Evaluating Controls on Arsenic Geochemistry at the Long Lake Gold Mine in Sudbury, ON

by

Brent Robert Verbuyst

A thesis

presented to the University of Waterloo

in fulfillment of the

thesis requirement for the degree of

Master of Science

in

Earth Sciences

Waterloo, Ontario, Canada, 2020

Author's Declaration

I hereby declare that I am the sole author of this thesis. This is a true copy of the thesis, including any required final revisions, as accepted by my examiners.

I understand that my thesis may be made electronically available to the public.

Abstract

The release of As from old mine sites can persist long after cessation of mining activities. This project combines field and laboratory research components at the Long Lake Gold Mine site, near Sudbury, Ontario. The mine was discovered in 1908 and operated intermittently from 1909 until 1939; the mine was later abandoned and is now the responsibility of the Ontario Ministry of Energy, Northern Development and Mines. Arsenic-bearing sulfide-rich tailings were deposited in three topographic depressions near the mill, named TA-01, TA-02 and TA-03. The purpose of this project is to evaluate controls on As biogeochemistry in the Long Lake tailings areas and to provide a detailed geochemical and mineralogical investigation of aqueous- and solid-phase As. During the past 100 years, extensive sulfide oxidation of sulfide minerals in the Long Lake tailings has resulted in acidic conditions and high concentrations of dissolved metals and SO_4 in the tailings pore water.

Four nests of monitoring equipment were installed within TA-01, to assist in the understanding of the biogeochemical behaviour of As in the tailings and groundwater. Core samples of the sand cap, tailings, and underlying soils were collected for geochemical, mineralogical, and microbiological characterization. Mineralogical and geochemical characterization of the TA-01 tailings showed a zone of sulfide oxidation extending ~0.3-1.0 m below the tailings surface. Arsenic K-edge X-ray absorption near edge structure (XANES) and bulk As K-edge high energy resolution fluorescence detection X-ray spectroscopy (HERFD-XAS) produced results consistent with the mineralogical investigation. Pore water within the near surface tailings was characterized by low pH (2.0-3.9) and elevated concentrations of dissolved metals and SO_4. Groundwater was characterized by circumneutral pH values and low concentrations of dissolved metals and SO_4. Arsenic concentrations of up to 500 mg L^{-1} were

measured in the tailings pore water and 70 mg L^{-1} in the underlying aquifer materials. The highest dissolved As concentrations were measured at shallow depths in the tailings corresponding with the lowest pH values and at the depth of the tailings profile near the organic layer interface. The tailings pore water and groundwater were characterized by $\delta^{34}S\text{-}SO_4$ and $\delta^{13}C$-DIC fractionation indicating the likelihood of dissimilatory sulfate reduction (DSR). Results of this study will be used to inform and complement remediation efforts being undertaken by the Ministry of Energy, Northern Development and Mines. This study will provide information on the nature of mechanisms that affect the release and attenuation of As in over 100 year old sub-aerially deposited sulfide tailings.

Acknowledgements

First, I would like to thank my supervisor Dr. David Blowes for his support and guidance throughout the course of this thesis. I would like to thank my committee members Dr. Carol Ptacek and Dr. Dogan Paktunc for their time and support in helping me, as well as providing insightful comments throughout this project.

The completion of this research would not have been possible without the assistance of many individuals in the field and laboratory. Thank you to Jeff Bain and Steve Holland for your instrumental help throughout the past few years. Thank you to everyone in the GGR Research Group including Krista Elena, Laura Groza, Joy Hu, and Sara Fellin.

I am thankful for the assistance that was provided by many individuals from the Ontario Ministry of Energy, Northern Development and Mines including Steve Reitzel and Heather White. Thank you for your help in the organization of field work that was performed throughout this project.

Thank you to all the graduate and coop students who helped me in the field and laboratory. This includes David Hilger, Mason McAlary, Emily Saurette, Eva Pakastova, Zhongwen Bao and many others. A special thank you to Joanne Angai for your invaluable help and support throughout this project. I will always be thankful for your friendship over the past two years.

I want to thank my parents, brother, sister and everyone else who have supported me over the years. I could not have done this without them. I also want to thank my friends who have supported me throughout this project.

Table of Contents

List of Figures

List of Tables

1 Introduction

1.1 Mine drainage geochemistry

1.1.1 Sulfide oxidation

The residual gangue produced during the recovery of ore minerals through milling and concentrating are classified as tailings. Mill tailings generated through the processing of sulfide ores can have negative impacts on the environment and water resources (Lindsay et al., 2015). Exposure to atmospheric oxygen results in oxidation of sulfide minerals in tailings and waste rock deposits, produces acidic water and releases hazardous elements (Blowes and Jambor, 1990; Nordstrom and Alpers, 1999). Several factors such as oxygen availability, pore-water pH, and the activity of S- and Fe-oxidizing bacteria control the rates of mineral oxidation (Lindsay et al., 2015, Nordstrom and Alpers, 1999). Pyrite and pyrrhotite are the main sulfide minerals associated with mine wastes that are susceptible to oxidation. The oxidation of pyrite and pyrrhotite by atmospheric oxygen is represented as:

$$(1) \quad FeS_{2(s)} + \frac{7}{2}O_2 + H_2O \rightarrow 2SO_4^{2-} + Fe^{2+} + 2H^+ \qquad (Pyrite)$$

$$(2) \quad Fe_{(1-x)}S + (2 - \frac{1}{2}x)O_2 + xH_2O \rightarrow (1-x)Fe^{2+} + SO_4^{2-} + 2xH^+ \qquad (Pyrrhotite)$$

Both pyrite and pyrrhotite may contain trace elements that occur as impurities such as As (Savage et al., 2000; Nordstrom, 2002; Paktunc et al., 2006) and other trace elements such as Pb, Sb, Bi, Cu, Co, Ni, Zn, Au, Ag, Se and Te (Deditius et al., 2011). In addition, arsenopyrite [FeAsS] and arsenian pyrite [$Fe(As_xS(1-x)_2$] are common sources of As in sulfide-ore deposits and mine wastes (Blowes et al., 2013; Lindsay et al., 2015). Sulfide oxidation can release these trace elements to the environment. The Fe(II) that is released by the oxidation of pyrite and

pyrrhotite can be oxidized to form Fe(III), which can precipitate as ferric oxyhydroxide under mildly acidic to near-neutral pH conditions.

$$(3) \quad Fe^{2+} + \tfrac{1}{4}O_2 + \tfrac{3}{2}H_2O \rightarrow \alpha FeOOH + 2H^+$$

Mineral dissolution reactions can neutralize acidity generated by sulfide-mineral oxidation and Fe(III) oxyhydroxide precipitation. The dissolution of calcite [$CaCO_3$], dolomite [$CaMg(CO_3)_2$] and other carbonate phases consumes H^+, which results in neutral mine drainage conditions through the following reactions (Blowes, 1997; Jurjovec et al., 2002).

$$(4) \quad CaCO_3 + H^+ \rightarrow Ca^{2+} + HCO_3^-$$

$$(5) \quad CaMg(CO_3)_{2(s)} + 2H^+ \rightarrow Ca^{2+} + Mg^{2+} + 2HCO_3^-$$

As the carbonate content decreases the pH remains near neutral. Acid mine drainage conditions occur following the depletion of carbonate minerals. After the carbonate minerals are depleted the pH of the pore-water decreases until it reaches equilibrium with the most soluble secondary hydroxide mineral, $Al(OH)_3$, maintaining the pH between 4.0 to 4.5 (Blowes, 1997). The pH will then lower until equilibrium with an Fe(III) oxyhydroxide has been attained which maintains the pH in the region of 2.5 to 3.5. With decreasing pH the solubility of Fe(III) increases and indirect oxidation becomes the dominant pathway of sulfide mineral oxidation (Nordstrom, 2003). Additional acidity and release of Fe(II), SO_4 and other metals are caused by indirect oxidation of pyrite by Fe(III):

$$(6) \quad FeS_{2(s)} + 14Fe^{3+} + 8H_2O \rightarrow 15Fe^{2+} + 2SO_4^{2-} + 16H^+$$

1.1.2 Arsenic geochemistry

Arsenic is a naturally occurring element found in the atmosphere, soils and rocks, natural waters, and organisms. Arsenic can be mobilized through natural processes such as weathering reactions,

biological activity and through anthropogenic causes. The occurrence of As contamination in the environment has greatly increased through releases associated with waste disposal, pesticides, As-bearing chemicals and mining (Morin and Calas, 2006). Mining activities in numerous locations in the world have contributed to As contamination (Williams, 2001). Although there are numerous pathways of exposure to As including air, food, water and soil, drinking water poses the greatest threat to human health associated with As contamination (Smedley and Kinniburgh, 2002).

On a worldwide scale As and F are recognised as the most serious inorganic contaminants in drinking water (Smedley and Kinniburgh, 2002). The limit of As in drinking water has changed over the years due to the growing evidence of the toxicological effects. The World Health Organization guideline value for As in drinking water is 10 μg L^{-1}, reduced from 50 μg L^{-1} in 1993. The maximum acceptable concentration of As for Canadian drinking water is 10 μg L^{-1}, while the interim maximum acceptable concentration for Ontario drinking water is 25 μg L^{-1}. In 2001 the US-EPA limit was reduced from 50 to 10 μg L^{-1}.

Arsenic occurs in many compounds and exists in the environment in five oxidation states (-III, -I, 0, III, V). Arsenic occurs in the -I oxidation state in sulfide minerals such as arsenopyrite [FeAsS] and arsenian pyrite [FeS_2] (Campbell and Nordstrom, 2014). Other primary sulfide minerals that contain As include orpiment [As_2S_3] and realgar [As_2S_2]; small amounts of As are commonly found in the structure of co-existing pyrite (Kocourkova et al., 2011). Arsenic is found in a variety of other forms such as As-sorbed species, poorly crystalline As-bearing solids and organic forms of As (Wang and Mulligan, 2009). Biological activity can produce organic forms of As, mainly in surface water where it has been significantly impacted by industrial pollution (Smedley and Kinniburgh, 2002). Organic forms of As include dimethylarsinate

(DMA) and monomethylarsonate (MMA), and are the least toxic As species (Miller et al., 2000). Organic As species are rarely quantitatively significant in groundwater except where industrial pollution occurs (Smedley and Kinniburgh, 2005).

In natural waters As commonly occurs as trivalent arsenite [As(III)] or pentavalent arsenate [As(V)] (Smedley and Kinniburgh, 2002). In anaerobic environments As(III) is the primary species, while in aerobic waters As(V) dominates (Nordstrom, 2002; Smedley and Kinniburgh, 2005). In the environment, As(V) and As(III) often co-exist due to relatively slow redox transformations (Raven et al., 1998). Arsenite has been reported as being 25-60 times more toxic than As(V) and is more mobile in the environment (Korte and Fernando, 1991).

The most important factors that control As speciation in aqueous systems are pH and redox potential (Smedley and Kinniburgh, 2005). In contrast to many other elements, As is soluble across a wide pH range (pH 1-12) (Williams, 2001). Arsenic is unique due to its sensitivity to mobilization in circumneutral waters under both oxidizing and reducing conditions (Smedley and Kinniburgh, 2002). Inorganic As forms the arsenate oxyanion (AsO_4^{3-}) at moderate and high redox potentials, while the arsenite oxyanion (AsO_3^{3-}) occurs under moderately reducing conditions at circumneutral or low pH. At lower pH values (less than 6.9) and oxidizing conditions H_3AsO_4 is dominant and AsO_4^{3-} is dominant under alkaline conditions (Smedley and Kinniburgh, 2002; O'Day, 2006). Uncharged $H_3AsO_3^0$ dominates under reducing conditions and at pH less than 9.2 (Smedley and Kinniburgh, 2005).

1.1.3 Sulfate reduction

Dissimilatory sulfate-reducing bacteria are found over an extensive pH range (Chang et al., 2001). Microbially mediated sulfate reduction can attenuate dissolved metals and SO_4 released by sulfide oxidation reactions and has been used to remediate acid mine drainage at the source

(Hulshof et al., 2003, 2006), in constructed wetlands (Ledin and Pederson, 1996) and in permeable reactive barriers (Blowes et al., 1998; Waybrant et al., 1998; Benner et al., 1999). The oxidation of organic carbon is catalyzed by sulfate-reducing bacteria and is coupled with the reduction of SO_4 to H_2S by the reaction:

$$(7) \quad SO_4^{2-} + 2CH_2O \rightarrow H_2S + 2HCO_3^-$$

Where CH_2O represents a generic organic compound (Berner, 1980). This reaction releases H_2S into pore waters which may result in the precipitation of metals through the follow reaction:

$$(8) \quad Me^{2+} + HS^- \rightarrow MeS + H^+$$

Where Me^{2+} represents a metal such as Cd, Co, Cu, Fe, Ni, and Zn. The net results from reactions (7) and (8) include decreased concentrations of SO_4, Fe, metal(loid)s and an increase in pH and alkalinity (Hammack and Edenborn, 1992; Benner et al., 1999).

1.2 Research objectives

The primary objective of this research was to provide information on the mechanisms that control the release and attenuation of As in a sub-aerially tailings impoundment where sulfide-bearing mill tailings were deposited starting over 100 years ago and ending 81 years ago. Results of this study will be used to inform and complement remediation efforts at the Long Lake mine site, which are being undertaken by the Ministry of Energy, Northern Development and Mines. Specific objectives of this research included:

- Providing a detailed geochemical and mineralogical investigation of aqueous and solid phase As, and
- Evaluate controls on As biogeochemistry in the tailings at the Long Lake mine site

The expected outcome of this project is to better understand the controls on As geochemistry in gold mine tailings and to characterize the site for future remediation. This project also describes the geochemistry of the tailings pore water and the mechanisms that control the concentrations of dissolved metals.

1.3 Site description

The Long Lake Gold Mine is a former Au mine and located in the Eden Township of the City of Greater Sudbury, roughly 1.3 km south of the south-western end of Long Lake (Figure 1). The ore deposit was discovered in 1908 and mined intermittently from 1908 until 1939, when the mine site was abandoned. The ore body contained impregnations of fine-grained, gold-bearing arsenopyrite and pyrite in Mississagi sandstone as a pipe-shaped mass approximately 150 feet by 250 feet (Gordon et al., 1979). The main ore minerals, gold-bearing arsenopyrite and pyrite replaced feldspars in the sandstone. Other minerals include chalcopyrite, pyrrhotite, and minor amounts of galena, magnetite, and hematite (CH2M Hill, 2014). The mineralization is spatially related to Nipissing type intrusions (Gordon et al., 1979). Underground mining methods were used to recover the Au ore. The mine consisted of four levels of underground drifts, winzes, a mine shaft and a small open pit. The underground workings and the open pit are currently flooded. Gold was recovered using a 20-ton stamp mill and cyanide plant. Ore may also have been roasted. The mine produced over 56,000 ounces of Au and over 600 ounces of Ag from approximately 196,000 tonnes of ore. Arsenic-bearing sulfide-rich tailings were deposited in three topographic depressions near the mill, named TA-01, TA-02 and TA-03, between the mine site and the south end of Long Lake. The three tailings areas are estimated to contain 163,000 m^3 of tailings (CH2M Hill, 2014).

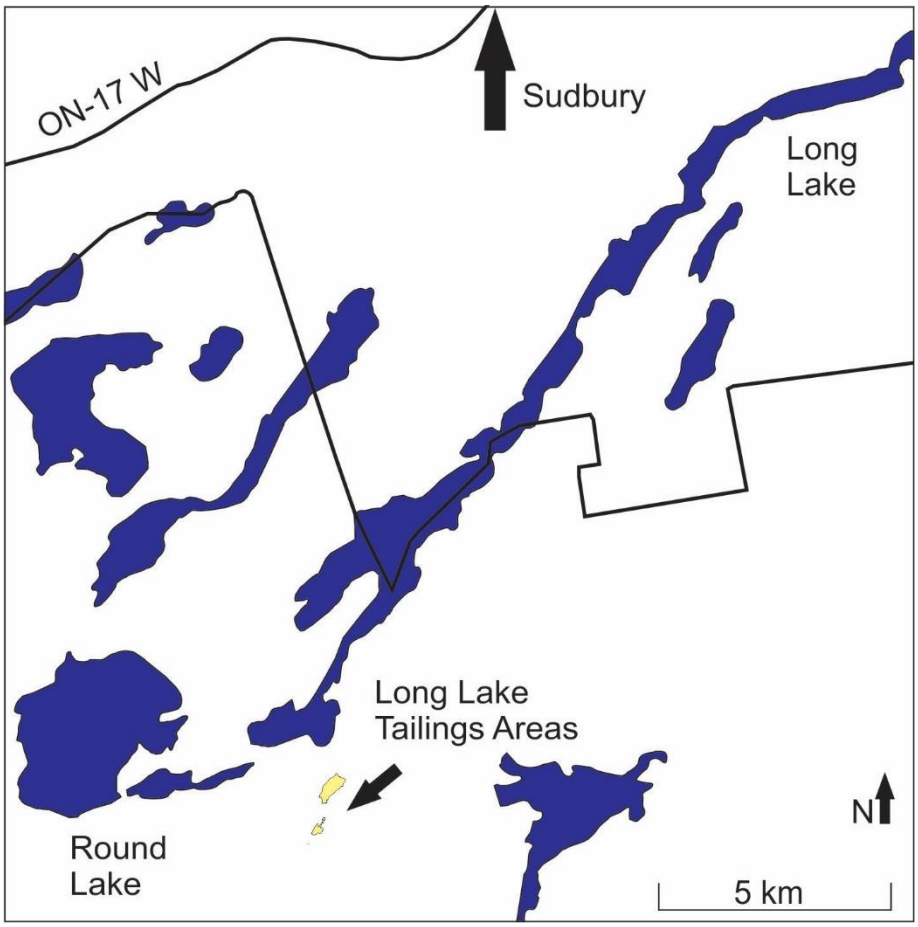

Figure 1: Image showing the location of the abandoned Long Lake Gold Mine, approximately 1.3 km south of the southwest end of Long Lake, south of the City of Greater Sudbury.

Since the mine was abandoned waterborne fugitive tailings have migrated northward through the surface water drainage between the three tailings areas. Tailings have also been observed in the downstream drainage and in Luke Creek, which discharges into Long Lake. These releases have resulted in a tailings delta formed at the southern end of Long Lake where Luke Creek discharges. In the early 1970s, the Ministry of labour capped tailings areas TA-01 and TA-02 with white sand as an attempt to reduce the exposure of As through tailings dusting. Since that time portions of the sand cap eroded, and exposed tailings are visible. The presence of plants on the tailings areas is limited due to the toxicity of the tailings (CH2M Hill, 2014).

The tailings at the Long Lake Gold Mine include sulfide minerals that can produce acidic drainage with high concentrations of dissolved metals when the tailings are exposed to air and water. The runoff from the tailings is acidic and contains elevated concentrations of dissolved metals. The element of primary concern at the Long Lake Gold Mine is As. The Ontario Ministry of the Energy, Northern Development and Mines (ENDM) has been monitoring the water quality in Long Lake since the 1970s. It has been determined that the As concentrations at the southwest end of Long Lake exceed the Ontario Drinking Water Standard of 25 µg/L and Health Canada's guideline of 10 µg/L. This concern has led to the Sudbury and District Health Unit issuing a Drinking Water Advisory to property owners located near the affected area of Long Lake (CH2M Hill, 2014).

In 2014, a site characterization study was conducted at the Long Lake Gold Mine (CH2M Hill, 2014). It was determined that there are three primary contaminant sources of concern to Long Lake. These contaminant sources are the three tailings areas (TA-01, TA-02, TA-03 and the related drainage paths), the fugitive tailings in Luke Creek and the wetland, and finally the tailings in Long Lake (tailings delta). The waste rock and the mine water from the open pit were not found to be substantial sources of contamination.

Much of the As in the tailings delta in Long Lake is in a stable sulfide phase. There is limited potential for oxidation of this sulfide phase if the tailings remain submerged and are not exposed to the atmosphere (CH2M Hill, 2014). In the submerged tailings in Long Lake about 25% of the As has co-precipitated with Fe(III) oxyhydroxide. Under low $O_{2(g)}$ conditions ferric hydroxide may be unstable and remobilize As. Because of the low reduction potential in the submerged tailings and adequate $O_{2(g)}$ concentrations, the remobilization of As is not expected to happen in Long Lake (CH2M Hill, 2014). As determined by CH2M Hill, the submerged tailings

were determined to not be a significant source of dissolved As. The sources of As that are contributing to the contamination of Long Lake vary seasonally. During low flow seasons, As is derived from the tailings in Luke Creek, which are exposed to atmospheric $O_{2(g)}$. The tailings areas are the source of the fugitive tailings and are therefore contributing to the As loading during higher flow periods. The tailings areas do not contribute to As loading during low flow. According to CH2M Hill, groundwater is not a major migration pathway of As from the tailings areas to Long Lake.

The Ministry of Energy, Northern Development and Mines is responsible for the remediation plan that will occur at the Long Lake Gold Mine. The goal of this remediation effort is to improve the water quality in Long Lake to meet the provincial safe drinking water limits. The tailings will be consolidated to reduce the As loading to the ecosystem and restore wildlife productivity and biodiversity. This remediation plan will involve the development of a tailings impoundment within TA-01 and consolidation of all of the tailings in a single impoundment area. The tailings that are in the delta in Long Lake will be excavated to a minimum depth of 2 m below the lake water level and moved to the tailings impoundment. The tailings that will remain in Long Lake will be capped with a layer of gravel to prevent re-suspension. After all the tailings are consolidated in the impoundment, the impoundment will be capped with an engineered cover. The cover will help to prevent infiltration into the impounded tailings. All areas where tailings are removed will be covered and vegetated.

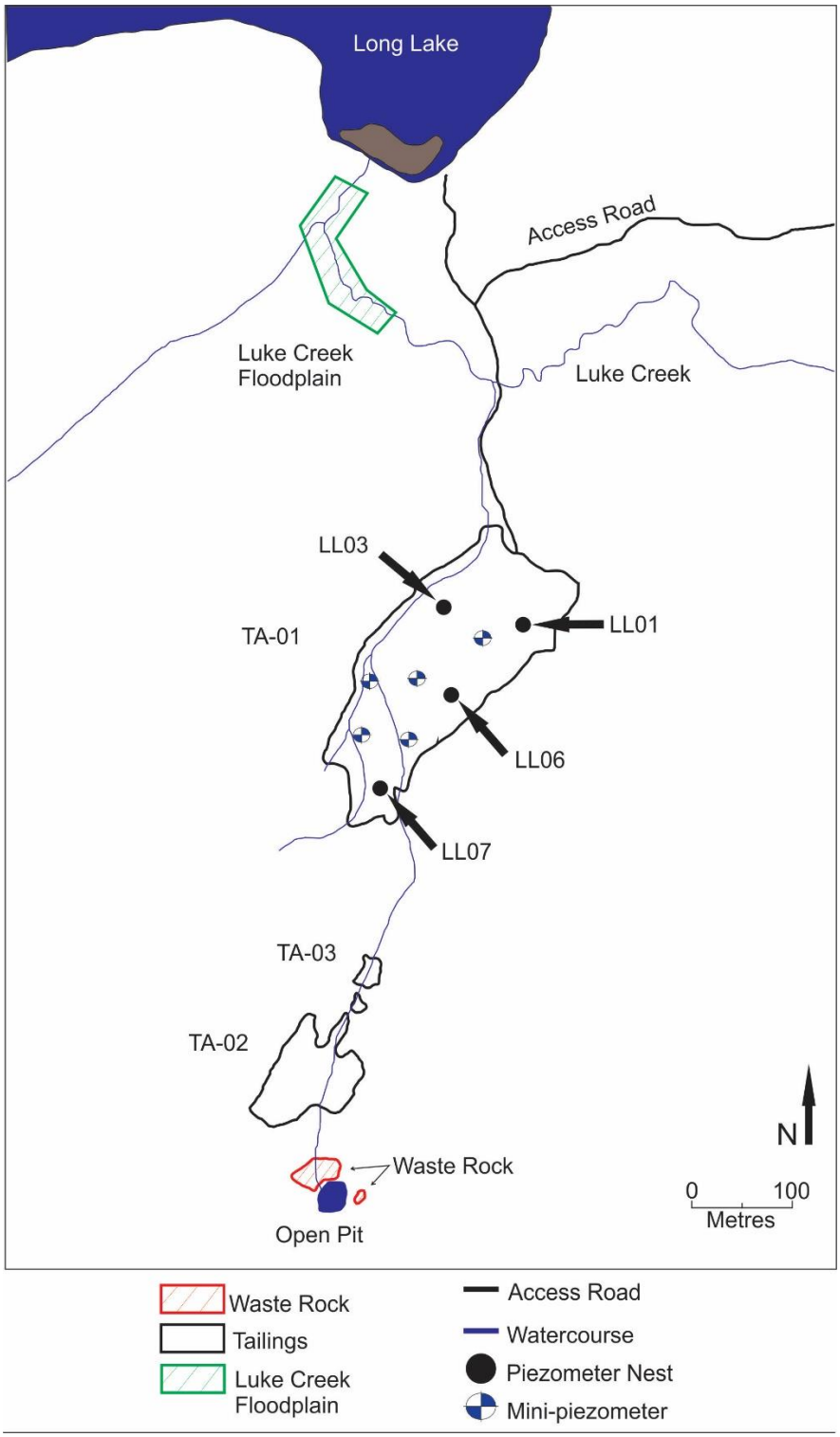

Figure 2: Detailed Long Lake Gold Mine site map, including the location of the four piezometer nests (LL01, LL03, LL06, and LL07) used for geochemical and mineralogical investigations and the location of the five mini-piezometers (P1 to P5) installed to measure the shallow groundwater flow.

2 Methods of Investigation

2.1 Piezometer network

A network of four piezometer nests and five water-table wells was installed within TA-01 tailings impoundment (Figure 2). Each piezometer nest consisted of several 5.08 cm (2-in.) diameter drive-point piezometers (total of 23) and one to two soil-water solution samplers (SWSS). The water-table wells were installed within TA-01 to further characterize the groundwater flow system (Figure 2). Hydraulic conductivity values were determined using a combination of piezometer-response tests and calculations based on grain size measurements (Table 1). Water levels and hydraulic head measurements were made on several occasions to determine the groundwater flow velocity within TA-01 (Appendix C).

2.2 Groundwater sampling

Water from the piezometers was collected using a peristaltic pump. Soil-water solution samplers were used to collect tailings pore water from the unsaturated zone. Measurements of pH (Orion Ross Ultra pH Electrode) and Eh (Thermo Orion Redox Sure Flow Electrode) were made in the field. All measurements of pH and Eh were maintained at groundwater temperature (~8-10 °C). The pH electrode was calibrated using pH 1.68, pH 4 and pH 7 buffers (traceable to NIST). The Eh electrode was verified using ZoBell's solution (Nordstrom, 1977) and Light's solution (Light, 1972). Alkalinity was determined on samples filtered through 0.45 um cellulose acetate membranes using a Hach Digital Titrator, 0.16 N or 1.6 N sulfuric acid and bromcresol green-methyl red indicator. The electrical conductivity was measured on unfiltered samples using an Oakton® Instruments EcoTestr (Conductivity and TDS pocket meter). Samples were filtered with cellulose nitrate membranes and split into high-density polyethylene (HDPE) or glass amber bottles for various geochemical analyses.

Samples for analysis of cations were preserved using trace-metal-grade HNO_3 to a pH < 2. Samples for anions were not preserved. All samples were refrigerated immediately after collection and stored at 5 °C until analysis. Cations concentrations were determined by inductively coupled plasma optical emission spectroscopy (ICP-OES) and inductively coupled plasma mass spectrometry (ICP-MS) for Ag, Al, As, B, Ba, Be, Ca, Cd, Co, Cr, Cs, Cu, Fe, K, Li, Mg, Mn, Mo, Na, Ni, P, Pb, S, Sb, Se, Si, Sn, Sr, Ti, Tl, U, V and Zn. Anion concentrations were determined by ion chromatography (IC) for Cl^-, Br^-, F^-, NO_2^-, NO_3^-, PO_4^{3-} and SO_4^{2-}.

Samples collected for As speciation were analyzed as soon as possible at the University of Waterloo by separating As(III) and As(V) using a modified version of the anion exchange method described by Ficklin (Ficklin, 1983). This method uses ion exchange of anionic arsenate from neutral arsenite under acidic conditions. The ion exchange is performed using gravity flow of the samples through an anion exchange resin using HCl as the eluant. The modified Ficklin method is inexpensive, fast and simple (Edwards et al., 1998). All samples were then refrigerated until analysis. After separation, the samples were analyzed by ICP-OES to determine the concentrations of both As(III) and As(V).

At the University of Waterloo, environmental-grade 3N HCl was used to adjust the pH of samples collected for $\delta^{34}S$ and $\delta^{18}O$ analysis. The addition of HCl acid ensured that the dissolved inorganic carbon was driven out of the solution. Sulfate for $\delta^{34}S$ and $\delta^{18}O$ isotope analysis was then precipitated as $BaSO_4$ using reagent grade $BaCl_2 \cdot 6H_2O$. The precipitate was rinsed with a minimum of 500 mL distilled water to remove any residual $BaCl_2$. The precipitated $BaSO_4$ was then converted into SO_2 in an elemental analyzer coupled to a mass spectrometer (Giesemann et al., 1994). Raw $\delta^{34}S$ values are normalized to the Vienna Canyon Diablo Troilite (VCDT) scale using reference materials and laboratory standards. Oxygen-isotope analysis on $BaSO_4$

precipitate was determined using a high temperature reactor coupled to an isotope ratio mass spectrometer in continuous flow mode. Results are expressed in the per mil notation relative to the international V-SMOW standard.

Dissolved organic carbon (DOC) samples were collected in 40 mL sealed amber glass bottles, preserved with H_2SO_4 and stored at 5 °C until analysis. Dissolved inorganic carbon (DIC) samples were collected in 60 mL HDPE bottles. Dissolved inorganic carbon samples contained no preservative and were kept frozen until analysis. Both DOC and DIC samples were analyzed at the University of Waterloo.

Water collected for cyanide analyses included samples for total cyanide, weak acid dissociable cyanide (WAD) and thiocyanate. Samples for total cyanide and WAD cyanide analyses were collected in the same sample bottle, which contained NaOH as a preservative. Samples for thiocyanate analysis were collected into separate 60 mL bottles containing HNO_3 as a preservative. Samples were shipped to ALS Environmental in Waterloo, ON, for analysis.

Unfiltered samples for methane (CH_4) analysis were collected, with no headspace, in 30 mL glass serum bottles sealed with a rubber septa and aluminum crimp seals. Samples were stored at 5 °C and inverted during transport to the University of Waterloo. In the laboratory, a headspace was created in the sample by injecting 10 mL He gas. The samples were shaken to equilibrate dissolved CH_4 with the He gas. An aliquot of the headspace gas was removed and injected into a gas chromatograph (Agilent 7890B GC System) with a flame ionization detector (GC-FID) for the determination of aqueous CH_4.

2.3 Pore-gas analysis

Pore-gas concentrations of $O_{2(g)}$ and $CO_{2(g)}$ were measured in the field. Stainless steel tubes, 0.63 cm in diameter, were driven into the tailings at 10 cm intervals and connected directly to a portable O_2/CO_2 analyzer (Quantek Instruments Oxygen/Carbon Dioxide Analyzer, Model 902P). Pore gas was pumped through the analyzer until the readings stabilized. The pore-gas concentrations were measured at each of the four nest locations. Measurements ended at the depth where saturated conditions were encountered.

2.4 Core sample collection

Continuous core samples for geochemical, mineralogical and microbiological investigations were collected at four piezometer nests within TA-01: LL01, LL03, LL06 and LL07 (Figure 2). All core samples were collected in thin-walled Al tubes either 7.62 cm (3-in.) or 5.08 cm (2-in.) in diameter, using the piston core-barrel method described by Starr and Ingleton (1992). The samples were frozen at the site and transported to the University of Waterloo where they were maintained frozen until analysis. Core samples collected in November 2016 were utilized for pore-water extraction, whereas samples collected in November 2017 were used for microbiological and mineralogical investigations. A correction factor was applied to each core section to compensate for compaction.

2.5 Pore-water extraction

Core samples collected in 2016 were used to collect pore water by the method described by Moncur et al. (2013). Measurements of pH, Eh and alkalinity were determined as described above, at least three times for each section of core to ensure representative results. The remaining pore water was passed through 0.45 um cellulose acetate filters and transferred to HDPE bottles.

One aliquot was collected for cation analysis and another aliquot collected for anion analysis. Samples were preserved as described above.

2.6 Geochemical modeling

The geochemical model PHREEQC 3.4.0 (Parkhurst and Appelo, 1999) using the WATEQ4F database (Ball and Nordstrom, 1991) was used to assist in the interpretation of the aqueous geochemical data and the mineralogical results. The model was also used to infer mineral phases that may be controlling concentrations of dissolved constituents. PHREEQC is an equilibrium speciation/mass transfer model that provides calculations of saturation indices (SI) for discrete mineral phases.

2.7 Physical properties

The bulk density, particle density, moisture content and porosity were determined at several depths at each piezometer nest. The particle density of the dry material was measured using a Beckman Model 930 Air Comparison Pycnometer. Volumetric moisture content and porosity were calculated from the measured values of bulk density, particle density and gravimetric moisture content. Particle-size distributions were determined using laser diffraction analysis on samples from several depths at each of the four nest locations. The hydraulic conductivity was then estimated using the Kozeny-Carmen equation from each grain size curve using the HydrogeoSieveXL2-3 program (Devlin, 2015). The uniformity coefficient (CU) was calculated for each grain-size distribution, where $CU = D_{60}/D_{10}$.

2.8 Solid-phase geochemistry and mineralogy

Core samples collected in November 2017 were sub-sampled for geochemical analyses and mineralogical study. Geochemical analyses included C/S determinations and whole-rock

analyses. Whole-rock assay samples were selected from one nest location, LL01, at six different depths. These samples were sent to three independent laboratories, ALS Global, Activation Laboratories Ltd. (Actlabs) and Bureau Veritas Minerals (BVM), for digestion with aqua regia followed by trace element analysis by ICP-MS.

X-ray Diffraction (XRD), optical microscopy and Scanning Electron Microscopy (SEM) were used to study the tailings mineralogy. Seven samples from each LL06 and LL07 were selected for examination. Samples included tailings from both the oxidized and unoxidized zones, the organic layer directly beneath the tailings and samples from the underlying sediment. Polished thin sections were prepared by Spectrum Petrographics in Vancouver, Washington. Sections were prepared in the absence of water and oxygen to prevent the dissolution of soluble phases or the oxidation of sulfide minerals. The polished thin sections were examined using optical microscopy under both transmitted and reflected light. All thin sections from LL07 were then coated with carbon and grains selected on the basis of optical microscopy were examined by scanning electron microscopy-energy dispersive spectrometry (SEM-EDS). The SEM-EDS utilized a Hitachi S-3200N instrument with a backscattered electron detector and a Hitachi TM3000 Table-top SEM coupled with a Bruker QUANTAX 70 EDS.

Bulk As K-edge high energy resolution fluorescence detection X-ray spectroscopy (HERFD-XAS) spectra were collected from tailings and native soil on the 20-ID beamline at the Advanced Photon Source (Argonne National Laboratory, Lemont, IL) to identify As species. Frozen core samples were freeze dried under vacuum at -50 °C and pulverized in an agate mortar and pestle. The powdered samples were pressed in Teflon holders and sealed with Kapton tape prior to analysis. Sample preparation was completed in an anaerobic glovebox. Nine mineral standards were examined including: arsenolite [As_4O_6], arsenopyrite [FeAsS], arsenic trioxide

[As_2O_3], getchellite [$AsSbS_3$], kankite [$Fe^{3+}AsO_4 \bullet 3.5(H_2O)$], orpiment [$As_2S_3$], realgar [α-$As_4S_4$], scorodite [$FeAsO_4 \bullet 2H_2O$], and sodium arsenate [$Na_3AsO_4$]. Three to ten scans were made on each sample. Linear combination fitting (LCF) of normalized spectra was performed using ATHENA (Ravel and Newville, 2005).

Synchrotron radiation-based μ-XRF and X-ray adsorption near edge structure spectroscopy (XANES) was used to examine As speciation for selected grains in addition to HERFD spectroscopy. Arsenic K-edge spectra were collected for reference standards. Experiments were performed on beamline 20-ID at the Advanced Photon Source located at Argonne National Laboratory in Lemont, Illinois. Grains were selected from thin section slides determined by optical and SEM examination. Scans were performed over an energy range of 11,667 to 12,720 eV. Three to five scans were made on each location selected for XANES spectra. Arsenopyrite [FeAsS], scorodite [$FeAsO_4 \bullet 2H_2O$], and schneiderhohnite [$Fe^{2+}Fe^{3+}{}_3As_5O_{13}$] were analyzed as reference standards. Data analysis of normalized spectra was performed using ATHENA (Ravel and Newville, 2005). Additional reference standards used included kankite [$FeAsO_4 \bullet 3.5H_2O$], sodium arsenite [$NaAsO_2$], orpiment [As_2S_3], realgar [α-As_4S_4], arsenic trioxide [As_2O_3], arsenic pentoxide [As_2O_5], and sodium arsenate [Na_3AsO_4].

3 Results and Discussion

3.1 Hydrogeology

Tailings area 01 (TA-01) is the largest tailings area of the three and is approximately 7.1 ha in size (Figure 2). Of the total 163,000 m^3 of tailings generated at Long Lake TA-01 contains 141,000 m^3 of tailings, approximately 87 percent of the total tailings by volume (CH2M Hill, 2014). A drainage channel enters the tailings area from the south-east and flows toward the western boundary of TA-01. From there the channel extends north, exiting TA-01 at the northern tip, toward Long Lake *via* Luke Creek.

The surficial geology consists of a bedrock-drift complex containing frequent bedrock outcrops and discontinuous glacial drift of variable thickness, consisting of a silty to sandy till (Boissoneau, 1965). The southern portion of TA-01 slopes northward towards the drainage channel. The remaining area of TA-01 generally slopes to the northwest. Measurements over the period from 1971 to 2010 from a meteorological station 21 km northeast of the site indicate that the average annual precipitation is 901 mm, with 74 percent occurring as rainfall and the remaining in the form of snow (CH2M Hill, 2014). Tailings thickness at TA-01 ranged between 1.0 and 2.5 m. The tailings are underlain by a thin peat/organic layer which overlies a clay/silty clay layer. Bedrock was encountered at one location by CH2M Hill at the northern end of TA-01 at a depth of 5.79 m.

Physical properties including bulk density, particle density, moisture content, porosity and grain-size distributions were measured on samples at various depths from the nest locations. The calculated uniformity coefficient ranged from 2.25 to 8.40 with an average value of 3.88, representing a poor to well graded grain-size distribution. The porosity of the tailings determined

using the volumetric moisture content, bulk density and particle density ranges from 44 to 66 % and averages 59 %. (Figure 3).

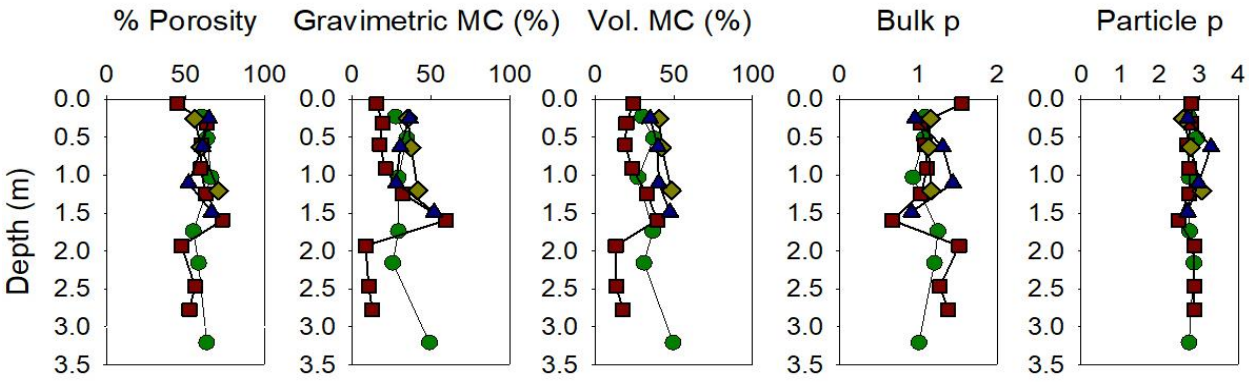

Figure 3: Depth profiles of porosity (n), gravimetric and volumetric moisture content, bulk (ρ_b) and particle (ρ_d) density for each piezometer nest location: LL01 (circle), LL03 (square), LL06 (diamond), and LL07 (triangle).

The grain-size diameter of the tailings at which 10 % by weight of the particles are finer (D_{10}) showed differences in values between the profiles (Appendix C). Grain-size distributions showed a mixture of well sorted, fine to medium grained sand/silt and gap graded sand/silt. The distribution of particles sizes ranged from < 0.001 to > 0.1 mm. Samples were characterized by a broad range of particle sizes or by two dominant particle sizes (Figure 4). The grain size was coarser at all depths at LL07, near where the tailings were discharged into the impoundment, compared to the other locations. At LL06 the D_{10} values are coarser near the surface and become finer with depth. The D_{10} values at LL03 increase to a maximum of 0.15 mm at a depth of 0.70 m, followed by a decrease at greater depths. The D_{10} values at LL01 are fairly consistent throughout the profile, ranging between 0.063 and 0.124 mm. The coarser nature of the tailings near the surface could be a result of cementation of particles by secondary minerals produced by weathering reactions, winnowing by wind, or segregation during tailings deposition.

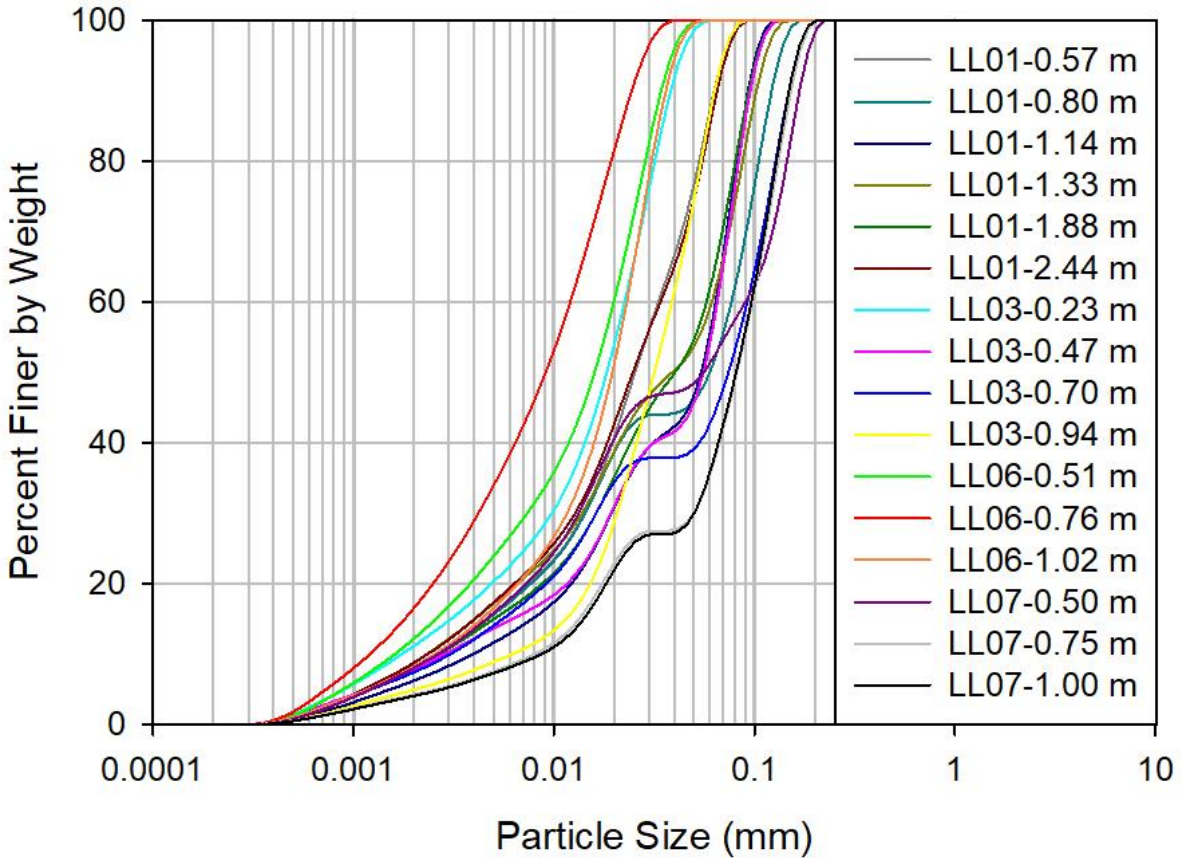

Figure 4: Grain-size distribution of tailings samples throughout TA-01.

Hydraulic conductivity (K) values were calculated from rising-head tests (Bower and Rice) and grain-size analyses (Kozeny-Carman). Due to the sampling method used to collect sediment for grain-size analyses, direct overlap between the two methods was not possible. The estimated K, as calculated from grain-size analysis using the Kozeny-Carman equation for the tailings samples from the four nest locations averaged 1.6×10^{-6} m s^{-1}, with a range of 3.4×10^{-7} m s^{-1} to 4.0×10^{-6} m s^{-1} (Table 1). This relatively high permeability is consistent with the soil classification of tailings. Hydraulic conductivity was also evaluated using rising-head tests averaging 5.6×10^{-6} m s^{-1} within the tailings and averaging 1.1×10^{-7} m s^{-1} within the underlying natural materials (Table 1). Hydraulic conductivities calculated from grain-size analyses are considered less reliable than pumping and slug tests (Pucko and Verbovsek, 2015). Hydraulic

conductivity values were also calculated using the Hazen method, but were found to be several orders of magnitude different than the Bower and Rice and Kozeny-Carman methods. The Hazen method was developed for loose, clean sands with a uniformity coefficient of less than 2 and should be limited to saturated sands with D_{10} values between 0.1 to 0.3 mm (Carrier, 2003). The Hazen formula is based only on the D_{10} particle size whereas the Kozeny-Carmen formula is based on the full particle size distribution, particle shape, and the void ratio. Therefore, the Hazen method is considered less accurate than the Kozeny-Carmen formula (Carrier, 2003). Grain-size analyses test a small area of sediment compared to field-scale tests and is the most probable cause of differences between the two methods. Hydraulic conductivity results determined using the Kozeny-Carman and Bower and Rice methods are generally consistent, with results within an order of magnitude. An independent-samples t-test was conducted to compare the means of the Bower and Rice and Kozeny-Carman hydraulic conductivity methods. There was not a significant difference in the results for the Bower and Rice ($M=1.6 \times 10^{-6}$, $SD=9.5 \times 10^{-7}$) and Kozeny-Carman ($M=2.6 \times 10^{-6}$, $SD=4.7 \times 10^{-6}$) methods; t (29), p=0.36. These results suggest that the two populations are not significantly different. Hydraulic conductivities below the tailings within the native soil are lower by several orders of magnitude, which is consistent with the fine particle size of the silt/clay lithology.

Table 1: Comparison of hydraulic conductivity values.

Location	Depth (m)	Matrix	K (m s^{-1}) [Kozeny-Carman]	K (m s^{-1}) [Bower and Rice]
	0.23	Sand	1.25×10^{-6}	
	0.57	Tailings	1.22×10^{-6}	
	0.80	Tailings	1.42×10^{-6}	
	1.14	Tailings	2.02×10^{-6}	
	1.33	Tailings	1.25×10^{-6}	
LL01	1.60	Tailings		1.60×10^{-6}
	1.88	Tailings	1.44×10^{-6}	
	1.97	Tailings		1.97×10^{-6}
	2.44	Tailings	1.23×10^{-6}	
	3.0	Organics		2.79×10^{-6}
	3.89	Soil		2.49×10^{-9}
	0.23	Tailings	6.56×10^{-7}	
	0.47	Tailings	1.38×10^{-6}	
	0.70	Tailings	1.45×10^{-6}	
LL03	0.94	Tailings	2.43×10^{-6}	
	1.00	Tailings		6.60×10^{-6}
	1.86	Soil		1.57×10^{-7}
	6.00	Soil		1.14×10^{-9}
	0.25	Sand	2.31×10^{-6}	
	0.51	Tailings	5.88×10^{-7}	
	0.76	Tailings	3.44×10^{-7}	
LL06	1.00	Tailings		1.77×10^{-6}
	1.02	Tailings	9.48×10^{-7}	
	2.00	Soil		3.49×10^{-7}
	4.55	Soil		2.06×10^{-9}
	0.25	Tailings	1.42×10^{-6}	
	0.50	Tailings	1.48×10^{-6}	
LL07	0.75	Tailings	3.74×10^{-6}	
	1.00	Tailings	4.00×10^{-6}	
	1.43	Organics		1.61×10^{-5}
	2.1	Soil		1.61×10^{-7}

Within TA-01, the groundwater levels ranged from 239.56 m above sea level (mASL) to 242.82 mASL between June 2017 and July 2019. The highest hydraulic head values were observed to be at the south-west end of the tailings area (Figure 5). These measurements indicate that groundwater is flowing north from the south end of TA-01. Groundwater level

measurements taken by CH2M Hill and the ENDM in 2013, 2015 and 2016 are included (Appendix C). The groundwater level measurements from CH2M Hill are consistent with observations during this project. Contour maps from between June 2018 and October 2018 show that the lowest hydraulic head values are at piezometer nest LL03 (Figure 5). Groundwater measurements from 2017 also suggest that groundwater is flowing north from LL07 towards the other three locations LL01, LL03 and LL06, as well as from LL01 toward LL03 (Appendix C). The addition of the mini-piezometers in 2018 provided a more comprehensive description of groundwater flow within TA-01.

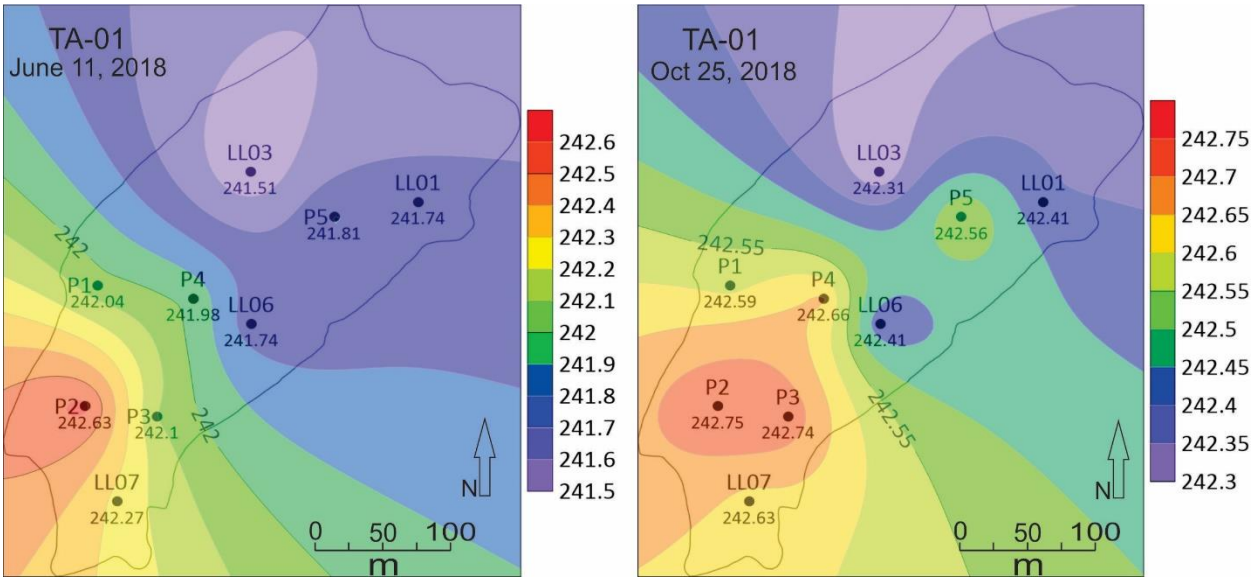

Figure 5: Groundwater elevation contour maps for TA-01 from June 11, 2018 and October 25, 2018 indicating groundwater flow from the south of TA-01 towards the northern point and towards Luke Creek and Long Lake.

The hydraulic head measurements suggest that there is a seasonal variation in the vertical gradient (Figure 6). At LL01 there is a downward gradient during November 2017 and 2018, and a slight upward gradient during June, July and September. A similar trend is observed at LL03 in November 2017 showing a downward gradient throughout the profile. During the other sampling

dates an upward gradient is observed. An upward vertical gradient is observed at LL06 during June, July, and September, while a downward gradient is observed during November.

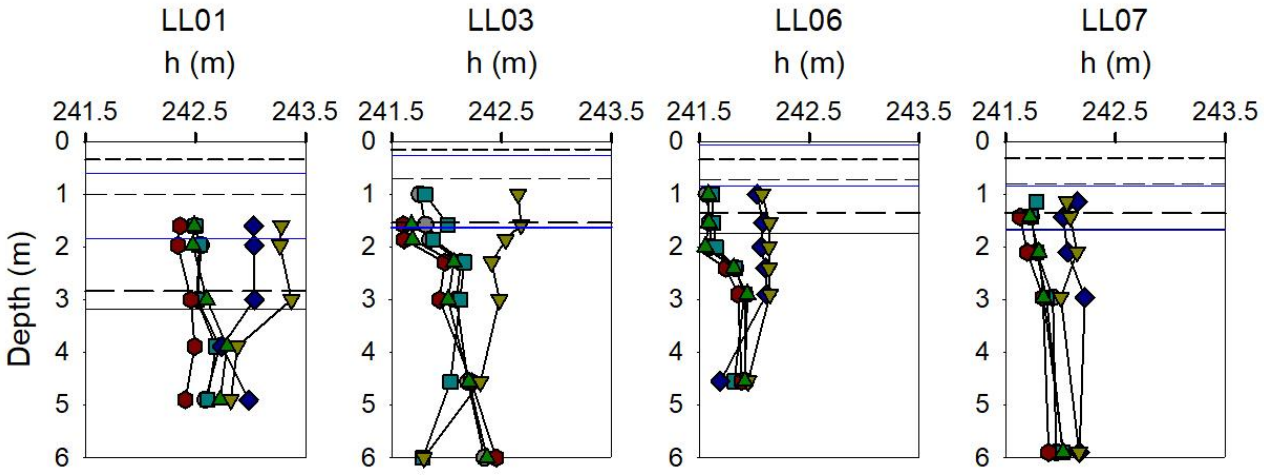

Figure 6: Depth profiles of hydraulic head (h) values. Short, medium, and long-dashed lines represent the depth of the sand layer, oxidized tailings, and unoxidized tailings, respectively. The solid line represents the depth of the organic layer. The solid blue lines represent the range of the water table. Symbols represent different sampling episodes: June 2017 (○), September 2017 (□), November 2017 (◊), June 2018 (⬡), November 2018 (▽), and July 2019 (△).

The average horizontal hydraulic gradient was estimated to be 0.0028, ranging from 0.0001 to 0.0102 between June 2017 and July 2019. This horizontal hydraulic gradient is consistent with previous findings that provided an estimate of lateral hydraulic gradient of 0.0040 within TA-01 in July and August 2013 (CH2M Hill, 2014). The average specific discharge was 1.39×10^{-8} m s^{-1}, ranging from 1.32×10^{-9} m s^{-1} to 6.09×10^{-8} m s^{-1}. The average estimated horizontal groundwater velocity was 1.78 m a^{-1}, ranging from 0.13 to 3.72 m a^{-1}. The average vertical hydraulic gradient was estimated to be 0.02, ranging from -0.87 to 1.11 between June 2017 and July 2019. A negative value represents upward flow while a positive value represents downward flow. The direction and magnitude of vertical hydraulic gradients is dependent on the piezometer nest location and the time of year. The vertical hydraulic conductivity calculated for each piezometer nest location was 1.08×10^{-8}, 1.65×10^{-9}, 3.67×10^{-9},

and 4.94 $\times 10^{-7}$ m s^{-1} for LL01, LL03, LL06, and LL07, respectively. Using the vertical hydraulic conductivity for each piezometer nest location and the average vertical hydraulic gradient, the average vertical groundwater velocity ranges from 0.007 to 0.944 m a^{-1}. The vertical groundwater velocity at location LL07 was the largest at 0.944 m a^{-1}, consistent with the coarser particle size of the tailings at this location.

The δ^2H and $\delta^{18}O$ ratios were determined at each piezometer nest location to help identify geochemical processes and groundwater surface water interactions. The tailings pore water and groundwater were plotted along the global meteoric water line (GMWL) at each piezometer nest location (Craig, 1961). The local meteoric water line (IAEA/WMO, 2020) was found to not be significantly different from the GMWL. Values of $\delta^{18}O$ and δ^2H ranged from approximately -14 to -9 ‰ and from -98 to -68 ‰, respectively (Figure 7). There were small variations between sampling events for values of $\delta^{18}O$ and δ^2H, suggesting a moderately uniform hydrological setting, which is consistent with the stability of the geochemical profiles over the course of this study. Values of $\delta^{18}O$ and δ^2H were slightly enriched in the near surface tailings pore water and became more negative with depth at piezometer nest locations LL01, LL03, and LL07. At piezometer nest location LL06, values of $\delta^{18}O$ and δ^2H showed the smallest change with depth and were consistent throughout the profile. The evaporation of water causes enrichment in values of $\delta^{18}O$ and δ^2H, while the oxidation of pyrite can also affect both $\delta^{18}O$ and δ^2H values, producing depleted $\delta^{18}O$ values (Spangenberg et al., 2007). Pore water that shows enriched isotope ratios occurred in the near surface tailings pore water, suggesting greater evaporation and water-rock interactions.

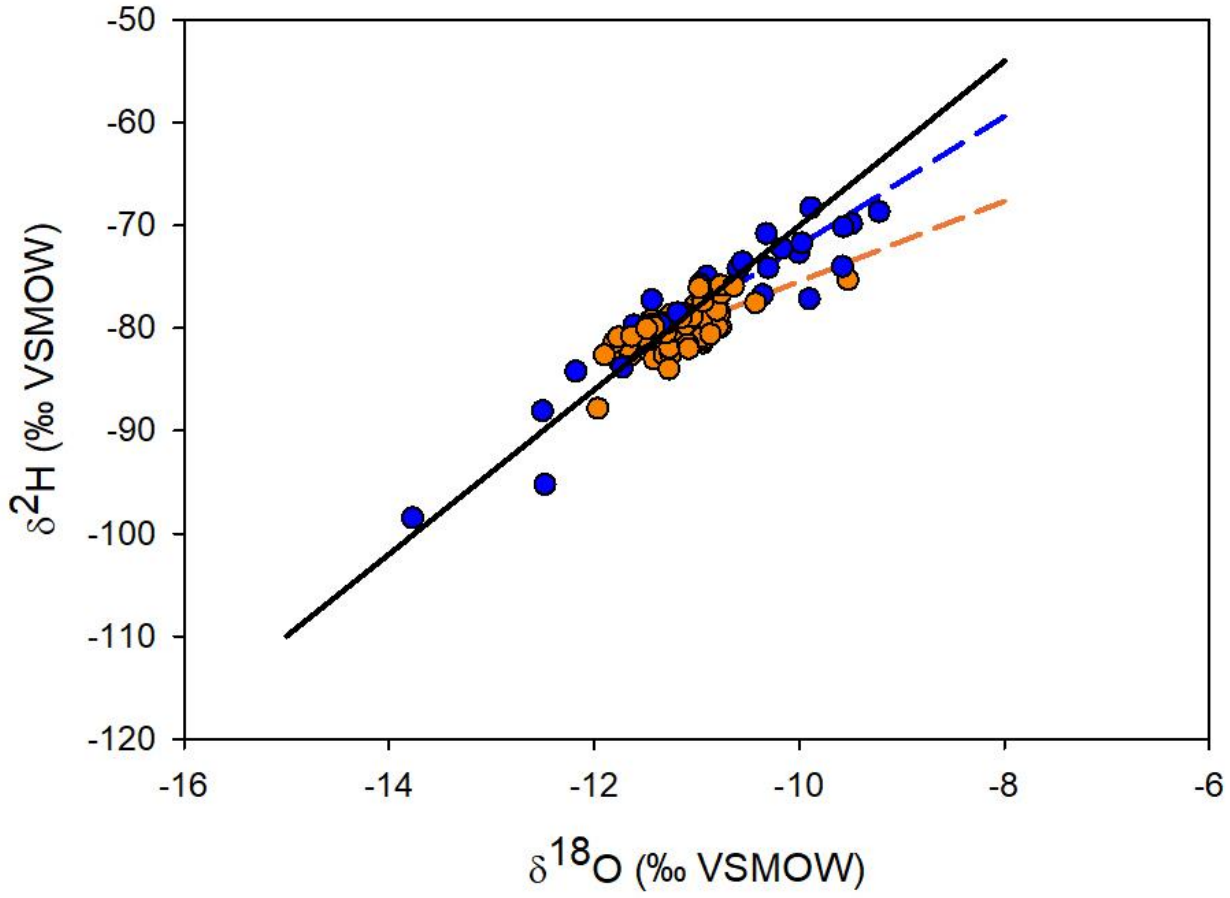

Figure 7: Plot of $\delta^{18}O$ versus $\delta^{2}H$ values measured from 2016 to 2019 from LL01, LL03, LL06, and LL07. Blue symbols represent tailings pore water while orange symbols represent groundwater. The solid black line represents the Global Meteoric Water Line (Craig, 1961). The medium-dashed blue line represents a linear regression for all tailings pore water samples and the short-dashed orange line represents a linear regression for all groundwater samples.

3.2 Lithology and mineralogy

Stratigraphy was similar at all four piezometer nests, consisting of a thin sand layer, followed by the tailings layer containing oxidized and unoxidized tailings, underlain by a layer of organic/peat followed by the native soil consisting of clay and clayey silt. The thickness of the tailings was greatest at LL01 at 2.5 m, while the thickness of the tailings at the other three sites fell in the range of 1.0 to 1.4 m (Figure 8). Core samples extracted from each piezometer nest showed little variation between the oxidized and unoxidized layers for the four sites. The sand cap was easily identifiable by the bright white colour of the sand. The core samples extracted

from beneath the sand cap showed a light grey colour throughout the oxidized zones, ranging from 0.41 to 0.57 m depending on location. The unoxidized layers were observed to be dark grey in colour. Visible Fe stains were observed at each location near the surface of the tailings and within the layer of sand, varying in colour from a rusty-red/orange to light yellow.

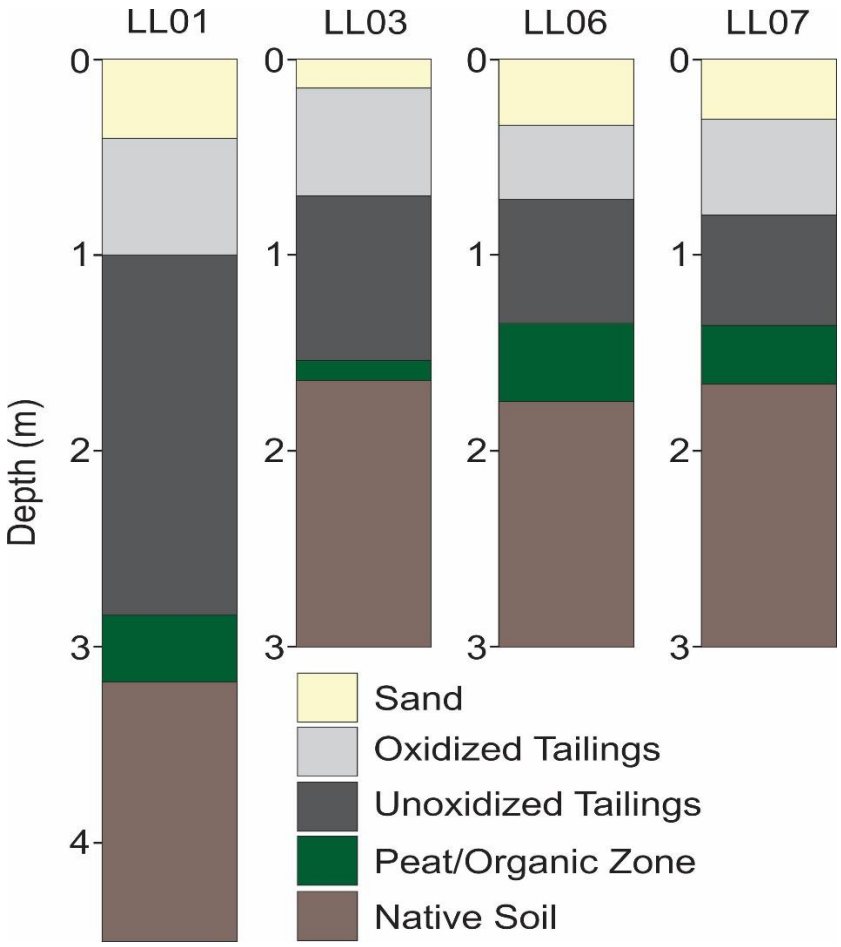

Figure 8: Stratigraphy of core samples taken at each piezometer nest location.

X-ray diffraction (XRD) performed on tailings and native soil samples indicated that the tailings consist primarily of quartz, albite and pyrite, with minor amounts of muscovite and orthoclase detected (Appendix D). XRD analysis performed previously indicate tailings samples from TA-01 primarily includes quartz, albite, pyrite and arsenopyrite (CH2M Hill, 2014). Results from using XRD Rietveld quantitative analysis indicate that albite is the most abundant

mineral at 54 %, followed by quartz at 27 %, with pyrite and arsenopyrite at 10 and 3.7 %, respectively (CH2M Hill, 2014). The results indicate that pyrite and arsenopyrite contents are high, which is consistent with the high As concentrations found within the tailings TA-01. Optical microscopy confirmed the presence of pyrite and arsenopyrite within the tailings samples. The occurrence of ferric oxyhydroxides has been observed in the shallow tailings (Figure 9, 10). Sulfide oxidation has depleted sulfide minerals in the near surface tailings below the sand layer (Figure 9, 11). The carbonate mineral content has also been depleted in the shallow tailings (Figure 11), indicating a decrease in the acid-neutralization capacity, and potential for ongoing generation of acidic drainage.

Optical microscopic study indicates that principal sulfides were pyrite and arsenopyrite with pyrite being the predominant sulfide mineral. Samples examined from LL07 under reflected light from 0.28 m below the ground surface contained trace sulfide grains ranging in size from 50 to 100 μm. Some of the sulfide grains indicated weathering or the formation of secondary phases (Figure 9). At a depth of > 0.75 m below ground surface the sulfide content increases considerably (Figure 11), with little to no alteration rims (Figure 9). The absence of alteration rims on some of the sulfide minerals can be attributed to the low pH values occurring within the oxidized portion of the tailings. The decline in oxidation intensity corresponds to the highest water table position, measured during November, as well as the depth to which measurable pore gas $O_{2(g)}$ was detected (Figure 12). Although samples obtained from the peat and aquifer materials underlying the tailings contain a lower abundance of sulfide grains than the tailings several small sulfide grains, possibly secondary sulfide minerals were observed.

Reflected light microscopy showed similar observations at LL06. Samples collected at a depth of 0.35 m contained trace sulfide grains ranging in size up to > 50 μm. The sulfides are

highly oxidized in the upper 0.44 m of tailings and becoming less oxidized to a depth of approximately 0.76 m. The lower limit of oxidation at LL06 is consistent with the $O_{2(g)}$ profile and the depth of the water table (~ 0.40 m below the ground surface), with limited oxidation below this depth. Samples observed at depths of 0.76, 1.00, and 1.21 m to the maximum depth of the tailings (1.62 m) contained abundant sulfide grains with some grains containing alteration rims and others showing no alteration. At depths of 1.62 and 1.89 m a trace amount of sulfide grains was observed.

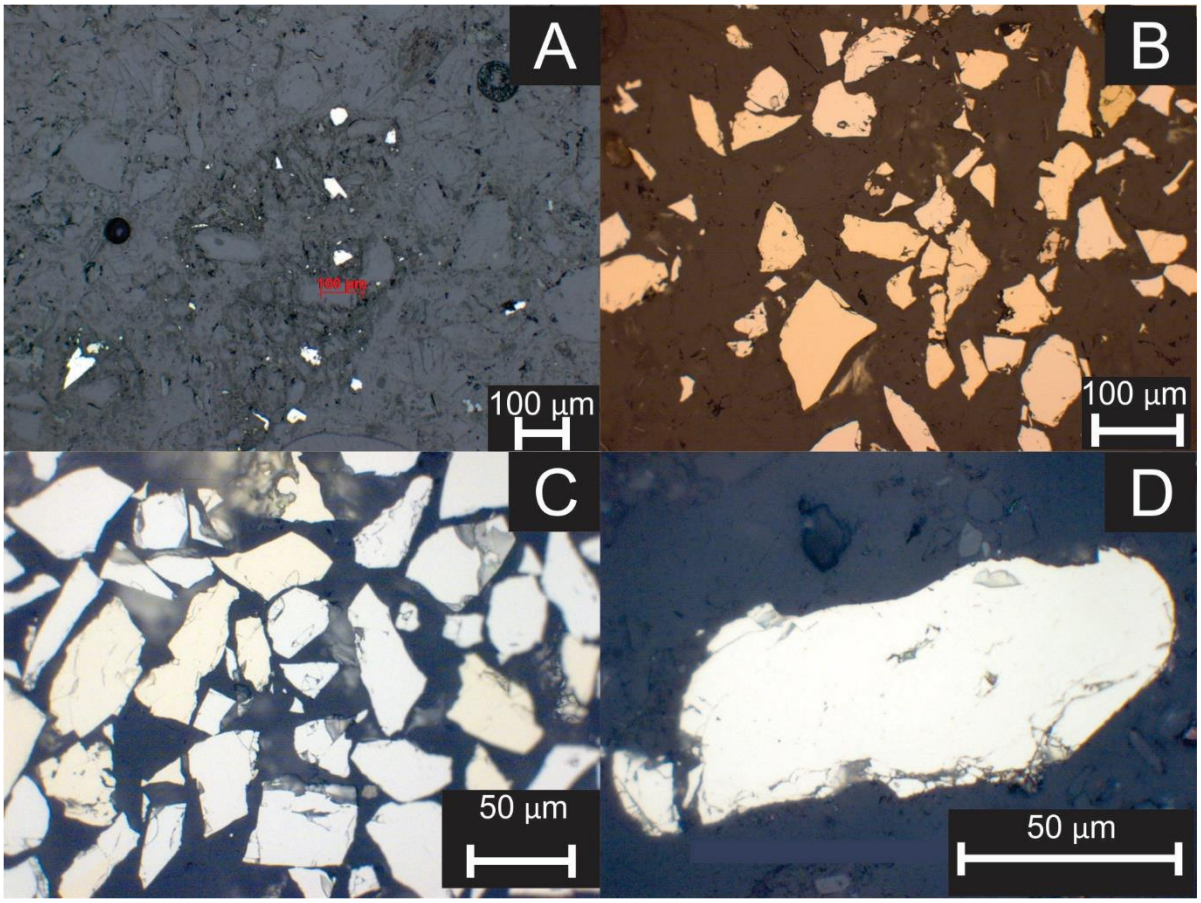

Figure 9: Optical photomicrographs of tailings thin sections from LL07 in reflected light (A) 0.28 m depth showing a few small sulfide grains 50 to 100 µm in size, (B) 0.75 m depth showing several unaltered sulfide grains, (C) 1.13 m depth containing many sulfide grains in close proximity, (D) 1.86 m depth showing one large sulfide grain approximately 100 µm in size.

Several grains from various depths at LL06 and LL07 were examined by SEM-EDS to determine their compositions and to identify potential grains for synchrotron studies. Occurrence of scorodite was common at LL07 in the shallow tailings (Figure 10). An iron-arsenic-sulfide solid phase was observed below the tailings at a depth of 1.54 m (Figure 10). Examination of other grains revealed traces of Ni, Mg, Al, and other metals within the secondary sulfide phases.

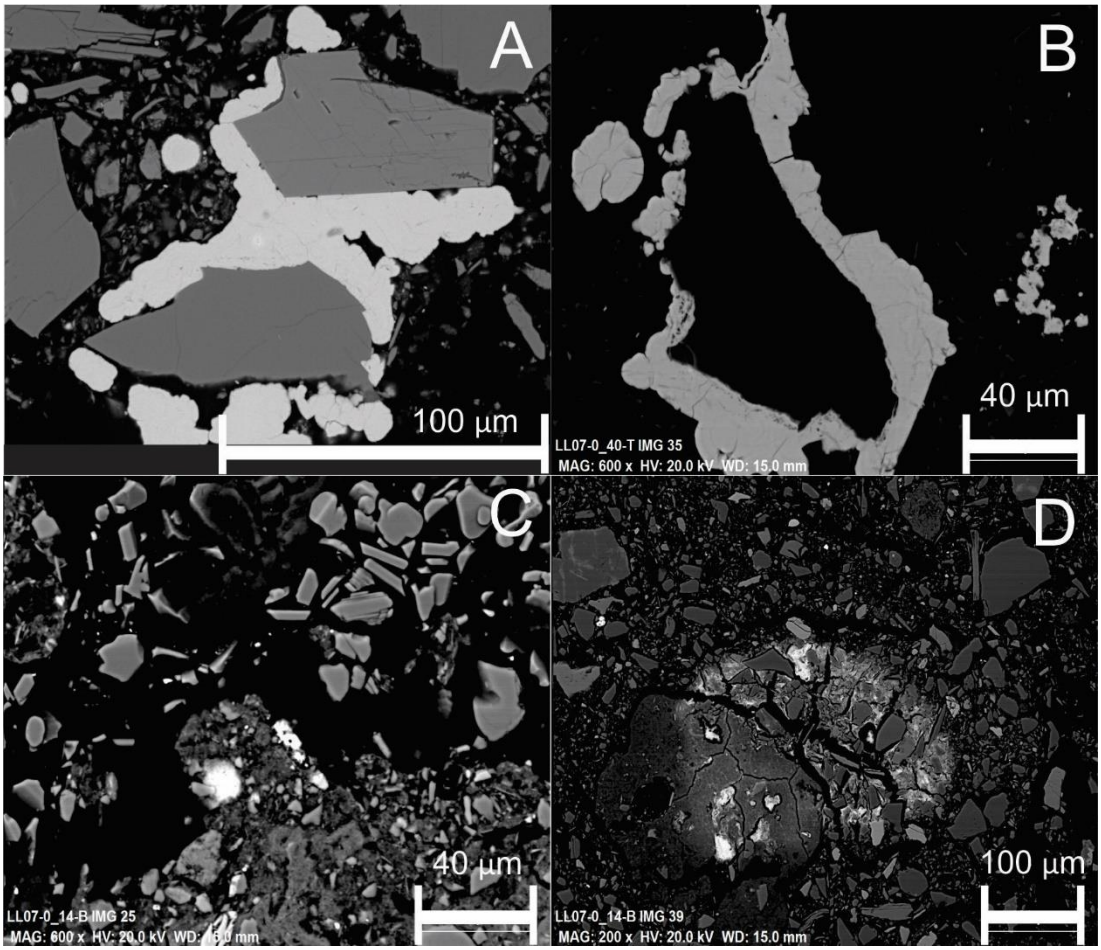

Figure 10: Scanning electron microscope pictures from location LL07 of (A) scorodite precipitation occurring at a depth of 0.28 m, (B) scorodite precipitation occurring at a depth of 0.50 m, (C) an iron-arsenic-sulfide solid phase at a depth of 1.54 m, (D) secondary As sulfide precipitation at a depth of 1.54 m.

Total S and C concentrations were measured from all nest locations throughout the sand cap, tailings layer and underlying aquifer materials. Concentration profiles from each location showed different depth-dependent trends (Figure 11). The average S content was determined to

be 3 wt. % at locations LL01, LL03 and LL06, while at LL07 the average S content was 8 wt. %. At LL01, LL06, and LL07 there is very low S in the sand layer, and the samples directly below the sand are depleted in S relative to the deeper samples within the tailings. The S content at LL03 in the sand layer and near surface tailings is higher compared to the other locations. The pattern at LL01 is intermediate between LL07 and LL03. At LL01 there is very low S content to a depth of 0.46 m, followed by an increase to approximately 2 to 6 wt. % in the deeper samples. The pattern at LL01 is consistent with the $O_{2(g)}$ measurements which indicate depletion at a depth of approximately 0.50 m. The S content in the natural materials are much lower than in the tailings averaging 0.3 wt. %.

The total C content was low at each location, averaging 0.36 wt. % for the tailings (Figure 11). The C content in the tailings at the time of deposition is present as carbonate minerals such as calcite and dolomite. Based on the C content within the tailings there has been extensive depletion of the carbonate minerals in all but the deepest tailings. This pattern of C content is consistent with the pH measurements observed at each piezometer nest. The highest C content was observed directly beneath the tailings layer at each of the sampling locations. The total C content directly beneath the tailings ranged between 3.5 to 24.8 wt. %. The large increase in C content is associated with the organic materials at the base of the impoundment. Total C decreases to low concentrations in the native soil. Although the TA-01 tailings are not vegetated there was decaying organic matter observed on the tailings surface that may contribute to the carbon content, but there was no decaying organic matter close to any of the sampling locations.

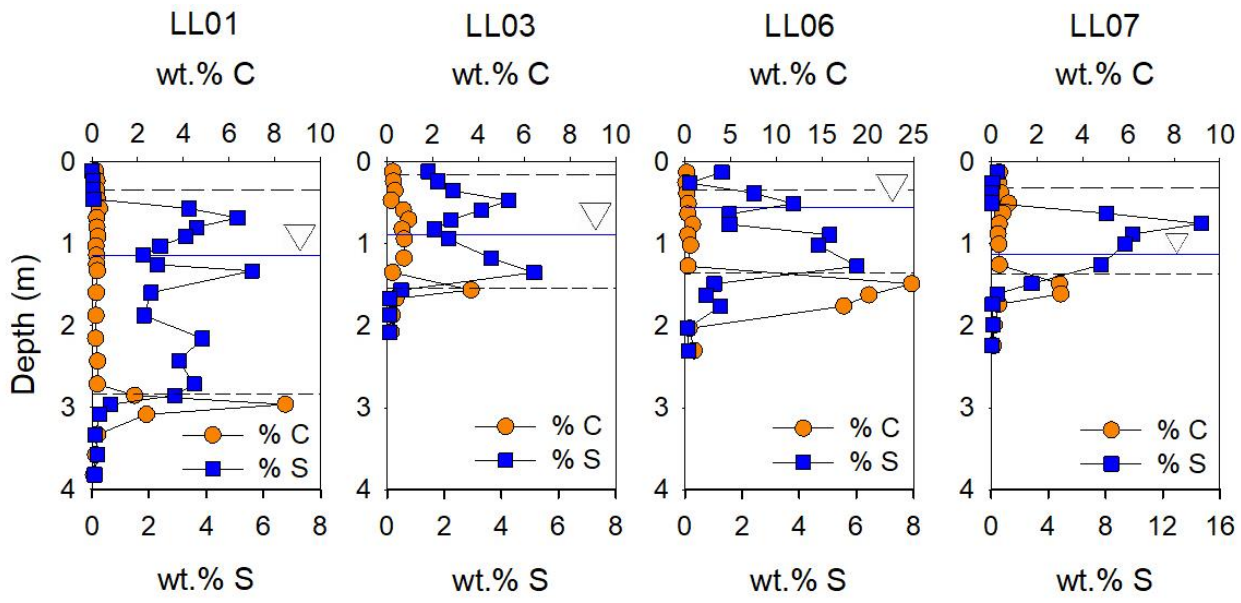

Figure 11: Depth profiles of weight percent of total sulfur (S) and carbon (C). The medium and short-dashed lines represent the depth of the sand layer and tailings, respectively. The solid blue line represents the water table at each location.

3.3 Pore gas

Pore-gas $O_{2(g)}$ concentrations show a downward decrease from atmospheric concentrations of 20.9 vol. % to less than 1.0 vol. % at depths of 0.3-0.7 m below ground surface (Figure 12). An increase in the total S content correspond with the decrease of pore-gas $O_{2(g)}$ at each of the nest locations. The increase in total S content and decrease in pore-gas $O_{2(g)}$ is a result of the consumption of $O_{2(g)}$ that is occurring from the oxidation of pyrite and arsenopyrite. The pattern of S content is consistent with depth profiles which show greater $O_{2(g)}$ penetration at LL07 than at LL03 (Figure 12), leading to more extensive depletion of the sulfide content in the shallow tailings at LL07 compared to LL03. Pore gas concentrations of CO_2 were undetectable or measured at very low concentrations (0.1-0.6 vol. %).

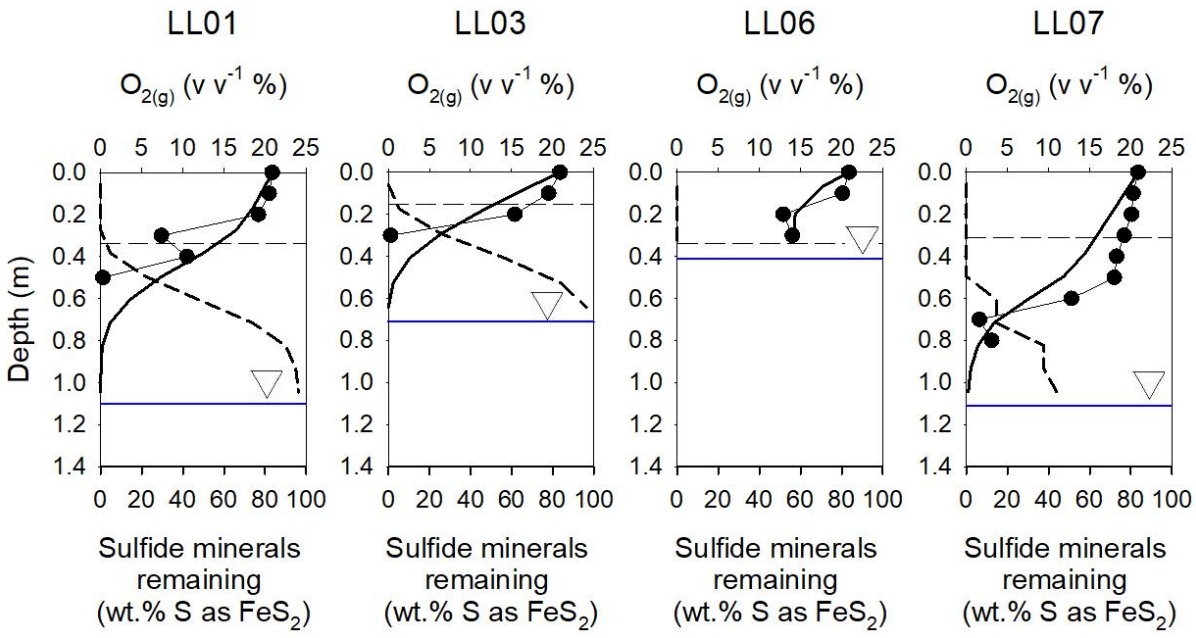

Figure 12: Depth profiles showing measured concentrations of $O_{2(g)}$ (circle), modelled concentrations of $O_{2(g)}$ (solid line), and the modelled percent of remaining sulfide minerals (dashed line). The horizonal dashed lines represents the depth of sand, while the solid blue lines represent the water table. The measurements were taken in 2018 and the model simulated sulfide oxidation from 1939 to 2019.

An oxygen-diffusion model (PYROX) for non-homogeneous media which simulates $O_{2(g)}$ transport by diffusion through the tailings pore spaces with a shrinking-core model was applied to simulate sulfide oxidation versus depth (Wunderly et al., 1996). Parameters used for the PYROX simulations for locations LL01, LL03, LL06, and LL07 including the grain radius, depth of the unsaturated zone, diffusion coefficient for the oxidized coating (D_2), porosity, bulk density, and the fraction that consists of sulfides were selected on the basis of the field observations (Table 2). The depth of the unsaturated zone used was the depth from the surface to the depth of the average water table level. The sulfide fraction was determined from the mean of the measured S content in the unoxidized section of the tailings. Grain size analyses were used to estimate the grain radius of the sulfide minerals. The bulk density and porosity measurements were determined from the average values for each location. The D_2 values were varied while keeping the other parameters constant until a best fit profile was determined with respect to the

measured $O_{2(g)}$ concentrations. The PYROX model calculates $O_{2(g)}$ concentrations and the fraction of reacted sulfide minerals with depth through the unsaturated zone. The time step used in the simulation was 0.01 years, while nodes were distributed evenly throughout the unsaturated zone at 0.1 m intervals.

Table 2: Input parameters used by PYROX to simulate sulfide oxidation reactions.

Location	Particle Size (mm)	Fraction S	D_2 (m^2 s^{-1})	Approximate time to complete oxidation (years)
LL01	0.0215	0.32	1.93×10^{-14}	157
LL03	0.0225	0.32	1.98×10^{-14}	101
LL06	0.0145	0.33	9.99×10^{-14}	< 10
LL07	0.0370	0.88	2.11×10^{-13}	157

Oxygen enters the tailings pore space from the tailings surface downwards toward the water table and therefore the diffusion of $O_{2(g)}$ is assumed to be a one-dimensional process (Wunderly et al., 1996). The concentration of $O_{2(g)}$ at the ground surface is constant, resulting in the surface of the tailings being a first-type boundary condition. The concentration gradient at the water table can be assumed to be zero; the water table is a second-type boundary condition. Oxidation reactions decrease during winter months when the tailings are covered in snow. Historic data from a meteorological station 21 km northeast of the site indicates that the mean temperature is above 0 °C for 5 months of the year (CH2M Hill, 2014). Therefore, sulfide oxidation was assumed to occur for 5 months of each year. Sulfide oxidation was assumed to begin when the deposition of tailings ended in 1939.

The calculated $O_{2(g)}$ profiles and the calculated fractions of sulfide minerals remaining for locations LL01, LL03, LL06, and LL07 are in good agreement with the field measurements

(Figure 12). The calculated fraction of sulfide minerals remaining are also in good agreement with observations made by optical microscopy of samples from LL06 and LL07. At LL07 the abundance of sulfide minerals observed by optical microscopy increases considerably at a depth of 0.75 m. This depth of 0.75 m corresponds well to the measured and modelled $O_{2(g)}$ concentrations at LL07.

At LL06, due to the shallow water table sulfide oxidation has consumed almost all the sulfide minerals available for oxidation in the unsaturated zone. A trace amount of sulfide minerals was observed in the shallow tailings at LL06 by reflected light microscopy (Appendix D). At a depth of 0.76 m few sulfide minerals were observed, indicating that sulfide oxidation has consumed the sulfide minerals to approximately this depth. The maximum depth of the water table at LL06 is approximately 0.80 m during the driest period of the year. The S content increases to > 5 % at 0.89 m.

The depth of the water table fluctuates by approximately 0.5 m throughout the year; Figure 12 shows the annual average depth. This variability exposes additional sulfide minerals to oxidation during dry periods. Similar $O_{2(g)}$ concentrations and sulfide mineral content profiles were observed for locations LL01 and LL03. At both locations the modelled $O_{2(g)}$ profiles penetrate slightly deeper than the measured $O_{2(g)}$ values. However, the depth profiles are in good agreement with the total sulfur values, which represent the depth to which sulfide-mineral depletion has occurred. Based on the observations of $O_{2(g)}$ concentrations, the sulfide content, and the water-table position measurements, the model results indicate that sulfide oxidation will continue to occur for many decades at locations LL01, LL03, and LL07, whereas sulfide oxidation is almost complete at LL06.

3.4 Solid-phase geochemistry

Samples were selected from various depths within the tailings and native soil at LL01 for ICP-OES/MS analysis after a modified aqua digestion to identify depth dependent trends in major and trace elements (Figure 13). Concentrations of Al were lower in the tailings (< 10,000 ppm), than in the underlying natural materials (24,000 ppm). Other elements that followed this trend include Cr, Mg and Ca. Elevated Fe concentrations were measured in the shallow tailings at 51,000 ppm and 45,000 ppm at depths of 0.57 m and 0.91 m, respectively. The concentration of Fe then decreases to 24,000 ppm at a depth of 1.88 m before increasing to a maximum of 68,000 ppm at a depth of 2.85 m, at the tailings and organic interface. In the native soil Fe concentrations are approximately 20,000 ppm. Arsenic concentrations were high at all depths throughout the profile. The highest concentrations of As occurred in the shallow tailings at > 40,000 ppm. Arsenic concentrations decreased with increasing depth through the tailings to approximately 20,000 ppm at the base of the tailings. Within the native soil As concentrations were measured to be approximately 1,000 ppm. Similar trends were observed for Cu, Ni, S and Au. The highest concentrations of Au, Cu, and Ni occur in the shallow tailings with concentrations decreasing with depth (Figure 13). Concentrations of Mg and Ca tend to increase from the oxidized to unoxidized portion of the tailings. The concentrations of Mg and Ca are consistent with the C content indicating that the carbonate minerals have been depleted in the oxidized tailings and some carbonate minerals are still present in the unoxidized tailings. The trends of the As, Fe, S, Ni, and Cu depth profiles suggest that these elements are tied primarily to sulfide minerals. At a depth of 0.57 m there is 1.1 mole per 1000 grams of S, 0.58 mole per 1000 grams of As, and 0.92 mole per 1000 grams of Fe. At a depth of 1.88 m there is 0.50 mole per 1000 grams of S, 0.18 mole per 1000 grams of As, and 0.43 mole per 1000 grams of Fe. These values indicate that there is not sufficient S content to account for all of the Fe and As at these depths for these

elements to occur only as sulfide minerals. This observation is consistent with the abundance of scorodite present in the shallow tailings. The concentrations of As, Fe, Cu, and Ni are well correlated except at the bottom of the profile where secondary precipitation is occurring.

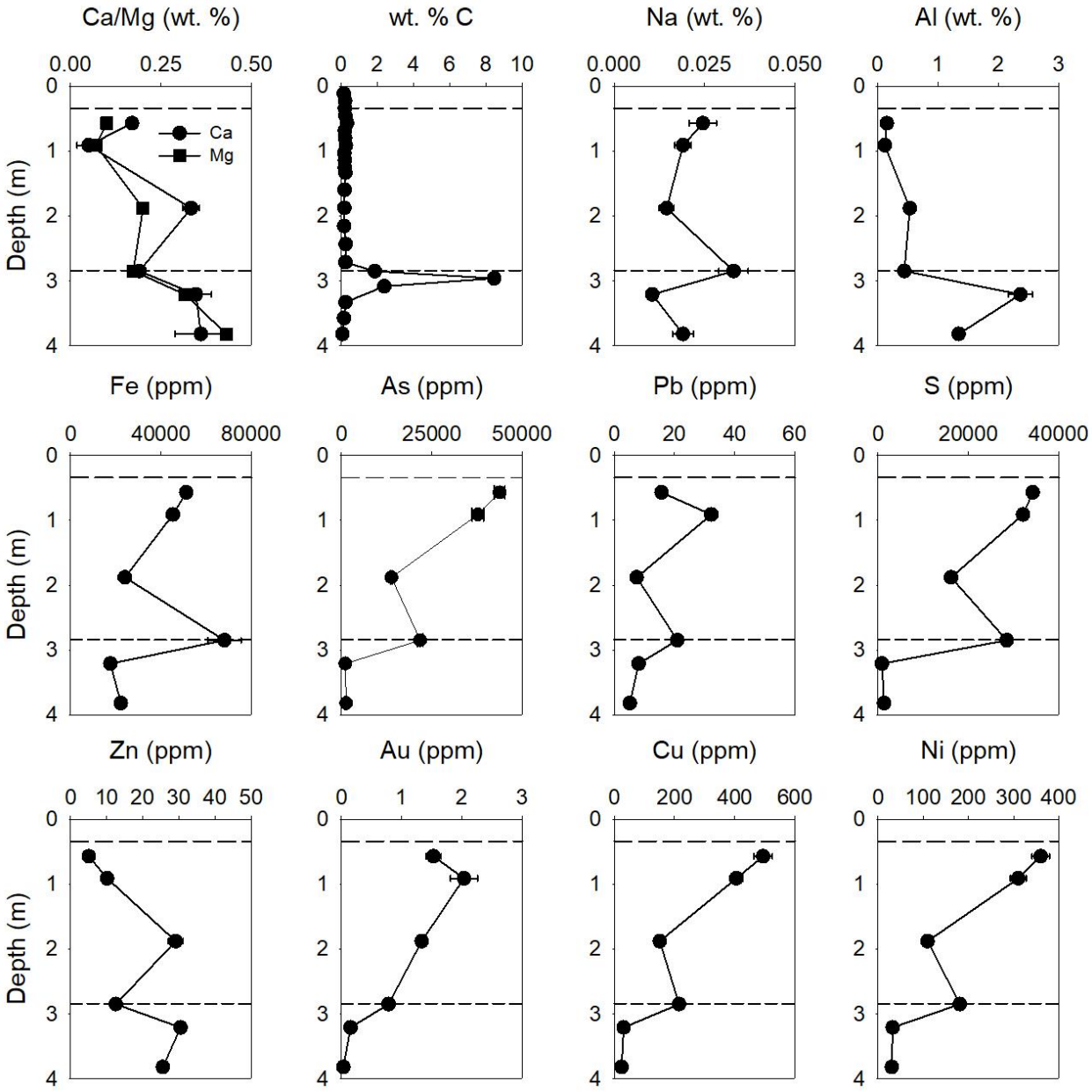

Figure 13: Depth profile through LL01 tailings showing solid-phase concentrations of major and trace elements. The medium and short-dashed lines represent the depth of the sand layer and tailings, respectively.

3.5 Pore-water geochemistry

The oxidation of sulfide minerals within the unsaturated zone of the tailings resulted in generation of low pH conditions (pH 2.0-3.9) and elevated concentrations of dissolved SO_4 (up to 5,427 mg L^{-1}), As (up to 406 mg L^{-1}), Fe (up to 1,827 mg L^{-1}) and other dissolved metals (Figures 14 to 17). The pH values of < 4 in the near surface tailings indicate the depletion of carbonate minerals. The measured Eh values were lowest directly beneath the tailings and in the underlying sediments, with the Eh decreasing with increasing depth at all the sampling locations. The lowest measured Eh values (0 mV) indicate reduced conditions. There was no detectable alkalinity measured at any of the locations in the vadose zone. The highest concentrations of dissolved metals were generally observed near the tailings surface, but elevated concentrations were observed throughout the profile of the tailings. These observations indicate that dissolved metals, released by sulfide-mineral oxidation, have migrated down through the tailings into the underlying native soils. These results are consistent with the estimated vertical hydraulic conductivity indicating that tailings pore water has migrated down past the depth of the tailings at each nest location. In contrast, the highest concentrations of dissolved Mn at LL01 occur in the natural materials below the tailings, suggesting that Mn has been released by reduction of Mn oxides in contact with the organic carbon-rich sediments.

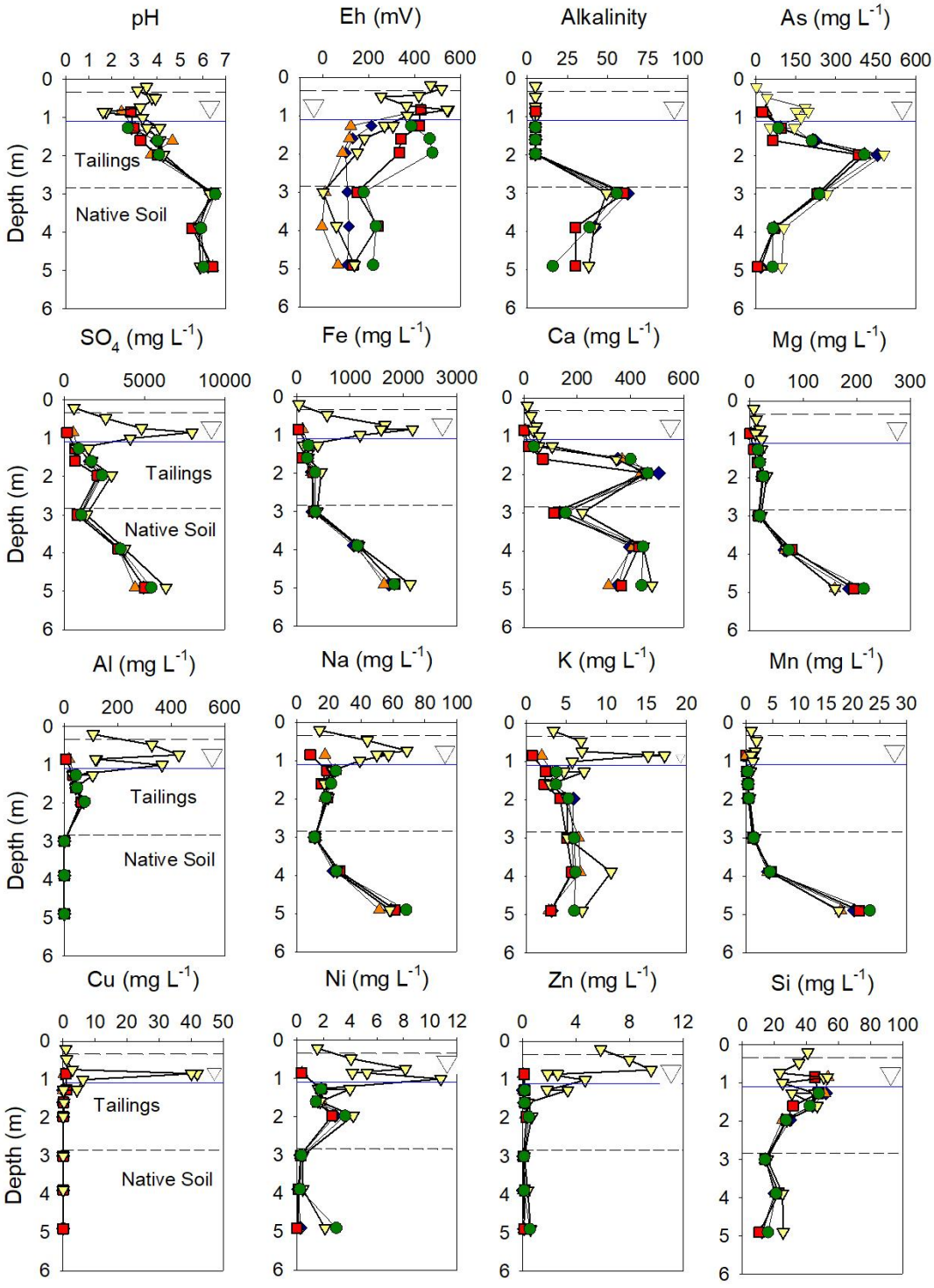

Figure 14: Depth profiles of groundwater chemistry from LL01 during various sampling episodes: December 2016 (▽), June 2017 (○), September 2017 (◊), November 2017 (△), and June 2018 (□). Solid blue line indicates the level of the water table. Medium-dashed line indicated the depth of the sand cap and the short-dashed line indicates the depth of the tailings.

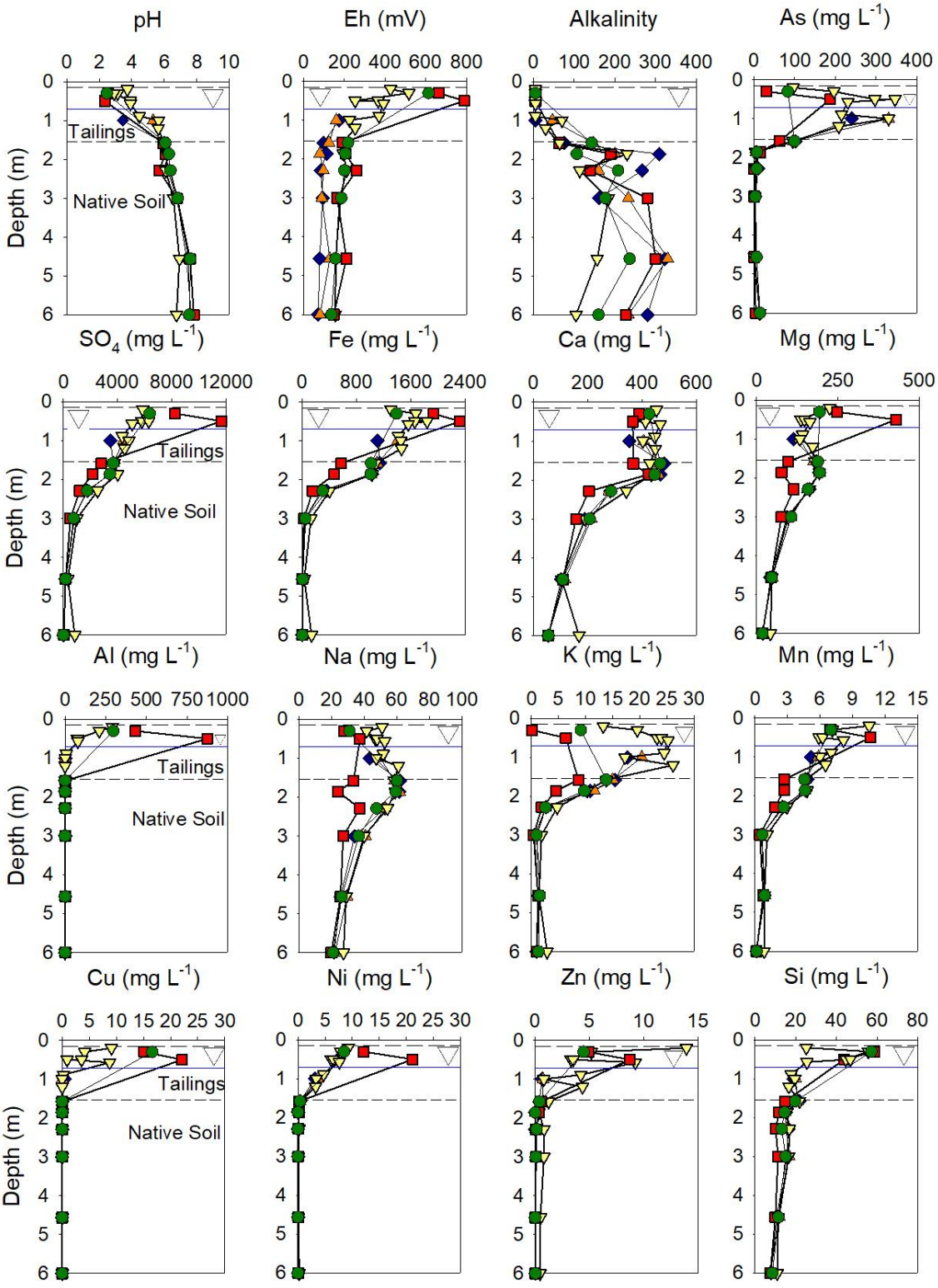

Figure 15: Depth profiles of groundwater chemistry from LL03 during various sampling episodes: December 2016 (▽), June 2017 (○), September 2017 (◊), November 2017 (△), and June 2018 (□). Solid blue line indicates the level of the water table. Medium-dashed line indicated the depth of the sand cap and the short-dashed line indicates the depth of the tailings.

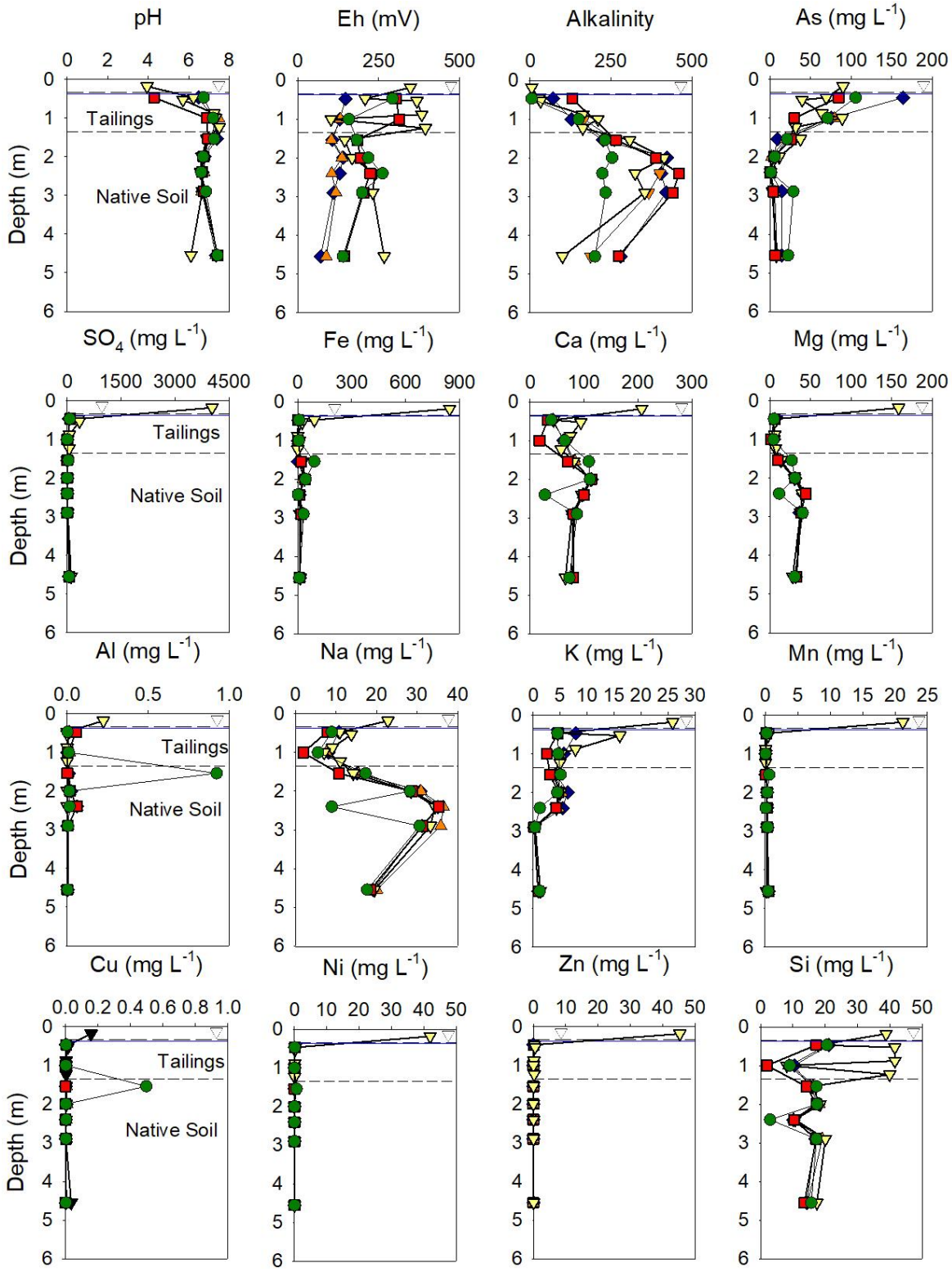

Figure 16: Depth profiles of groundwater chemistry from LL06 during various sampling episodes: December 2016 (▽), June 2017 (○), September 2017 (◊), November 2017 (△), and June 2018 (□). Solid blue line indicates the level of the water table. Medium-dashed line indicated the depth of the sand cap and the short-dashed line indicates the depth of the tailings.

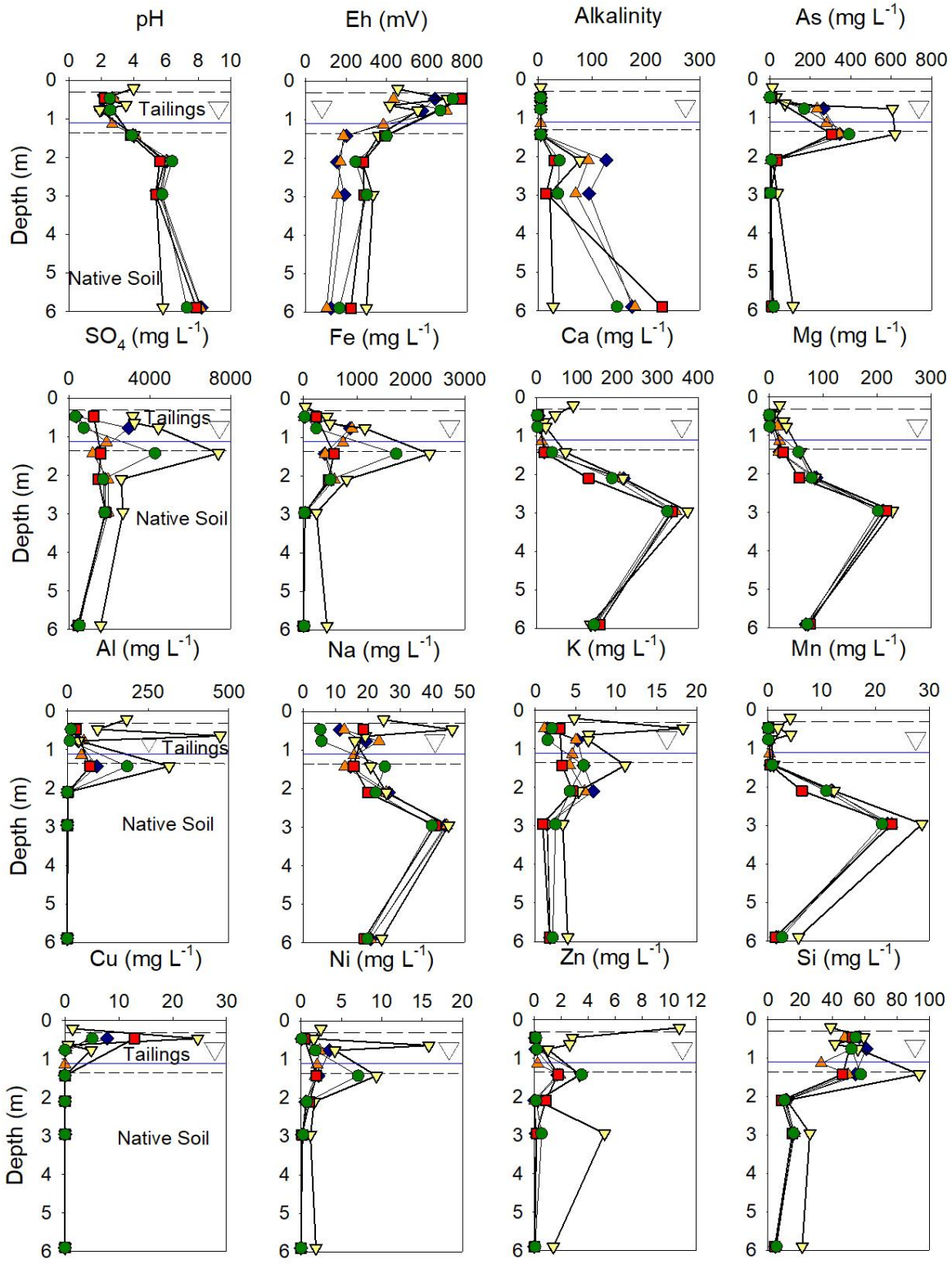

Figure 17: Depth profiles of groundwater chemistry from LL07 during various sampling episodes: December 2016 (▽), June 2017 (○), September 2017 (◊), November 2017 (△), and June 2018 (□). Solid blue line indicates the level of the water table. Medium-dashed line indicated the depth of the sand cap and the short-dashed line indicates the depth of the tailings.

Low pH values (pH 2.72-4.01) were measured at LL01 between 1.27 to 1.6 m below ground surface. The pH conditions become circumneutral with depth (Figure 14). The Eh reached over 400 mV at LL01 within the tailings, near the surface of the impoundment, where $O_{2(g)}$ is abundant in the tailings pore gas. The minimum Eh values of < 200 mV were observed beneath the tailings in the underlying natural materials. Arsenic concentrations of up to 400 mg L^{-1} were measured in the tailings pore water and 60 mg L^{-1} present in the underlying aquifer materials. The highest dissolved As concentrations were measured at shallow depths within the tailings corresponding with the lowest pH values. Depth profiles of pH and Eh values were consistent over the period of this project between 2016 and 2019 (Figures 14 to 17). Alkalinity values range between from below detection to 63 mg L^{-1} as $CaCO_3$, with the highest values measured at the base of the tailings profile. Concentrations of SO_4 were greatest (> 5,000 mg L^{-1}) at the base of the profile. High concentrations of Fe, Ni, Cu, and Zn are present in the vadose zone, at depths that correspond with the maximum SO_4 concentrations. The maximum concentration of Cu occurred at 0.85 m below the tailings surface at a depth that correspond to the depletion of $O_{2(g)}$. Up to 2,100 mg L^{-1} Fe occurred in the shallow tailings, decreasing to a minimum of 200 mg L^{-1}, then increasing to a maximum of 1,800 mg L^{-1} at 4.9 m below ground surface. Concentrations of dissolved Mn differ from other dissolved metals with low concentrations (0.34 mg L^{-1} at 1.27 m) present in the tailings and higher concentrations present in the underlying natural materials (> 23 mg L^{-1} at 4.9 m). The increases in Fe and Mn concentrations in the natural sediments beneath the tailings suggest that these metals are released by reductive dissolution of Fe and Mn oxides.

Low pH values (pH 2.47) were observed at 0.3 m below ground surface at LL03. The pH increases with increasing depth and becomes circumneutral at 1.0 m (Figure 15). The highest Eh

values (up to 600 mV) were observed within the vadose zone at 0.3 m, followed by a decrease in Eh to < 200 mV at 1.58 m depth. Alkalinity values ranges from below detection in the vadose zone of the tailings to between 47 and 330 mg L^{-1} as $CaCO_3$, with the highest concentrations present in the natural materials below the tailings. Arsenic concentrations of up to 100 mg L^{-1} occur at a depth of 1.58 m below ground surface and < 10 mg L^{-1} in the underlying materials. Arsenic concentrations increased as the Eh decreased, with the highest As concentrations associated with the lower Eh values. Similar to LL01, high concentrations of metals and SO_4 were observed at shallow depths within the tailings and near the peat/organic horizon. Concentrations of SO_4 were measured to be the greatest at a depth of 0.3 m and 1.58m at 6,300 mg L^{-1} and 3,600 mg L^{-1}, respectively. Concentrations of SO_4 decrease with depth at LL03 to < 10 mg L^{-1} at 6.0 m, the deepest sampling point. Concentrations of Fe followed the same trend as SO_4, with concentrations of 1,300 mg L^{-1} observed in the tailings and a decrease to < 300 mg L^{-1} with depth. Unlike LL01, the highest concentration of Mn (10 mg L^{-1}) occurs in the vadose zone of the tailings, at the same depth as the highest concentration of Fe. The concentration of Mn decreases with depth, to concentrations < 1 mg L^{-1}. The concentrations of other dissolved metals were highest in the vadose zone and decreased in concentration with depth.

Depth profiles of pH at LL06 show neutral pH values (pH 6.11 to 7.43) at depths of 1.0 to 4.55 m below ground surface (Figure 16). A pH value of 3.94 was measured from the squeezing samples at a depth of 0.18 m below ground surface. At LL06 a minimum Eh value was measured at a depth of 4.55 m at 71 mV with a maximum value of 314 mV at a depth of 1.0 m. Alkalinity was below detection in the vadose zone. Alkalinity concentrations range between 28 and 460 mg L^{-1} as $CaCO_3$, with the highest values measured beneath the tailings. Arsenic is weakly adsorbed under neutral pH conditions which is consistent with elevated As

concentrations of up to 164 mg L^{-1} were observed in the tailings pore water. A minimum of 0.25 mg L^{-1} of dissolved As was observed at a depth of 2.4 m below the tailings, followed by an increase in As concentration to > 20 mg L^{-1} at greater depths. The concentrations of SO_4 at LL06 differ from the other three nest locations. The greatest SO_4 concentration was observed at a depth of 0.18 m at > 4,000 mg L^{-1}. Concentrations of SO_4 decrease to 72 mg L^{-1} at a depth of 0.47 m and to approximately 1 mg L^{-1} in the groundwater. At a depth of 4.55 m the SO_4 concentration increases to 48 mg L^{-1}. Concentrations of Fe, Mg, Al and other metals follow a similar trend with the greatest concentrations occurring in the near surface tailings pore water and decrease with depth. Concentrations of Fe tend to slightly increase directly below the tailings to approximately 50 mg L^{-1}, before decreasing again with depth. One high concentration of dissolved Al was measured during the June 2017 sampling episode at 0.92 mg L^{-1} at a depth of 1.54 m. When compared to LL01, LL03 and LL07, the concentrations of SO_4, Fe, Mg, Al and other metals are notably lower at location LL06.

Acidic pH values (pH 2.52-3.88) were observed at LL07 at shallow depths within the tailings (Figure 17). The pH values then became neutral with depth with pH ranging from 5.76 to 7.29 in the native materials. The measured Eh values ranged from 400 to 700 mV in the near surface tailings at LL07 with a minimum of 104 mV measured at a depth of 2.96 m in the underlying materials. Measured alkalinity values at LL07 follow similar trends, ranging from below detection in the vadose zone to between 22 and 230 mg L^{-1} as $CaCO_3$ in the deeper tailings and the underlying natural materials. Arsenic concentrations of up to 392 mg L^{-1} were measured in the tailings pore water and 33 mg L^{-1} in the underlying aquifer materials. Sulfate concentrations were observed to be greatest at the interface between the tailings and the

peat/organic layer at > 4,000 mg L^{-1}. Concentrations of metals such as Fe, Ni and Zn are greatest directly beneath the tailings followed by a sharp decrease with depth.

The geochemical reactions occurring within the TA-01 tailings at Long Lake can be separated into different redox zones. The first is the oxic zone which occurs in the near surface tailings. The oxic zone contains low dissolved Fe concentrations, oxidized sulfide grains and is characterized by the presence of $O_{2(g)}$. The oxic zone is followed by the anoxic zone, which is characterized by the absence of $O_{2(g)}$ and smaller alteration rims or the absence of alteration rims on sulfide grains. The anoxic zone also contains higher dissolved Fe and SO_4 concentrations. Following the anoxic zone is the reducing zone which occurs near the peat layer. The reducing zone is characterized by lower concentrations of SO_4 and dissolved metals, suggesting SO_4 reduction and precipitation of insoluble sulfides.

High concentrations of dissolved As were observed at all four of the nest locations within TA-01. Pyrite, a common carrier of As and arsenopyrite, are abundant in the unoxidized tailings (Figure 9). The occurrence of As in pyrite particles has been observed in tailings samples from TA-01 (Appendix D). Oxidation of these minerals can release As, Fe, SO_4, and other elements (Nordstrom, 2002). The occurrence of oxidized pyrite and arsenopyrite in the vadose zone of the tailings impoundment indicate the source of As and Fe is the oxidation of sulfide minerals. The oxidation of arsenopyrite can be described by the following reaction:

$$(9) \qquad FeAsS + \frac{11}{4}O_2 + \frac{3}{2}H_2O \rightarrow Fe^{2+} + SO_4^{2-} + H_3AsO_3$$

Arsenate can adsorb to Fe oxyhydroxide minerals under circumneutral pH and oxidizing conditions (Dixit and Hering, 2003), or precipitate as arsenate-bearing minerals. Scorodite is observed in the near surface tailings at LL07. Under acidic conditions scorodite is the most

common secondary As mineral, commonly forming from the oxidation of arsenopyrite or As-bearing pyrite (Drahota and Filippi, 2009). The solubility of scorodite may control dissolved As concentrations in acidic environments with a pH < 3. The dissolution of scorodite at low pH is described by the following reaction:

$$(10) \quad FeAsO_4 \cdot 2H_2O + H^+ \rightarrow H_2AsO_4^- + Fe(OH)^{2+} + H_2O$$

The solubility of scorodite increases with pH and will dissolve incongruently to form Fe oxyhydroxide with adsorbed As(V) under low pH conditions (Walker et al., 2009). The theoretical Fe/As molar ratios for common arsenate minerals, such as scorodite, range between 1 and 1.5 (Paktunc et al., 2004; Corriveau et al., 2011). The ratios of Fe to As in tailings samples collected from LL01 range from 1.2 to 1.7. Samples at depths of 0.57 and 0.91 m have a Fe/As ratio of 1.2 and the sample at a depth of 1.88 m has a Fe/As ratio of 1.7. Beneath the tailings profile the Fe/As ratios increase to 3.1 at a depth of 2.85 m, with ratios of 16.9 and 17.2 at depths of 3.21 and 3.82 m, respectively. The Fe/As ratios of the tailings samples are similar to molar ratios present in scorodite or other arsenate minerals, which have been observed in tailings samples at LL07 by optical microscopy and SEM. Ferric arsenates with Fe/As molar ratios less than 4 are also significant As carriers (Paktunc et al., 2004). Therefore, continued release of As is expected to occur from the tailings.

Dissolved As concentrations decrease sharply at the bottom of the tailings profile, correlating with the organic-rich zone. At LL01 dissolved As concentrations decrease from 237.6 mg L^{-1} at 3.0 m to 65 mg L^{-1} at 3.89 m, while at LL03 As concentrations decrease from 99.7 mg L^{-1} at 1.58 m to 7.44 mg L^{-1} at 1.86 m. Similar trends are observed at LL06 and LL07. The decrease in dissolved As and Fe concentrations coupled with a decrease in SO_4 and increases in dissolved H_2S, indicates the potential for precipitation of secondary sulfide phases (Berner, 1969;

McCreadie et al., 2007; Ludwig et al., 2009). The decrease in As and Fe suggest that these elements reprecipitated with H_2S as a sulfide-bearing phase. Dissolved As is present beneath the tailings at concentrations of approximately 5 to 30 mg L^{-1}, suggesting that sulfide precipitation is not sufficient to remove all of the As from solution.

The pH of the tailings pore water increases in a series of steps, occurring at pH values of approximately 2.6, 4.0, 6.1, and 7.5. Results of geochemical modelling and field studies have shown that pH plateaus of 2.8, 4.0, 5.5, and 6.5 can be attributed to the successive dissolution of ferrihydrite, aluminium hydroxide, siderite and calcite (Dubrovsky, 1986), while similar progressions have been reported at other sulfide tailings impoundments (Blowes et al., 1990). The geochemical modelling and pore water data suggest that similar reactions may be controlling the pH of the Long Lake TA-01 tailings.

In areas where the pH ranges from approximately 3.7 to 4.6 the pore water contains higher concentrations of dissolved Al (> 100 mg L^{-1}). The dissolution of aluminosilicate minerals in the near surface tailings is likely the initial source of dissolved Al in the tailings pore water. A decrease in dissolved Al concentrations corresponds to an increase in pH values. Aluminum hydroxide can dissolve while increasing the pH and releasing Al to the pore water:

(11) $Al(OH)_3 + 3H^+ \rightarrow Al^{3+} + 3H_2O$

The dissolution of aluminosilicate minerals may also release Ca, K, Mg, Na, and Si to the tailings pore water, Ca and Mg can also be released by the dissolution of calcite and dolomite. The depletion of these elements in the oxidized portion of the tailings suggests that aluminosilicate dissolution has occurred (Appendix D). The depletion of concentrations is more apparent for solid phase concentrations of Ca and Mg. Solid phase data from whole-rock

analyses indicate that the order of abundance of metals in the unoxidized tailings is Fe > Al > Cu > Co > Ni > Mn > Cr > Zn > Pb > Cd (Appendix D). A similar order is observed in the dissolved concentrations (Figure 14).

The concentrations of dissolved Ni correspond to changes in pH. At sites LL01, LL03, and LL07, dissolved Ni concentrations decreased from > 10 mg L^{-1} to < 1 mg L^{-1} where the pH increased from pH < 4 to pH > 6. Concentrations of dissolved Ni are consistently low throughout the profile at LL06, except for at a depth of 0.18 m where the concentration reaches 40 mg L^{-1}. Whole-rock analyses indicate that the concentration of Mn increases slightly from the oxidized tailings to the unoxidized tailings. Dissolved Mn concentrations reach a maximum of approximately 20-30 mg L^{-1}. The greatest dissolved Mn concentrations generally occur where dissolved Fe and SO_4 concentrations are greatest, except at site LL07 where the greatest dissolved Mn concentration occurs approximately 1 m below maximum Fe and SO_4 concentrations. The oxidation of chalcopyrite is the most probable cause for the release of dissolved Cu to the tailings pore water. Dissolved Cu concentrations reach a maximum of 40 mg L^{-1} within the oxidized zone of the tailings. Below the base of the oxidized zone dissolved Cu concentrations decrease sharply to < 0.5 mg L^{-1}. At LL01 solid phase Zn concentrations increase slightly from the oxidized zone to the unoxidized zone of the tailings. Dissolved Zn concentrations are greatest (up to 9.5 mg L^{-1}) in the near surface tailings pore water, where the pH is < 5, followed by a decrease to < 0.5 mg L^{-1} with an increase in pH. Dissolved Zn concentrations follow the same trends at similar depths as Ni, Cu and Co.

Gold was extracted from the ore using cyanide (CN^-). Water samples were collected for measurement of total cyanide, weak acid dissociable cyanide (WAD) and thiocyanate. Samples were collected from various depths at all four nest locations within TA-01. Thiocyanate and

WAD results show only one sample each that was above the detection limit. At LL01 at a depth of 1.27 m WAD was 0.0062 mg L^{-1}, at a depth of 1.97 m thiocyanate was observed to be 0.55 mg L^{-1}. Values for total cyanide were all observed to be less than the Guideline for Canadian Drinking Water Quality of 0.2 mg L^{-1} (Appendix A). These observations indicate that cyanide included in the tailings pore water during deposition has degraded or been displaced from the tailings.

3.6 Inorganic and organic carbon

Dissolved organic carbon and dissolved inorganic carbon concentrations varied based on location throughout TA-01 but followed similar trends. The average DOC and DIC concentrations in the tailings groundwater was 3.77 mg L^{-1} and 3.94 mg L^{-1}, respectively. Dissolved organic carbon concentrations at LL01 were relatively low within the tailings (2.0 mg L^{-1}). Directly beneath the tailings in the organic layer DOC concentrations increased to 10.1 mg L^{-1} followed by a concentration of 5.7 mg L^{-1} at a depth of 4.9 m. Concentrations of DIC were low at LL01, ranging between 0.65 to 2.09 mg L^{-1}. Concentrations of DOC within the tailings at LL03 were close to 5.0 mg L^{-1}. Like LL01, directly below the tailings DOC concentrations increased to 19.6 mg L^{-1} with a maximum concentration of 54.2 mg L^{-1} at a depth of 2.29 m. At LL03 DIC concentrations were measured between 3.30 to 4.45 mg L^{-1} at depths of 1.58 to 2.29 m. Concentrations of DIC increased to 40.16 mg L^{-1} at a depth of 3.0 m and reached a maximum of 60.23 mg L^{-1} at a depth of 4.56 m. Similar pore water concentrations of DOC were observed at LL06 at between 2 to 5 mg L^{-1}. Concentrations sharply increased beneath the tailings and in the underlying aquifer materials to a maximum of 34.8 mg L^{-1}. Concentrations of DIC are highest at LL06, ranging between 9.70 to 85.6 mg L^{-1}. The highest concentrations of DIC occur beneath the tailings in the underlying aquifer materials. At LL07 DOC concentrations follow the

same trend observed at the LL01 location, with DOC reaching a maximum of 10.2 mg L^{-1} at a depth of 2.1 m, beneath the tailings. Concentrations of DIC were measured to be 4.69 and 4.27 mg L^{-1} at depths of 2.1 and 2.96 m, respectively, before increasing to 36.1 mg L^{-1} at a depth of 5.9 m. Organic carbon can originate from the peat layer at the base of the tailings impoundment and can be transported through groundwater flow.

3.7 Sulfate reduction

Dissimilatory sulfate reduction (DSR) releases sulfide and results in a decrease in dissolved SO_4 concentrations. Sulfate reducing bacteria preferentially reduce $^{32}S\text{-}SO_4$ over $^{34}S\text{-}SO_4$, resulting in enrichment of $^{34}S\text{-}SO_4$ values (Jones and Starkey, 1957). Sulfate reduction will normally produce $\delta^{34}S\text{-}SO_4$ in the range of -30 ‰ to 10 ‰ (Mayer, 2005). Values of $\delta^{34}S$ for primary sulfide minerals range from 0.2 to 2.6 ‰ (Moncur et al., 2009), while values of $\delta^{34}S$ for five tailings samples from TA-01 averaged 5.1 ‰. Values of $\delta^{34}S$ and $\delta^{18}O$ for dissolved sulfate were more positive than the primary sulfide minerals. These positive values are consistent with the fractionation that is associated with DSR (Figure 18). The $\delta^{34}S$ values in TA-01 ranged from 3.9 ‰ to 32.3 ‰, while $\delta^{18}O$ values ranged from -7.7 ‰ to 12.3 ‰. Along with values of $\delta^{34}S$ and $\delta^{18}O$ other geochemical parameters measured indicate that SO_4 reduction is occurring near the base of the tailings layer and in the organic carbon layer at the base of TA-01. The sequence of reactions (7) and (8) describes the decrease of metals and SO_4 with an increase in pH and alkalinity that accompany DSR. Dissolved organic carbon concentrations range from 1.9 to 25.8 mg L^{-1} near the organic zone. Low concentrations of H_2S were measured at all the sampling locations. The concentrations of H_2S were generally greater in underlying materials, beneath the tailings. At LL03, the concentration of H_2S increased from 0.006 mg L^{-1} at 1.58 m to 0.112 mg L^{-1} at 6.0 m. The increased in H_2S corresponds to a decrease in SO_4 concentrations from 6,366

mg L^{-1} at 1.58 m to 7.88 mg L^{-1} at 6.0 m. Similar increases in H_2S and decreases in SO_4 were observed at LL06 and LL07. The depth trends of increased pH, alkalinity, and H_2S with the decrease of As, Fe, SO_4 and other metals at LL01, LL03, LL06 and LL07 are consistent with SO_4 reduction and metal(loid)-sulfide precipitation. Elevated Fe concentrations at depth throughout the profiles suggest that there may be insufficient dissolved H_2S to precipitate all the Fe as a sulfide phase.

There is an observed correlation between the depth of ^{34}S-SO_4 enrichment with dissolved As concentrations. At LL03 As concentrations decrease at the base of the tailings profile from approximately 100 mg L^{-1} to less than 10 mg L^{-1}. Similar trends are observed at the other sampling locations throughout TA-01. The low dissolved As concentrations at the bottom of the profile suggest that As is removed at the base of the impoundment and within the peat through As-sulfide precipitation.

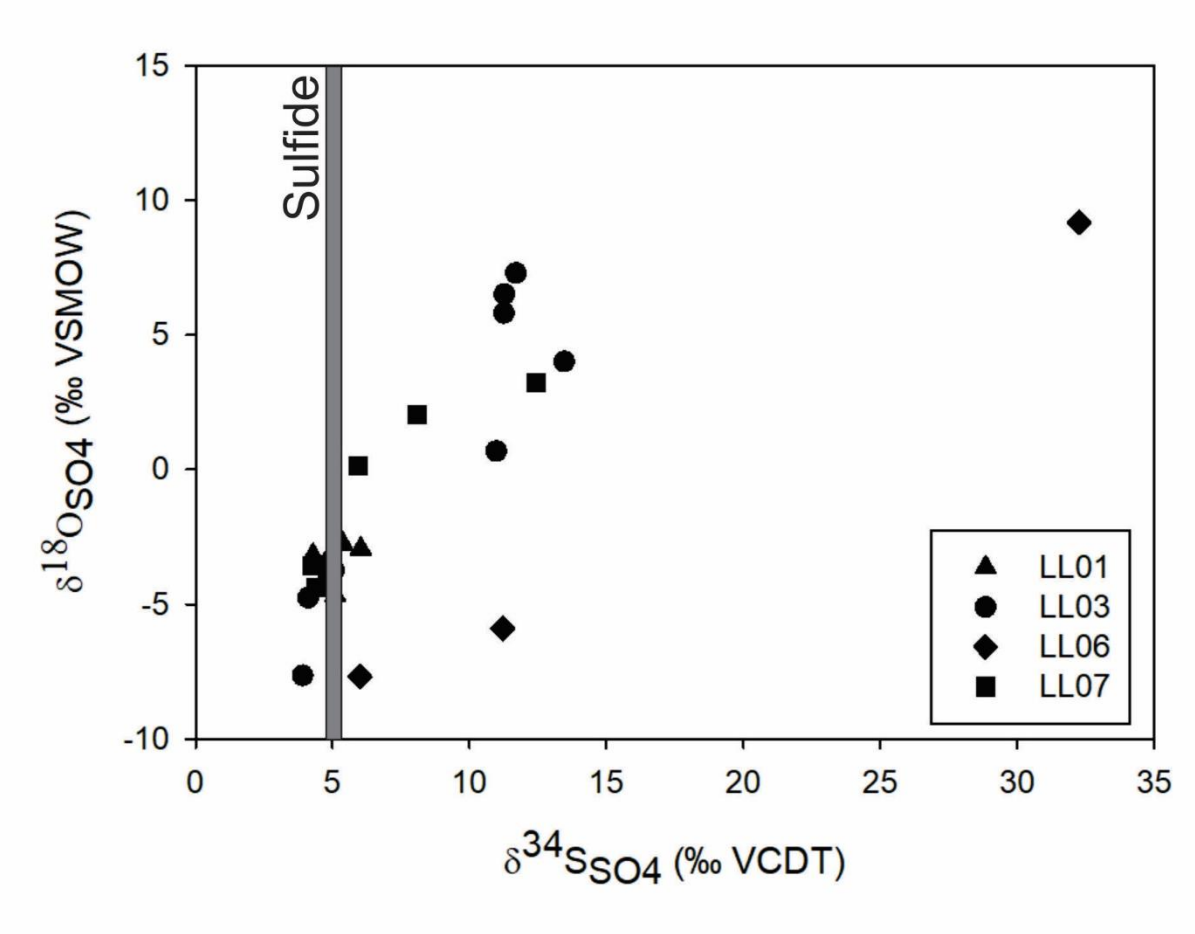

Figure 18: Plot of δ^{34}S-SO_4 versus δ^{18}O-SO_4 values of dissolved sulfate from LL01, LL03, LL06 and LL07 in TA-01. The shaded area represents the average δ^{34}S values measured from five TA-01 tailings samples. VCDT: Vienna Canyon Diablo Troilite; VSMOW: Vienna Standard Mean Ocean Water.

Although δ^{34}S and δ^{18}O values vary between the nest locations (Figure 18), there are consistent trends. The δ^{34}S-SO_4 values in the oxidation zone at the top of the tailings range from 3.9-5.1 ‰ and δ^{18}O-SO_4 range from -7.7 to -3.2 ‰. These δ^{34}S values are similar to the primary sulfide minerals present in the tailings. Values of δ^{34}S-SO_4 and δ^{18}O-SO_4 increase (to δ^{34}S-SO_4 between 11.0 and 29.1 ‰ and δ^{18}O-SO_4 between 4.0 and 9.2 ‰) at the base of the tailings and in the underlying peat beneath the tailings. These trends indicate δ^{34}S-SO_4 and δ^{18}O-SO_4 fractionation associated with sulfate reduction (Mayer, 2005).

3.8 Methanogenesis

Maximum concentrations of CH_4 were measured at the base of the tailings within the peat/organic layer, while lower concentrations of CH_4 were measured in the tailings pore water. In the shallow tailings at LL01 CH_4 concentrations were below detection limit. At a depth of 3 m directly beneath the tailings CH_4 concentrations were highest at 0.22 mg L^{-1}, followed by a decrease to < 0.1 mg L^{-1} towards the base of the profile. Methane concentrations at LL03 followed a similar trend with the highest concentration occurring at the base of the tailings at a depth of 1.58 m and a concentration of 0.17 mg L^{-1}. Concentrations of CH_4 decrease toward the base of the profile. At LL06 concentrations of CH_4 are notably higher when compared to the other locations. In the tailings pore water, the CH_4 concentration were 8.97 mg L^{-1} at a depth of 1.0 m. At the base of the tailings at 1.54 m, CH_4 concentrations were 60.01 mg L^{-1}. Methane concentrations reached a maximum of 74.58 mg L^{-1} at a depth of 2.0 m and decreased to 0.06 mg L^{-1} at 4.55 m. The concentration of CH_4 near the peat at LL07 was 1.07 mg L^{-1} at a depth of 2.1 m, with a decrease to 0.11 mg L^{-1} and 0.02 mg L^{-1} at depths of 2.96 m and 5.9 m, respectively.

Methanogenesis influences the ^{13}C signature on DIC by preferentially using lighter ^{12}C isotopes in DIC and reducing it to CH_4. The reduction to CH_4 causes remaining DIC to become enriched in ^{13}C (Chapelle et al., 1988; Murphy et al., 1989). The carbon isotope signatures on DIC from LL06 were depleted at -24.75 ‰ near the ground surface and becomes more enriched with depth (Figure 19). A maximum enriched ^{13}C value of 2.52 ‰ was observed at a depth of 2.0 m, corresponding to the highest CH_4 concentration, suggesting methanogenic conditions. Groundwater collected from LL06 indicates enriched ^{13}C values between 1.0 and 2.9 m depths. At a depth of 4.55 m the ^{13}C signature on DIC becomes depleted at -13.79 ‰, corresponding to a decrease in CH_4 concentration to 0.06 mg L^{-1}. The depletion of ^{13}C on DIC also may be due to

greater SO_4 reduction occurring at that depth. The carbon isotopic signatures on DIC from locations LL01, LL03, and LL07 were relatively depleted compared to LL06. The depletion of ^{13}C (-11.22 to -24.25 ‰) along with low CH_4 concentrations (0 to 1.07 mg L^{-1}), suggest that methanogenesis is not occurring through these profiles, or is occurring to a lesser extent than at LL06.

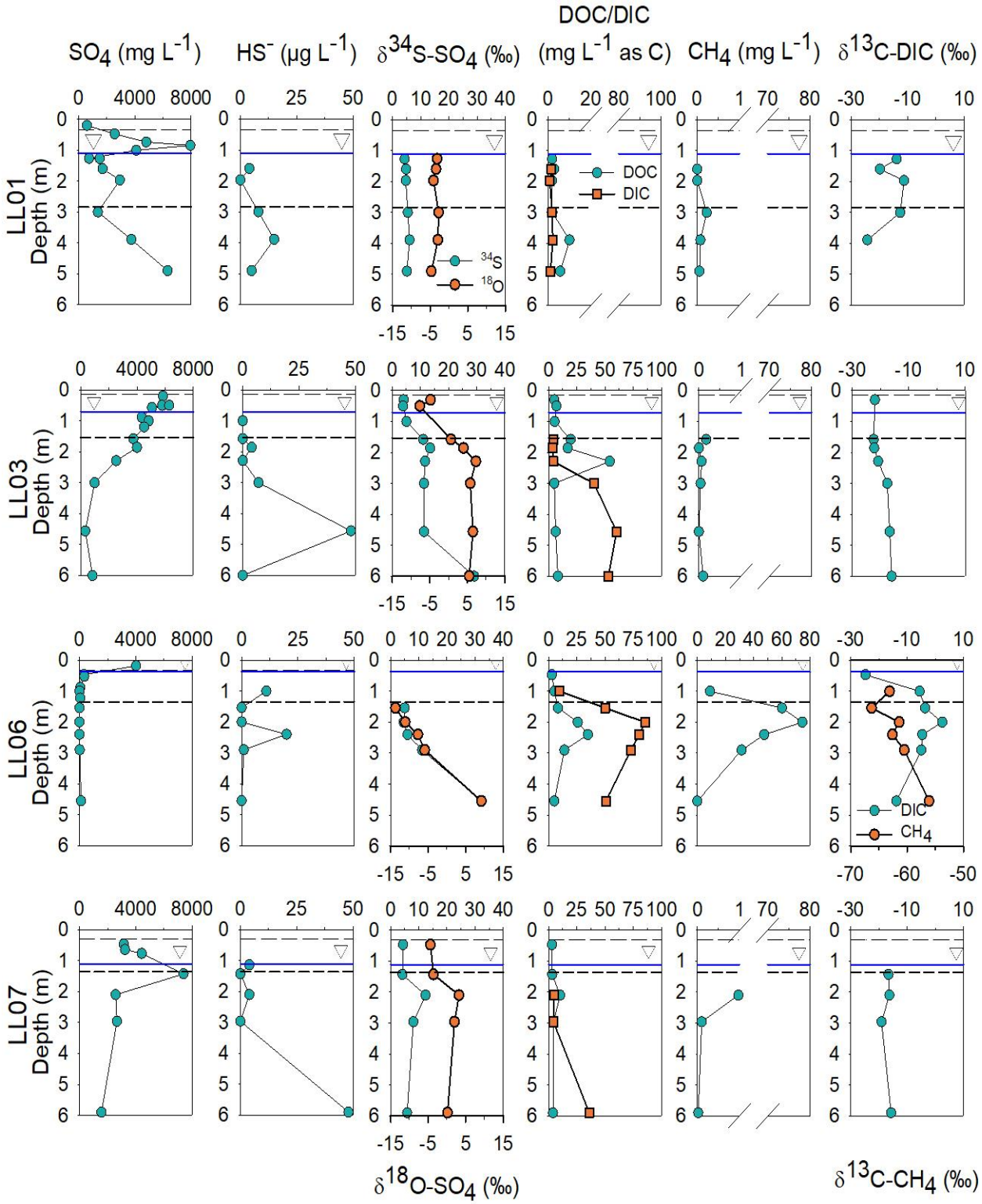

Figure 19: Depth profiles of SO_4, HS^-, $\delta^{34}S$-SO_4, $\delta^{18}O$-SO_4, DOC, DIC, CH_4, $\delta^{13}C$-DIC, and $\delta^{13}C$-CH_4. The medium and short dashed lines represent the depths of the sand and tailings layer, respectively. The solid blue line represents the water table.

Carbon isotope ratios were determined on dissolved inorganic carbon. Carbon isotope ratios on CH_4 samples were also determined on samples from LL06 due to the high concentrations of aqueous CH_4 measured at that location. Values of $\delta^{13}C_{DIC}$ were measured to identify whether SO_4 reduction is occurring throughout the tailings and native soils within TA-01. The $\delta^{13}C_{DIC}$ signature from groundwater and tailings pore water ranged from -24.75 to 2.52 ‰. Values of $\delta^{13}C$ at LL01 range from -19.78 to -11.22 ‰ in the tailings pore water, with a value of -12.59 ‰ directly beneath the tailings. There is a large depletion of $\delta^{13}C_{DIC}$ deeper in the native soil at a value of -24.25 ‰. Values of $\delta^{13}C_{DIC}$ at LL03 are more depleted near the surface of the tailings (-21.94 ‰ at 0.3 m) and become enriched with depth (-16.04 ‰ at 6.0 m). At LL06 values of $\delta^{13}C_{DIC}$ are more negative toward the tailings surface at a value of -24.75 ‰. These values become more enriched throughout the depth of the profile, reaching a maximum of 2.52 ‰ directly beneath the tailings layer within the organic/peat zone. In the underlying aquifer materials, values of $\delta^{13}C_{DIC}$ range between –4.60 to -13.79 ‰. Values of $\delta^{13}C_{DIC}$ at LL07 were determined on samples only collected from beneath the tailings and range between -19.08 and -15.66 ‰. Carbon isotope ratios determined on CH_4 samples from LL06 ranged between -66.3 to -56.1 ‰ (Figure 19). The ^{13}C-CH_4 ratio reached a minimum of -66.3 ‰ at a depth of 1.54 m and reached a maximum of -56.1 ‰ at a depth of 4.55 m.

3.9 Arsenic speciation

The redox status of the aquifer is an important control on the ratio of As(III) to As(V) in groundwater. The abundance of redox-active solids, such as organic carbon and potential oxidants are important in the speciation of arsenic in groundwater (Smedley and Kinniburgh, 2005). For As species, the lack of redox equilibrium can be attributed to systems characterized by high levels of microbial activity, since microorganisms play a key role in redox reactions.

Reduced sulfur and carbonate ligands may form aqueous complexes with As(III) and As(V). Dissolved As sulfide species can also be formed at low pH and where there are very high concentrations of reduced dissolved sulfur (Smedley and Kinniburgh, 2005). Precipitation of realgar, orpiment and other sulfide minerals that contain As are favoured under reducing conditions (Cullen and Reimer, 1989).

Two processes affect the solubility and mobility of dissolved As: adsorption/desorption and precipitation/dissolution reactions. Bacterially-mediated oxidative dissolution of sulfides and bacterially-mediated reductive dissolution of metal hydroxides are the primary mechanisms for the release of As from the mineral phases. Reductive dissolution can enhance the desorption of As oxyanions from hydroxide surfaces, resulting in As release to pore-water. (Moore et al., 1988; Saunders et al., 1997).

Iron oxyhydroxides have an important role on the mobility of As and it is therefore important to understand the impact that Fe has on As. In acidic mine waters dissolved As is removed as Fe is oxidized and precipitated, while As is scavenged through adsorption (Smedley and Kinniburgh, 2002). Arsenic oxyanions are sorbed strongly to Fe oxyhydroxide surfaces at low pH values (Dzombak and Morel, 1990; Romero et al., 2004). Arsenic can also precipitate as an arsenate such as ferric arsenate or scorodite. The surface charge of Fe oxyhydroxide becomes negative at pH values greater than 8, and adsorption of As oxyanions declines. The mobilization of As(V) and As(III) is influenced by the adsorption characteristics of both species (Mok, 1994). At low pH As(V) is strongly adsorbed by hydrous ferric oxides and desorption occurs as pH increases, while As(III) is adsorbed to a lesser extent but over a wider range of pH values (Dzombak and Morel, 1990). The highest concentrations of As(V) found in Fe oxyhydroxides are associated with the oxidized surface portion of mine tailings. Lower concentrations of As(V)

are found in acidic soils or reducing conditions (Bowell, 1994). In saturated tailings the reduction of ferric oxide phase can affect the release and transport of As from tailings below the water table (McCreadie et al., 2000).

The speciation of As in groundwater is important because the properties of As(III) and As(V) vary with pH. However, pH affects the As sorption differently between As(III) and As(V) (Bednar et al., 2005). Speciation of As showed that As is predominantly in the trivalent form throughout the four profiles (Figure 20). These observations are consistent with reports of As(III) present as the primary species in anaerobic water (Nordstrom, 2002; Smedley and Kinniburgh, 2005). These observations are also consistent with previous findings that As(III) is the dominant As species at TA-01 (CH2M Hill, 2014). Arsenic is present in arsenopyrite and other As bearing sulfides as As(-I). The oxidation of reduced As to As(III) can occur under mildly oxidizing conditions and can result in increased concentrations of As(III) and enhanced mobility in groundwater.

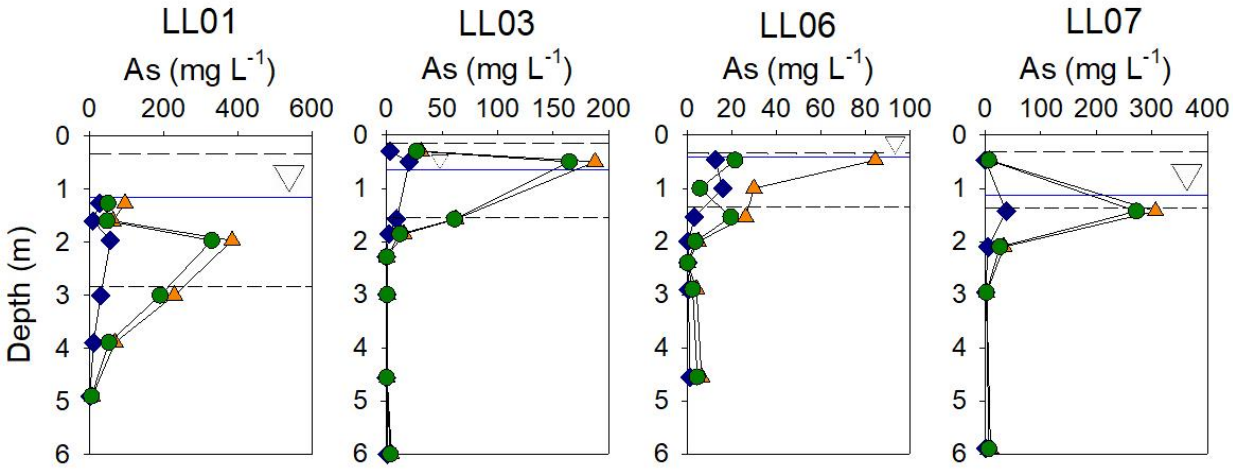

Figure 20: Depth profiles of As speciation showing As[III] (○), As[V] (◊), and As[T] (Δ) concentrations. Results are from June 2018. The medium-dashed and short-dashed lines represent the depth of the sand cap and tailings layer, respectively. The solid blue line represents the water table.

The ratio of As(III) to As(V) ranged from 0.4 to 30 at all locations sampled in June 2018. The greatest abundance of As(V) occurred near the tailings surface, where low pH conditions and high redox potentials prevail. Arsenate minerals can precipitate from solutions rich in Fe and As. The adsorption of As to iron oxyhydroxides can be a significant control on the mobility of As, however, the presence of scorodite in the tailings suggests that this is the predominant form of As immobilization in the oxidized tailings. The highest ratio of As(III) to As(V) generally occurred where the concentrations of As were highest and near the organic/peat layer directly underneath the tailings. Zones with a high organic carbon content and sulfate-reducing conditions show greater reduction of As(V) to As(III). The maximum As(III) concentrations coincide with the highest organic carbon content at the bottom of the tailings profile near the native soil, where $\delta^{34}S\text{-}SO_4$ ratios and the presence of dissolved H_2S indicate sulfate reduction. An important role of organic matter is the ability to facilitate microbial activity and create reducing conditions that affect the speciation and mobility of As (Campbell and Nordstorm, 2014).

The effect of Fe plays an important role in controlling the speciation of As in low pH waters. Soluble Fe and Mn are in their reduced forms at higher pH and can indicate an environment for predominance of As(III) due to a lower Eh (McGeehan and Naylor, 1994). Arsenate has a higher degree of sorption over As(III) to oxyhydroxides and results in As(III) dominating at a higher pH (Bednar et al., 2005). At a pH less than 3.5 and in the presence of dissolved Fe(III), As(III) will be oxidized to As(V):

(12) $H_3AsO_3 + H_2O + 2Fe^{3+} \rightarrow H_2AsO_4^- + 3H^+ + 2Fe^{2+}$

Although As(III) was the dominant species throughout the tailings, a greater abundance of As(V) was present in the shallow tailings where low pH values occurred. At LL01 at a depth of 1.27 m

the concentration of As(V) was 27.5 mg L^{-1}, or approximately 29 % of the total As. Throughout the rest of the profile As(V) accounted for 13 to 16 % of the total As. At LL03 the As(V) concentrations range from 2.9 to 20 mg L^{-1} within the tailings and 0.08 to 2.1 mg L^{-1} in the underlying materials. A similar trend is observed at LL06 where As(V) concentrations were greater in the near surface tailings, ranging from 3.2 to 15.9 mg L^{-1}. At LL07 the greatest concentration of As(V) at a depth of 1.43 m was 37.7 mg L^{-1}.

The concentration of total As was compared to the sum of As(III) and As(V). While the differences were modest at most locations, there were some locations where large differences were observed. The majority of the As speciation samples reported the sum of As(III) and As(V) concentrations to be within 20 % of the total As concentrations, with 70 out of 95 samples within that range. The samples with the largest differences had total As concentrations of 2 mg L^{-1} or less. These samples with large differences were collected at the same locations and sampling depths throughout each sampling episode, and generally occurred beneath the tailings profile in the underlying aquifer materials. High dilution factors may account for some loss in accuracy in the other samples due to the high concentrations of measured As.

3.10 Geochemical modelling

Saturation indices for potential mineral phases were calculated using the geochemical model PHREEQC 3.4.0. Saturation index values indicate the tendency for precipitation or dissolution of a phase to occur, where a SI > 0 represents supersaturated conditions, SI < 0 represents undersaturated conditions and a SI = 0 represents equilibrium conditions. Water that is supersaturated with respect to a mineral phase suggests the tendency for that mineral to precipitate while undersaturation suggests a tendency for dissolution. Saturation indices of

various mineral phases were calculated for every sampling event at each nest location (Figures 21 to 28, Appendix B).

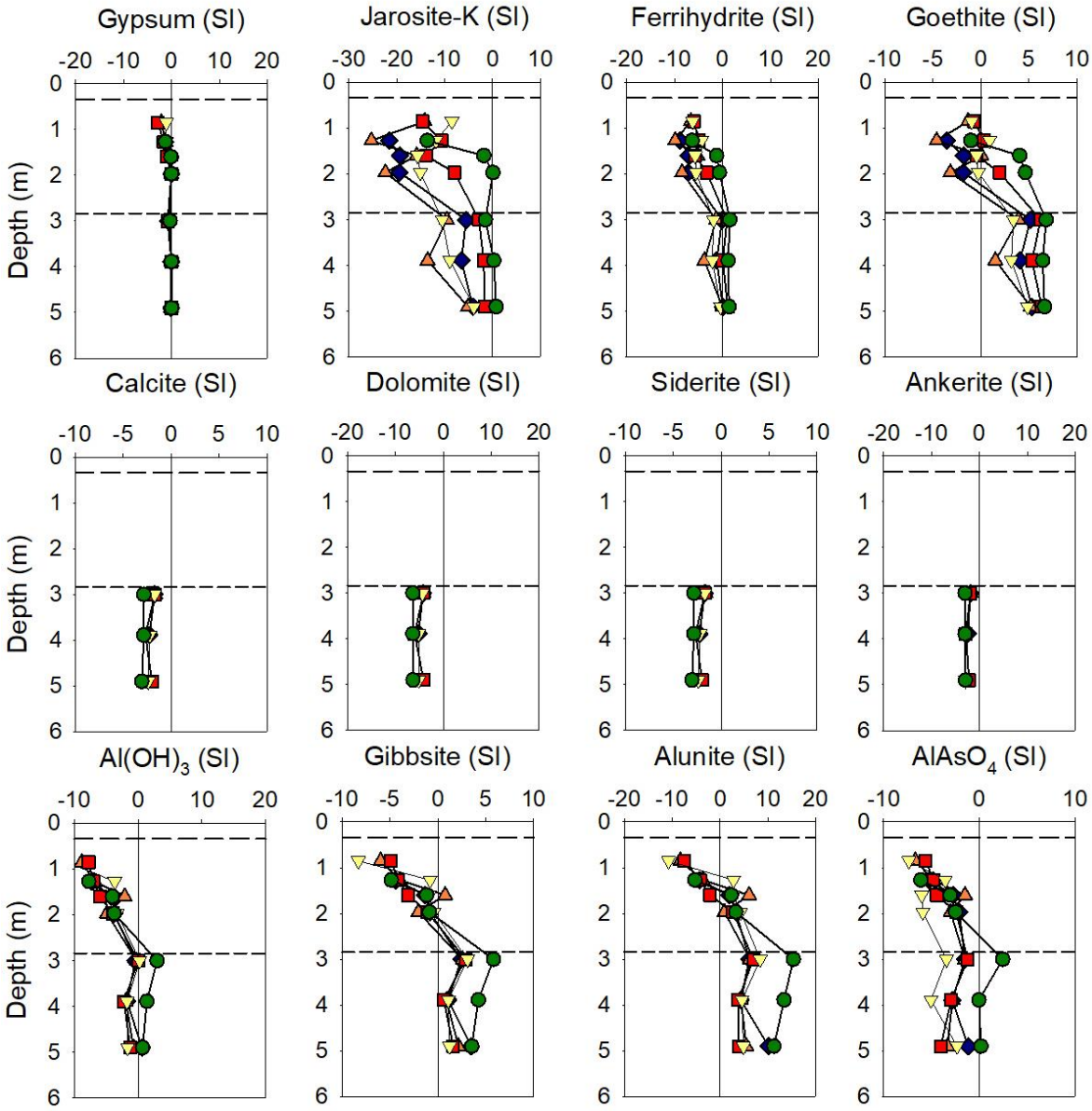

Figure 21: Depth profiles through LL01 showing calculated saturation indices from December 2016 (▽), June 2017 (○), September 2017 (◊), November 2017 (△), and June 2018 (□). The medium and short dashed lines represent the depth of the sand layer and tailings, respectively.

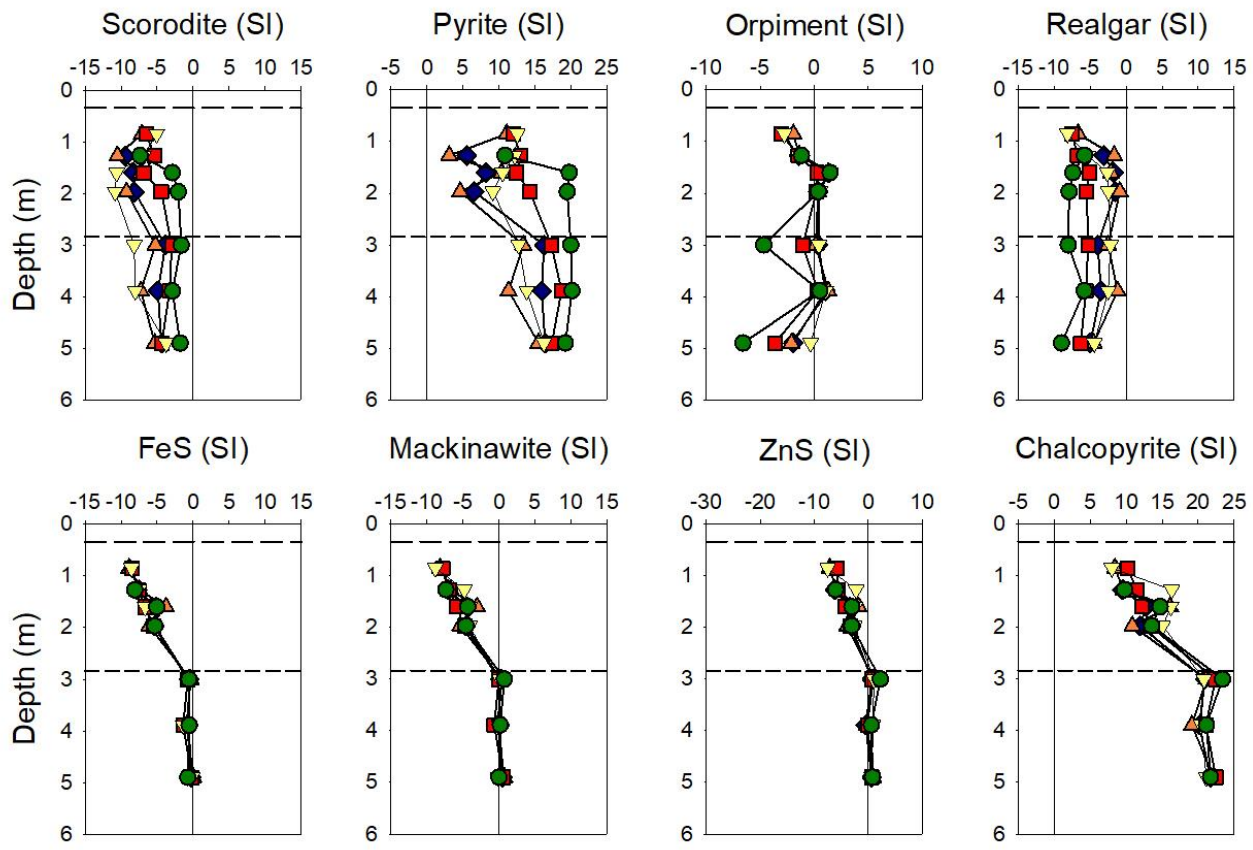

Figure 22: Depth profiles through LL01 showing calculated saturation indices of scorodite and sulfide minerals from December 2016 (▽), June 2017 (○), September 2017 (◊), November 2017 (△), and June 2018 (□). The medium and short dashed lines represent the depth of the sand layer and tailings, respectively.

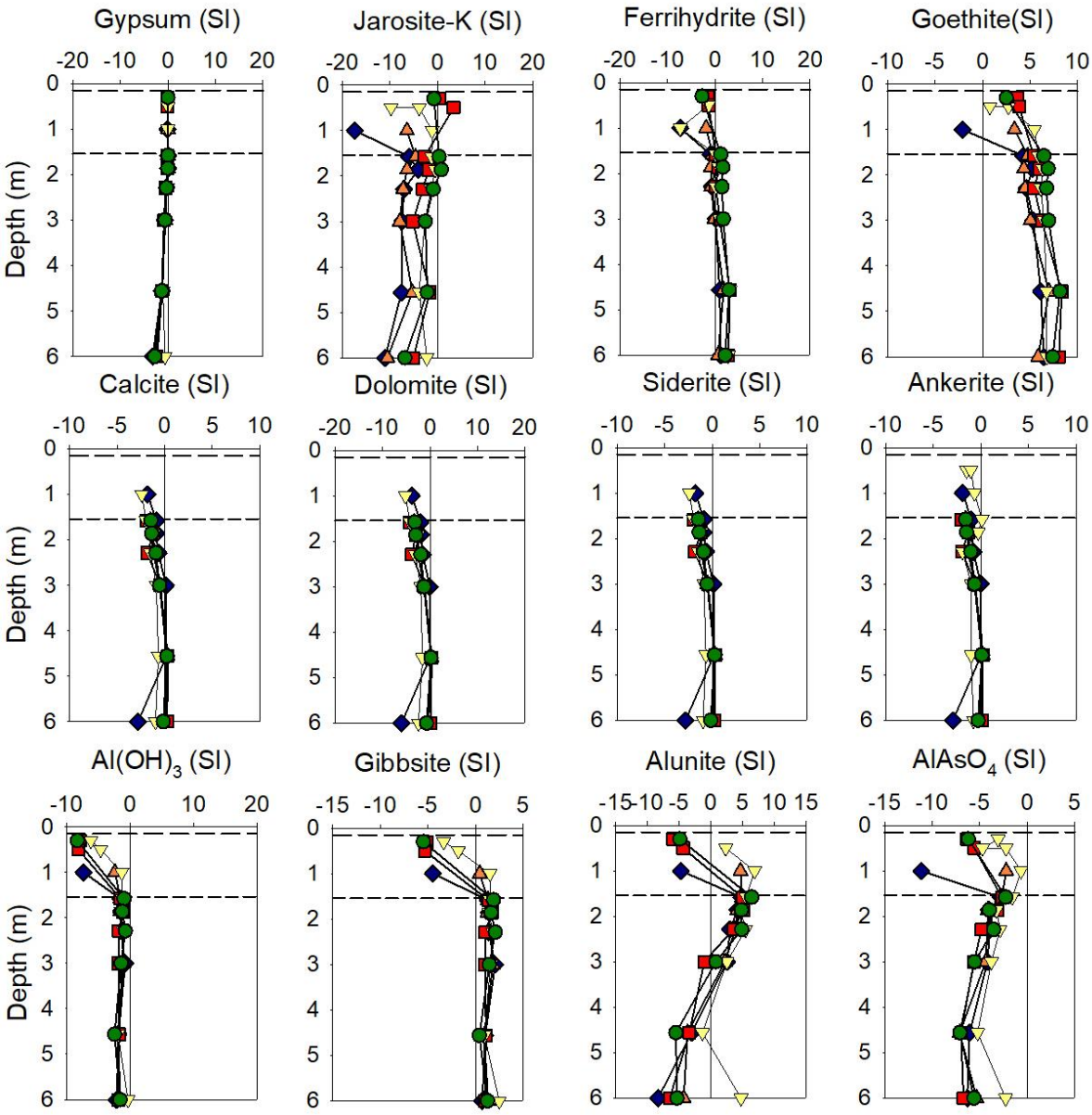

Figure 23: Depth profiles through LL03 showing calculated saturation indices from December 2016 (▽), June 2017 (○), September 2017 (◊), November 2017 (△), and June 2018 (□). The medium and short dashed lines represent the depth of the sand layer and tailings, respectively.

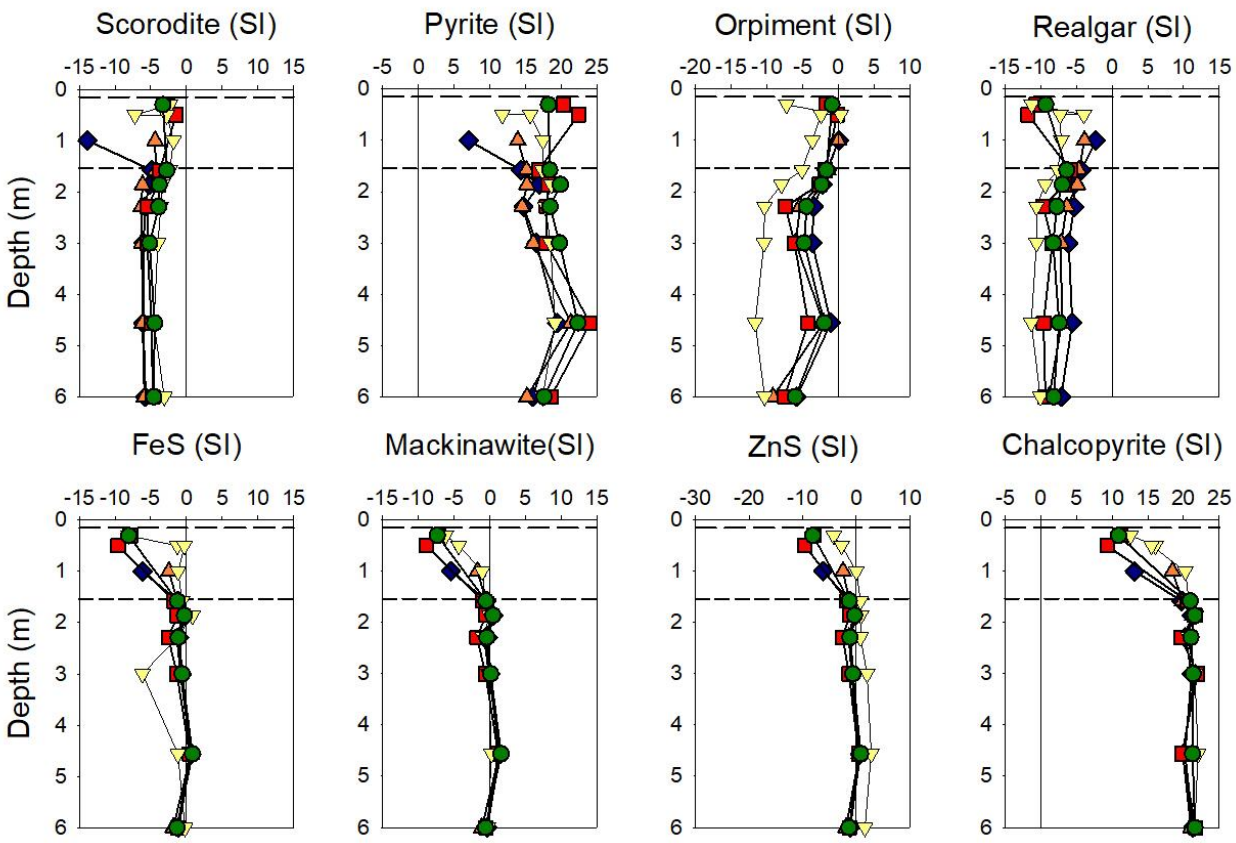

Figure 24: Depth profiles through LL03 showing calculated saturation indices of scorodite and sulfide minerals from December 2016 (▽), June 2017 (○), September 2017 (◊), November 2017 (△), and June 2018 (□). The medium and short dashed lines represent the depth of the sand layer and tailings, respectively.

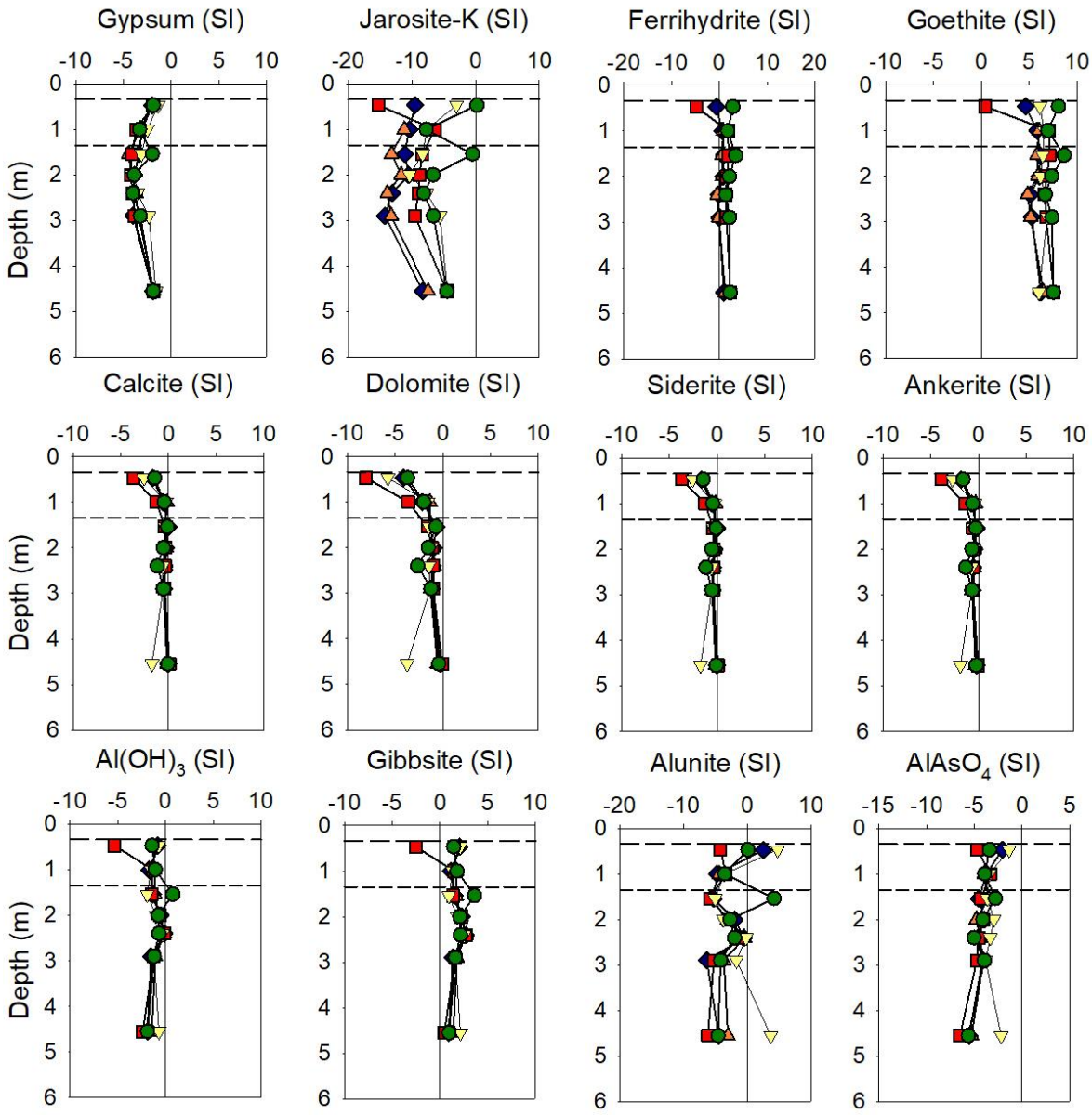

Figure 25: Depth profiles through LL06 showing calculated saturation indices from December 2016 (▽), June 2017 (○), September 2017 (◊), November 2017 (△), and June 2018 (□). The medium and short dashed lines represent the depth of the sand layer and tailings, respectively.

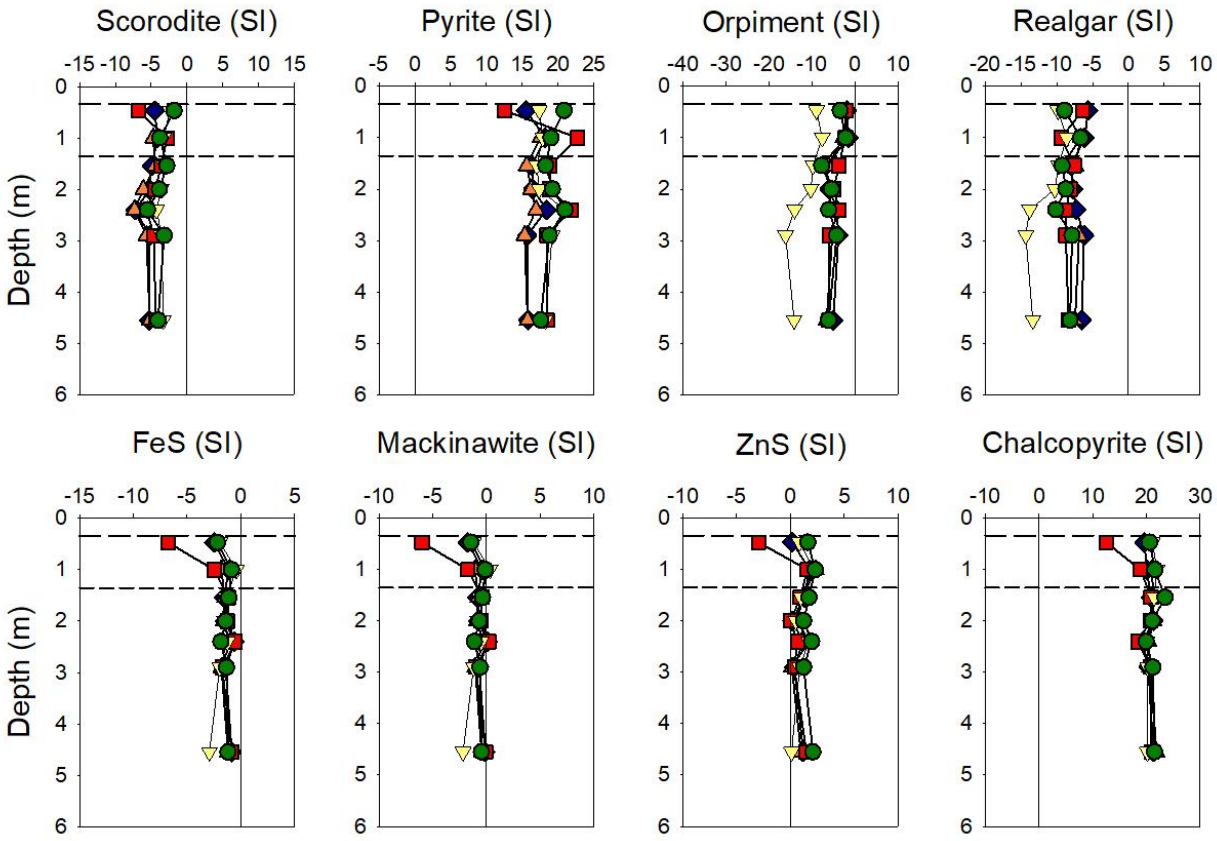

Figure 26: Depth profiles through LL06 showing calculated saturation indices of scorodite and sulfide minerals from December 2016 (▽), June 2017 (○), September 2017 (◊), November 2017 (△), and June 2018 (□). The medium and short dashed lines represent the depth of the sand layer and tailings, respectively.

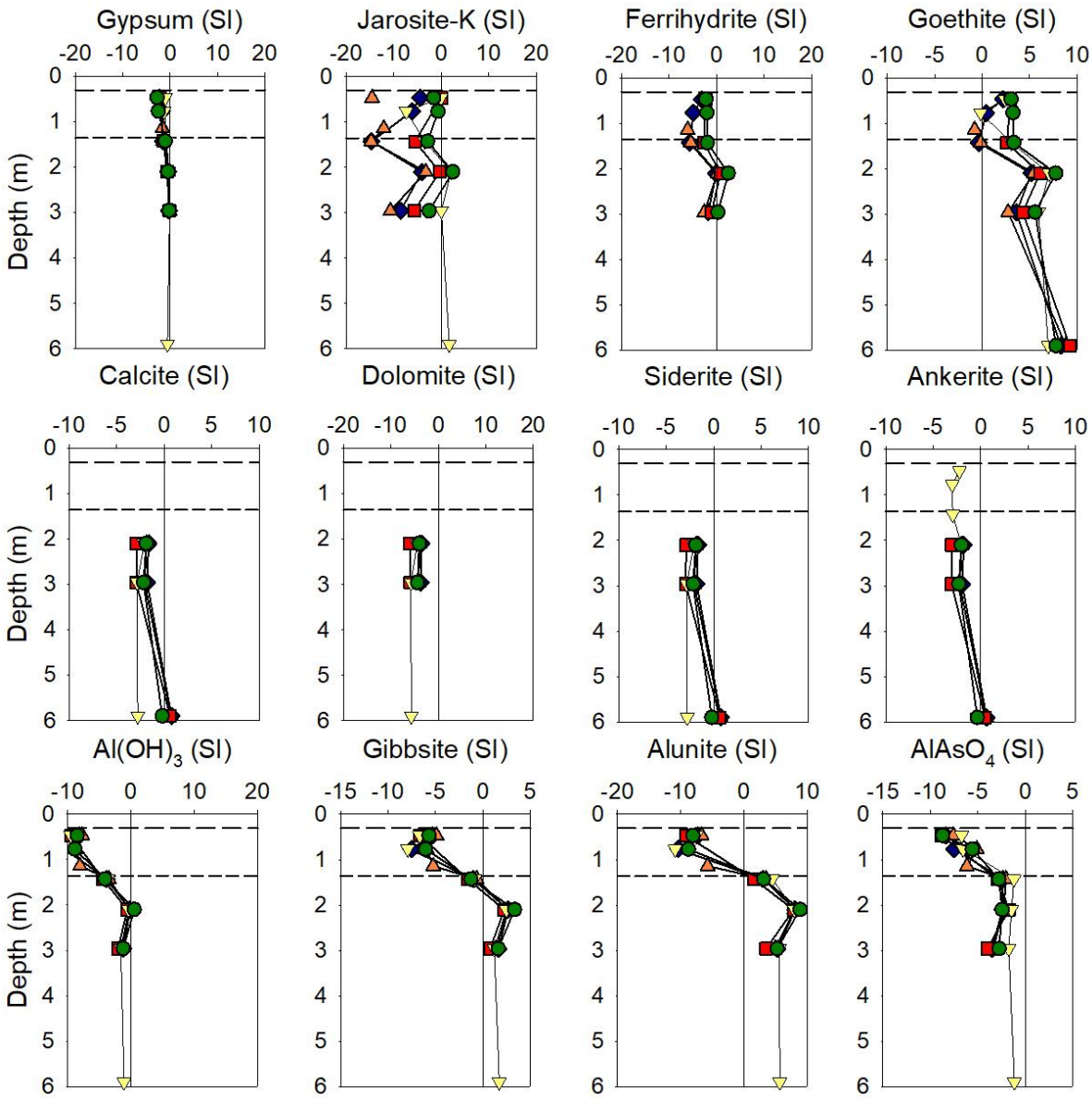

Figure 27: Depth profiles through LL07 showing calculated saturation indices from December 2016 (▽), June 2017 (○), September 2017 (◊), November 2017 (△), and June 2018 (□). The medium and short dashed lines represent the depth of the sand layer and tailings, respectively.

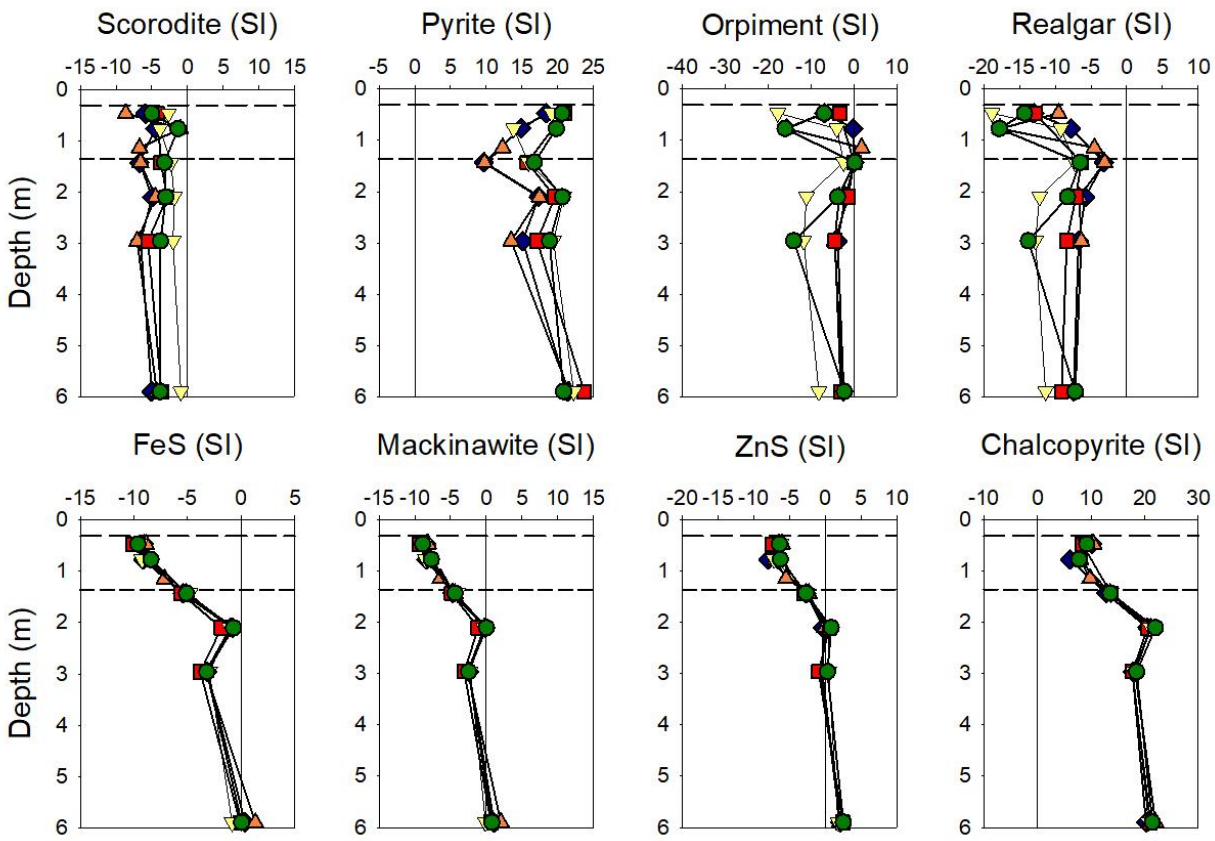

Figure 28: Depth profiles through LL07 showing calculated saturation indices of scorodite and sulfide minerals from December 2016 (▽), June 2017 (○), September 2017 (◊), November 2017 (△), and June 2018 (□). The medium and short dashed lines represent the depth of the sand layer and tailings, respectively.

The groundwater and tailings pore water are highly supersaturated with respect to pyrite (SI 10-20) at all sampling locations (Figures 22, 24, 26, and 28). Groundwater and tailings pore water is undersaturated with respect to orpiment at many sampling locations. Near saturation with respect to orpiment is observed at some locations in the tailings above the native soil, where high concentrations of dissolved As(III) and H_2S are observed, suggesting that orpiment is near equilibrium within the tailings. The tailings pore waters is undersaturated with respect to realgar throughout the tailings area and in the native soil. The precipitation of realgar and orpiment is favoured under reducing conditions (Smedley and Kinniburgh, 2002).

The groundwater and tailings pore water are undersaturated with respect to mackinawite within the tailings and saturated with respect to this mineral at the base of the tailings and within the native soil, where enriched $\delta^{34}S\text{-}SO_4$ values are observed. Tailings pore water at LL01, LL03 and LL07 was undersaturated with respect to ZnS within the tailings and were saturated at deeper depths, below the tailings in the underlying soils (Figures 22, 24, and 28). At LL06 the water were slightly supersaturated with respect to ZnS at all sampling depths. This phase may be controlling Zn and H_2S concentrations. These results are consistent with the concentrations of Ni and Zn observed at each piezometer nest. Concentrations of Zn and Ni are highest within the shallow tailings pore water at LL01, LL03, and LL07 before decreasing in the native soil, corresponding to depths were SI values indicate saturation or supersaturation with respect to mackinawite and ZnS. At LL06 the concentrations of Zn and Ni are consistently low throughout the profile except for one sampling point near the surface of the profile.

The groundwater and tailings pore water were supersaturated at all piezometer nest locations with respect to covellite [CuS] (Appendix B). Covellite can act as a solid-phase sink for Cu and may be controlling Cu concentrations in the tailings pore water. As covellite is exposed to oxidizing conditions Cu will be released to the pore waters. The increases in concentrations of Cu at each piezometer nest location correspond with the depth of $O_{2(g)}$ depletion. Maximum dissolved Cu concentrations decline below the oxidation front, suggesting that Cu released by sulfide oxidation are removed from solution by formation of covellite.

Tailings pore water and groundwater at LL03 and LL06 were saturated with respect to siderite throughout the profiles, suggesting that precipitation of siderite, or a less crystalline precursor, may be controlling dissolved Fe(II) concentrations (Figures 23 and 25). The saturation index values indicate that the tailings pore water and groundwater below the tailings approaches

equilibrium with respect to calcite and dolomite throughout the depth profile of LL03, LL06, and LL07. Groundwater and tailings pore water that approach saturation with respect to calcite and siderite suggest that these minerals may be maintaining circumneutral pH conditions. Groundwater at LL01 is undersaturated with respect to carbonate minerals calcite and dolomite (Figure 21).

Groundwater and tailings pore water is saturated or undersaturated with respect to ferrihydrite throughout the profiles (Figures 21, 23, 25, and 27). At LL01 waters are undersaturated with respect to ferrihydrite throughout the tailings and slightly undersaturated or saturated in the underlying aquifer materials. Throughout the profile of LL03 waters are slightly undersaturated or saturated with respect to ferrihydrite throughout all sampling depths. The SI values indicate that throughout the profile at LL06 the water is slightly supersaturated or saturated with respect to ferrihydrite, whereas the SI values at LL07 indicate that water is undersaturated in the tailings, and becomes saturated with respect to ferrihydrite directly beneath the tailings layer and supersaturated at a depth of 5.9 m.

All sampling locations show waters are supersaturated with respect to goethite throughout the depth profiles. When other Fe(III) oxyhydroxides are at saturation mine waters are normally supersaturated with respect to goethite (Moncur et al., 2015). This does not necessarily suggest that direct precipitation of goethite is occurring (Alpers and Nordstrom, 1999).

The groundwater and tailings pore water were undersaturated with respect to the arsenite-containing phases arsenolite (As_4O_6) and claudetite (As_2O_3) at all sampling locations and depths (Appendix B). These calculations suggest that As(III) concentrations are not controlled by precipitation of these minerals. The tailings pore water and underlying groundwater were also

undersaturated with respect to the arsenate phases $AlAsO_4$, $Ca_3(AsO_4)_2$ and $Mn_3(AsO_4)_2$ at all sampling locations and depths (Appendix B). These arsenate phases are unlikely to limit dissolved As(V) concentrations. Arsenate concentrations in the groundwater and tailings pore water were much lower than concentrations of As(III), therefore the negative saturation indices are expected. The tailings pore water and groundwater were undersaturated with respect to scorodite at all sampling locations and depths. However, scorodite precipitation was observed in the near surface tailings at LL07, suggesting that scorodite may be controlling dissolved As concentrations in the near surface tailings.

Saturation indices of gypsum were slightly undersaturated within the tailings and at equilibrium in the underlying materials at LL01 and LL07. At LL03 waters were at saturation with respect to gypsum throughout the profile except at a depth of 6 m where waters were slightly undersaturated (Figure 23). Water was undersaturated with respect to gypsum throughout the profile at LL06 (Figure 25). The pore water was mainly undersaturated with respect to jarosite, with few sampling depths at saturation. Jarosite could be controlling dissolved concentrations of SO_4, Fe, and K.

The groundwater and tailings pore water were undersaturated at LL01, LL03 and LL07 with respect to $Al(OH)_3$ in the tailings. Saturation indices of $Al(OH)_3$ indicate saturation or supersaturation with respect to $Al(OH)_3$ in the underlying aquifer materials, directly below the tailings profile. This change corresponds to a decrease in tailings pore water and groundwater Al concentrations, as well as an increase in pH. Geochemical calculations indicate that the groundwater and pore water in the tailings is undersaturated with respect to gibbsite and becomes saturated or supersaturated beneath the tailings at LL01, LL03, and LL07. At LL06 waters are supersaturated with respect to gibbsite at all depths. At depths where the water becomes

supersaturated with respect to gibbsite, the concentrations of Al decrease to < 1 mg L^{-1}. Calculations indicate that the saturation indices of alunite follow similar trends as $Al(OH)_3$, with water becoming saturated or supersaturated beneath the tailings layer at LL01, LL03, and LL07. At LL06 all water samples are undersaturated with respect to alunite at all depths.

3.11 X-ray absorption spectroscopy

The oxidation state (-I, III, V) of As can be determined from the position of the absorption edges from As K-edge XANES spectra. In minerals such as arsenopyrite and arsenian pyrite, As can occur in the -I oxidation state and is susceptible to oxidation (Campbell and Nordstrom, 2014; Paktunc, 2008). The main absorption peaks for As(-I), As(III), and As(V) occur at 11,865.4 eV, 11,868.9 eV, and 11,873 eV, respectively. Arsenic K-edge HERFD-XAS measurements were collected for tailings from various depths at LL01, LL03, LL06, and LL07. The HERFD-XAS technique provides sharper absorption edges and spectral features for quantitative analysis. Linear combination fitting (LCF) of the HERFD-XAS spectra indicate that arsenopyrite was the dominant As species in the majority of tailings samples (Table 3).

Scorodite is abundant, and the principal As-bearing phase in the oxidized tailings in the shallow vadose zone at all locations except LL06. Minor to major amounts of scorodite (1-27 %) are present below the near surface tailings, within the unoxidized tailings and natural materials. Below the depth of active oxidation arsenopyrite is the dominant form of As, accompanied by trace concentrations of arsenolite. Realgar and orpiment cannot be distinguished using the HERFD-XAS. Realgar/orpiment comprise a significant component, up to 81 % of the As in the peat layer at the base of the tailings and the underlying natural materials. The presence of minor species (< 5 %) was confirmed by performing significance tests. Linear combination fitting was performed with and without the addition of the minor species to determine if the inclusion

improved the fit quality. If the fit quality with the inclusion of the minor species improved by 1 % or greater the minor species was included. In all the samples that contained minor species, the reduced chi square values were lower with the addition of the minor species and improved the quality of fit by greater than 1 %.

The precipitation of scorodite has been confirmed in the near surface tailings at LL07 through optical microscopy and SEM (Figure 10). At LL03 and LL07 waters approach near equilibrium with respect to orpiment suggesting a tendency for orpiment precipitation. The depths at which orpiment approaches equilibrium correspond to the depths where orpiment/realgar was detected by LCF, at the bottom of the tailings profile near the organic/peat layer. Orpiment was at or near equilibrium at LL01 for many of the sampling depths, including at the bottom of the tailings profile, but orpiment was detected in only one sample at a depth of 3.02 m. At LL06, the pore water and groundwater were undersaturated with respect to orpiment at all sampling depths. However, orpiment was detected at depths of 1.36 and 1.62 m at LL06, but orpiment did not comprise the majority of the As spectra.

Table 3: Results of LCF analysis of As K-edge HERFD spectra for TA-01 tailings and soil. Fitted reference spectra included aresenolite [As_4O_6], arsenopyrite [FeAsS], arsenic trioxide [As_2O_3], getchellite [$AsSbS_3$], kankite [$Fe^{3+}AsO_4 \cdot 3.5(H_2O)$], orpiment [$As_2S_3$], realgar [$\alpha$-$As_4S_4$], scorodite [$FeAsO_4 \cdot 2H_2O$], and sodium arsenate [$Na_3AsO_4$]. The R factor is the mean-square misfit between the measured and modeled spectra. Fitting range: 11,851-11,901 eV.

Location	Depth (m)	Arsenolite	Arsenopyrite	Orpiment/ Realgar	Scorodite	R factor
	0.34		0.19		0.81	0.0049
	0.59		0.96		0.04	0.0044
	0.85		0.97		0.03	0.0003
	1.19		0.87		0.13	0.0024
LL01	1.72	0.17	0.71		0.12	0.0109
	2.38	0.19	0.75		0.06	0.0077
	2.85		0.95		0.05	0.0060
	3.02	0.29		0.48	0.22	0.0098
	3.27		0.83		0.17	0.0017
	0.41		0.10		0.90	0.0117
	0.74	0.26	0.03		0.71	0.0123
	1.06	0.34	0.29		0.37	0.0144
LL03	1.41		0.95		0.05	0.0048
	1.47		0.41	0.47	0.12	0.0140
	1.56			0.89	0.11	0.0084
	1.77		0.49	0.23	0.29	0.0237
	0.44		0.97		0.03	0.0048
	0.76		0.76		0.24	0.0101
	1.00	0.39	0.11		0.50	0.0028
LL06	1.21		0.99		0.01	0.0060
	1.36		0.72	0.15	0.13	0.0098
	1.62		0.52	0.42	0.07	0.0251
	1.89		0.82		0.18	0.0090
	0.28				1.00	0.0099
	0.50				1.00	0.0100
	0.75		0.97		0.03	0.0080
LL07	1.13		0.96		0.04	0.0094
	1.37		0.94		0.06	0.0030
	1.54		0.07	0.81	0.12	0.0082
	1.86		0.73		0.27	0.0025

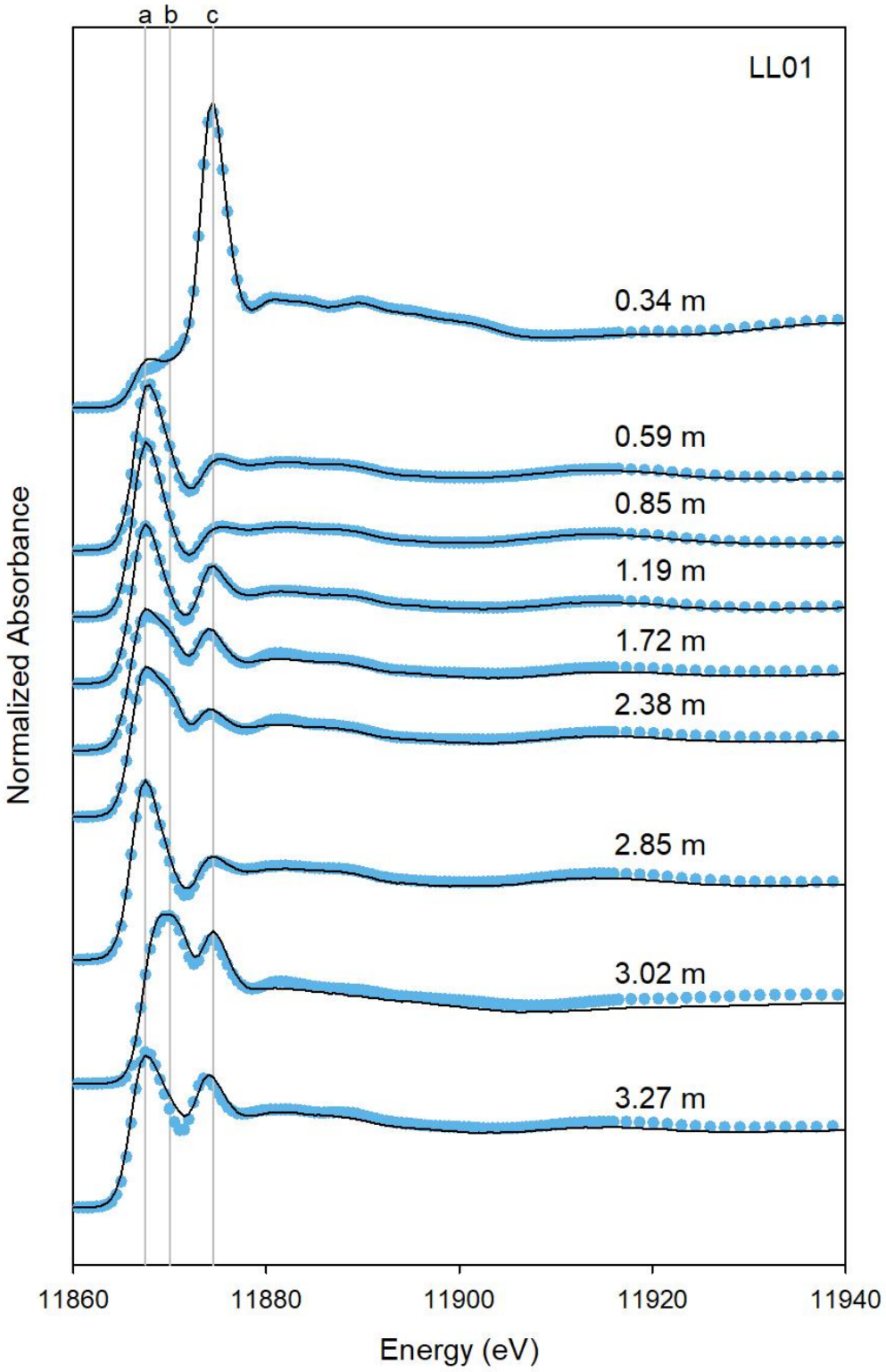

Figure 29: Measured (line) and modeled (circles) As K-edge HERFD spectra for TA-01 tailings samples from LL01. Vertical shaded lines represent measured As K-edge white line maxima for (a) arsenopyrite, (b) arsenolite, and (c) scorodite reference standards.

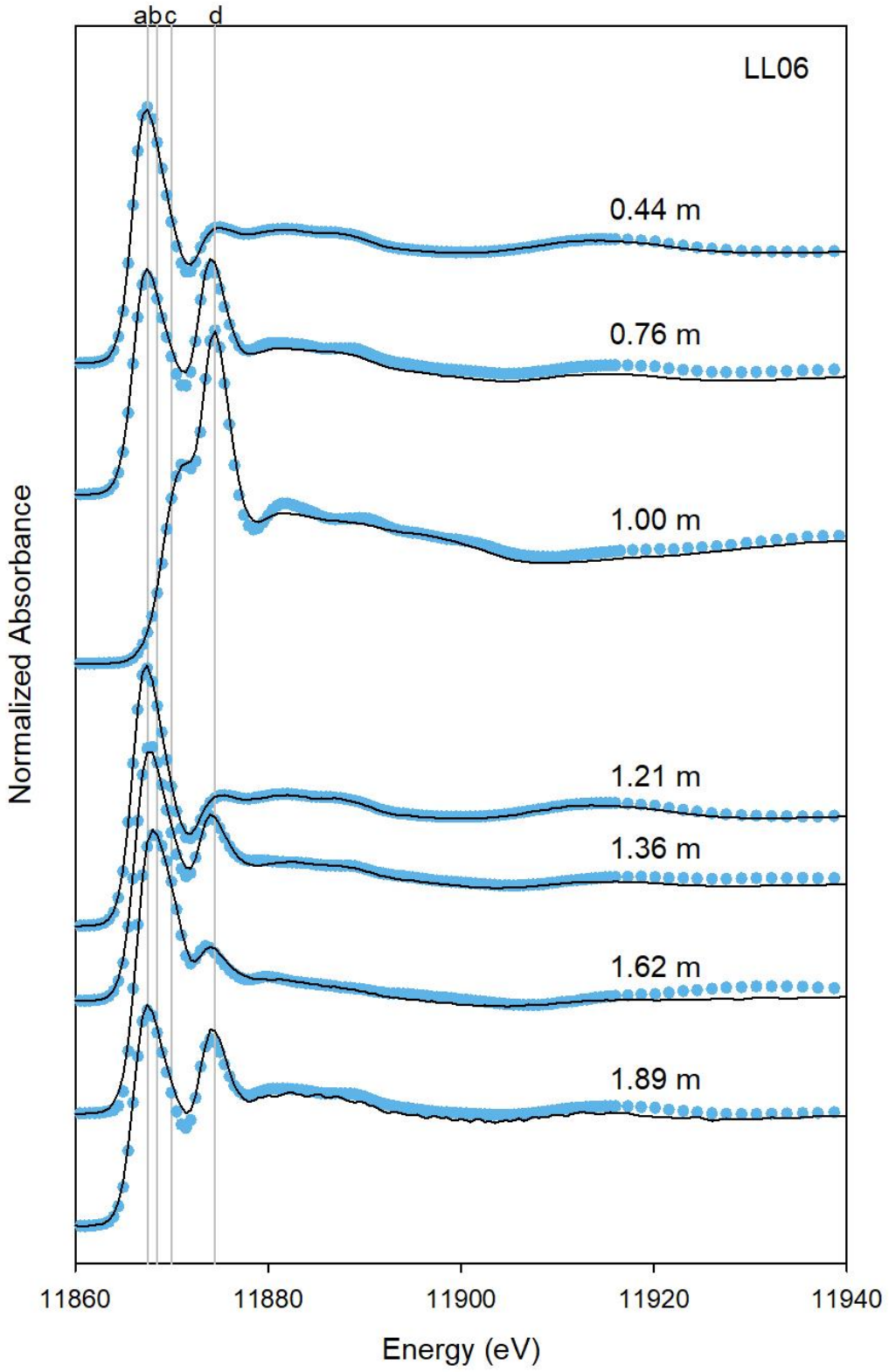

Figure 30: Measured (line) and modeled (circles) As K-edge HERFD spectra for TA-01 tailings samples from LL06. Vertical shaded lines represent measured As K-edge white line maxima for (a) arsenopyrite, (b) orpiment, (c) arsenolite, and (d) scorodite reference standards.

Four As K-edge spectra were collected from a grain at a depth of 0.28 m along with μ-XRF mapping for As, Fe, Cu, and Ca (Figure 31). All four XANES spectra indicate that As(V) is the dominant species, consistent with the scorodite reference spectrum. Elemental mapping indicates high concentrations of As occurring around the edges of the two grains, as shown in the SEM photomicrograph where a white precipitate has formed. Mapping of Fe was found to be similar to that of As, in lower concentrations. All four XANES spectra indicate the precipitate that has formed is scorodite. The sample from LL07 at a depth of 0.50 m displayed a similar XANES spectra with As(V) being the dominant species (Figure 32). These results are consistent with the HERFD spectra indicating that scorodite accounted for 100 % of the As spectra for samples at depths of 0.28 and 0.50 m (Table 3).

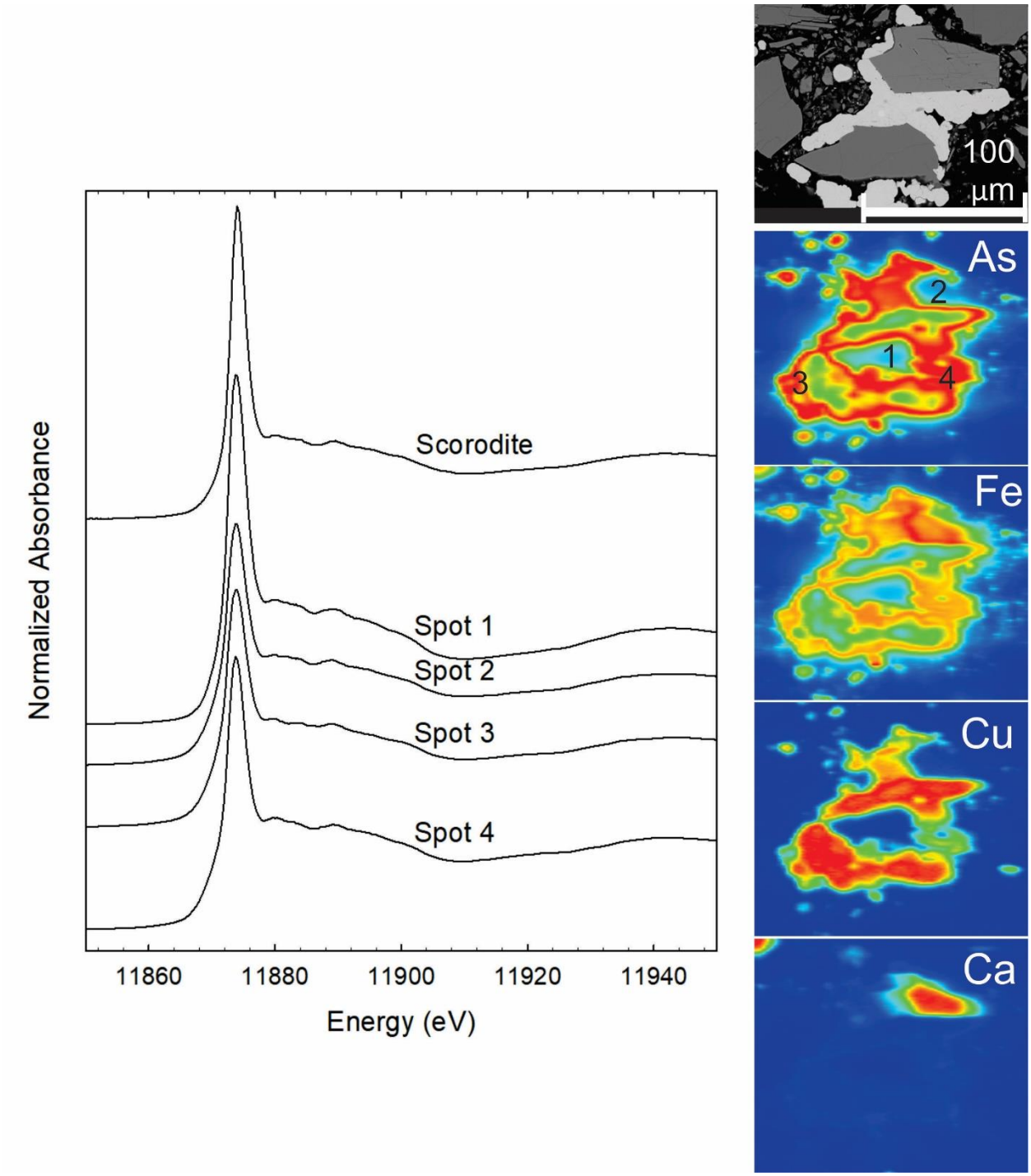

Figure 31: µ-XRF imaging and As K-edge XANES spectra of scorodite precipitation from LL07-0.28 m and scorodite reference standard.

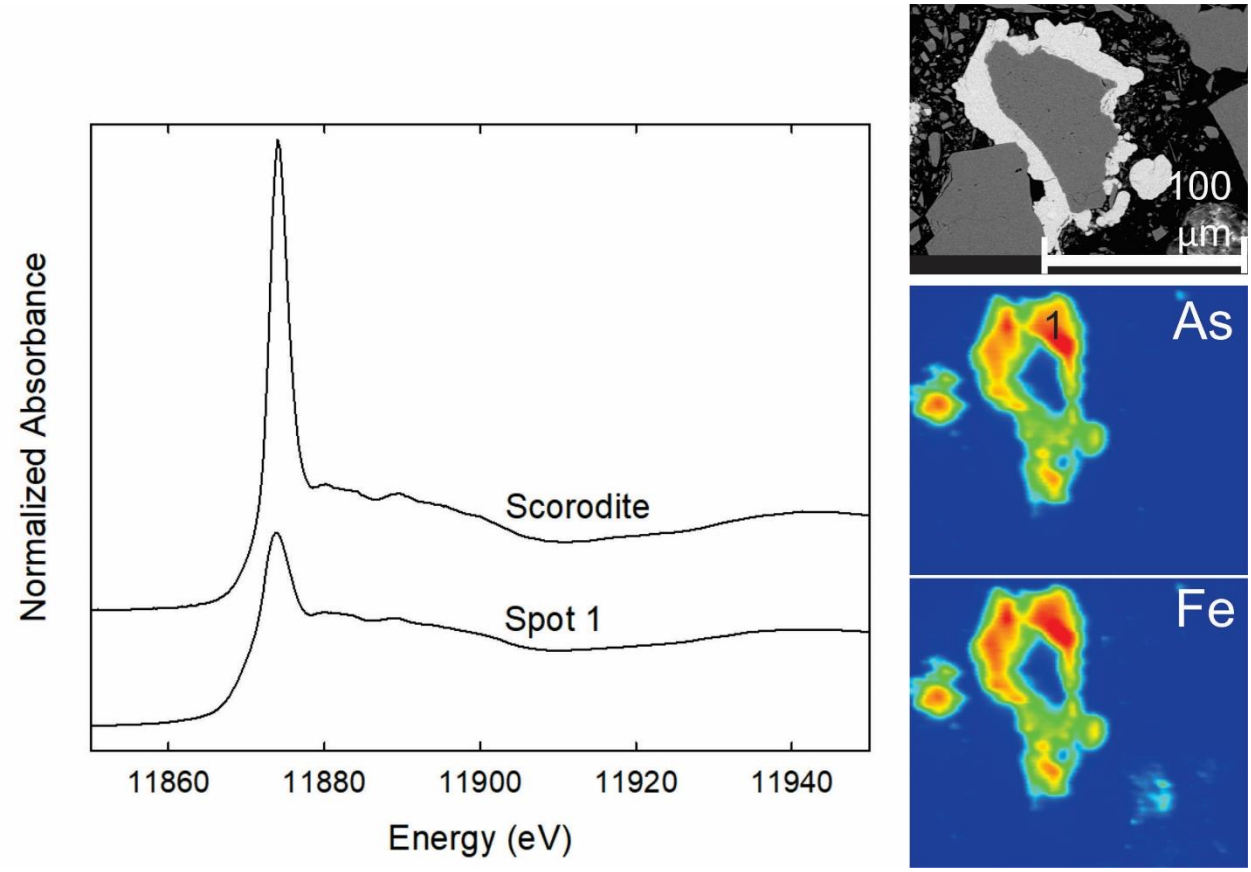

Figure 32: µ-XRF imaging and As K-edge XANES spectra of an albite particle surrounded by scorodite from LL07-0.50 m and scorodite reference standard.

The spectra for samples from 0.75 and 1.13 m depths displayed differences in their As K-edges compared to the near surface samples (Figures 33 to 35). The spectra of a sample from 0.75 m depth had the main absorption peak occurring close to that of arsenopyrite or arsenian pyrite at 11,865.3 eV, indicating the presence of As(-I), along with a minor amount of As(V). Samples from 1.13 m depth also show the main absorption peak occurring at 11,865.3 eV. The occurrence of As(-I) at depths of 0.75 and 1.13 m are consistent with sulfide minerals such as arsenopyrite that were observed in the unoxidized sections of the tailings and with the HERFD results indicating that arsenopyrite accounts for greater than 90 % of the spectra. Minor amounts of As(III) were observed in almost all of the samples analyzed.

Other elements detected in the selected grains included As, Fe, Cu, Cr, and Ca. The distribution of these elements is shown along with a BSE image for each analyzed grain (Figures 31 to 35). In the near surface tailings at depths of 0.28 and 0.50 m the grains are surrounded by a white precipitate, which was identified to be scorodite from the As XANES spectra. High concentrations of As and Fe were observed within this precipitate.

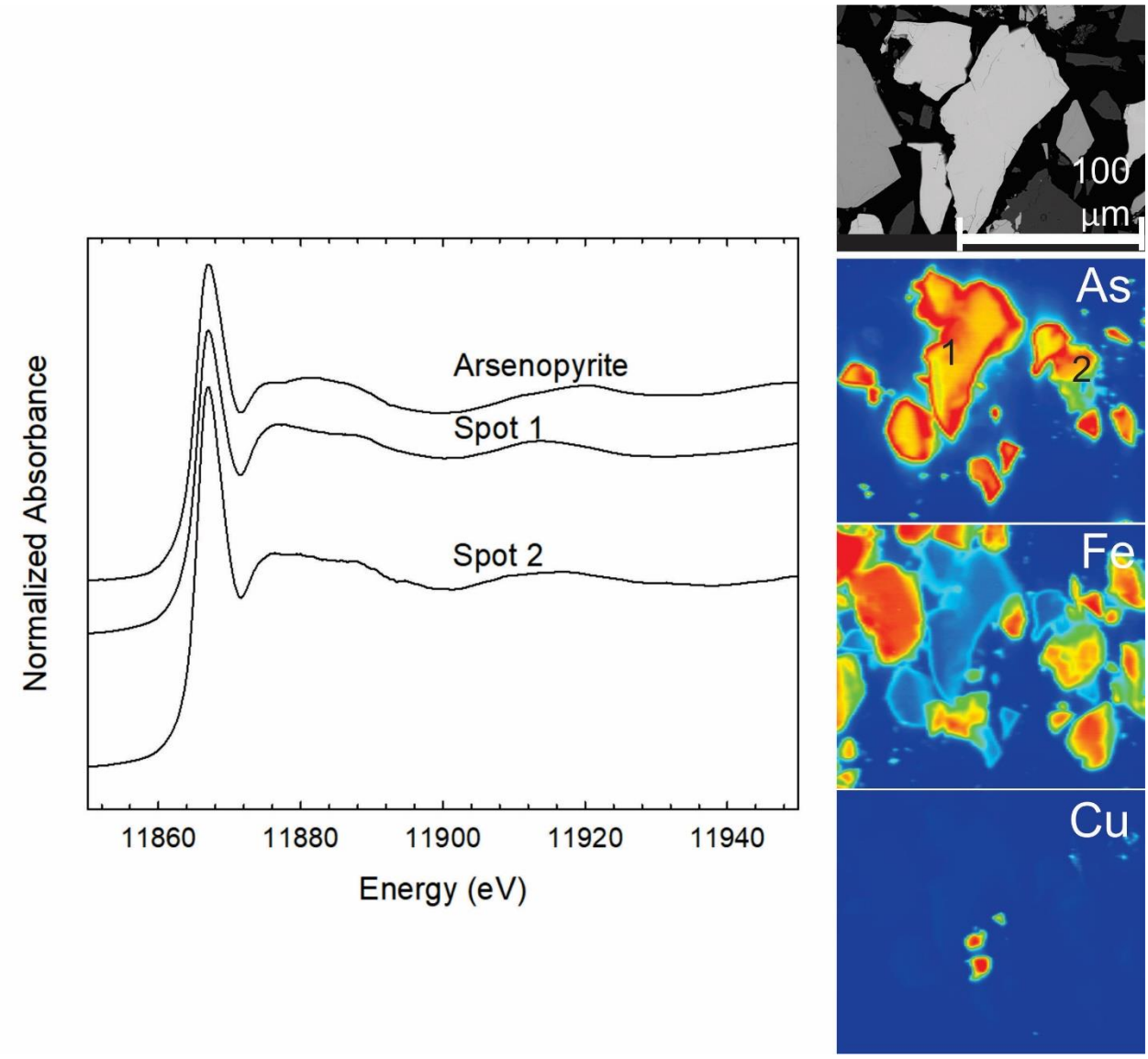

Figure 33: µ-XRF imaging and As K-edge XANES spectra of an arsenopyrite particle from LL07-0.75 m and an arsenopyrite reference standard.

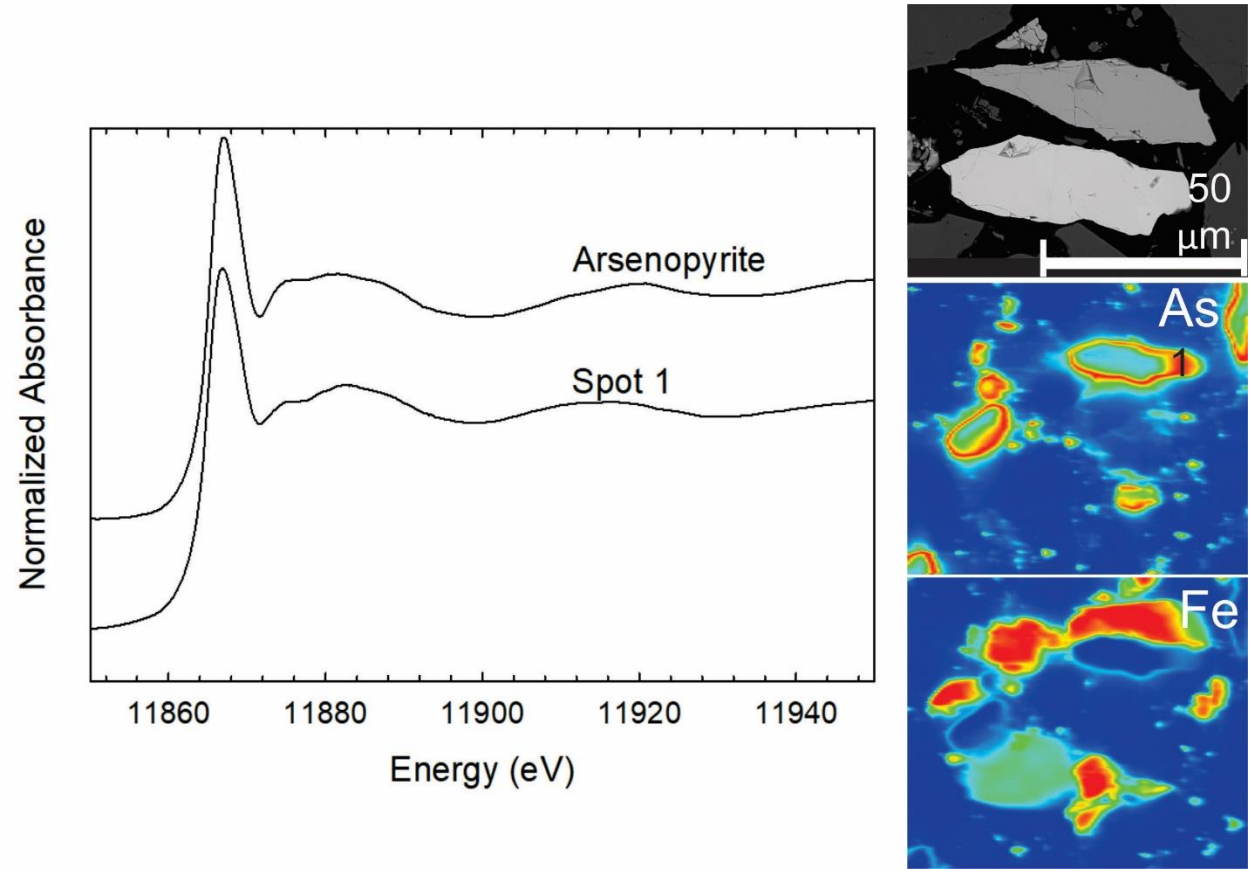

Figure 34: µ-XRF imaging and As K-edge XANES spectra of a pyrite particle from LL07-1.13 m and an arsenopyrite reference standard.

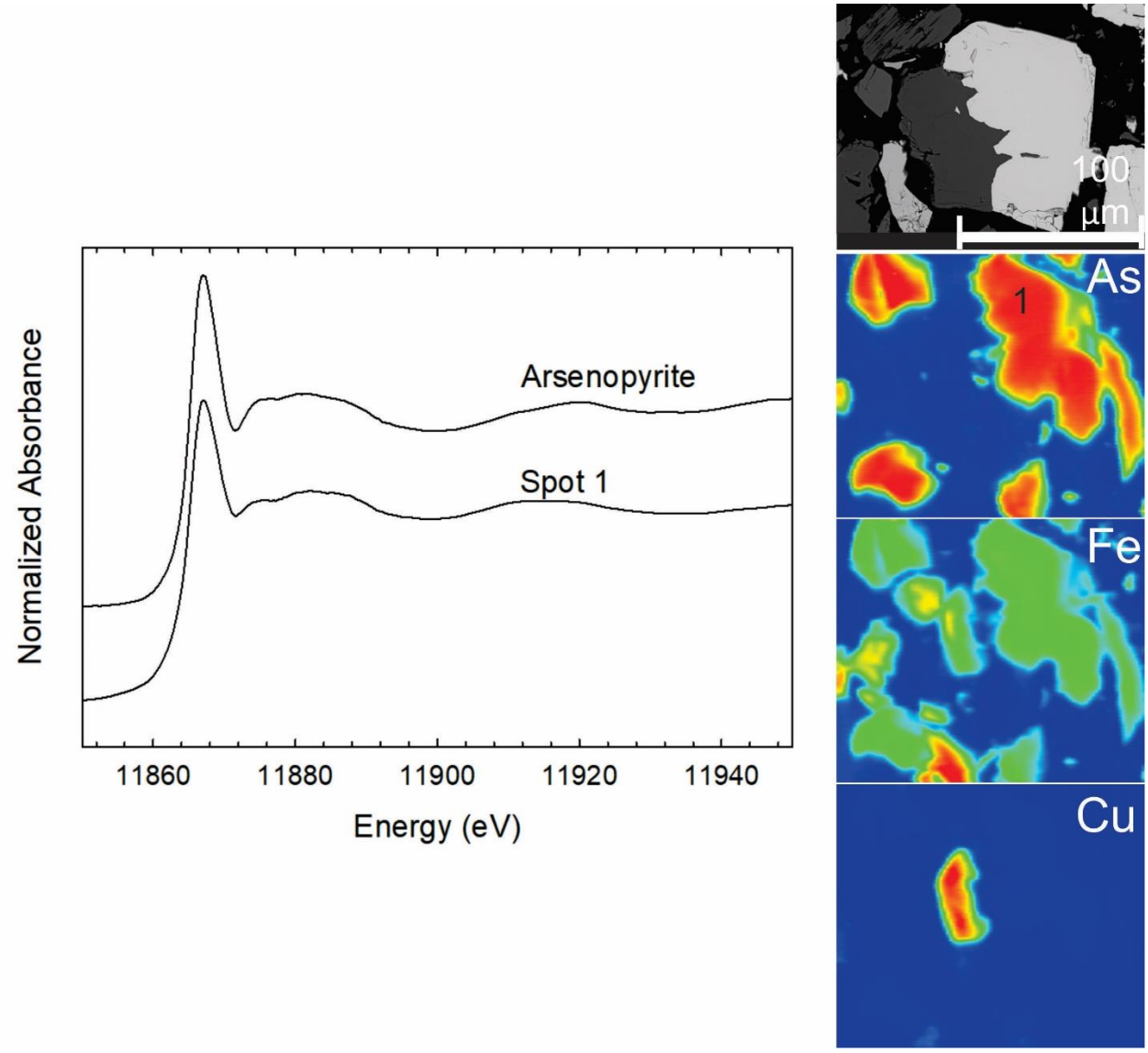

Figure 35: µ-XRF imaging and As K-edge XANES spectra of an arsenopyrite particle from LL07-1.13 m and an arsenopyrite reference standard.

3.12 Arsenic sulfide paragenesis

A conceptual model is proposed for the temporal evolution of geochemical conditions within the Long Lake tailings (Figure 36). Early state microbial mediated oxidation of arsenopyrite and arsenian pyrite (Figure 36A) in the tailings releases Fe(III), Fe(II), $H_2AsO_4^-$, and H^+ leading to the formation of As-rich Fe(III) oxyhydroxide rims (Figure 36B). As oxidation continues more H^+ is generated, and the pH decreases leading to dissolution of these rims and releasing elevated concentrations of $H_2AsO_4^-$ and Fe(III) to the pore water, which exceeds the solubility limit of

scorodite leading to precipitation within the pore space (Figure 36C, D). After longer times, the rate of sulfide-mineral oxidation declines and infiltrating precipitation leads to undersaturation with respect to scorodite, releasing Fe and $H_2AsO_4^-$ which is displaced downward into the profile. Because of the large mass of scorodite, many pore volumes of infiltration will be required prior to complete dissolution (Figure 36E). At this time, ongoing oxidation of As-rich sulfides will continue to release additional Fe, As, and H^+ as the oxidation front progresses further.

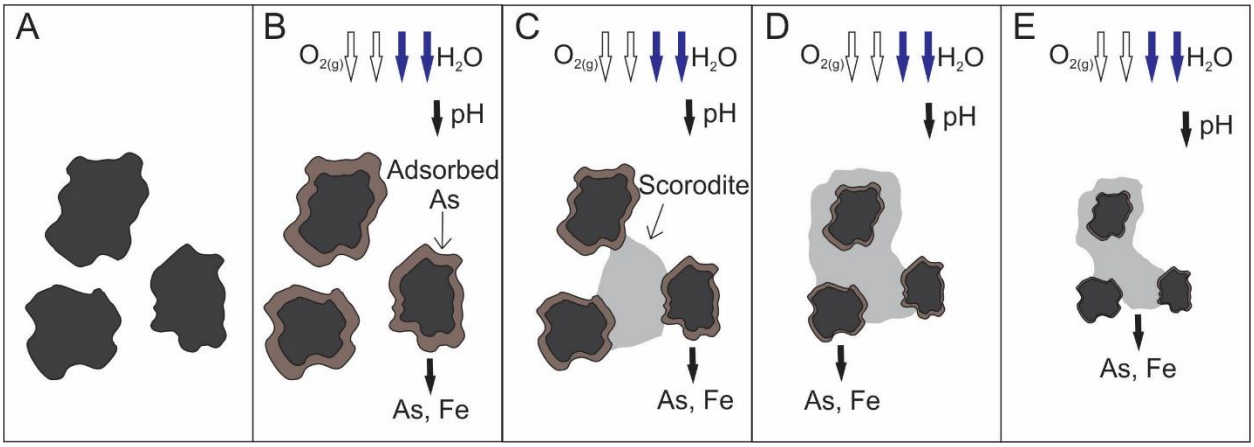

Figure 36: Conceptual model of the oxidation of sulfide minerals in the Long Lake tailings showing oxygen diffusion and infiltration of precipitation with (A) unaltered sulfide grains, (B) oxidation of sulfide minerals leading to As-rich Fe(III) oxyhydroxide rims, (C) precipitation of scorodite, (D) dissolution of As-rich Fe(III) oxyhydroxide rims and further scorodite precipitation, (E) infiltration of precipitation waters and scorodite dissolution.

4 Conclusions

Sulfide mine tailings were deposited at the Long Lake gold mine within TA-01 starting 100 years ago and ending 32 years later. Exposure of the tailings to atmospheric oxygen resulted in oxidation of the principal sulfide minerals pyrite and arsenopyrite. The tailings at TA-01 displayed an oxidation zone with sulfide mineral depletion extending from the surface to a depth of 0.3-1.0 m. At greater depths sulfide minerals remained unaltered. Scorodite precipitation was common in the near surface tailings as observed by optical microscopy and SEM analysis.

Pore water collected from the TA-01 near surface tailings was characterized by low pH, depleted alkalinity, and elevated concentrations of dissolved SO_4 and metals, especially As and Fe. Generally, the highest concentrations of dissolved As were measured within the tailings pore water and in close association with the organic layer. As depth increased, the tailings pore water and groundwater were characterized by circumneutral pH, low concentrations of dissolved SO_4 and metals, indicating strong reducing conditions. Elevated concentrations of H_2S and $\delta^{34}S\text{-}SO_4$ enrichment was measured beneath the tailings in the native soil, suggesting dissimilatory sulfate reduction (DSR). Concentrations of SO_4 decreased from over 6,000 mg L^{-1} to less than 100 mg L^{-1}. Areas of sulfate reduction corresponded to decreases in As concentrations as well as an increase in pH. Detectable concentrations of H_2S were measured, with the lowest concentrations measured near the organic/peat interface, suggesting the precipitation of metal sulfides. The decrease in As and Fe concentrations near the organic/peat interface suggests that dissolved As concentrations are controlled by the precipitation of secondary As sulfides. Pore water within the Long Lake TA-01 tailings contains elevated concentrations of dissolved Al, Ni, Zn, and Cu. As the pore water pH increases with depth, the concentrations of these dissolved metals decrease.

Speciation of As showed that As(III) is the dominant form throughout TA-01 in the tailings pore water and groundwater. Areas of high organic carbon and sulfate-reducing conditions showed greater As(III) concentrations, while a greater abundance of As(V) was present in the near surface tailings pore water. The results of this project show the effect of reducing conditions on As geochemistry within sulfide mine tailings.

Arsenic K-edge X-ray absorption near edge structure (XANES) and bulk As K-edge high energy resolution fluorescence detection X-ray spectroscopy (HERFD-XAS) results were consistent with other mineralogical and geochemical observations. XANES and HERFD spectra indicated that the near surface oxidized tailings were dominated by As(V) species with features similar to those of scorodite. XANES and HERFD spectra collected for unoxidized tailings samples indicated the presence of reduced As species (As(-I)) with features characteristic of arsenopyrite and arsenian pyrite. Realgar/orpiment comprise a significant component of the As in the organic layer at the base of the tailings and the underlying natural materials.

High dissolved As concentrations were measured in the groundwater beneath the tailings profile, indicating that the precipitation of secondary As sulfides did not completely remove As from the water. The oxidation sulfide minerals and release of dissolved As is expected to continue for many decades throughout TA-01. If the dissolved SO_4 is depleted, sulfate reduction and the precipitation of metal sulfides will no longer remove As from solution.

References

Alpers, C.N., Nordstrom, D.K., 1999. Geochemical modeling of water-rock interactions in mining environments. In: Plumlee, G.S., Logsdon, M.J. (Eds.). Reviews in Economic Geology, vol. 6A. The Environmental Geochemistry of Mineral Deposits, Part A, Processes, Methods and Health Issues, 289-324.

Ball, J.W., Nordstrom, D.K., 1991. User's manual for WATEQ4F with revised thermodynamic data base and test cases for calculating speciation of major, trace and redox elements in natural waters. U.S. Geol. Surv. Open-File Rep. pp. 91-183.

Bednar, A.J., Garbarino, J.R., Ranville, J.F., Wildeman, T.R., 2005. Effects of iron on arsenic speciation and redox chemistry in acid mine water. Journal of Geochemical Exploration. 85, 55-62.

Benner, S.G., Blowes, D.W., Gould, W.D., Herbert, R.B., Jr., Ptacek, C.J., 1999. Geochemistry of a permeable reactive barrier for metals and acid mine drainage. Environmental Science and Technology. 33, 2793-2799.

Berner, R.A., 1969. Migration of iron and sulfur with anaerobic sediments during early diagenesis. American Journal of Science. 267, 19-42.

Berner, R.A., 1980. Early Diagenesis: A Theoretical Approach. Princeton University Press, Princeton, N.J. 241 pp.

Blowes, D.W., Jambor, J.L., 1990. The pore-water chemistry and the mineralogy of the vadose zone of sulfide tailings, Waite Amulet, Quebec. Applied Geochemistry 5, 327-346.

Blowes, D.W., Reardon, E.J., Jambor, J.L., Cherry, J.A., 1990. The formation and potential importance of cemented layers in inactive sulfide mine tailings. Geochimica et Cosmochimica Acta. 55, 965-978.

Blowes, D.W. The environmental effects of mine wastes. In: Gubins AG, editor. Proceedings of Exploration 97, Fourth Decennial International Conference on Mineral Exploration, Toronto, 1997. p. 887–92

Blowes, D.W., Ptacek, C.J., Benner, S.G., Waybrant, K.R., Bain, J.G., 1998. Porous reactive walls for the prevention of acid mine drainage: a review. Mineral Processing and Extractive Metallurgy Review. 19(1), 25-37.

Blowes, D.W., Ptacek, C.J., Jambor, J.L., 2013. Mineralogy of mine wastes and strategies for remediation. In: Vaughan, D.J., Wogelius, R.A. (Eds.). Environmental Mineralogy II, European Mineralogical Union Notes in Mineralogy. 13, 295-338.

Boissoneau, A.N., 1965. Surficial geology: Algoma, Sudbury, Timiskaming and Nipissing. Lands and Surveys Branch,Ontario. Department of Lands and Forests.

Bowell, R.J., 1994. Sorption of arsenic by iron oxides and oxyhydroxides in soils. Applied Geochemistry. 9, 279-286.

Campbell, K.M., Nordstrom, D.K., 2014. Arsenic speciation and sorption in natural environments. In: Bowell, R.J., Alpers, C.N., Jamieson, H.E., Nordstrom, D.K., Majzlan, J., (Eds.), Arsenic: Environmental Geochemistry, Mineralogy, and Microbiology. Reviews in Mineralogy and Geochemistry. 79, 185-216.

Carrier, W.D., 2003. Goodbye, Hazen; Hello, Kozeny-Carman. Journal of Geotechnical and Geoenvironmental Engineering. 129(11), 1054-1056.

Chang, Y., Peacock, A.D., Long, P.E., Stephen, J.R., McKinley, J.P., Macnaughton, S.J., Hussain, A.K.M.A., Saxton, A.M., White, D.C., 2001. Diversity and characterization of sulfate-reducing bacteria in groundwater at a uranium mill tailings site. Applied and Environmental Microbiology. 67(7), 3149-3160.

Chapelle, F.H., Morris, J.T., McMahon, P.B., Zelibor, J.L., Jr., 1988. Bacterial metabolism and the $\delta^{13}C$ composition of ground water, Floridan aquifer system, South Carolina. Geology. 16, 117-121.

CH2M Hill. (2014). Site Characterization Report and Data Analyses – Long Lake Gold Mine Tailings Areas, Eden Township, Ontario. Toronto, ON: CH2M Hill.

Corriveau, M.C., Jamieson, H.E., Parsons, M.B., Hall, G.E.M., 2011. Mineralogical characterization of arsenic in gold mine tailings from three sites in Nova Scotia. Geochemistry: Exploration, Environment, Analysis. 11, 179-192.

Craig, H., 1961. Isotopic variations in meteoric waters. Science. 133, 1702-1703.

Cullen, W.R., Reimer, K.J., 1989. Arsenic speciation in the environment. Chemical Reviews. 89, 713-764.

Deditius, A.P., Utsunomiya, S., Reich, M., Kesler, S.E., Ewing, R.C., Hough, R., Walsh, J., 2011. Trace metal nanoparticles in pyrite. Ore Geology Reviews. 42, 32-46.

Devlin, J.F., 2015. HydrogeoSieveXL: an Excel-based tool to estimate hydraulic conductivity from grain-size analysis. Hydrogeology Journal. 23, 837-844.

Dixit, S., Hering, J.G., 2003. Comparison of arsenic(V) and arsenic(III) sorption onto iron oxide minerals: Implications for arsenic mobility. Environmental Science and Technology. 37, 4182-4189.

Drahota, P., Filippi, M., 2009. Secondary arsenic minerals in the environment: A review. Environmental International. 35, 1243-1255.

Dubrovsky, N.M., 1986. Geochemical evolution of inactive pyritic tailings in the Elliot Lake uranium district. PhD Thesis. University of Waterloo, Waterloo, Ontario.

Dzombak, D.A., Morel, F.M.M., 1990. Surface Complexation Modelling- Hydrous Ferric Oxide. John Wiley, New York.

Edwards, M., Patel, S., McNeill, L., Chen, H., Frey, M., Eaton, A.D., Antweiler, R.C., Taylor, H.E., 1998. Considerations in As analysis and speciation. American Water Works Association. 90(3), 103-113.

Ficklin, W.H., 1983. Separation of arsenic(III) and arsenic(V) in ground waters by ion-exchange. Talanta. 30(5), 371-373.

Giesemann, A., Jaeger, H.J., Norman, A.L., Krouse, A.L., Krouse, H.R., Brand, W.A., 1994. On-line sulfur isotope determination using a elemental analyzer coupled to a mass spectrometer. Analytical Chemistry. 66, 2816.

Gordon, J.B., Lovell, H.L., de Grijs, Jan, Davie, R.F., 1979. Gold Deposits of Ontario, Part 2: Part of District of Cochrane, Districts of Muskoka, Nipissing, Parry Sound, Sudbury, Timiskaming, and Counties of Southern Ontario. Ontario Geological Survey, Mineral Deposits Circular. 18, 253p.

Hammack, R.W., Edenborn, H.M., 1992. The removal of nickel from mine waters using bacterial sulfate reduction. Applied Microbiology and Biotechnology. 37(5), 674-678.

Hulshof, A.H.M., Blowes, D.W., Ptacek, C.J., Gould, W.D., 2003. Microbial and nutrient investigations into the use of in situ layers for treatment of tailings effluent. Environmental Science and Technology. 37, 5027-5033.

Hulshof, A.H.M., Blowes, D.W., Gould, W.D., 2006. Evaluation of in situ layers for treatment of acid mine drainage: A field comparison. Water Research. 40, 1816-1826.

IAEA/WMO. (2020). Global Network of Isotopes in Precipitation. The GNIP Database. Retrieved from https://nucleus.iaea.org/wiser.

Jones, G.E., Starkey, R.L., 1957. Fractionation of stable isotopes of sulphur my microorganisms and their role in deposition of native sulphur. Applied Microbiology. 5, 111-118.

Jurjovec, J., Ptacek, C.J., Blowes, D.W., 2002. Acid neutralization mechanisms and metal release in mine tailings: A laboratory column experiment. Geochimica et Cosmochimica Acta. 66, 1511-1523.

Kocourkova, E., Sracek, O., Houzar S., Cempirek, J., Losos, Z., Filip, J., Hrselova, P., 2011. Geochemical and mineralogical control on the mobility of arsenic in a waste rock pile at Dlouha Ves, Czech Republic. Journal of Geochemical Exploration. 110, 61-73.

Korte, M.E., Fernando, Q., 1991. A review of arsenic (III) in groundwater. Critical Reviews in Environmental Control. 21, 1-39.

Ledin, M., Pedersen, K., 1996. The environmental impact of mine wastes – Roles of microorganisms and their significance in treatment of mine wastes. Earth-Science Reviews. 41, 67-108

Light, T.S., 1972. Standard solution for redox potential measurements. Analytical Chemistry. 44, 1038-1039.

Lindsay M.B.J., Moncur, M.C., Bain, J.G., Jambor, J.L., Ptacek, C.J., Blowes, D.W., 2015. Geochemical and mineralogical aspects of sulfide mine tailings. Applied Geochemistry. 57, 157-177.

Ludwig, R.D., Smyth, D.J.A., Blowes, D.W., Spink, L.E., Wilkin, R.T., Jewett, D.G., Weisener, C.J., 2009. Treatment of arsenic, heavy metals, and acidity using a mixed ZVI-compost PRB. Environmental Science and Technology. 43, 1970-1976.

Mayer, B., 2005. Assessing sources and transformations of sulfate and nitrate in the hydrosphere using isotope techniques. In: Aggarwal, P.K., Gat, J.R., Froehlich, K.F.O., (Eds.), Isotopes in the Water Cycle: Past, Present and Future of a Developing Science. International Atomic Energy Agency, Springer, Dordrecht, Netherlands, p. 67-89.

McCreadie, H., Blowes, D.W., Ptacek, C.J., Jambor, J.L., 2000. Influence of reduction reactions and solid-phase composition on porewater concentrations of arsenic. Environmental Science and Technology. 34, 3159-3166.

McGeehan, S.L., Naylor, D.V., 1994. Sorption and redox transformations of arsenite and arsenate in two flooded soils. Soil Science Society of America Journal. 58, 337-342.

Miller, G.P., Norman, D.I., Frisch, P.L., 2000. A comment on arsenic species separation using ion exchange. Water Research. 34(4), 1397-1400.

Mirza, B.S., Muruganandam, S., Meng, X., Sorensen, D.L., Dupont, R.R., McLean, J.E., 2014. Arsenic reduction in relation to iron(III) transformation and molecular characterization of the structural and functional microbial community in sediments of a basin-fill aquifer in northern Utah. Applied and Environmental Microbiology. 80(10), 3198-3208.

Mok, W.M., 1994. Mobilization of arsenic in contaminated river waters. In Arsenic in the Environment, Part 1: Cycling and Characterization. Edited by J.O. Nriagu. John Wiley & Sons, New Yourk. Pp. 99-117

Moncur, M.C., Jambor, J.L., Ptacek, C.J., Blowes, D.W., 2009. Mine drainage from the weathering of sulfide minerals and magnetite. Applied Geochemistry. 24, 2362-2373.

Moncur, M.C., Blowes, D.W., Ptacek, C.J., 2013. Pore-water extraction from the unsaturated and saturated zones. Canadian Journal of Earth Sciences. 50, 1051-1058.

Moncur, M.C., Paktunc, D., Birks, S.J., Ptacek, C.J., Welsh, B., Thibault, Y., 2015. Source and distribution of naturally occurring arsenic in groundwater from Alberta's Southern Oil Sands Region. Applied Geochemistry. 62, 171-185.

Moore, J.N., Ficklin, W.H., Johns, C., 1988. Partitioning of arsenic and metals in reducing sulfidic sediments. Environmental Science and Technology. 22, 432-437.

Morin, G., Calas, G., 2006. Arsenic in soils, mine tailings, and former industrial sites. Elements. 2, 97-101.

Murphy, E.M., Davis, S.N., Long, A., Donahue, D., Jull, A.J.T., 1989. Characterization and isotopic composition of organic and inorganic carbon in the Milk River Aquifer. Water Resources Research. 8, 1893-1905.

Nordstrom, D.K., 1977. Thermochemical redox equilibria in Zobell's solution. Geochimica et Cosmochimica Acta. 41, 1835-1841.

Nordstrom, D.K., Alpers, C.N., 1999. Negative pH, efflorescence mineralogy, and consequences for environmental restoration at the Iron Mountain Superfund site. In National Academy of Sciences USA. 96, 3455-3462

Nordstrom, D.K., 2002. Worldwide occurrence of arsenic in ground water. Science. 21, 2143-2145.

Nordstrom, D.K., 2003. Effects of microbiological and geochemical interactions in mine drainage. In: Environmental Aspects of Mine Wastes, Short Course Series Vol. 31, Jambor, J.L., Blowes, D.W., and Ritchie, A.I.M. (Eds.), Mineralogical Association of Canada, Ottawa, 2003. pp. 227–238.

O'Day, P.A., 2006. Chemistry and Mineralogy of Arsenic. Elements. 2, 77-83

Paktunc, D., Foster, A., Heald, S., Laflamme, G., 2004. Speciation and characterization of arsenic in gold ores and cyanidation tailings using X-ray absorption spectroscopy. Geochimica et Cosmochimica Acta. 68, 969-983.

Paktunc, D., Kingston, D., Pratt, A., McMullen, J., 2006. Distribution of gold in pyrite and in products of its transformation resulting from roasting of refractory gold ore. The Canadian Mineralogist. 44, 213-227.

Paktunc, D., 2008. Speciation of arsenic in pyrite by micro-X-ray absorption fine- structure spectroscopy (XAFS). Proc. 9th Int. Cong. App. Mineral. (ICAM2008) 8-10 September 2008, Brisbane, Queensland, Australasian Inst. Mining Metall., 155-158.

Parkhurst, D.L., Appelo, C.A.J., 1999. User's guide to PHREEQC (version 2) - a computer program for speciation, batch-reaction, one-dimensional transport, and inverse geochemical calculations. US Geol. Survey, Water-Resour. Inv. Rep. 99-4259, pp. 312.

Parkhurst, D.L., Appelo, C.A.J., 2013. Description of input and examples for PHREEQC version 3—A computer program for speciation, batch-reaction, one-dimensional transport, and inverse geochemical calculations. U.S. Geological Survey Techniques and Methods, Book 6, Chapter A43, 497.

Pucko, T., Verbovsek, T., 2015. Comparison of hydraulic conductivities by grain-size analysis, pumping, and slug tests in Quaternary gravels, NE Slovenia. Open Geosciences. 7, 308-317.

Ravel, B., Newville, M., 2005. ATHENA, ARTEMIS, HEPHAESTUS: data analysis for X-ray absorption spectroscopy using IFEFFIT. Journal of Synchrotron Radiation. 12(4), 537-541.

Raven, K.P., Jain, A., Loeppert, R.H., 1998. Arsenite and arsenate adsorption on ferrihydrite: Kinetics, equilibrium, and adsorption envelopes. Environmental Science and Technology. 32, 344-349.

Romero, F.M., Armienta, M.A., Carrillo-Chavez, A., 2004. Arsenic sorption by carbonate-rich aquifer material, a control on arsenic mobility at Zimapan, Mexico. Environmental Contamination and Toxicology. 47, 1-13.

Saunders, J.A., Pritchett, M.A., Cook, R.B., 1997. Geochemistry of biogenic pyrite and ferromanganese coatings from a small watershed: a bacterial connection? Geomicrobiology. 14, 203-217.

Savage, K.S., Tingle, T.N., O'Day, P.A., Waychunas, G.A., Bird, D.K., 2000. Arsenic speciation in pyrite and secondary weathering phases, Mother Lode gold district, Tuolumne County, California. Applied Geochemistry. 15, 1219-1244.

Smedley, P.L., Kinniburgh, D.G., 2002. A review of the source, behaviour and distribution of arsenic in natural waters. Applied Geochemistry. 17, 517-568.

Smedley, P.L., Kinniburgh, D.G., 2005. Arsenic in groundwater and the environment. *In* Essentials of Medical Geology. British Geological Survey. pp. 263-299.

Spangenberg, J.E., Dold, B., Vogt, M.L., Pfeifer, H,R., Stable hydrogen and oxygen isotope composition of waters from mine tailings in different climatic environments. Environmental Science and Technology. 41, 1870-1876.

Starr, R.C., Ingleton, R.A., 1992. A new method for collecting core samples without a drill rig. Groundwater Monitoring & Remediation. 12, 91-95.

Walker, S.R., Parsons, M.B., Jamieson, H.E., Lanzirotti, A., 2009. Arsenic mineralogy of near-surface tailings and soils: influences on arsenic mobility and bioaccessibility in the Nova Scotia gold mining districts. The Canadian Mineralogist. 47, 533-556.

Wang, S., Mulligan, C.N., 2009. Effect of natural organic matter on arsenic mobilization from mine tailings. Journal of Hazardous Materials. 168, 721-726.

Waybrant, K.R., Blowes, D.W., Ptacek, C.J., 1998. Selection of reactive mixtures for use in permeable reactive walls for treatment of mine drainage. Environmental Science and Technology. 32, 1972-1979.

Williams, M., 2001. Arsenic in mine waters: an international study. Environmental Geology. 40, 267-278.

Wunderly, M.D., Blowes, D.W., Frind, E.O., Ptacek, C.J., 1996. Sulfide mineral oxidation and subsequent reactive transport of oxidation products in mine tailings impoundments: a numerical model. Water Resources Research. 32, 3173-3187.

Appendix A: Geochemistry

Table A.1 Summary of general chemistry from December 2016.

Location	Depth (m)	Date	pH	E_h (mV)	Alk (mg L^{-1} as $CaCO_3$)	EC (mS/cm)
LL01-1E	0.3	5-Dec-2016	3.14	517		6.60
LL01-1E	0.5	5-Dec-2016	3.92	253		5.37
LL01-1E	0.85	5-Dec-2016	1.77	546		12.9
LL01-1E	0.85	6-Dec-2016	1.64	541		
LL01-1E	1.27	5-Dec-2016	4.11	268		1.28
LL01-1E	1.6	5-Dec-2016	4.12	180		2.27
LL01-1E	1.97	5-Dec-2016	4.28	149		3.33
LL01-1E	3	5-Dec-2016	6.30	0	49	2.08
LL01-1E	3.89	5-Dec-2016	5.82	58	42	4.46
LL01-1E	4.9	5-Dec-2016	5.88	137	38	6.30
LL03-1E	0.3	5-Dec-2016	3.14	517		6.60
LL03-1E	0.3	6-Dec-2016	2.91	517		7.10
LL03-1E	0.5	5-Dec-2016	3.92	253		5.37
LL03-1E	0.5	6-Dec-2016	3.92	366		6.38
LL03-1E	1	6-Dec-2016	5.65	225	70	5.04
LL03-1E	1.58	6-Dec-2016	5.99	193	64	5.18
LL03-1E	1.86	6-Dec-2016	6.16	194	230	4.92
LL03-1E	2.29	6-Dec-2016	6.09	211	114	3.75
LL03-1E	3	6-Dec-2016	6.56	178	184	1.82
LL03-1E	4.56	6-Dec-2016	6.93	158	157	1.06
LL03-1E	6	6-Dec-2016	6.75	155	105	1.61
LL06-1E	0.47	6-Dec-2016	6.23	208	28	0.62
LL06-1E	1	6-Dec-2016	7.33	103	209	0.45
LL06-1E	1.54	6-Dec-2016	6.89	145	308	0.67
LL06-1E	2	6-Dec-2016	6.65	168	414	1.01
LL06-1E	2.4	6-Dec-2016	6.59	238	324	0.91
LL06-1E	2.9	6-Dec-2016	6.67	232	354	1.08
LL06-1E	4.55	6-Dec-2016	6.11	267	100	0.87
LL07-1E	0.47	7-Dec-2016	2.13	702		10.7
LL07-1E	0.77	7-Dec-2016	1.89	555		13.6
LL07-1E	1.43	7-Dec-2016	4.01	360		6.14
LL07-1E	2.1	7-Dec-2016	5.91	279	78	3.42
LL07-1E	2.96	7-Dec-2016	5.38	333	22	4.52
LL07-1E	5.9	7-Dec-2016	5.8	301	28	3.03

Table A.2 Summary of anion concentrations from December 2016.

Location	Depth (m)	Date	Aqueous Concentration (mg L^{-1})						
			Fluoride	**Chloride**	**Nitrite**	**Bromide**	**Nitrate**	**Phosphate**	**Sulfate**
LL01-1E	0.85	6-Dec-2016	0.45	17.30	< 0.2	< 0.2	< 0.2	< 0.2	7957.54
LL01-1E	1.27	5-Dec-2016	< 0.2	9.46	< 0.2	< 0.2	< 0.2	< 0.2	754.56
LL01-1E	1.6	5-Dec-2016	< 0.2	2.04	< 0.2	< 0.2	< 0.2	< 0.2	1727.68
LL01-1E	1.97	5-Dec-2016	1.36	1.68	< 0.2	< 0.2	< 0.2	< 0.2	2948.55
LL01-1E	3	5-Dec-2016	1.81	0.84	< 0.2	< 0.2	< 0.2	< 0.2	1388.47
LL01-1E	3.89	5-Dec-2016	< 0.2	3.40	< 0.2	< 0.2	< 0.2	< 0.2	3765.67
LL01-1E	4.9	5-Dec-2016	< 0.2	6.02	< 0.2	< 0.2	< 0.2	< 0.2	6336.35
LL03-1E	0.5	5-Dec-2016	3.31	6.78	< 0.2	< 0.2	< 0.2	< 0.2	5782.45
LL03-1E	0.5	6-Dec-2016	3.69	7.62	< 0.2	< 0.2	< 0.2	< 0.2	6293.47
LL03-1E	1	6-Dec-2016	0.86	5.15	< 0.2	< 0.2	< 0.2	< 0.2	4834.99
LL03-1E	1.58	6-Dec-2016	0.25	5.10	< 0.2	< 0.2	< 0.2	< 0.2	3750.50
LL03-1E	1.86	6-Dec-2016	< 0.2	4.97	< 0.2	< 0.2	< 0.2	< 0.2	4005.51
LL03-1E	2.29	6-Dec-2016	< 0.2	5.73	< 0.2	< 0.2	< 0.2	< 0.2	2527.28
LL03-1E	3	6-Dec-2016	< 0.2	3.78	< 0.2	< 0.2	< 0.2	< 0.2	993.12
LL03-1E	4.56	6-Dec-2016	< 0.2	3.99	< 0.2	< 0.2	< 0.2	< 0.2	332.06
LL03-1E	6	6-Dec-2016	< 0.2	2.99	< 0.2	< 0.2	< 0.2	< 0.2	840.04
LL06-1E	0.47	6-Dec-2016	< 0.2	0.23	< 0.2	< 0.2	< 0.2	< 0.2	316.12
LL06-1E	1	6-Dec-2016	0.39	0.61	< 0.2	< 0.2	< 0.2	< 0.2	10.77
LL06-1E	1.54	6-Dec-2016	0.20	1.06	< 0.2	< 0.2	< 0.2	< 0.2	2.54
LL06-1E	2	6-Dec-2016	0.08	2.01	< 0.2	< 0.2	< 0.2	< 0.2	0.23
LL06-1E	2.4	6-Dec-2016	< 0.2	2.41	< 0.2	< 0.2	< 0.2	< 0.2	0.95
LL06-1E	2.9	6-Dec-2016	0.07	2.93	< 0.2	< 0.2	< 0.2	< 0.2	17.33
LL06-1E	4.55	6-Dec-2016	< 0.2	1.17	< 0.2	< 0.2	< 0.2	< 0.2	107.35
LL07-1E	0.47	7-Dec-2016	0.63	43.30	< 0.2	< 0.2	< 0.2	< 0.2	3147.62
LL07-1E	0.77	7-Dec-2016	1.45	7.82	< 0.2	< 0.2	< 0.2	2.58	4414.89
LL07-1E	1.43	7-Dec-2016	3.31	8.23	< 0.2	< 0.2	< 0.2	< 0.2	7386.35
LL07-1E	2.1	7-Dec-2016	1.05	2.64	< 0.2	< 0.2	< 0.2	< 0.2	2573.56
LL07-1E	2.96	7-Dec-2016	1.22	3.94	< 0.2	< 0.2	< 0.2	< 0.2	2658.25
LL07-1E	5.9	7-Dec-2016	< 0.2	3.14	< 0.2	< 0.2	< 0.2	< 0.2	1562.96

Table A.3 Summary of cation and metal concentrations from December 2016.

Location	Depth (m)	Date	Aqueous Concentration (mg L^{-1})							
			Al	**As**	**B**	**Ca**	**Cd**	**Co**	**Cr**	**Cu**
LL01-1E	0.85	05-Dec-16	120.9	152.5	1.04	38.79	0.0018	2.55	0.281	41.81
LL01-1E	0.85	06-Dec-16	117.2	196.4	1.35	36.24	0.0016	3.07	0.300	39.98
LL01-1E	1.27	05-Dec-16	31.47	54.26	0.06	56.21	0.0010	2.43	0.020	4.317
LL01-1E	1.6	05-Dec-16	43.03	208.0	0.03	346.3	0.0031	2.31	0.035	0.257
LL01-1E	1.97	05-Dec-16	72.53	479.6	0.03	458.7	0.0025	5.21	0.045	0.051
LL01-1E	3	05-Dec-16	0.36	266.6	0.03	219.5	0.0001	2.08	0.011	0.009
LL01-1E	3.89	05-Dec-16	0.07	105.2	0.94	447.3	< 0.0001	0.82	0.001	0.003
LL01-1E	4.9	05-Dec-16	0.10	96.97	1.52	479.8	0.0002	1.44	0.003	0.004
LL03-1E	0.3	06-Dec-16	210.6	196.4	1.36	397.7	0.0119	10.2	0.860	4.14
LL03-1E	0.5	05-Dec-16	75.44	297.3	1.25	372.5	0.0044	8.53	0.045	3.59
LL03-1E	0.5	06-Dec-16	79.05	346.6	1.33	413.2	0.0045	9.14	0.063	0.925
LL03-1E	1	06-Dec-16	0.96	331.0	1.09	403.5	0.0003	5.90	0.004	0.013
LL03-1E	1.58	06-Dec-16	0.08	95.42	0.82	429.6	0.0001	1.17	0.006	0.004
LL03-1E	1.86	06-Dec-16	0.03	4.14	0.76	434.7	< 0.0001	0.10	0.002	0.004
LL03-1E	2.29	06-Dec-16	0.07	3.49	0.05	342.7	0.0004	0.28	0.005	0.007
LL03-1E	3	06-Dec-16	< 0.005	1.95	0.03	190.7	0.0001	0.13	0.002	0.002
LL03-1E	4.56	06-Dec-16	< 0.001	0.86	0.05	104.5	< 0.0001	0.12	0.001	0.005
LL03-1E	6	06-Dec-16	0.04	14.44	0.06	168.4	0.0001	0.38	0.001	0.002
LL06-1E	0.47	06-Dec-16	0.03	69.33	0.02	43.64	0.0001	0.20	0.002	0.016
LL06-1E	1	06-Dec-16	< 0.005	89.10	0.01	69.38	0.0001	0.01	0.001	0.003
LL06-1E	1.54	06-Dec-16	< 0.001	37.57	0.02	80.63	< 0.0001	0.01	0.001	0.003
LL06-1E	2	06-Dec-16	0.01	11.16	0.04	112.3	< 0.0001	0.01	0.002	0.002
LL06-1E	2.4	06-Dec-16	0.04	0.80	0.02	95.96	< 0.0001	0.01	0.002	0.003
LL06-1E	2.9	06-Dec-16	< 0.005	2.75	0.02	77.61	0.0001	0.01	0.002	0.001
LL06-1E	4.55	06-Dec-16	0.04	7.74	0.04	65.43	0.0002	0.03	0.002	0.035
LL07-1E	0.47	07-Dec-17	94.00	30.49	0.18	46.02	0.0031	1.84	0.087	24.65
LL07-1E	0.77	07-Dec-17	36.01	606.4	0.79	23.03	0.0016	5.18	0.199	4.89
LL07-1E	1.43	07-Dec-17	315.2	619.7	1.61	71.74	0.0282	11.7	0.437	0.006
LL07-1E	2.1	07-Dec-17	0.78	13.31	0.07	214.3	0.0001	2.88	0.002	0.004
LL07-1E	2.96	07-Dec-17	1.34	37.04	0.05	374.2	0.0001	1.52	0.002	0.003
LL07-1E	5.9	07-Dec-17	0.25	114.5	0.10	134.1	0.0002	2.34	0.008	0.005

Table A.3 Continued.

Location	Depth (m)	Date	Aqueous Concentration (mg L^{-1})							
			Fe	**K**	**Li**	**Mg**	**Mn**	**Na**	**Ni**	**Pb**
LL01-1E	0.85	05-Dec-16	1580	17.25	0.174	10.75	1.23	50.01	4.17	0.5797
LL01-1E	0.85	06-Dec-16	2170	15.21	0.112	11.26	0.99	57.33	5.28	1.3740
LL01-1E	1.27	05-Dec-16	130.3	4.71	0.056	16.79	0.75	22.00	1.62	0.0008
LL01-1E	1.6	05-Dec-16	214.8	3.01	0.011	18.91	0.38	17.34	1.77	0.0217
LL01-1E	1.97	05-Dec-16	461.9	5.06	0.045	31.61	0.67	19.65	4.24	0.0585
LL01-1E	3	05-Dec-16	383.7	5.15	0.056	21.28	1.62	11.55	0.48	0.0016
LL01-1E	3.89	05-Dec-16	1161	10.58	0.048	68.86	4.39	25.09	0.47	0.0003
LL01-1E	4.9	05-Dec-16	2124	6.99	0.117	159.6	17.34	58.11	2.13	0.0005
LL03-1E	0.3	06-Dec-16	1678	19.5	0.408	193.9	7.13	41.29	7.86	0.0176
LL03-1E	0.5	05-Dec-16	1662	23.2	0.304	135.8	5.90	46.74	6.11	0.0009
LL03-1E	0.5	06-Dec-16	1844	24.0	0.279	146.9	6.23	47.82	6.50	0.0008
LL03-1E	1	06-Dec-16	1456	17.2	0.156	132.9	5.98	47.26	3.38	0.0480
LL03-1E	1.58	06-Dec-16	1086	13.8	0.050	178.5	4.69	58.30	0.41	0.0007
LL03-1E	1.86	06-Dec-16	1032	10.3	0.015	192.5	4.81	58.83	0.04	0.0010
LL03-1E	2.29	06-Dec-16	403.8	4.76	0.014	162.6	2.94	54.15	0.19	0.0010
LL03-1E	3	06-Dec-16	131.7	1.86	0.007	96.73	1.11	39.84	0.09	0.0002
LL03-1E	4.56	06-Dec-16	33.00	1.39	0.007	47.24	0.87	28.82	0.07	0.0002
LL03-1E	6	06-Dec-16	139.7	2.89	0.014	42.15	0.84	27.17	0.25	0.0001
LL06-1E	0.47	06-Dec-16	92.81	4.57	0.041	7.95	0.42	10.89	0.277	0.0002
LL06-1E	1	06-Dec-16	10.35	5.16	0.005	4.96	0.08	7.01	0.006	0.0005
LL06-1E	1.54	06-Dec-16	28.65	3.62	0.004	13.66	0.10	14.21	0.007	0.0005
LL06-1E	2	06-Dec-16	38.07	5.08	0.003	30.03	0.24	28.46	0.004	0.0003
LL06-1E	2.4	06-Dec-16	8.88	4.29	< 0.003	39.67	0.26	34.38	0.010	0.0020
LL06-1E	2.9	06-Dec-16	11.80	0.39	0.004	37.48	0.25	33.26	0.012	0.0004
LL06-1E	4.55	06-Dec-16	14.56	1.33	0.005	27.86	0.18	19.44	0.038	0.0006
LL07-1E	0.47	07-Dec-17	435.5	18.3	0.139	8.52	1.84	46.04	1.59	0.0149
LL07-1E	0.77	07-Dec-17	1144	6.56	0.137	32.03	0.60	15.94	4.20	0.2566
LL07-1E	1.43	07-Dec-17	2342	11.1	0.191	57.95	1.05	20.83	9.35	0.0366
LL07-1E	2.1	07-Dec-17	805.4	5.37	0.037	84.98	12.27	25.69	1.66	0.0004
LL07-1E	2.96	07-Dec-17	243.5	3.39	0.070	228.9	28.58	44.95	1.18	0.0014
LL07-1E	5.9	07-Dec-17	439.2	4.00	0.058	72.19	5.67	24.20	1.85	0.0007

Table A.3 Continued.

Location	Depth (m)	Date	Aqueous Concentration (mg L^{-1})								
			S	**Sb**	**Se**	**Si**	**Sr**	**Ti**	**Tl**	**V**	**Zn**
LL01-1E	0.85	05-Dec-16	1510	0.0020	< 1	50.77	< 1	1.77	< 2	0.67	2.64
LL01-1E	0.85	06-Dec-16	1928	0.0024	< 1	53.07	< 1	1.62	< 2	< 0.2	1.87
LL01-1E	1.27	05-Dec-16	197.3	0.0017	< 1	45.41	< 1	< 0.1	< 2	< 0.2	1.83
LL01-1E	1.6	05-Dec-16	478.5	0.0010	< 1	46.64	< 1	< 0.1	< 2	< 0.2	0.39
LL01-1E	1.97	05-Dec-16	769.8	0.0040	< 1	27.66	< 1	< 0.1	< 2	< 0.2	0.68
LL01-1E	3	05-Dec-16	385.5	0.0022	< 1	15.53	< 0.3	< 0.1	< 2	< 0.2	0.13
LL01-1E	3.89	05-Dec-16	1036	0.0006	< 1	24.93	< 1	< 0.1	< 2	< 0.2	0.39
LL01-1E	4.9	05-Dec-16	1690	0.0033	< 1	25.38	< 1	< 0.1	< 2	< 0.4	0.60
LL03-1E	0.3	06-Dec-16	1820	0.0014	< 1	55.70	< 1	< 0.3	< 2	< 0.2	5.18
LL03-1E	0.5	05-Dec-16	1479	0.0010	< 1	44.68	< 1	< 0.1	< 2	< 0.2	3.33
LL03-1E	0.5	06-Dec-16	1623	0.0010	< 1	46.88	< 1	< 0.1	< 2	< 0.2	3.52
LL03-1E	1	06-Dec-16	1254	0.0005	< 1	19.58	< 1	< 0.1	< 2	< 0.2	0.81
LL03-1E	1.58	06-Dec-16	1100	0.0033	< 1	21.85	< 1	< 0.1	< 2	< 0.4	1.25
LL03-1E	1.86	06-Dec-16	1076	0.0011	< 1	15.72	0.90	< 0.1	< 2	< 0.4	0.37
LL03-1E	2.29	06-Dec-16	670.8	0.0006	< 1	16.87	< 1	< 0.1	< 2	< 0.4	0.83
LL03-1E	3	06-Dec-16	290.4	0.0003	< 1	16.54	< 1	< 0.1	< 2	< 0.4	0.82
LL03-1E	4.56	06-Dec-16	104.5	0.0068	< 1	11.43	< 1	< 0.1	< 2	< 0.2	0.50
LL03-1E	6	06-Dec-16	232.5	0.0023	< 1	10.96	< 0.3	< 0.1	< 2	< 0.2	0.45
LL06-1E	0.47	06-Dec-16	91.44	0.0015	< 1	17.85	< 0.3	< 0.1	< 2	< 0.2	0.36
LL06-1E	1	06-Dec-16	5.14	0.0008	< 1	8.13	< 0.3	< 0.1	< 2	< 0.2	0.04
LL06-1E	1.54	06-Dec-16	2.52	0.0004	< 1	15.91	< 0.3	< 0.1	< 2	< 0.2	0.04
LL06-1E	2	06-Dec-16	2.51	0.0004	< 1	18.41	< 1	< 0.1	< 2	< 0.2	0.03
LL06-1E	2.4	06-Dec-16	2.66	0.0005	< 1	10.68	< 1	< 0.1	< 2	< 0.2	0.07
LL06-1E	2.9	06-Dec-16	6.86	0.0007	< 1	20.03	< 1	< 0.1	< 2	< 0.2	0.05
LL06-1E	4.55	06-Dec-16	36.44	0.0018	< 1	17.40	< 0.3	< 0.1	< 2	< 0.2	0.10
LL07-1E	0.47	07-Dec-17	685.8	0.0016	< 1	59.15	1.23	0.50	< 2	< 0.2	2.83
LL07-1E	0.77	07-Dec-17	1050	0.0041	< 1	55.62	< 0.3	0.55	< 2	< 0.2	1.01
LL07-1E	1.43	07-Dec-17	1823	0.0014	< 1	93.57	< 0.3	< 0.1	< 2	< 0.2	3.37
LL07-1E	2.1	07-Dec-17	670.1	0.0006	< 1	11.58	< 1	< 0.1	< 2	< 0.2	0.27
LL07-1E	2.96	07-Dec-17	724.2	0.0012	< 1	25.88	< 1	< 0.1	< 2	0.42	5.22
LL07-1E	5.9	07-Dec-17	416.5	0.0011	< 1	21.21	< 1	< 0.1	< 2	< 0.4	1.42

Table A.3 Continued.

Location	Depth (m)	Date	Aqueous Concentration (µg L^{-1})							
			Be	**P**	**Mo**	**Ag**	**Sn**	**Cs**	**Ba**	**U**
LL01-1E	0.85	05-Dec-16	4.35	5054	169.4	1.09	6.89	< 0.06	33.46	65.38
LL01-1E	0.85	06-Dec-16	2.77	4579	143.6	0.59	6.28	< 0.06	20.73	42.34
LL01-1E	1.27	05-Dec-16	1.17	< 70	15.68	2.82	4.05	< 0.06	64.67	5.07
LL01-1E	1.6	05-Dec-16	0.81	< 200	1.51	3.22	4.82	< 0.06	13.49	4.09
LL01-1E	1.97	05-Dec-16	1.81	< 70	6.42	39.47	4.61	< 0.06	12.61	7.75
LL01-1E	3	05-Dec-16	< 0.16	< 70	4.12	26.14	< 3	< 0.06	8.84	0.34
LL01-1E	3.89	05-Dec-16	< 0.16	< 70	2.23	2.18	7.70	< 0.06	12.25	0.11
LL01-1E	4.9	05-Dec-16	< 0.5	< 70	13.79	1.92	< 3	< 0.06	10.08	0.47
LL03-1E	0.3	06-Dec-16	6.47	< 70	14.90	2.27	< 3	< 0.06	27.09	141.00
LL03-1E	0.5	05-Dec-16	2.31	< 70	7.13	15.13	8.01	< 0.06	38.68	6.65
LL03-1E	0.5	06-Dec-16	2.42	< 70	3.87	2.06	< 3	< 0.06	10.41	4.39
LL03-1E	1	06-Dec-16	< 0.5	< 70	0.50	1.75	2.85	< 0.06	3.21	0.90
LL03-1E	1.58	06-Dec-16	< 0.16	< 70	7.26	11.07	< 3	< 0.06	5.38	0.51
LL03-1E	1.86	06-Dec-16	< 0.5	< 70	1.27	2.14	3.26	< 0.06	1.59	1.13
LL03-1E	2.29	06-Dec-16	< 0.5	< 70	0.71	5.71	6.93	< 0.06	1.68	0.63
LL03-1E	3	06-Dec-16	< 0.16	< 70	0.53	0.52	5.25	< 0.06	3.06	0.84
LL03-1E	4.56	06-Dec-16	< 0.16	< 70	10.60	0.86	4.15	< 0.06	6.70	2.46
LL03-1E	6	06-Dec-16	< 0.16	< 70	3.60	0.66	8.97	< 0.06	5.59	1.51
LL06-1E	0.47	06-Dec-16	< 0.16	< 70	27.95	< 0.3	8.11	< 0.06	18.87	0.06
LL06-1E	1	06-Dec-16	< 0.16	< 70	5.38	0.80	< 3	< 0.06	5.78	1.72
LL06-1E	1.54	06-Dec-16	< 0.16	< 70	1.62	10.54	< 3	< 0.06	12.66	0.49
LL06-1E	2	06-Dec-16	< 0.16	< 70	0.86	0.73	< 0.8	< 0.06	55.51	0.38
LL06-1E	2.4	06-Dec-16	< 0.16	< 70	0.44	1.10	6.10	< 0.06	75.09	0.41
LL06-1E	2.9	06-Dec-16	< 0.16	< 70	0.76	1.03	< 3	< 0.06	17.28	0.96
LL06-1E	4.55	06-Dec-16	< 0.5	< 70	4.58	0.74	6.10	< 0.06	9.41	1.83
LL07-1E	0.47	07-Dec-17	2.34	2713	59.00	3.12	7.61	< 0.06	102.90	41.44
LL07-1E	0.77	07-Dec-17	1.42	4122	33.00	3.02	3.20	< 0.06	27.62	24.53
LL07-1E	1.43	07-Dec-17	3.67	8146	2.34	1.50	5.86	< 0.06	19.81	25.97
LL07-1E	2.1	07-Dec-17	0.53	< 70	0.80	2.71	< 3	< 0.06	16.74	0.39
LL07-1E	2.96	07-Dec-17	< 0.5	< 70	1.49	1.77	< 3	< 0.06	15.43	0.23
LL07-1E	5.9	07-Dec-17	< 0.5	< 70	1.93	7.93	3.24	< 0.06	17.10	0.07

Table A.4 Summary of general chemistry from June 2017.

Location	Depth (m)	Date	pH	E_h (mV)	Alk (mg L^{-1} as $CaCO_3$)	EC (mS/cm)	H_2S (mg L^{-1})
LL01-1E	1.27	14-Jun-17	2.72	385		1.8	
LL01-1E	1.6	14-Jun-17	4.01	465		2.3	
LL01-1E	1.97	14-Jun-17	4.08	477		2.9	
LL01-1E	3	14-Jun-17	6.53	177	55	1.7	
LL01-1E	3.89	14-Jun-17	5.92	231	39	4	
LL01-1E	Steel (4.9)	14-Jun-17	6.02	218	16		
LL03-1E	0.3	15-Jun-17	2.47	614			
LL03-1E	1.58	15-Jun-17	6.06	218	140	4.3	0.006
LL03-1E	1.86	15-Jun-17	6.28	205	107	4	0
LL03-1E	2.29	15-Jun-17	6.38	201	208	2.6	0
LL03-1E	3	15-Jun-17	6.82	185	177	1.6	0.047
LL03-1E	4.56	15-Jun-17	7.6	156	237	0.8	0.039
LL03-1E	6	15-Jun-17	7.54	136	160	0.4	0.112
LL06-1E	0.47	15-Jun-17	6.74	293	71	0.30	
LL06-1E	1	15-Jun-17	7.2	158	150	0.4	0.001
LL06-1E	1.54	16-Jun-17	7.25	183	231	0.9	0.001
LL06-1E	2	16-Jun-17	6.71	218	253	0.9	0.005
LL06-1E	2.4	16-Jun-17	6.62	262	223	0.6	
LL06-1E	2.9	16-Jun-17	6.85	199	233	0.7	0.009
LL06-1E	4.55	16-Jun-17	7.42	140	200	0.6	0.06
LL07-1E	0.47	17-Jun-17	2.52	729		1.3	
LL07-1E	0.77	17-Jun-17	2.55	667		1.8	
LL07-1E	1.43	17-Jun-17	3.88	401		3.4	
LL07-1E	2.1	17-Jun-17	6.37	247	40	2	0.005
LL07-1E	2.96	17-Jun-17	5.76	302	37	2.1	
LL0X-1E	Steel	17-Jun-17	7.29	167	147	1.3	

Table A.5 Summary of anion concentrations from June 2017.

Location	Depth (m)	Date	Aqueous Concentration (mg L^{-1})						
			Fluoride	**Chloride**	**Nitrite**	**Bromide**	**Nitrate**	**Phosphate**	**Sulfate**
LL01-1E	1.27	14-Jun-17	0.15	0.35	< 0.2	< 0.4	< 0.2	< 0.4	906.84
LL01-1E	1.6	14-Jun-17	0.25	0.41	< 0.2	< 0.4	< 0.2	< 0.4	1692.26
LL01-1E	1.97	14-Jun-17	1.09	0.56	< 0.2	< 0.4	< 0.2	< 0.4	2357.08
LL01-1E	3	14-Jun-17	2.27	0.53	< 0.2	< 0.4	< 0.2	< 0.4	1061.94
LL01-1E	3.89	14-Jun-17	0.18	1.20	< 0.2	< 0.4	0.18	< 0.4	3500.21
LL01-1E	4.9	14-Jun-17	0.43	2.48	< 0.2	< 0.4	0.24	< 0.4	5427.16
LL03-1E	0.3	15-Jun-17	6.15	2.41	< 0.2	< 0.4	< 0.2	< 0.4	6366.10
LL03-1E	1.58	15-Jun-17	0.30	2.86	< 0.2	< 0.4	< 0.2	< 0.4	3675.55
LL03-1E	1.86	15-Jun-17	< 0.4	2.89	< 0.2	< 0.4	< 0.2	< 0.4	3431.55
LL03-1E	2.29	15-Jun-17	< 0.4	3.12	< 0.2	< 0.4	0.10	< 0.4	1740.96
LL03-1E	3	15-Jun-17	0.20	3.26	< 0.2	< 0.4	0.18	< 0.4	753.74
LL03-1E	4.56	15-Jun-17	0.17	2.57	< 0.2	< 0.4	< 0.2	< 0.4	164.61
LL03-1E	6	15-Jun-17	0.17	1.58	< 0.2	< 0.4	< 0.2	< 0.4	7.88
LL06-1E	0.47	15-Jun-17	0.30	0.36	< 0.2	< 0.4	< 0.2	< 0.4	72.18
LL06-1E	1	15-Jun-17	0.38	0.31	< 0.2	< 0.4	< 0.2	< 0.4	1.64
LL06-1E	1.54	16-Jun-17	0.19	0.57	< 0.2	< 0.4	< 0.2	< 0.4	32.31
LL06-1E	2	16-Jun-17	0.12	0.80	< 0.2	< 0.4	< 0.2	< 0.4	0.38
LL06-1E	2.4	16-Jun-17	< 0.4	1.11	< 0.2	< 0.4	< 0.2	< 0.4	0.73
LL06-1E	2.9	16-Jun-17	0.13	1.77	< 0.2	< 0.4	< 0.2	< 0.4	2.00
LL06-1E	4.55	16-Jun-17	0.16	1.07	< 0.2	< 0.4	< 0.2	< 0.4	48.93
LL07-1E	0.47	17-Jun-17	< 0.4	0.36	< 0.2	< 0.4	0.68	< 0.4	308.30
LL07-1E	0.77	17-Jun-17	< 0.4	0.32	< 0.2	< 0.4	0.12	< 0.4	721.04
LL07-1E	1.43	17-Jun-17	2.89	0.75	< 0.2	< 0.4	< 0.2	< 0.4	4249.53
LL07-1E	2.1	17-Jun-17	0.72	1.26	< 0.2	< 0.4	< 0.2	< 0.4	1679.26
LL07-1E	2.96	17-Jun-17	0.28	3.00	< 0.2	< 0.4	0.13	< 0.4	1755.23
LL07-1E	5.9	17-Jun-17	< 0.4	2.58	< 0.2	< 0.4	0.60	< 0.4	510.68

Table A.6 Summary of cation and metal concentrations from June 2017.

Location	Depth (m)	Date	Aqueous Concentration (mg L^{-1})							
			Al	**As**	**B**	**Ca**	**Cd**	**Co**	**Cr**	**Cu**
LL01-1E	1.27	14-Jun-17	44.35	84.87	0.02	37.77	0.0011	2.52	0.096	0.283
LL01-1E	1.6	14-Jun-17	47.93	210.1	0.02	399.6	0.0015	1.92	0.044	0.020
LL01-1E	1.97	14-Jun-17	76.03	406.7	0.02	464.5	0.0005	4.47	0.051	0.007
LL01-1E	3	14-Jun-17	114.2	237.6	0.04	157.2	0.0002	1.92	0.001	0.002
LL01-1E	3.89	14-Jun-17	48.63	65.0	0.03	446.4	0.0001	0.56	0.002	0.003
LL01-1E	4.9	14-Jun-17	7.74	63.52	0.03	441.2	0.0001	1.06	0.001	0.006
LL03-1E	0.3	15-Jun-17	296.5	83.12	1.13	427.6	0.0157	10.7	1.57	16.62
LL03-1E	1.58	15-Jun-17	0.12	99.72	0.92	468.2	< 0.00004	1.08	0.003	0.005
LL03-1E	1.86	15-Jun-17	0.02	7.44	0.74	446.4	< 0.00004	0.03	0.003	0.001
LL03-1E	2.29	15-Jun-17	0.03	7.05	0.02	286.5	< 0.00004	0.01	0.001	0.002
LL03-1E	3	15-Jun-17	< 0.003	3.68	0.05	207.6	< 0.00004	0.01	0.002	0.001
LL03-1E	4.56	15-Jun-17	< 0.001	6.47	0.06	108.2	< 0.0001	0.01	0.001	0.002
LL03-1E	6	15-Jun-17	0.01	15.04	0.08	54.92	< 0.00004	0.01	0.001	0.002
LL06-1E	0.47	15-Jun-17	< 0.003	105.6	0.02	39.20	< 0.00004	0.12	0.002	0.002
LL06-1E	1	15-Jun-17	0.01	70.92	0.02	64.45	< 0.00004	0.01	0.001	0.002
LL06-1E	1.54	16-Jun-17	0.92	21.00	0.04	109.0	0.0005	0.88	0.002	0.498
LL06-1E	2	16-Jun-17	0.01	5.76	0.05	111.1	0.0006	0.00	0.004	0.002
LL06-1E	2.4	16-Jun-17	0.02	0.24	0.02	27.61	0.0006	0.00	0.002	0.003
LL06-1E	2.9	16-Jun-17	0.01	28.79	0.02	86.83	0.0004	0.01	0.003	0.002
LL06-1E	4.55	16-Jun-17	< 0.003	22.21	0.05	72.93	0.0001	0.01	0.002	0.002
LL07-1E	0.47	17-Jun-17	11.90	0.89	0.02	1.94	0.0002	0.15	0.010	5.09
LL07-1E	0.77	17-Jun-17	8.11	169.9	0.02	2.26	0.0003	3.97	0.017	0.013
LL07-1E	1.43	17-Jun-17	185.7	392.0	0.06	38.78	0.0097	9.16	0.137	0.016
LL07-1E	2.1	17-Jun-17	0.53	8.69	0.07	186.9	< 0.0001	1.32	0.003	0.004
LL07-1E	2.96	17-Jun-17	0.23	3.50	0.03	324.0	< 0.00004	0.27	0.002	0.004
LL07-1E	5.9	17-Jun-17	0.01	19.38	0.12	142.4	< 0.0001	0.01	0.003	0.004

Table A.6 Continued.

Location	Depth (m)	Date	Aqueous Concentration (mg L^{-1})							
			Fe	**K**	**Li**	**Mg**	**Mn**	**Na**	**Ni**	**Pb**
LL01-1E	1.27	14-Jun-17	220.1	3.78	0.007	15.60	0.34	24.57	1.83	0.6394
LL01-1E	1.6	14-Jun-17	196.0	3.71	0.011	18.68	0.44	21.57	1.45	0.0103
LL01-1E	1.97	14-Jun-17	348.8	5.28	0.038	25.91	0.57	18.26	3.63	0.0037
LL01-1E	3	14-Jun-17	351.55	5.98	0.051	19.08	1.46	11.09	0.35	0.0003
LL01-1E	3.89	14-Jun-17	1140	6.16	0.052	73.22	4.49	24.88	0.24	0.0006
LL01-1E	4.9	14-Jun-17	1827	5.99	0.120	213.5	23.15	68.36	2.97	0.0006
LL03-1E	0.3	15-Jun-17	1395	9.11	0.379	193.5	7.00	30.88	8.51	0.0406
LL03-1E	1.58	15-Jun-17	1017	13.8	0.046	188.2	4.56	60.06	0.37	0.0003
LL03-1E	1.86	15-Jun-17	1013	9.76	0.011	194.1	4.62	59.30	0.01	0.0001
LL03-1E	2.29	15-Jun-17	305.1	2.59	0.004	158.2	2.64	47.46	0.01	0.0002
LL03-1E	3	15-Jun-17	47.45	0.93	0.010	106.1	0.66	36.55	0.002	0.0003
LL03-1E	4.56	15-Jun-17	9.66	1.51	0.008	46.46	0.89	26.13	0.004	0.0007
LL03-1E	6	15-Jun-17	3.72	1.29	0.004	17.94	0.15	20.73	0.01	0.0002
LL06-1E	0.47	15-Jun-17	7.80	4.51	0.019	4.74	0.23	8.89	0.120	0.0002
LL06-1E	1	15-Jun-17	6.65	4.65	0.008	4.27	0.05	5.50	0.003	0.0005
LL06-1E	1.54	16-Jun-17	92.99	5.09	0.035	26.77	0.61	17.23	0.677	0.0011
LL06-1E	2	16-Jun-17	44.35	4.49	0.004	30.82	0.30	28.23	0.002	0.0008
LL06-1E	2.4	16-Jun-17	2.56	1.26	< 0.0008	11.24	0.08	8.93	0.004	0.0009
LL06-1E	2.9	16-Jun-17	33.22	0.38	0.005	40.16	0.36	30.60	0.002	0.0007
LL06-1E	4.55	16-Jun-17	9.57	1.21	0.007	30.41	0.41	17.63	0.002	0.0006
LL07-1E	0.47	17-Jun-17	23.61	2.04	0.006	0.21	0.03	5.27	0.11	0.0044
LL07-1E	0.77	17-Jun-17	241.70	1.53	0.003	0.82	0.04	5.61	1.78	0.0500
LL07-1E	1.43	17-Jun-17	1726	5.98	0.192	54.62	0.77	25.23	7.08	0.0059
LL07-1E	2.1	17-Jun-17	500.7	4.28	0.032	78.72	10.81	22.36	0.73	0.0008
LL07-1E	2.96	17-Jun-17	23.32	2.49	0.049	202.1	21.19	39.81	0.24	0.0003
LL07-1E	5.9	17-Jun-17	15.27	2.14	0.010	71.12	2.61	19.79	0.02	0.0011

Table A.6 Continued.

Location	Depth (m)	Date	Aqueous Concentration (mg L^{-1})								
			S	**Sb**	**Se**	**Si**	**Sr**	**Ti**	**Tl**	**V**	**Zn**
LL01-1E	1.27	14-Jun-17	274.0	0.0011	< 1	47.62	< 0.3	< 0.1	< 2	< 0.2	0.17
LL01-1E	1.6	14-Jun-17	514.2	0.0009	< 1	42.06	< 1	< 0.1	< 2	< 0.4	0.16
LL01-1E	1.97	14-Jun-17	675.2	0.0009	< 1	27.19	< 1	< 0.1	< 2	0.57	0.47
LL01-1E	3	14-Jun-17	320.0	0.0006	< 1	14.02	< 0.3	< 0.1	< 2	< 0.2	0.12
LL01-1E	3.89	14-Jun-17	1025	0.0005	< 1	21.05	< 1	< 0.3	< 2	< 0.2	0.12
LL01-1E	4.9	14-Jun-17	1503	0.0006	< 1	15.97	< 1	< 0.3	< 2	< 0.2	0.54
LL03-1E	0.3	15-Jun-17	1883	0.0013	< 1	57.21	< 0.3	0.58	< 2	0.98	4.49
LL03-1E	1.58	15-Jun-17	1028	0.0003	< 1	19.73	< 1	< 0.1	< 2	< 0.2	0.42
LL03-1E	1.86	15-Jun-17	1035	< 0.00018	< 1	14.47	< 1	< 0.1	< 2	< 0.2	0.03
LL03-1E	2.29	15-Jun-17	526.4	0.0002	< 1	13.12	< 1	< 0.1	< 2	< 0.2	0.15
LL03-1E	3	15-Jun-17	248.0	0.0007	< 1	15.04	< 1	< 0.1	< 2	< 0.2	0.07
LL03-1E	4.56	15-Jun-17	56.06	0.0005	< 1	11.44	< 1	< 0.1	< 2	< 0.2	0.03
LL03-1E	6	15-Jun-17	4.86	0.0004	< 1	8.54	< 0.3	< 0.1	< 2	< 0.2	0.05
LL06-1E	0.47	15-Jun-17	23.54	0.0008	< 1	20.50	< 0.3	< 0.1	< 2	< 0.2	0.30
LL06-1E	1	15-Jun-17	1.96	0.0002	< 1	9.04	< 0.3	< 0.1	< 2	< 0.2	0.07
LL06-1E	1.54	16-Jun-17	138.9	< 0.00018	< 1	17.27	< 0.3	< 0.1	< 2	< 0.2	0.46
LL06-1E	2	16-Jun-17	2.52	0.0009	< 1	17.45	< 1	< 0.1	< 2	< 0.2	0.13
LL06-1E	2.4	16-Jun-17	1.00	0.0007	< 1	2.99	< 0.3	< 0.1	< 2	< 0.2	0.13
LL06-1E	2.9	16-Jun-17	2.56	0.0004	< 1	17.27	< 1	< 0.1	< 2	< 0.2	0.08
LL06-1E	4.55	16-Jun-17	15.18	0.0004	< 1	15.69	< 0.3	< 0.1	< 2	< 0.2	0.15
LL07-1E	0.47	17-Jun-17	95.4	0.0004	< 1	54.17	< 0.3	< 0.3	< 2	< 0.2	0.13
LL07-1E	0.77	17-Jun-17	218.0	0.0032	< 1	51.67	< 0.3	< 0.1	< 2	< 0.2	0.20
LL07-1E	1.43	17-Jun-17	1293	0.0009	< 1	57.39	< 0.3	< 0.1	< 2	0.93	3.53
LL07-1E	2.1	17-Jun-17	477.8	0.0006	< 1	10.12	< 1	< 0.1	< 2	< 0.2	0.13
LL07-1E	2.96	17-Jun-17	534.3	0.0014	< 1	15.80	< 1	< 0.1	< 2	< 0.2	0.55
LL07-1E	5.9	17-Jun-17	166.8	0.0004	< 1	5.26	< 1	< 0.1	< 2	< 0.2	0.07

Table A.6 Continued.

Location	Depth (m)	Date	Aqueous Concentration (µg L^{-1})							
			Be	**P**	**Mo**	**Ag**	**Sn**	**Cs**	**Ba**	**U**
LL01-1E	1.27	14-Jun-17	1.35	427.3	8.35	3.49	15.57	1.29	18.63	8.66
LL01-1E	1.6	14-Jun-17	1.13	435.1	2.71	13.14	19.85	< 0.2	11.60	2.84
LL01-1E	1.97	14-Jun-17	2.01	< 200	1.28	0.71	10.82	0.27	11.27	7.89
LL01-1E	3	14-Jun-17	< 0.5	< 200	6.13	0.74	8.99	< 0.2	7.93	0.10
LL01-1E	3.89	14-Jun-17	< 0.5	< 70	3.55	1.61	22.45	< 0.2	9.25	0.18
LL01-1E	4.9	14-Jun-17	< 0.16	< 70	7.73	2.08	12.72	< 0.2	7.48	1.50
LL03-1E	0.3	15-Jun-17	8.52	< 200	8.48	1.96	17.46	1.00	17.99	265.50
LL03-1E	1.58	15-Jun-17	< 0.16	< 70	1.06	1.41	15.25	< 0.2	5.17	1.32
LL03-1E	1.86	15-Jun-17	< 0.16	< 70	0.38	0.92	12.13	< 0.2	2.88	1.11
LL03-1E	2.29	15-Jun-17	< 0.16	< 70	2.41	0.67	13.45	< 0.2	2.11	1.09
LL03-1E	3	15-Jun-17	< 0.16	< 70	4.03	4.73	13.82	< 0.2	9.40	0.35
LL03-1E	4.56	15-Jun-17	< 0.16	< 70	7.25	1.37	19.83	< 0.2	9.96	3.11
LL03-1E	6	15-Jun-17	< 0.16	< 70	5.52	1.53	62.03	< 0.06	4.03	4.97
LL06-1E	0.47	15-Jun-17	< 0.16	< 70	9.18	0.79	11.92	< 0.2	3.61	0.04
LL06-1E	1	15-Jun-17	< 0.16	< 70	7.00	0.60	13.74	< 0.2	4.30	1.49
LL06-1E	1.54	16-Jun-17	< 0.5	< 70	1.86	1.85	7.74	0.20	24.19	0.60
LL06-1E	2	16-Jun-17	0.66	261.0	1.82	2.56	12.76	< 0.2	98.49	0.14
LL06-1E	2.4	16-Jun-17	0.66	< 70	1.52	0.93	14.48	< 0.06	29.22	0.07
LL06-1E	2.9	16-Jun-17	< 0.5	< 70	1.35	1.23	19.44	< 0.2	162.40	0.40
LL06-1E	4.55	16-Jun-17	< 0.5	< 70	3.58	1.59	26.04	< 0.2	20.23	2.51
LL07-1E	0.47	17-Jun-17	< 0.5	< 70	6.88	0.94	18.46	0.23	36.37	2.92
LL07-1E	0.77	17-Jun-17	< 0.5	< 70	17.06	4.03	19.24	< 0.2	23.31	12.32
LL07-1E	1.43	17-Jun-17	2.50	3033	4.17	2.42	13.00	< 0.2	12.91	10.69
LL07-1E	2.1	17-Jun-17	< 0.5	< 70	3.33	0.96	20.82	< 0.2	12.98	0.23
LL07-1E	2.96	17-Jun-17	< 0.5	< 70	2.39	0.86	14.86	< 0.2	16.17	0.08
LL07-1E	5.9	17-Jun-17	< 0.16	< 200	14.55	0.48	15.60	< 0.06	12.88	3.31

Table A.7 Summary of general chemistry from September 2017.

Location	Depth (m)	Date	pH	E_h (mV)	Alk (mg L^{-1} as $CaCO_3$)	EC (mS/cm)	PO_4^{3-} (mg L^{-1})	NH_3 (mg L^{-1})
LL01-1E	1.27	19-Sep-17	2.88	210		1.7		
LL01-1E	1.6	18-Sep-17	3.96	130		2.1	11.3	0.24
LL01-1E	1.97	18-Sep-17	4.1	99		2.5	3.58	0.18
LL01-1E	3	19-Sep-17	6.35	106	63	1.4	0.8	0.61
LL01-1E	3.89	18-Sep-17	5.82	112	42	4	0.41	0.78
LL01-1E	Steel	18-Sep-17	6.22	106				
LL03-1E	1	19-Sep-17	3.44	174		3.5	1.13	3.83
LL03-1E	1.58	19-Sep-17	6.01	97	75	3.8	1.3	4.88
LL03-1E	1.86	19-Sep-17	6.28	112	309	3.9	0.19	5.99
LL03-1E	2.29	19-Sep-17	6.32	84	267	2.6	0.06	2.71
LL03-1E	3	19-Sep-17	6.79	93	162	1.5	0.05	0.46
LL03-1E	4.56	19-Sep-17	7.37	79	323	0.7	0.52	0.63
LL03-1E	6	19-Sep-17	7.65	71	280	0.6	0.69	0.52
LL06-1E	0.47	20-Sep-17	6.49	148	70	0.3		
LL06-1E	1	20-Sep-17	7.21	130	127.5	0.3	0.14	1.29
LL06-1E	1.54	19-Sep-17	7.39	107	225	0.5	1.11	3.7
LL06-1E	2	19-Sep-17	6.77	141	422.5	0.8	1.09	10.1
LL06-1E	2.4	19-Sep-17	6.67	129	405	0.9	0.07	10.1
LL06-1E	2.9	19-Sep-17	6.69	110	420	0.7	0.06	0.32
LL06-1E	4.55	19-Sep-17	7.34	71	280	0.6	0.13	0.23
LL07-1E	0.47	20-Sep-17	2.65	639		1.5		
LL07-1E	0.77	20-Sep-17	1.98	577		7.2		
LL07-1E	1.43	20-Sep-17	3.94	201		1.6	23.8	0.66
LL07-1E	2.1	20-Sep-17	6.03	156	127	2.1	0.12	2.31
LL07-1E	2.96	20-Sep-17	5.71	191	95	2.4	0.06	0.38
LL07-1E	Steel	20-Sep-17	8.17	124	175	0.9	1.01	0.33

Table A.8 Summary of anion concentrations from September 2017.

Location	Depth (m)	Date	Aqueous Concentration (mg L^{-1})						
			Fluoride	**Chloride**	**Nitrite**	**Bromide**	**Nitrate**	**Phosphate**	**Sulfate**
LL01-1E	1.27	19-Sep-17	0.12	0.27	< 0.4	< 0.4	< 0.4	1.13	880.77
LL01-1E	1.6	18-Sep-17	0.25	0.35	< 0.4	< 0.4	< 0.4	0.92	1605.25
LL01-1E	1.97	18-Sep-17	0.93	0.37	< 0.4	< 0.4	< 0.4	< 0.4	2112.33
LL01-1E	3	19-Sep-17	2.79	0.46	< 0.4	< 0.4	< 0.4	< 0.4	992.95
LL01-1E	3.89	18-Sep-17	0.25	0.77	< 0.4	< 0.4	< 0.4	< 0.4	3476.10
LL01-1E	Steel	18-Sep-17	0.48	1.44	< 0.4	< 0.4	< 0.4	< 0.4	4957.08
LL03-1E	1	19-Sep-17	1.13	1.84	< 0.4	< 0.4	< 0.4	< 0.4	3463.89
LL03-1E	1.58	19-Sep-17	0.44	2.89	< 0.4	< 0.4	< 0.4	< 0.4	3681.75
LL03-1E	1.86	19-Sep-17	0.05	2.95	< 0.4	< 0.4	< 0.4	< 0.4	3440.37
LL03-1E	2.29	19-Sep-17	0.18	3.37	< 0.4	< 0.4	< 0.4	< 0.4	1804.75
LL03-1E	3	19-Sep-17	0.19	3.42	< 0.4	< 0.4	< 0.4	< 0.4	751.47
LL03-1E	4.56	19-Sep-17	0.18	3.18	< 0.4	< 0.4	0.10	< 0.4	169.19
LL03-1E	6	19-Sep-17	0.14	1.54	< 0.4	< 0.4	< 0.4	< 0.4	2.83
LL06-1E	0.47	20-Sep-17	0.49	0.35	< 0.4	< 0.4	< 0.4	< 0.4	48.49
LL06-1E	1	20-Sep-17	0.52	0.37	< 0.4	< 0.4	< 0.4	< 0.4	3.35
LL06-1E	1.54	19-Sep-17	0.20	0.70	< 0.4	< 0.4	< 0.4	< 0.4	1.24
LL06-1E	2	19-Sep-17	0.16	0.97	< 0.4	< 0.4	< 0.4	< 0.4	< 0.4
LL06-1E	2.4	19-Sep-17	0.04	1.47	< 0.4	< 0.4	< 0.4	< 0.4	0.43
LL06-1E	2.9	19-Sep-17	0.15	2.07	< 0.4	< 0.4	< 0.4	< 0.4	< 0.4
LL06-1E	4.55	19-Sep-17	0.22	1.03	< 0.4	< 0.4	< 0.4	< 0.4	48.14
LL07-1E	0.47	20-Sep-17	0.11	1.70	< 0.4	< 0.4	< 0.4	< 0.4	366.36
LL07-1E	0.77	20-Sep-17	0.23	0.37	< 0.4	< 0.4	< 0.4	< 0.4	2936.32
LL07-1E	1.43	20-Sep-17	1.63	0.50	< 0.4	< 0.4	< 0.4	< 0.4	1402.43
LL07-1E	2.1	20-Sep-17	0.94	1.22	< 0.4	< 0.4	< 0.4	< 0.4	1777.15
LL07-1E	2.96	20-Sep-17	0.22	2.57	< 0.4	< 0.4	< 0.4	< 0.4	1767.65
LL07-1E	Steel	20-Sep-17	0.12	1.89	< 0.4	< 0.4	< 0.4	< 0.4	408.51

Table A.9 Summary of cation and metal concentrations from September 2017.

Location	Depth (m)	Date	Aqueous Concentration (mg L^{-1})							
			Al	**As**	**B**	**Ca**	**Cd**	**Co**	**Cr**	**Cu**
LL01-1E	1.27	19-Sep-17	42.54	91.81	< 0.008	35.19	0.0005	2.52	0.063	0.030
LL01-1E	1.6	18-Sep-17	44.48	222.9	< 0.008	353.0	0.0012	2.06	0.050	< 0.00075
LL01-1E	1.97	18-Sep-17	65.18	456.5	< 0.008	504.4	0.0003	3.46	0.049	< 0.00075
LL01-1E	3	19-Sep-17	0.06	239.6	< 0.008	134.8	< 0.00007	1.76	< 0.00033	< 0.00075
LL01-1E	3.89	18-Sep-17	0.07	67.07	0.64	397.8	< 0.00007	0.49	< 0.00033	< 0.00075
LL01-1E	Steel	18-Sep-17	< 0.0025	18.6	1.12	352.8	0.0029	0.50	0.003	< 0.0025
LL03-1E	1	19-Sep-17	2.66	240.4	0.75	354.7	0.0005	5.31	0.003	0.465
LL03-1E	1.58	19-Sep-17	0.04	101.9	0.74	482.0	0.0004	1.15	0.002	< 0.00075
LL03-1E	1.86	19-Sep-17	0.01	6.94	0.63	468.6	< 0.00025	0.03	0.002	< 0.00075
LL03-1E	2.29	19-Sep-17	< 0.007	10.47	< 0.008	283.7	< 0.00025	0.01	< 0.0011	< 0.00075
LL03-1E	3	19-Sep-17	0.01	3.31	< 0.008	189.2	< 0.00007	0.01	< 0.0011	< 0.00075
LL03-1E	4.56	19-Sep-17	< 0.0025	3.12	< 0.026	102.0	< 0.00007	0.00	< 0.00033	< 0.00075
LL03-1E	6	19-Sep-17	< 0.0025	12.88	0.03	54.20	< 0.00007	0.00	< 0.00033	< 0.00075
LL06-1E	0.47	20-Sep-17	0.01	164.3	< 0.008	42.72	< 0.00007	0.05	< 0.00033	< 0.00075
LL06-1E	1	20-Sep-17	< 0.0025	75.32	< 0.008	62.06	< 0.00007	0.01	< 0.00033	< 0.00075
LL06-1E	1.54	19-Sep-17	0.01	9.54	< 0.008	80.55	< 0.00007	0.01	< 0.00033	< 0.00075
LL06-1E	2	19-Sep-17	0.02	4.53	0.03	113.8	0.0093	0.01	0.012	0.007
LL06-1E	2.4	19-Sep-17	0.06	0.25	< 0.008	99.25	0.0034	0.01	0.004	< 0.00075
LL06-1E	2.9	19-Sep-17	< 0.0025	14.37	< 0.008	79.35	0.0020	0.01	0.004	< 0.00075
LL06-1E	4.55	19-Sep-17	< 0.0025	14.7	< 0.026	76.60	0.0012	0.01	< 0.0011	< 0.00075
LL07-1E	0.47	20-Sep-17	12.97	0.80	< 0.008	5.36	0.0008	0.07	0.007	7.86
LL07-1E	0.77	20-Sep-17	32.86	265.5	< 0.008	8.66	0.0008	5.82	0.097	0.032
LL07-1E	1.43	20-Sep-17	92.11	346.0	0.03	18.87	0.0027	2.28	0.063	0.003
LL07-1E	2.1	20-Sep-17	0.54	8.63	0.04	216.1	< 0.00007	1.12	0.002	< 0.00075
LL07-1E	2.96	20-Sep-17	0.25	7.17	< 0.008	334.4	< 0.00007	0.16	< 0.0011	< 0.00075
LL07-1E	Steel	20-Sep-17	< 0.007	15.38	0.04	144.4	< 0.00007	0.00	< 0.00033	< 0.00075

Table A.9 Continued.

Location	Depth (m)	Date	Aqueous Concentration (mg L^{-1})							
			Fe	**K**	**Li**	**Mg**	**Mn**	**Na**	**Ni**	**Pb**
LL01-1E	1.27	19-Sep-17	227.4	3.85	< 0.006	17.49	0.31	24.14	1.86	0.5694
LL01-1E	1.6	18-Sep-17	196.5	3.29	0.010	17.94	0.39	18.73	1.58	0.0110
LL01-1E	1.97	18-Sep-17	286.5	5.90	0.038	23.99	0.48	18.75	2.89	0.0040
LL01-1E	3	19-Sep-17	297.7	5.74	0.046	16.61	1.30	11.13	0.30	< 0.00005
LL01-1E	3.89	18-Sep-17	1072	5.85	0.043	65.27	4.11	23.14	0.14	< 0.00005
LL01-1E	Steel	18-Sep-17	1732	3.19	0.117	185.6	20.23	58.87	0.27	0.0021
LL03-1E	1	19-Sep-17	1112	17.7	0.129	113.5	5.18	43.12	3.10	0.0020
LL03-1E	1.58	19-Sep-17	1148	15.4	0.048	183.8	4.84	61.81	0.38	0.0002
LL03-1E	1.86	19-Sep-17	1034	10.9	0.011	191.6	4.67	61.30	0.01	< 0.00005
LL03-1E	2.29	19-Sep-17	361.5	2.66	< 0.006	161.1	2.56	52.68	0.003	< 0.00005
LL03-1E	3	19-Sep-17	52.65	0.60	0.008	92.95	0.61	33.96	0.006	< 0.00005
LL03-1E	4.56	19-Sep-17	9.99	1.22	< 0.006	42.74	0.86	25.36	0.001	< 0.00005
LL03-1E	6	19-Sep-17	3.02	0.94	< 0.006	19.33	0.16	21.42	0.002	< 0.00005
LL06-1E	0.47	20-Sep-17	4.34	7.91	0.014	5.68	0.09	10.63	0.068	< 0.00005
LL06-1E	1	20-Sep-17	1.38	5.73	0.007	5.13	0.02	8.04	0.003	< 0.00005
LL06-1E	1.54	19-Sep-17	2.06	4.28	< 0.006	13.10	0.04	15.25	0.003	< 0.00005
LL06-1E	2	19-Sep-17	37.61	6.42	< 0.006	31.39	0.27	30.88	0.010	0.0078
LL06-1E	2.4	19-Sep-17	11.49	5.42	< 0.006	40.86	0.26	35.10	0.004	0.0026
LL06-1E	2.9	19-Sep-17	30.06	0.16	< 0.006	36.34	0.32	31.17	0.002	0.0017
LL06-1E	4.55	19-Sep-17	13.49	0.97	< 0.006	31.73	0.49	19.11	0.002	0.0009
LL07-1E	0.47	20-Sep-17	24.77	1.51	< 0.006	1.19	0.10	11.28	0.08	0.0048
LL07-1E	0.77	20-Sep-17	871.3	5.22	< 0.006	4.32	0.16	19.31	3.55	0.2320
LL07-1E	1.43	20-Sep-17	402.1	5.97	0.183	19.81	0.43	14.64	2.15	0.0005
LL07-1E	2.1	20-Sep-17	516.9	7.16	0.030	87.57	11.89	26.50	0.59	< 0.00005
LL07-1E	2.96	20-Sep-17	28.24	1.45	0.043	209.8	22.16	43.92	0.16	< 0.00005
LL07-1E	Steel	20-Sep-17	0.84	1.83	< 0.006	68.54	1.46	20.82	0.00	< 0.00005

Table A.9 Continued.

Location	Depth (m)	Date	Aqueous Concentration (mg L^{-1})								
			S	**Sb**	**Se**	**Si**	**Sr**	**Ti**	**Tl**	**V**	**Zn**
LL01-1E	1.27	19-Sep-17	292.3	0.0011	< 1	52.13	< 0.3	< 0.1	< 2	< 0.2	0.06
LL01-1E	1.6	18-Sep-17	489.7	0.0015	< 1	43.55	< 1	< 0.1	< 2	< 0.4	0.09
LL01-1E	1.97	18-Sep-17	711.1	0.0004	< 1	29.84	< 1	< 0.1	< 2	0.65	0.32
LL01-1E	3	19-Sep-17	285.7	< 0.0005	< 1	14.41	< 0.3	< 0.1	< 2	< 0.2	< 0.0405
LL01-1E	3.89	18-Sep-17	993.5	< 0.00013	< 1	19.94	< 1	< 0.1	< 2	< 0.2	< 0.0125
LL01-1E	Steel	18-Sep-17	1512	0.0028	< 1	12.27	< 1	< 0.1	< 2	< 0.2	0.12
LL03-1E	1	19-Sep-17	1091	0.0007	< 1	18.89	< 1	< 0.1	< 2	< 0.2	0.65
LL03-1E	1.58	19-Sep-17	1267	0.0005	< 1	21.93	0.87	< 0.1	< 2	< 0.2	0.39
LL03-1E	1.86	19-Sep-17	1162	< 0.0005	< 1	15.16	0.99	< 0.1	< 2	< 0.2	< 0.0125
LL03-1E	2.29	19-Sep-17	576.7	< 0.0005	< 1	16.39	< 1	< 0.1	< 2	< 0.2	< 0.0125
LL03-1E	3	19-Sep-17	239.0	< 0.0005	< 1	15.58	< 1	< 0.1	< 2	< 0.2	0.11
LL03-1E	4.56	19-Sep-17	53.84	0.0006	< 1	10.77	< 1	< 0.1	< 2	< 0.2	< 0.0125
LL03-1E	6	19-Sep-17	3.74	< 0.0005	< 1	7.86	< 0.3	< 0.1	< 2	< 0.2	< 0.0125
LL06-1E	0.47	20-Sep-17	15.69	0.0007	< 1	21.18	< 0.3	< 0.1	< 2	< 0.2	< 0.0125
LL06-1E	1	20-Sep-17	2.55	< 0.0005	< 1	10.42	< 0.3	< 0.1	< 2	< 0.2	< 0.0125
LL06-1E	1.54	19-Sep-17	2.39	< 0.0005	< 1	15.31	< 0.3	< 0.1	< 2	< 0.2	< 0.0125
LL06-1E	2	19-Sep-17	2.67	0.0083	< 1	17.85	< 1	< 0.1	< 2	< 0.2	< 0.0125
LL06-1E	2.4	19-Sep-17	2.82	0.0031	< 1	10.13	< 1	< 0.1	< 2	< 0.2	< 0.0125
LL06-1E	2.9	19-Sep-17	2.01	0.0019	< 1	16.92	< 1	< 0.1	< 2	< 0.2	< 0.0125
LL06-1E	4.55	19-Sep-17	18.20	0.0013	< 1	14.30	< 1	< 0.1	< 2	< 0.2	< 0.0125
LL07-1E	0.47	20-Sep-17	116.7	0.0007	< 1	56.46	< 0.3	< 0.1	< 2	< 0.2	0.07
LL07-1E	0.77	20-Sep-17	933.5	0.0028	< 1	60.78	< 0.3	0.49	< 2	< 0.2	0.09
LL07-1E	1.43	20-Sep-17	423.3	0.0008	< 1	54.13	< 0.3	< 0.1	< 2	0.50	1.72
LL07-1E	2.1	20-Sep-17	548.9	< 0.0005	< 1	11.44	< 1	< 0.1	< 2	< 0.2	< 0.0125
LL07-1E	2.96	20-Sep-17	575.9	< 0.0005	< 1	16.14	< 1	< 0.1	< 2	< 0.2	0.11
LL07-1E	Steel	20-Sep-17	150.2	< 0.00013	< 1	4.55	< 1	< 0.1	< 2	< 0.2	< 0.0125

Table A.9 Continued.

Location	Depth (m)	Date	Aqueous Concentration (µg L^{-1})							
			Be	**P**	**Mo**	**Ag**	**Sn**	**Cs**	**Ba**	**U**
LL01-1E	1.27	19-Sep-17	< 1.25	< 500	10.16	< 0.75	< 1.7	1.82	14.44	7.70
LL01-1E	1.6	18-Sep-17	< 1.25	< 500	2.35	< 0.25	< 6.5	< 0.15	8.15	3.75
LL01-1E	1.97	18-Sep-17	1.74	< 150	1.12	< 0.75	< 1.7	< 0.15	13.55	8.99
LL01-1E	3	19-Sep-17	< 0.4	< 150	1.90	< 0.75	< 1.7	< 0.15	7.84	0.12
LL01-1E	3.89	18-Sep-17	< 0.4	< 150	< 0.8	< 0.25	< 1.7	< 0.15	8.11	0.10
LL01-1E	Steel	18-Sep-17	2.01	< 150	6.93	2.75	< 1.7	< 0.15	11.63	1.61
LL03-1E	1	19-Sep-17	< 1.25	< 150	1.28	< 0.75	< 6.5	0.88	5.70	2.45
LL03-1E	1.58	19-Sep-17	< 1.25	< 150	1.11	< 0.75	< 1.7	< 0.5	7.41	0.90
LL03-1E	1.86	19-Sep-17	< 0.4	< 150	< 0.8	< 0.25	< 1.7	0.66	3.93	0.65
LL03-1E	2.29	19-Sep-17	< 0.4	< 150	< 0.8	< 0.25	< 1.7	< 0.5	4.39	0.75
LL03-1E	3	19-Sep-17	< 0.4	< 150	< 0.8	< 0.25	6.76	< 0.15	13.57	0.22
LL03-1E	4.56	19-Sep-17	< 0.4	< 150	7.31	< 0.25	< 1.7	< 0.15	19.97	0.99
LL03-1E	6	19-Sep-17	< 0.4	< 150	4.36	< 0.25	< 6.5	< 0.15	4.74	3.29
LL06-1E	0.47	20-Sep-17	< 0.4	< 150	9.17	< 0.25	< 1.7	< 0.15	2.75	< 0.1
LL06-1E	1	20-Sep-17	< 0.4	< 150	8.11	< 0.25	< 1.7	< 0.15	3.36	1.48
LL06-1E	1.54	19-Sep-17	< 0.4	< 150	1.46	< 0.25	< 1.7	< 0.15	4.37	0.38
LL06-1E	2	19-Sep-17	8.81	< 500	10.55	8.02	< 1.7	< 0.15	105.70	< 0.1
LL06-1E	2.4	19-Sep-17	3.39	< 150	3.80	2.56	< 6.5	< 0.15	111.50	0.12
LL06-1E	2.9	19-Sep-17	2.16	< 150	2.46	1.54	< 6.5	< 0.15	177.80	0.22
LL06-1E	4.55	19-Sep-17	< 1.25	< 150	3.16	1.19	< 1.7	< 0.15	35.83	1.26
LL07-1E	0.47	20-Sep-17	< 1.25	< 150	5.31	< 0.75	< 1.7	< 0.15	28.59	1.89
LL07-1E	0.77	20-Sep-17	< 1.25	< 500	10.65	< 0.75	< 1.7	< 0.5	17.40	45.14
LL07-1E	1.43	20-Sep-17	2.56	< 150	4.54	< 0.75	< 1.7	< 0.15	11.66	6.43
LL07-1E	2.1	20-Sep-17	< 0.4	< 150	1.26	< 0.75	< 1.7	< 0.15	18.13	0.23
LL07-1E	2.96	20-Sep-17	< 0.4	< 150	0.95	< 0.25	< 1.7	< 0.15	16.78	0.15
LL07-1E	Steel	20-Sep-17	< 0.4	< 150	10.39	< 0.25	< 1.7	< 0.15	14.72	0.75

Table A.10 Summary of general chemistry from November 2017.

Location	Depth (m)	Date	**pH**	**E_h (mV)**	**Alk (mg L^{-1} as $CaCO_3$)**	**EC (mS/cm)**	**NH_3 (mg L^{-1})**
LL01-1E	0.85	09-Nov-17	2.44	432			
LL01-1E	1.27	09-Nov-17	3.03	121			
LL01-1E	1.6	09-Nov-17	4.66	114		1.796	0.11
LL01-1E	1.97	08-Nov-17	3.73	85		2.71	0.12
LL01-1E	3	08-Nov-17	6.48	9	53	1.53	0.68
LL01-1E	3.89	08-Nov-17	5.62	-5			
LL01-1E	Steel	08-Nov-17	6.42	65			
LL03-1E	1	09-Nov-17	5.32	160	47	3.87	0.67
LL03-1E	1.58	09-Nov-17	6.01	124	147	3.93	7.53
LL03-1E	1.86	09-Nov-17	6.15	79	200	0.00003	9.33
LL03-1E	2.29	09-Nov-17	6.22	97	160		
LL03-1E	3	09-Nov-17	6.75	89	233	1.604	0.67
LL03-1E	4.56	11-Nov-17	7.5	128	330	0.8	0.38
LL03-1E	6	09-Nov-17	7.55	80	233	0.466	
LL06-1E	1	10-Nov-17	7.47	132	167	0.337	1.38
LL06-1E	1.54	10-Nov-17	7.01	104	260	0.48	3.33
LL06-1E	2	10-Nov-17	6.77	137	413	0.854	8.17
LL06-1E	2.4	10-Nov-17	6.75	105	400	0.657	8.01
LL06-1E	2.9	10-Nov-17	6.65	118	367	0.597	0.36
LL06-1E	4.55	10-Nov-17	7.35	88	187	0.566	0.39
LL07-1E	0.47	11-Nov-17	2.77	435			0.85
LL07-1E	0.77	11-Nov-17	2.15	696			
LL07-1E	1.14	11-Nov-17	2.67	385			
LL07-1E	1.43	11-Nov-17	4.08	187		1.50	0.32
LL07-1E	2.1	11-Nov-17	6.01	172	93	2.42	3
LL07-1E	2.96	11-Nov-17	5.58	157	70	0.0033	0.2
LL07-1E	Steel	11-Nov-17	8.12	104	180	0.0002	0.23

Table A.11 Summary of anion concentrations from November 2017.

Location	Depth (m)	Date	Aqueous Concentration (mg L^{-1})						
			Fluoride	**Chloride**	**Nitrite**	**Bromide**	**Nitrate**	**Phosphate**	**Sulfate**
LL01-1E	0.85	09-Nov-17	< 0.4	0.36	< 0.4	< 0.4	< 0.4	< 0.4	557.34
LL01-1E	1.27	09-Nov-17	0.08	0.28	< 0.4	< 0.4	< 0.4	< 0.4	869.46
LL01-1E	1.6	09-Nov-17	0.22	0.32	< 0.4	< 0.4	< 0.4	< 0.4	1592.81
LL01-1E	1.97	08-Nov-17	0.95	0.35	< 0.4	< 0.4	< 0.4	< 0.4	2209.11
LL01-1E	3	08-Nov-17	2.55	0.44	< 0.4	< 0.4	< 0.4	< 0.4	1051.31
LL01-1E	3.89	08-Nov-17	0.22	0.74	< 0.4	< 0.4	< 0.4	< 0.4	3395.02
LL01-1E	Steel	08-Nov-17	0.33	1.25	< 0.4	< 0.4	< 0.4	< 0.4	4420.82
LL03-1E	1	09-Nov-17	0.94	2.28	< 0.4	< 0.4	< 0.4	< 0.4	4415.44
LL03-1E	1.58	09-Nov-17	0.30	3.05	< 0.4	< 0.4	< 0.4	< 0.4	3698.44
LL03-1E	1.86	09-Nov-17	< 0.4	3.19	< 0.4	< 0.4	< 0.4	< 0.4	3450.55
LL03-1E	2.29	09-Nov-17	< 0.4	3.42	< 0.4	< 0.4	< 0.4	< 0.4	1724.01
LL03-1E	3	09-Nov-17	0.12	3.56	< 0.4	< 0.4	< 0.4	< 0.4	811.81
LL03-1E	4.56	11-Nov-17	0.17	2.62	< 0.4	< 0.4	< 0.4	< 0.4	184.33
LL03-1E	6	09-Nov-17	0.16	1.34	< 0.4	< 0.4	< 0.4	< 0.4	25.75
LL06-1E	1	10-Nov-17	0.55	0.36	< 0.4	< 0.4	< 0.4	< 0.4	1.99
LL06-1E	1.54	10-Nov-17	0.21	0.57	< 0.4	< 0.4	< 0.4	< 0.4	0.11
LL06-1E	2	10-Nov-17	0.15	1.07	< 0.4	< 0.4	< 0.4	< 0.4	0.20
LL06-1E	2.4	10-Nov-17	0.03	1.40	< 0.4	< 0.4	< 0.4	< 0.4	0.68
LL06-1E	2.9	10-Nov-17	0.14	1.90	< 0.4	< 0.4	< 0.4	< 0.4	1.41
LL06-1E	4.55	10-Nov-17	0.18	1.20	< 0.4	< 0.4	< 0.4	< 0.4	51.61
LL07-1E	0.47	11-Nov-17	0.02	0.90	< 0.4	< 0.4	< 0.4	< 0.4	280.48
LL07-1E	1.14	11-Nov-17	0.49	0.46	< 0.4	< 0.4	< 0.4	< 0.4	1850.13
LL07-1E	1.43	11-Nov-17	1.19	0.47	< 0.4	< 0.4	< 0.4	< 0.4	1164.76
LL07-1E	2.1	11-Nov-17	0.91	1.27	< 0.4	< 0.4	< 0.4	< 0.4	1914.43
LL07-1E	2.96	11-Nov-17	0.22	2.80	< 0.4	< 0.4	< 0.4	< 0.4	1934.71
LL07-1E	Steel	11-Nov-17	0.08	2.33	< 0.4	< 0.4	< 0.4	< 0.4	446.60

Table A.12 Summary of cation and metal concentrations from November 2017.

Location	Depth (m)	Date	Aqueous Concentration (mg L^{-1})							
			Al	**As**	**B**	**Ca**	**Cd**	**Co**	**Cr**	**Cu**
LL01-1E	0.85	09-Nov-17	17.32	38.58	< 0.008	6.62	0.0004	0.40	0.017	0.257
LL01-1E	1.27	09-Nov-17	39.43	93.66	< 0.008	40.10	0.0005	2.56	0.055	0.032
LL01-1E	1.6	09-Nov-17	43.40	215.3	< 0.008	368.0	0.0010	2.58	0.041	0.004
LL01-1E	1.97	08-Nov-17	61.01	407.7	0.62	439.6	< 0.00025	3.33	0.042	0.003
LL01-1E	3	08-Nov-17	0.06	239.7	0.79	156.9	< 0.00007	1.75	< 0.0011	0.005
LL01-1E	3.89	08-Nov-17	0.16	70.33	2.39	408.4	0.0010	0.52	0.003	0.003
LL01-1E	Steel	08-Nov-17	0.04	20.12	3.55	317.9	0.0005	0.43	0.002	0.005
LL03-1E	1	09-Nov-17	0.68	331.1	3.20	406.6	0.0004	6.31	0.002	0.005
LL03-1E	1.58	09-Nov-17	0.04	96.97	2.40	450.5	< 0.00025	1.18	0.002	< 0.00075
LL03-1E	1.86	09-Nov-17	0.02	4.52	2.22	460.3	< 0.00025	0.06	0.004	< 0.0025
LL03-1E	2.29	09-Nov-17	0.02	1.73	< 0.008	278.3	< 0.00007	0.01	0.001	0.005
LL03-1E	3	09-Nov-17	< 0.007	1.36	< 0.026	213.7	< 0.00007	0.02	< 0.0011	0.003
LL03-1E	4.56	11-Nov-17	0.0025	0.95	0.04	116.5	< 0.00007	0.00	< 0.00033	< 0.00075
LL03-1E	6	09-Nov-17	0.01	4.75	0.05	54.98	< 0.00007	0.00	< 0.00033	< 0.0025
LL06-1E	1	10-Nov-17	0.01	79.41	< 0.008	63.42	< 0.00007	0.01	< 0.00033	0.004
LL06-1E	1.54	10-Nov-17	< 0.007	19.16	< 0.026	83.23	< 0.00007	0.00	< 0.0011	0.004
LL06-1E	2	10-Nov-17	0.02	1.99	0.04	112.2	0.0042	0.01	0.006	0.008
LL06-1E	2.4	10-Nov-17	0.06	0.55	< 0.008	97.51	0.0021	0.01	0.004	0.004
LL06-1E	2.9	10-Nov-17	< 0.007	5.82	< 0.026	82.78	0.0013	0.01	0.003	0.004
LL06-1E	4.55	10-Nov-17	0.01	8.73	0.03	78.04	0.0010	0.01	0.002	0.006
LL07-1E	0.47	11-Nov-17	13.23	2.56	< 0.026	5.08	0.0003	0.14	0.009	4.74
LL07-1E	0.77	11-Nov-17	51.35	233.8	1.83	14.70	0.0005	2.60	0.351	0.194
LL07-1E	1.14	11-Nov-17	44.02	280.6	1.58	12.85	0.0008	1.88	0.397	0.016
LL07-1E	1.43	11-Nov-17	71.49	344.2	0.88	22.23	0.0018	1.80	0.049	0.004
LL07-1E	2.1	11-Nov-17	0.48	5.55	1.31	206.2	< 0.00007	1.28	0.002	0.003
LL07-1E	2.96	11-Nov-17	0.36	4.63	< 0.008	345.3	< 0.00025	0.17	0.001	0.007
LL07-1E	Steel	11-Nov-17	0.03	10.09	0.06	147.1	< 0.00007	0.01	< 0.0011	0.005

Table A.12 Continued.

Location	Depth (m)	Date	Aqueous Concentration (mg L^{-1})							
			Fe	**K**	**Li**	**Mg**	**Mn**	**Na**	**Ni**	**Pb**
LL01-1E	0.85	09-Nov-17	109.6	1.94	< 0.006	2.87	0.06	17.74	0.41	0.2535
LL01-1E	1.27	09-Nov-17	225.3	3.15	< 0.006	18.48	0.31	24.32	1.90	0.2358
LL01-1E	1.6	09-Nov-17	211.1	3.29	0.011	17.86	0.35	19.97	1.90	0.0016
LL01-1E	1.97	08-Nov-17	276.7	4.80	0.036	22.67	0.57	17.33	2.70	0.0008
LL01-1E	3	08-Nov-17	327.1	6.55	0.050	17.75	1.31	12.06	0.27	< 0.00005
LL01-1E	3.89	08-Nov-17	1119	6.74	0.048	66.86	4.12	24.97	0.15	0.0007
LL01-1E	Steel	08-Nov-17	1637	2.80	0.124	159.4	17.76	51.60	0.12	0.0005
LL03-1E	1	09-Nov-17	1410	20.3	0.162	131.6	5.84	49.93	3.67	0.0003
LL03-1E	1.58	09-Nov-17	1104	15.0	0.050	174.3	4.63	58.35	0.38	< 0.00005
LL03-1E	1.86	09-Nov-17	1020	11.6	0.013	192.9	4.58	61.64	0.02	< 0.00005
LL03-1E	2.29	09-Nov-17	283.8	2.65	< 0.006	156.0	2.50	52.60	0.005	< 0.00015
LL03-1E	3	09-Nov-17	44.40	1.05	0.010	105.2	0.65	40.58	0.007	< 0.00005
LL03-1E	4.56	11-Nov-17	4.40	1.46	0.007	47.81	0.92	29.30	0.003	< 0.00005
LL03-1E	6	09-Nov-17	1.05	1.01	< 0.006	18.25	0.15	21.93	0.007	< 0.00005
LL06-1E	1	10-Nov-17	0.34	4.93	< 0.006	4.70	0.02	7.59	0.007	< 0.00005
LL06-1E	1.54	10-Nov-17	14.58	4.07	< 0.006	13.21	0.09	15.53	< 0.0021	< 0.00005
LL06-1E	2	10-Nov-17	29.46	5.21	< 0.006	30.23	0.26	30.94	0.006	0.0033
LL06-1E	2.4	10-Nov-17	9.01	4.63	< 0.002	40.63	0.27	36.48	0.003	0.0019
LL06-1E	2.9	10-Nov-17	21.41	0.22	< 0.006	38.16	0.32	35.80	0.003	0.0010
LL06-1E	4.55	10-Nov-17	10.77	1.00	0.007	31.84	0.49	20.05	0.004	0.0009
LL07-1E	0.47	11-Nov-17	21.13	1.12	< 0.006	1.08	0.09	12.64	0.11	0.0042
LL07-1E	0.77	11-Nov-17	900.5	5.03	0.029	15.16	0.25	23.44	2.29	0.1973
LL07-1E	1.14	11-Nov-17	735.1	4.57	0.054	19.27	0.27	15.67	1.99	1.0400
LL07-1E	1.43	11-Nov-17	405.2	4.25	0.167	17.96	0.51	12.84	1.77	0.0004
LL07-1E	2.1	11-Nov-17	574.6	6.10	0.031	83.19	11.65	25.67	0.63	< 0.00015
LL07-1E	2.96	11-Nov-17	36.15	1.51	0.049	212.1	22.95	44.41	0.15	< 0.00015
LL07-1E	Steel	11-Nov-17	7.78	1.85	0.007	67.99	1.94	20.78	0.01	< 0.00005

Table A.12 Continued.

Location	Depth (m)	Date	Aqueous Concentration (mg L^{-1})								
			S	**Sb**	**Se**	**Si**	**Sr**	**Ti**	**Tl**	**V**	**Zn**
LL01-1E	0.85	09-Nov-17	185.4	0.0015	< 1	53.36	< 0.3	< 0.1	< 2	< 0.2	< 0.0405
LL01-1E	1.27	09-Nov-17	285.6	0.0006	< 1	51.26	< 0.3	< 0.1	< 2	< 0.2	0.07
LL01-1E	1.6	09-Nov-17	537.5	0.0005	< 1	43.51	< 1	< 0.3	< 2	< 0.4	0.15
LL01-1E	1.97	08-Nov-17	673.9	< 0.0005	< 1	24.96	< 1	< 0.3	< 2	0.68	0.33
LL01-1E	3	08-Nov-17	325.2	< 0.0005	< 1	14.03	< 0.3	< 0.1	< 2	< 0.2	0.05
LL01-1E	3.89	08-Nov-17	1072	0.0025	< 1	20.84	< 1	< 0.3	< 2	< 0.2	0.05
LL01-1E	Steel	08-Nov-17	1429	0.0011	< 1	12.44	< 1	< 0.3	< 2	< 0.2	0.10
LL03-1E	1	09-Nov-17	1352	0.0008	< 1	19.94	< 1	< 0.3	< 2	< 0.2	0.73
LL03-1E	1.58	09-Nov-17	1248	0.0005	< 1	21.03	< 1	< 0.3	< 2	< 0.2	0.72
LL03-1E	1.86	09-Nov-17	1174	< 0.0005	< 1	14.90	0.95	< 0.1	< 2	< 0.2	< 0.0405
LL03-1E	2.29	09-Nov-17	579.0	< 0.0005	< 1	15.34	< 1	< 0.1	< 2	< 0.2	0.06
LL03-1E	3	09-Nov-17	275.2	<0.00013	< 1	16.76	< 1	< 0.1	< 2	< 0.2	< 0.0405
LL03-1E	4.56	11-Nov-17	62.49	< 0.0005	< 1	11.92	< 1	< 0.1	< 2	< 0.2	< 0.0125
LL03-1E	6	09-Nov-17	10.69	0.0006	< 1	7.53	< 0.3	< 0.1	< 2	< 0.2	< 0.0405
LL06-1E	1	10-Nov-17	2.73	< 0.0005	< 1	8.77	< 0.3	< 0.1	< 2	< 0.2	< 0.0405
LL06-1E	1.54	10-Nov-17	2.27	< 0.0005	< 1	16.22	< 0.3	< 0.1	< 2	< 0.2	< 0.0405
LL06-1E	2	10-Nov-17	3.13	0.0037	< 1	18.14	< 1	< 0.1	< 2	< 0.2	< 0.0405
LL06-1E	2.4	10-Nov-17	3.35	0.0025	< 1	10.24	< 1	< 0.1	< 2	< 0.2	< 0.0405
LL06-1E	2.9	10-Nov-17	3.11	0.0014	< 1	19.05	< 1	< 0.1	< 2	< 0.2	< 0.0125
LL06-1E	4.55	10-Nov-17	18.86	0.0011	< 1	14.60	< 1	< 0.1	< 2	< 0.2	< 0.0125
LL07-1E	0.47	11-Nov-17	94.6	< 0.0005	< 1	47.45	< 0.3	< 0.1	< 2	< 0.2	0.09
LL07-1E	0.77	11-Nov-17	1043	0.0020	< 1	51.85	< 0.3	0.36	< 2	< 0.4	0.20
LL07-1E	1.14	11-Nov-17	601.4	0.0008	< 1	32.91	< 0.3	< 0.3	< 2	< 0.4	0.25
LL07-1E	1.43	11-Nov-17	397.1	< 0.0005	< 1	49.57	< 0.3	< 0.1	< 2	0.49	1.90
LL07-1E	2.1	11-Nov-17	611.4	<0.00013	< 1	11.05	< 1	< 0.1	< 2	< 0.2	< 0.0405
LL07-1E	2.96	11-Nov-17	618.8	< 0.0005	< 1	16.35	< 1	< 0.1	< 2	< 0.2	0.14
LL07-1E	Steel	11-Nov-17	157.9	< 0.0005	< 1	4.75	< 1	< 0.1	< 2	< 0.2	< 0.0125

Table A.12 Continued.

Location	Depth (m)	Date	Aqueous Concentration (µg L^{-1})							
			Be	**P**	**Mo**	**Ag**	**Sn**	**Cs**	**Ba**	**U**
LL01-1E	0.85	09-Nov-17	< 0.4	< 150	2.72	< 0.25	< 1.7	< 0.5	29.56	1.14
LL01-1E	1.27	09-Nov-17	<1.25	< 150	4.10	< 0.25	< 1.7	1.69	11.33	5.14
LL01-1E	1.6	09-Nov-17	<1.25	< 150	< 0.8	< 0.25	< 6.5	< 0.15	11.64	2.16
LL01-1E	1.97	08-Nov-17	<1.25	< 150	< 0.8	< 0.25	< 1.7	< 0.15	10.00	5.69
LL01-1E	3	08-Nov-17	< 0.4	< 150	1.66	< 0.75	11.08	< 0.15	7.36	< 0.1
LL01-1E	3.89	08-Nov-17	1.52	< 150	10.09	< 0.75	16.01	< 0.5	9.03	0.11
LL01-1E	Steel	08-Nov-17	<1.25	< 150	5.44	6.83	< 6.5	< 0.15	6.72	0.82
LL03-1E	1	09-Nov-17	<1.25	< 150	1.39	< 0.75	7.96	< 0.15	3.49	0.12
LL03-1E	1.58	09-Nov-17	< 0.4	< 150	< 0.8	< 0.25	< 1.7	< 0.15	6.08	0.41
LL03-1E	1.86	09-Nov-17	< 0.4	< 150	< 0.8	< 0.25	< 1.7	< 0.15	4.26	0.36
LL03-1E	2.29	09-Nov-17	< 0.4	< 150	< 0.25	< 0.75	16.39	< 0.15	5.34	0.22
LL03-1E	3	09-Nov-17	< 0.4	< 150	< 0.25	< 0.25	11.34	< 0.15	18.16	< 0.1
LL03-1E	4.56	11-Nov-17	< 0.4	< 150	4.89	< 0.25	< 1.7	< 0.15	29.94	0.43
LL03-1E	6	09-Nov-17	< 0.4	< 150	3.41	< 0.25	< 6.5	< 0.15	13.69	2.69
LL06-1E	1	10-Nov-17	< 0.4	< 150	8.49	< 0.25	21.88	< 0.15	1.03	4.23
LL06-1E	1.54	10-Nov-17	< 0.4	< 150	1.18	< 0.25	11.84	< 0.15	9.96	0.26
LL06-1E	2	10-Nov-17	4.22	< 150	5.65	3.40	23.77	< 0.15	59.41	< 0.1
LL06-1E	2.4	10-Nov-17	2.12	< 150	4.65	2.95	15.15	< 0.15	99.16	< 0.1
LL06-1E	2.9	10-Nov-17	1.61	< 150	2.07	< 0.75	< 6.5	< 0.15	138.90	< 0.1
LL06-1E	4.55	10-Nov-17	1.34	< 150	2.92	6.80	< 6.5	< 0.15	35.66	0.77
LL07-1E	0.47	11-Nov-17	< 0.4	< 150	2.61	< 0.75	< 6.5	< 0.15	17.84	1.39
LL07-1E	0.77	11-Nov-17	<1.25	< 500	12.35	< 0.75	< 1.7	< 0.5	12.80	42.03
LL07-1E	1.14	11-Nov-17	<1.25	< 150	3.02	< 0.25	< 1.7	0.50	4.33	30.21
LL07-1E	1.43	11-Nov-17	1.73	< 150	< 0.25	< 0.25	< 1.7	< 0.15	7.78	2.81
LL07-1E	2.1	11-Nov-17	<1.25	< 150	< 0.25	< 0.25	8.02	< 0.15	15.06	< 0.1
LL07-1E	2.96	11-Nov-17	< 0.4	< 150	< 0.8	< 0.75	23.61	< 0.15	14.59	0.13
LL07-1E	Steel	11-Nov-17	< 0.4	< 150	5.31	< 0.75	< 6.5	< 0.15	12.68	1.37

Table A.13 Summary of general chemistry from June 2018.

Location	Depth (m)	Date	pH	E_h (mV)	Alk (mg L^{-1} as $CaCO_3$)	EC (mS/cm)	NH_3 (mg L^{-1})	H_2S (mg L^{-1})
LL01-1E	0.85	15-Jun-18	2.84	425				
LL01-1E	1.27	15-Jun-18	2.98	419		1.2	0.4	
LL01-1E	1.6	14-Jun-18	3.27	339		1.1		0.004
LL01-1E	1.97	14-Jun-18	4.02	333		2	0.15	0
LL01-1E	3	14-Jun-18	6.45	148	60	1.1	1.06	0.008
LL01-1E	3.89	14-Jun-18	5.51	238	30	3.3	1.11	0.015
LL01-1E	Steel	14-Jun-18	6.41	131	30	4.3	4.39	0.005
LL03-1E	0.3	16-Jun-18	2.56	663		5.1	0.001	
LL03-1E	0.5	16-Jun-18	2.34	789		4.9	0.0009	
LL03-1E	1.58	16-Jun-18	5.92	191	63	2.8	7.5	0
LL03-1E	1.86	14-Jun-18	6.07	205	190	2.3	6.9	0.004
LL03-1E	2.29	14-Jun-18	5.68	260	140			0
LL03-1E	3	14-Jun-18	6.77	165	280	1.4	0.4	0.007
LL03-1E	4.56	14-Jun-18	7.58	210	300	0.8	0.3	0.048
LL03-1E	6	14-Jun-18	7.82	148	227	0.4	0.3	0
LL06-1E	0.47	15-Jun-18	4.28	303	130	0.3	1	
LL06-1E	1	15-Jun-18	6.88	314				0.011
LL06-1E	1.54	15-Jun-18	6.95	184	265	0.4	3.6	0
LL06-1E	2	15-Jun-18	6.72	194	388	0.8	13.3	0
LL06-1E	2.4	15-Jun-18	6.66	224	460	0.7	10.6	0.02
LL06-1E	2.9	15-Jun-18	6.73	203	440	0.6	0.5	0.001
LL06-1E	4.55	15-Jun-18	7.43	144	273	0.5	0.3	0
LL07-1E	0.47	16-Jun-18	2.19	770		2.6		
LL07-1E	1.43	16-Jun-18	3.8	392		1.7		0.004
LL07-1E	2.1	16-Jun-18	5.6	284	30	1.4	3.1	0.004
LL07-1E	2.96	16-Jun-18	5.36	290	15	2.1	0.2	0
LL07-1E	Steel	16-Jun-18	7.86	224	230	1		0.048

Table A.14 Summary of anion concentrations from June 2018.

Location	Depth (m)	Date	Aqueous Concentration (mg L^{-1})						
			Fluoride	**Chloride**	**Nitrite**	**Bromide**	**Nitrate**	**Phosphate**	**Sulfate**
LL01-1E	0.85	15-Jun-18	< 1	1.03	< 1	< 1	< 1	< 1	171.82
LL01-1E	1.27	15-Jun-18	< 1	< 1	< 1	< 1	< 1	< 1	666.27
LL01-1E	1.6	14-Jun-18	< 1	0.30	< 1	< 1	< 1	< 1	653.30
LL01-1E	1.97	14-Jun-18	0.49	0.28	< 1	< 1	< 1	< 1	2079.80
LL01-1E	3	14-Jun-18	1.71	0.41	< 1	< 1	< 1	< 1	813.75
LL01-1E	3.89	14-Jun-18	< 1	0.61	< 1	< 1	< 1	< 1	3362.96
LL01-1E	Steel	14-Jun-18	0.202	1.12	< 1	< 1	< 1	< 1	5018.28
LL03-1E	0.3	16-Jun-18	6.67	2.20	< 1	< 1	< 1	< 1	8236.81
LL03-1E	0.5	16-Jun-18	13.71	2.83	< 1	< 1	< 1	< 1	11655.01
LL03-1E	1.58	16-Jun-18	0.26	1.80	< 1	< 1	< 1	< 1	2808.85
LL03-1E	1.86	14-Jun-18	< 1	1.12	< 1	< 1	< 1	< 1	2174.77
LL03-1E	2.29	14-Jun-18	< 1	1.64	< 1	< 1	< 1	< 1	1193.56
LL03-1E	3	14-Jun-18	< 1	1.72	< 1	< 1	< 1	< 1	513.32
LL03-1E	4.56	14-Jun-18	0.10	2.00	< 1	< 1	< 1	< 1	168.29
LL03-1E	6	14-Jun-18	0.14	1.48	< 1	< 1	< 1	< 1	18.28
LL06-1E	0.47	15-Jun-18	0.15	0.41	< 1	< 1	< 1	< 1	84.38
LL06-1E	1	15-Jun-18	0.20	0.69	< 0.1	< 0.1	< 0.1	< 0.1	2.04
LL06-1E	1.54	15-Jun-18	0.21	0.40	< 0.1	< 0.1	< 0.1	< 0.1	0.27
LL06-1E	2	15-Jun-18	0.13	0.94	< 0.1	< 0.1	< 0.1	< 0.1	0.17
LL06-1E	2.4	15-Jun-18	< 1	1.35	< 0.1	< 0.1	< 0.1	< 0.1	0.30
LL06-1E	2.9	15-Jun-18	0.13	1.73	< 0.1	< 0.1	< 0.1	< 0.1	0.55
LL06-1E	4.55	15-Jun-18	0.15	1.20	< 0.1	< 0.1	< 0.1	< 0.1	51.93
LL07-1E	0.47	16-Jun-18	< 1	< 1	< 1	< 1	< 1	< 1	1220.25
LL07-1E	1.43	16-Jun-18	0.95	0.66	< 1	< 1	< 1	< 1	1564.81
LL07-1E	2.1	16-Jun-18	0.61	1.06	< 1	< 1	< 1	< 1	1440.23
LL07-1E	2.96	16-Jun-18	< 1	1.94	< 1	< 1	< 1	< 1	1801.34
LL07-1E	Steel	16-Jun-18	< 1	1.42	< 1	< 1	< 1	< 1	453.87

Table A.15 Summary of cation and metal concentrations from June 2018.

Location	Depth (m)	Date	Aqueous Concentration (mg L^{-1})							
			Al	**As**	**B**	**Ca**	**Cd**	**Co**	**Cr**	**Cu**
LL01-1E	0.85	15-Jun-18	5.95	25.41	< 0.004	2.10	0.0001	0.55	0.001	0.759
LL01-1E	1.27	15-Jun-18	32.62	96.01	< 0.011	18.03	0.0004	2.52	0.032	1.17
LL01-1E	1.6	14-Jun-18	42.47	63.8	< 0.004	71.79	0.0006	2.23	0.018	0.053
LL01-1E	1.97	14-Jun-18	64.33	385.6	< 0.004	458.6	< 0.0001	3.33	0.030	0.007
LL01-1E	3	14-Jun-18	0.13	229.5	< 0.004	112.8	< 0.00004	1.53	0.001	0.011
LL01-1E	3.89	14-Jun-18	0.17	69.4	0.77	430.4	< 0.0001	0.54	0.001	0.020
LL01-1E	Steel	14-Jun-18	0.01	7.77	1.16	364.7	< 0.00004	0.26	0.001	0.006
LL03-1E	0.3	16-Jun-18	430.7	31.24	1.34	390.3	0.0159	14.4	1.531	15.13
LL03-1E	0.5	16-Jun-18	873.6	187.7	1.57	366.0	0.0229	25.9	2.114	22.13
LL03-1E	1.58	16-Jun-18	0.07	62.57	0.01	367.9	< 0.00004	0.62	0.002	0.007
LL03-1E	1.86	14-Jun-18	0.06	15.66	0.01	422.8	< 0.0001	0.26	0.001	0.013
LL03-1E	2.29	14-Jun-18	0.08	0.26	< 0.004	205.0	< 0.0001	0.03	0.001	0.015
LL03-1E	3	14-Jun-18	< 0.001	0.78	< 0.004	156.8	0.0008	0.02	0.004	0.008
LL03-1E	4.56	14-Jun-18	0.00	0.46	0.04	109.4	0.0005	0.00	0.001	0.001
LL03-1E	6	14-Jun-18	0.01	4.51	0.05	55.21	0.0002	0.00	0.001	0.002
LL06-1E	0.47	15-Jun-18	0.06	84.54	< 0.011	33.06	0.0001	0.13	< 0.0006	0.005
LL06-1E	1	15-Jun-18	0.00	29.88	< 0.004	17.39	0.0001	0.00	0.002	0.001
LL06-1E	1.54	15-Jun-18	< 0.003	26.17	< 0.011	69.48	< 0.00004	0.00	0.001	0.000
LL06-1E	2	15-Jun-18	0.02	4.85	0.03	113.7	< 0.00004	0.00	0.003	0.001
LL06-1E	2.4	15-Jun-18	0.06	0.07	< 0.011	99.47	< 0.00004	0.00	0.001	0.0002
LL06-1E	2.9	15-Jun-18	0.01	4.12	< 0.011	80.53	< 0.00004	0.00	0.002	0.003
LL06-1E	4.55	15-Jun-18	< 0.001	6.32	0.03	79.75	< 0.00004	0.00	< 0.0006	0.000
LL07-1E	0.47	16-Jun-18	26.19	7.43	< 0.004	4.19	0.0002	0.22	0.014	12.86
LL07-1E	1.43	16-Jun-18	70.99	306.7	< 0.004	19.94	0.0064	1.77	0.037	0.061
LL07-1E	2.1	16-Jun-18	2.31	33.78	0.02	129.1	0.0016	1.70	0.004	0.015
LL07-1E	2.96	16-Jun-18	0.44	2.70	< 0.004	336.3	0.0007	0.16	0.003	0.011
LL07-1E	Steel	16-Jun-18	0.02	9.67	0.06	157.0	0.0004	0.00	0.001	0.006

Table A.15 Continued.

Location	Depth (m)	Date	Aqueous Concentration (mg L^{-1})							
			Fe	**K**	**Li**	**Mg**	**Mn**	**Na**	**Ni**	**Pb**
LL01-1E	0.85	15-Jun-18	30.09	0.76	0.004	0.73	0.03	8.52	0.38	0.0227
LL01-1E	1.27	15-Jun-18	208.6	2.41	0.002	8.23	0.17	19.00	1.82	0.1006
LL01-1E	1.6	14-Jun-18	105.9	2.27	0.005	14.52	0.38	15.33	1.54	0.0008
LL01-1E	1.97	14-Jun-18	302.0	4.22	0.030	23.88	0.46	19.14	2.65	0.0007
LL01-1E	3	14-Jun-18	318.2	5.07	0.041	16.88	1.23	11.39	0.30	0.0001
LL01-1E	3.89	14-Jun-18	1154	5.71	0.052	79.37	4.76	26.83	0.15	0.0011
LL01-1E	Steel	14-Jun-18	1840	3.05	0.152	195.1	21.18	61.37	0.02	0.0001
LL03-1E	0.3	16-Jun-18	1936	0.09	0.444	247.5	6.96	27.60	12.07	0.0058
LL03-1E	0.5	16-Jun-18	2326	6.33	0.713	428.1	10.66	37.27	21.13	0.0156
LL03-1E	1.58	16-Jun-18	579.2	8.68	0.031	97.19	2.70	33.38	0.24	< 0.00008
LL03-1E	1.86	14-Jun-18	476.4	4.54	0.012	76.43	2.68	23.76	0.21	0.0001
LL03-1E	2.29	14-Jun-18	156.3	1.90	0.003	114.1	1.83	37.27	0.026	< 0.00008
LL03-1E	3	14-Jun-18	27.44	0.39	0.009	76.13	0.45	26.94	0.013	0.0008
LL03-1E	4.56	14-Jun-18	2.30	1.21	0.008	45.20	0.77	25.29	0.008	0.0004
LL03-1E	6	14-Jun-18	1.85	0.98	0.003	18.25	0.15	19.69	0.013	0.0001
LL06-1E	0.47	15-Jun-18	2.86	4.58	0.012	5.70	0.14	7.78	0.111	< 0.00008
LL06-1E	1	15-Jun-18	0.18	2.48	< 0.003	1.11	0.01	1.85	0.004	0.0002
LL06-1E	1.54	15-Jun-18	19.65	3.14	0.004	9.81	0.07	10.68	0.001	< 0.00002
LL06-1E	2	15-Jun-18	39.73	4.66	0.003	30.90	0.25	28.69	0.000	< 0.00002
LL06-1E	2.4	15-Jun-18	10.34	4.23	< 0.0008	43.99	0.27	35.31	0.001	< 0.00002
LL06-1E	2.9	15-Jun-18	19.18	0.18	0.005	38.12	0.30	31.30	0.000	< 0.00008
LL06-1E	4.55	15-Jun-18	9.36	0.90	0.007	32.65	0.49	18.50	0.002	< 0.00002
LL07-1E	0.47	16-Jun-18	245.9	3.04	0.004	1.19	0.06	18.57	0.43	0.0112
LL07-1E	1.43	16-Jun-18	567.3	3.32	0.145	25.75	0.42	15.54	1.92	0.0037
LL07-1E	2.1	16-Jun-18	466.8	4.61	0.057	56.01	6.32	20.00	1.04	0.0045
LL07-1E	2.96	16-Jun-18	29.07	0.90	0.045	217.4	22.98	40.85	0.14	0.0009
LL07-1E	Steel	16-Jun-18	2.31	1.78	0.004	75.32	1.36	18.92	0.02	0.0004

Table A.15 Continued.

Location	Depth (m)	Date	Aqueous Concentration (mg L^{-1})								
			S	**Sb**	**Se**	**Si**	**Sr**	**Ti**	**Tl**	**V**	**Zn**
LL01-1E	0.85	15-Jun-18	60.87	< 0.00018	< 1	45.11	< 0.3	< 0.1	< 2	< 0.2	0.12
LL01-1E	1.27	15-Jun-18	211.6	0.0060	< 1	47.32	< 0.3	< 0.1	< 2	< 0.2	0.15
LL01-1E	1.6	14-Jun-18	211.3	0.0018	< 1	31.54	< 0.3	< 0.1	< 2	< 0.4	0.19
LL01-1E	1.97	14-Jun-18	620.6	0.0012	< 1	27.50	< 1	< 0.1	< 2	0.56	0.30
LL01-1E	3	14-Jun-18	266.1	0.0008	< 1	14.08	< 0.3	< 0.1	< 2	< 0.2	0.06
LL01-1E	3.89	14-Jun-18	1015	0.0017	< 1	22.85	< 1	< 0.1	< 2	< 0.2	0.18
LL01-1E	Steel	14-Jun-18	1507	0.0005	< 1	10.50	0.87	< 0.1	< 2	< 0.2	0.10
LL03-1E	0.3	16-Jun-18	2599	0.0009	< 1	58.78	< 0.3	0.30	< 2	0.41	4.95
LL03-1E	0.5	16-Jun-18	3492	0.0008	< 1	43.93	< 0.3	< 0.3	< 2	0.95	8.72
LL03-1E	1.58	16-Jun-18	680.9	0.0005	< 1	14.89	< 1	< 0.1	< 2	< 0.2	0.59
LL03-1E	1.86	14-Jun-18	645.6	0.0004	< 1	11.87	< 1	< 0.1	< 2	< 0.2	0.38
LL03-1E	2.29	14-Jun-18	394.5	0.0002	< 1	10.17	< 1	< 0.1	< 2	< 0.2	0.10
LL03-1E	3	14-Jun-18	174.4	0.0013	< 1	11.37	< 1	< 0.1	< 2	< 0.2	0.09
LL03-1E	4.56	14-Jun-18	56.60	0.0013	< 1	10.04	< 1	< 0.1	< 2	< 0.2	< 0.017
LL03-1E	6	14-Jun-18	7.92	0.0009	< 1	7.54	< 0.3	< 0.1	< 2	< 0.2	< 0.017
LL06-1E	0.47	15-Jun-18	26.97	0.0005	< 1	17.19	< 0.3	< 0.1	< 2	< 0.2	0.11
LL06-1E	1	15-Jun-18	0.80	0.0008	< 1	1.97	< 0.3	< 0.1	< 2	< 0.2	< 0.017
LL06-1E	1.54	15-Jun-18	0.85	0.0002	< 1	14.21	< 0.3	< 0.1	< 2	< 0.2	< 0.017
LL06-1E	2	15-Jun-18	1.61	< 0.00018	< 1	17.22	< 1	< 0.1	< 2	< 0.2	< 0.005
LL06-1E	2.4	15-Jun-18	1.73	< 0.00018	< 1	10.31	< 1	< 0.1	< 2	< 0.2	< 0.005
LL06-1E	2.9	15-Jun-18	1.19	< 0.00018	< 1	17.14	< 1	< 0.1	< 2	< 0.2	< 0.017
LL06-1E	4.55	15-Jun-18	17.55	< 0.00018	< 1	13.60	< 1	< 0.1	< 2	< 0.2	< 0.017
LL07-1E	0.47	16-Jun-18	379.9	0.0004	< 1	52.27	< 0.3	0.34	< 2	< 0.2	0.09
LL07-1E	1.43	16-Jun-18	454.3	0.0032	< 1	46.28	< 0.3	< 0.1	< 2	< 0.4	1.77
LL07-1E	2.1	16-Jun-18	425.1	0.0015	< 1	8.46	< 1	< 0.1	< 2	< 0.2	0.85
LL07-1E	2.96	16-Jun-18	538.3	0.0008	< 1	15.04	< 1	< 0.1	< 2	< 0.2	0.17
LL07-1E	Steel	16-Jun-18	154.5	0.0027	< 1	4.28	< 1	< 0.1	< 2	< 0.2	0.03

Table A.15 Continued.

Location	Depth (m)	Date	Aqueous Concentration (µg L^{-1})							
			Be	**P**	**Mo**	**Ag**	**Sn**	**Cs**	**Ba**	**U**
LL01-1E	0.85	15-Jun-18	< 0.5	< 70	0.50	< 0.3	< 3	0.21	31.22	0.22
LL01-1E	1.27	15-Jun-18	0.81	317.3	6.12	0.61	< 3	1.68	11.84	3.79
LL01-1E	1.6	14-Jun-18	< 0.5	< 70	0.89	0.44	3.32	< 0.2	6.77	2.36
LL01-1E	1.97	14-Jun-18	1.10	< 70	0.58	< 0.3	< 3	< 0.2	8.96	4.59
LL01-1E	3	14-Jun-18	< 0.16	< 70	1.73	< 0.3	< 3	< 0.2	5.65	0.11
LL01-1E	3.89	14-Jun-18	0.66	< 70	2.10	0.31	3.43	< 0.2	7.81	0.07
LL01-1E	Steel	14-Jun-18	< 0.5	< 70	2.58	< 0.3	< 3	< 0.2	8.86	0.27
LL03-1E	0.3	16-Jun-18	6.94	< 70	5.95	< 0.3	3.32	0.99	1.15	327.40
LL03-1E	0.5	16-Jun-18	13.77	821.1	6.21	0.74	4.74	2.08	1.04	346.00
LL03-1E	1.58	16-Jun-18	< 0.16	< 70	< 0.4	0.33	< 3	< 0.2	8.79	0.51
LL03-1E	1.86	14-Jun-18	< 0.16	< 70	0.36	0.37	< 3	< 0.2	8.65	0.85
LL03-1E	2.29	14-Jun-18	< 0.16	< 70	< 0.4	0.45	3.03	< 0.06	6.69	< 0.04
LL03-1E	3	14-Jun-18	0.81	< 70	1.11	1.46	2.80	< 0.2	13.78	0.07
LL03-1E	4.56	14-Jun-18	< 0.5	< 70	11.00	0.33	2.70	< 0.2	34.80	1.17
LL03-1E	6	14-Jun-18	< 0.5	< 70	3.70	< 0.3	2.43	< 0.2	17.79	3.18
LL06-1E	0.47	15-Jun-18	< 0.16	< 70	1.54	< 0.1	< 0.8	< 0.2	1.91	< 0.012
LL06-1E	1	15-Jun-18	< 0.16	< 70	2.97	< 0.1	< 3	< 0.2	2.04	< 0.04
LL06-1E	1.54	15-Jun-18	< 0.16	< 70	1.09	< 0.1	< 0.8	< 0.2	22.75	0.13
LL06-1E	2	15-Jun-18	< 0.16	398.5	0.35	< 0.1	< 0.8	< 0.06	87.82	< 0.04
LL06-1E	2.4	15-Jun-18	< 0.16	< 70	0.32	< 0.1	< 3	< 0.06	103.20	0.07
LL06-1E	2.9	15-Jun-18	< 0.16	< 70	< 0.4	< 0.3	< 3	< 0.06	133.20	0.06
LL06-1E	4.55	15-Jun-18	< 0.16	< 70	1.47	< 0.1	< 3	< 0.06	46.18	0.67
LL07-1E	0.47	16-Jun-18	< 0.16	484.5	8.92	0.54	3.09	0.30	23.11	4.70
LL07-1E	1.43	16-Jun-18	4.22	344.3	3.80	2.47	< 3	< 0.2	10.78	5.76
LL07-1E	2.1	16-Jun-18	2.79	< 70	1.78	1.48	< 3	< 0.2	15.37	0.07
LL07-1E	2.96	16-Jun-18	0.89	< 70	0.94	1.04	2.39	< 0.2	12.40	0.13
LL07-1E	Steel	16-Jun-18	0.59	< 70	8.36	0.44	< 3	< 0.06	14.81	32.86

Table A.16 Summary of As speciation from June 2017.

Location	Depth (m)	Aqueous concentration (mg L^{-1})		
		As(III)	As(V)	As (T)
LL01-1E	1.27	69.2	4.3	84.9
LL01-1E	1.6	194.9	16.1	210.1
LL01-1E	1.97	403.2	34.0	406.7
LL01-1E	3	213.4	27.4	237.6
LL01-1E	3.89	59.0	6.2	65.0
LL01-1E	4.9	------	------	------
LL03-1E	0.3	74.1	8.6	83.1
LL03-1E	0.5	------	------	------
LL03-1E	1	------	------	------
LL03-1E	1.58	86.8	10.3	99.7
LL03-1E	1.86	6.3	0.6	7.4
LL03-1E	2.29	5.8	0.9	7.0
LL03-1E	3	0.7	0.1	3.7
LL03-1E	4.56	2.8	0.5	6.5
LL03-1E	6	12.8	1.6	15.0
LL06-1E	0.47	84.1	11.5	105.6
LL06-1E	1	54.5	6.4	70.9
LL06-1E	1.54	12.8	1.7	21.0
LL06-1E	2	4.1	0.5	5.8
LL06-1E	2.4	0.1	0.04	0.2
LL06-1E	2.9	27.6	3.5	28.8
LL06-1E	4.55	16.0	2.6	22.2
LL07-1E	0.47	0.1	0.05	0.9
LL07-1E	0.77	------	------	------
LL07-1E	1.43	312.6	28.5	392.0
LL07-1E	2.1	6.6	0.6	8.7
LL07-1E	2.96	------	------	------
LL07-1E	5.9	13.3	1.8	19.4

Table A.17 Summary of As speciation from September 2017.

Location	Depth (m)	Aqueous concentration (mg L^{-1})		
		As(III)	As(V)	As (T)
LL01-1E	1.27	53.6	15.0	91.8
LL01-1E	1.6	166.2	40.7	222.9
LL01-1E	1.97	408.0	80.5	456.5
LL01-1E	3	218.6	35.2	239.6
LL01-1E	3.89	63.6	11.0	67.1
LL01-1E	4.9	------	------	------
LL03-1E	0.3	------	------	------
LL03-1E	0.5	------	------	------
LL03-1E	1	------	------	------
LL03-1E	1.58	60.3	10.5	101.9
LL03-1E	1.86	5.2	0.9	6.9
LL03-1E	2.29	7.9	1.4	10.5
LL03-1E	3	2.8	0.5	3.3
LL03-1E	4.56	2.7	0.5	3.1
LL03-1E	6	9.1	1.7	12.9
LL06-1E	0.47	119.8	29.9	164.3
LL06-1E	1	27.1	41.9	75.3
LL06-1E	1.54	2.1	6.4	9.5
LL06-1E	2	3.2	0.5	4.5
LL06-1E	2.4	0.1	0.04	0.3
LL06-1E	2.9	12.6	2.7	14.4
LL06-1E	4.55	14.0	2.4	14.7
LL07-1E	0.47	0.1	0.06	0.8
LL07-1E	0.77	226.4	33.8	265.5
LL07-1E	1.43	322.6	48.9	346.0
LL07-1E	2.1	6.5	1.2	8.6
LL07-1E	2.96	4.4	0.5	7.2
LL07-1E	5.9	13.2	1.5	15.4

Table A.18 Summary of As speciation from November 2017.

Location	Depth (m)	Aqueous concentration (mg L^{-1})		
		As(III)	As(V)	As (T)
LL01-1E	1.27	56.4	20.3	93.7
LL01-1E	1.6	183.8	29.9	215.3
LL01-1E	1.97	400.4	65.7	407.7
LL01-1E	3	226.8	34.7	239.7
LL01-1E	3.89	65.9	10.6	70.3
LL01-1E	4.9	------	------	------
LL03-1E	0.3	------	------	------
LL03-1E	0.5	------	------	------
LL03-1E	1	316	49	331
LL03-1E	1.58	84.9	13.5	97.0
LL03-1E	1.86	3.5	0.7	4.5
LL03-1E	2.29	1.2	0.4	1.7
LL03-1E	3	0.2	0.5	1.4
LL03-1E	4.56	0.7	0.1	1.0
LL03-1E	6	0.3	2.8	4.8
LL06-1E	0.47	------	------	------
LL06-1E	1	52.9	18.4	79.4
LL06-1E	1.54	2.9	11.4	19.2
LL06-1E	2	0.0	0.1	2.0
LL06-1E	2.4	0.0	0.07	0.6
LL06-1E	2.9	4.5	1.1	5.8
LL06-1E	4.55	7.1	1.5	8.7
LL07-1E	0.47	0.1	0.17	2.6
LL07-1E	0.77	------	------	------
LL07-1E	1.43	300.4	58.9	344.2
LL07-1E	2.1	2.5	1.8	5.5
LL07-1E	2.96	2.0	0.9	4.6
LL07-1E	5.9	8.8	1.7	10.1

Table A.19 Summary of As speciation from June 2018.

Location	Depth (m)	Aqueous concentration (mg L^{-1})		
		As(III)	As(V)	As (T)
LL01-1E	1.27	50.5	27.5	96.0
LL01-1E	1.6	47.9	10.2	63.8
LL01-1E	1.97	330.6	57.4	385.6
LL01-1E	3	191.2	30.6	229.5
LL01-1E	3.89	53.1	11.5	69.4
LL01-1E	4.9	6	1	8
LL03-1E	0.3	5.7	1.3	7.8
LL03-1E	0.5	165	20	188
LL03-1E	1	27	3	31
LL03-1E	1.58	164.6	20.5	187.7
LL03-1E	1.86	61.3	9.4	62.6
LL03-1E	2.29	12.0	2.1	15.7
LL03-1E	3	0.1	0.1	0.3
LL03-1E	4.56	0.6	0.2	0.8
LL03-1E	6	0.1	0.1	0.5
LL06-1E	0.47	3.3	0.8	4.5
LL06-1E	1	21.4	12.6	84.5
LL06-1E	1.54	5.6	15.9	29.9
LL06-1E	2	19.5	3.2	26.2
LL06-1E	2.4	3.5	0.42	4.8
LL06-1E	2.9	0.1	0.0	0.1
LL06-1E	4.55	2.3	0.4	4.1
LL07-1E	0.47	4.4	1.12	6.3
LL07-1E	0.77	6.3	0.2	7.4
LL07-1E	1.43	272.0	37.7	306.7
LL07-1E	2.1	26.4	5.6	33.8
LL07-1E	2.96	2.0	0.5	2.7
LL07-1E	5.9	6.7	1.0	9.7

Table A.20 Summary of water isotope data from December 2016.

Location	Depth (m)	Date	**$\delta^{18}O$ (‰ VSMOW)**	**$\delta^{2}H$ (‰ VSMOW)**
LL01-1E	1.27	05-Dec-16	-10.32	-70.80
LL01-1E	1.6	05-Dec-16	-11.44	-77.27
LL01-1E	1.97	05-Dec-16	-11.45	-79.32
LL01-1E	3	05-Dec-16	-11.81	-81.42
LL03-1E	1	06-Dec-16	-10.90	-74.99
LL03-1E	1.58	06-Dec-16	-10.97	-75.71
LL03-1E	1.86	06-Dec-16	-10.97	-76.06
LL03-1E	2.29	06-Dec-16	-10.76	-75.84
LL03-1E	3	06-Dec-16	-10.64	-75.92
LL03-1E	6	06-Dec-16	-11.44	-79.21
LL06-1E	0.47	06-Dec-16	-11.19	-78.50
LL06-1E	1	06-Dec-16	-11.35	-79.70
LL06-1E	1.54	06-Dec-16	-11.76	-80.90
LL06-1E	2	06-Dec-16	-11.49	-79.93
LL06-1E	2.4	06-Dec-16	-11.43	-79.60
LL06-1E	2.9	06-Dec-16	-11.43	-79.68
LL06-1E	4.55	06-Dec-16	-11.63	-80.80
LL07-1E	0.77	07-Dec-16	-12.18	-84.21
LL07-1E	1.43	07-Dec-16	-11.90	-82.62
LL07-1E	2.1	07-Dec-16	-11.41	-79.85
LL07-1E	5.9	07-Dec-16	-11.49	-80.06

Table A.21 Summary of water isotope data from June 2017.

Location	Depth (m)	Date	$\delta^{18}O$ (‰ VSMOW)	$\delta^{2}H$ (‰ VSMOW)
LL01-1E	1.27	14-Jun-17	-9.89	-68.29
LL01-1E	1.6	14-Jun-17	-10.87	-75.42
LL01-1E	1.97	14-Jun-17	-11.46	-79.85
LL01-1E	3	14-Jun-17	-10.77	-79.91
LL01-1E	3.89	14-Jun-17	-11.67	-81.98
LL03-1E	1.58	15-Jun-17	-10.80	-76.40
LL03-1E	1.86	15-Jun-17	-10.94	-76.99
LL03-1E	3	15-Jun-17	-11.02	-77.84
LL03-1E	4.56	15-Jun-17	-11.38	-79.66
LL03-1E	6	15-Jun-17	-11.49	-80.35
LL06-1E	0.47	15-Jun-17	-11.74	-81.58
LL06-1E	1	15-Jun-17	-11.61	-79.70
LL06-1E	1.54	16-Jun-17	-11.80	-81.89
LL06-1E	2	16-Jun-17	-11.66	-81.33
LL06-1E	2.4	16-Jun-17	-11.54	-80.99
LL06-1E	2.9	16-Jun-17	-10.94	-81.46
LL06-1E	4.55	16-Jun-17	-11.61	-81.51
LL07-1E	0.47	17-Jun-17	-13.77	-98.48
LL07-1E	1.43	17-Jun-17	-10.76	-75.91
LL07-1E	2.1	17-Jun-17	-11.33	-80.39

Table A.22 Summary of water isotope data from September 2017.

Location	Depth (m)	Date	$\delta^{18}O$ (‰ VSMOW)	$\delta^{2}H$ (‰ VSMOW)
LL01-1E	1.27	19-Sep-17	-9.49	-69.84
LL01-1E	1.6	18-Sep-17	-10.00	-72.66
LL01-1E	1.97	18-Sep-17	-9.90	-77.15
LL01-1E	3	19-Sep-17	-11.15	-81.73
LL01-1E	3.89	18-Sep-17	-11.41	-83.03
LL03-1E	1.58	18-Sep-17	-10.35	-76.77
LL03-1E	1.86	18-Sep-17	-9.52	-75.28
LL03-1E	2.29	18-Sep-17	-10.43	-77.56
LL03-1E	3	18-Sep-17	-10.77	-78.58
LL03-1E	4.56	19-Sep-17	-10.79	-79.89
LL03-1E	6	19-Sep-17	-10.97	-80.83
LL06-1E	0.47	20-Sep-17	-11.13	-81.69
LL06-1E	1	20-Sep-17	-11.16	-81.44
LL06-1E	1.54	19-Sep-17	-11.31	-81.88
LL06-1E	2	19-Sep-17	-11.32	-82.19
LL06-1E	2.4	19-Sep-17	-11.23	-82.00
LL06-1E	2.9	19-Sep-17	-11.32	-82.63
LL06-1E	4.55	19-Sep-17	-11.25	-82.59
LL07-1E	0.47	20-Sep-17	-9.58	-74.01
LL07-1E	0.77	20-Sep-17	-12.48	-95.23
LL07-1E	1.43	20-Sep-17	-11.00	-80.82
LL07-1E	2.1	20-Sep-17	-10.93	-81.10
LL07-1E	5.9	20-Sep-17	-11.48	-80.69

Table A.23 Summary of water isotope data from November 2017.

Location	Depth (m)	Date	$\delta^{18}O$ (‰ VSMOW)	$\delta^{2}H$ (‰ VSMOW)
LL01-1E	1.27	09-Nov-17	-9.57	-70.15
LL01-1E	1.6	09-Nov-17	-10.17	-72.26
LL01-1E	1.97	08-Nov-17	-11.11	-78.64
LL01-1E	3	08-Nov-17	-11.27	-81.91
LL01-1E	3.89	08-Nov-17	-11.71	-83.51
LL03-1E	1	09-Nov-17	-10.87	-77.72
LL03-1E	1.58	09-Nov-17	-10.80	-77.65
LL03-1E	1.86	09-Nov-17	-10.98	-78.41
LL03-1E	2.29	09-Nov-17	-10.83	-78.18
LL03-1E	3	09-Nov-17	-10.94	-79.12
LL03-1E	4.56	11-Nov-17	-11.23	-80.30
LL06-1E	1	10-Nov-17	-11.68	-82.04
LL06-1E	1.54	10-Nov-17	-11.75	-83.35
LL06-1E	2	10-Nov-17	-10.96	-80.93
LL06-1E	2.4	10-Nov-17	-11.70	-82.78
LL06-1E	2.9	10-Nov-17	-11.64	-82.64
LL06-1E	4.55	10-Nov-17	-11.08	-81.55
LL07-1E	0.47	11-Nov-17	-9.22	-68.67
LL07-1E	1.43	11-Nov-17	-10.86	-80.62
LL07-1E	2.1	11-Nov-17	-11.27	-83.99
LL07-1E	5.9	11-Nov-17	-11.08	-82.01

Table A.24 Summary of water isotope data from June 2018.

Location	Depth (m)	Date	$\delta^{18}O$ (‰ VSMOW)	$\delta^{2}H$ (‰ VSMOW)
LL01-1E	1.27	14-Jun-18	-10.96	-75.91
LL01-1E	1.97	14-Jun-18	-10.60	-74.22
LL01-1E	3	14-Jun-18	-11.10	-79.69
LL01-1E	3.89	14-Jun-18	-11.68	-81.78
LL01-1E	4.9	14-Jun-18	-10.80	-78.30
LL03-1E	0.3	16-Jun-18	-9.97	-71.73
LL03-1E	0.5	16-Jun-18	-10.30	-74.14
LL03-1E	1.58	16-Jun-18	-11.72	-83.84
LL03-1E	1.86	14-Jun-18	-11.96	-87.82
LL03-1E	2.29	16-Jun-18	-10.76	-76.63
LL03-1E	3	14-Jun-18	-10.94	-77.26
LL03-1E	4.56	16-Jun-18	-11.25	-78.67
LL03-1E	6	14-Jun-18	-11.49	-81.20
LL06-1E	0.47	15-Jun-18	-12.50	-88.07
LL06-1E	1.54	15-Jun-18	-11.33	-80.37
LL06-1E	2	15-Jun-18	-11.53	-80.81
LL06-1E	2.4	15-Jun-18	-11.41	-80.07
LL06-1E	2.9	15-Jun-18	-11.04	-78.92
LL06-1E	4.55	15-Jun-18	-11.31	-79.61
LL07-1E	0.47	16-Jun-18	-10.55	-73.58
LL07-1E	1.43	16-Jun-18	-11.30	-80.45
LL07-1E	2.1	16-Jun-18	-10.93	-77.43
LL07-1E	2.96	16-Jun-18	-11.29	-79.52
LL07-1E	5.9	16-Jun-18	-11.15	-78.99

Table A.25 Summary of DIC, DOC, $\delta^{34}S\text{-}SO_4$, $\delta^{18}O\text{-}SO_4$, $\delta^{13}C\text{-}DIC$, $\delta^{13}C\text{-}CH_4$, and CH_4 data.

Location	Depth (m)	DIC (mg L^{-1} as C)	DOC	$\delta^{34}S\text{-}SO_4$ (‰ VCDT)	$\delta^{18}O\text{-}SO_4$ (‰ VSMOW)	$\delta^{13}C\text{-}DIC$	$\delta^{13}C\text{-}CH_4$	CH_4 (mg L^{-1})
LL01-1E	1.27	----	1.83	4.3	-3.2	-13.8	----	----
LL01-1E	1.6	1.48	2.78	4.8	-3.4	-19.8	----	0
LL01-1E	1.97	0.65	1.68	4.7	-4.1	-11.2	----	0
LL01-1E	3	1.84	1.91	5.4	-2.8	-12.6	----	0.22
LL01-1E	3.89	2.09	10.1	6	-2.9	-24.3	----	0.08
LL01-1E	4.9	1.07	5.69	5.1	-4.7	----	----	0.05
LL03-1E	0.3	----	5.04	4.1	-4.8	-21.9	----	----
LL03-1E	0.5	----	6.90	3.9	-7.7	----	----	----
LL03-1E	1	----	5.38	5.1	----	----	----	----
LL03-1E	1.58	4.45	19.6	11	0.7	-22.4	----	0.174
LL03-1E	1.86	3.30	16.9	13.5	4.0	-22.2	----	0
LL03-1E	2.29	4.02	54.2	11.7	7.3	-20.8	----	0.06
LL03-1E	3	40.16	5.06	11.3	5.8	-17.6	----	0.04
LL03-1E	4.56	60.23	6.13	11.3	6.5	-16.7	----	0
LL03-1E	6	52.90	8.22	29.1	5.5	-16.0	----	0.10
LL06-1E	0.47	----	2.82	----	----	-24.8	----	----
LL06-1E	1	9.70	5.14	----	----	-5.6	-63.1	8.97
LL06-1E	1.54	50.06	8.34	5.0	-13.7	-3.6	-66.3	60.09
LL06-1E	2	85.58	25.8	4.6	-11.1	2.5	-61.4	74.58
LL06-1E	2.4	80.49	34.8	6.0	-7.7	-4.6	-62.6	47.44
LL06-1E	2.9	72.92	13.9	11.2	-5.9	-4.9	-60.5	31.49
LL06-1E	4.55	50.87	5.04	32.3	9.2	-13.8	-56.1	0.06
LL07-1E	0.47	----	2.94	4.4	-4.4	----	----	----
LL07-1E	1.43	----	3.17	4.2	-3.6	-16.6	----	----
LL07-1E	2.1	4.69	10.2	12.4	3.2	-16.3	----	1.07
LL07-1E	2.96	4.27	4.32	8.1	2.0	-19.1	----	0.11
LL07-1E	5.9	36.07	3.81	5.9	0.2	-15.7	----	0.02

Table A.26 Summary of total cyanide, thiocyanate and WAD cyanide.

Location	Depth (m)	Cyanide, Weak Acid Diss (mg L^{-1})	Total Cyanide (mg L^{-1})	Thiocyanate (mg L^{-1})
LL01-1.27	1.27	0.0062	0.0099	<0.50
LL01-1.97	1.97	<0.0020	0.0035	0.55
LL01-3.0	3.00	<0.0020	0.0095	<0.50
LL01-3.89	3.89	<0.0020	0.0081	<0.50
LL01-4.9	4.90	<0.0020	0.0075	------
LL06-0.47	0.47	<0.0020	0.0047	<0.50
LL06-1.54	1.54	<0.0020	0.0094	<0.50
LL06-2.0	2.00	<0.0020	0.0127	<0.50
LL06-2.4	2.40	<0.0020	0.0047	<0.50
LL06-2.9	2.90	<0.0020	0.0119	<0.50
LL06-4.55	4.55	<0.0020	0.0110	<0.50

Appendix B: Saturation indices

Table B.1 Saturation indices for samples from December 2017 calculated using PHREEQC.

		Mineral saturation indices calculated with PHREEQC										
Location	Depth (m)	$Al(OH)_3$ (amorph.)	$AlAsO_4$	Alunite ($KAl_3(SO_4)_2(OH)_6$]	Anglesite [$PbSO_4$]	Anhydrite [$CaSO_4$]	Ankerite [$Ca(Fe,Mg,Mn)(CO_3)_2$]	Arsenolite [As_4O_6]	$Ca_3(AsO_4)_2$	Calcite [$CaCO_3$]	Chalcopyrite [$CuFeS_2$]	Claudetite [As_2O_3]
LL01-1E	0.85	-11.1	-7.4	-10.7	-0.2	-1.3		-6.0	-30.4		8.0	-6.1
LL01-1E	1.27	-3.7	-3.6	2.8	-3.6	-1.3		-4.6	-21.4		16.3	-4.7
LL01-1E	1.6	-3.7	-6.0	2.8	-2.1	-0.4		-3.4	-24.0		16.2	-3.5
LL01-1E	1.97	-3.3	-5.9	4.3	-1.6	-0.2		-2.7	-23.8		15.1	-2.7
LL01-1E	3	0.3	-3.4	8.4	-3.3	-0.7	-3.0	-3.2	-14.4	-1.7	20.8	-3.3
LL01-1E	3.89	-1.7	-5.1	4.6	-3.9	-0.2	-3.0	-4.0	-16.0	-2.2	20.4	-4.1
LL01-1E	4.9	-1.6	-2.3	4.9	-3.7	-0.1	-2.9	-4.4	-10.6	-2.4	21.1	-4.4
LL03-1E	0.3	-6.2	-3.0				-1.6	-10.6	-20.4		12.6	-10.7
LL03-1E	0.5	-4.6	-4.7	2.3	-3.4	-0.3	-1.5	-3.1	-21.6		16.1	-3.1
LL03-1E	0.5	-4.7	-2.2	2.4	-3.4	-0.2	-1.1	-5.8	-16.5		15.5	-5.9
LL03-1E	1	-1.3	-0.7	6.9	-1.7	-0.2	-0.7	-6.7	-9.6	-2.4	20.3	-6.7
LL03-1E	1.58	-1.3	-1.6	5.6	-3.6	-0.3	0.1	-7.7	-9.1	-2.0	20.7	-7.7
LL03-1E	1.86	-1.4	-3.2	4.7	-3.5	-0.2	-0.3	-11.5	-11.2	-1.2	21.7	-11.5
LL03-1E	2.29	-1.0	-2.9	5.5	-3.5	-0.4	-1.9	-12.5	-11.6	-1.5	20.7	-12.6
LL03-1E	3	-1.3	-3.8	2.5	-4.7	-0.8	-1.0	-13.3	-10.8	-0.9	21.6	-13.4
LL03-1E	4.56	-1.9	-5.2	-1.3	-5.1	-1.3	-1.0	-15.1	-10.6	-0.7	22.0	-15.1
LL03-1E	6	-0.4	-2.3	4.8	-4.8	-0.9	-0.8	-11.4	-8.4	-0.9	21.6	-11.5
LL06-1E	0.47	-0.7	-1.3	4.8	-4.3	-1.6	-2.7	-10.4	-10.2	-2.6	21.1	-10.5
LL06-1E	1	-1.5	-3.4	-3.6	-6.5	-2.8	-0.4	-10.2	-5.5	-0.2	22.0	-10.2
LL06-1E	1.54	-1.9	-3.6	-5.1	-7.0	-3.4	-0.5	-10.8	-7.4	-0.4	21.4	-10.9
LL06-1E	2	-1.0	-2.9	-3.7	-8.3	-4.4	-0.5	-12.0	-8.9	-0.4	20.9	-12.0
LL06-1E	2.4	-0.3	-3.3	-0.2	-6.7	-3.8	-0.7	-18.7	-11.5	-0.6	20.1	-18.8
LL06-1E	2.9	-1.2	-3.8	-1.7	-6.2	-2.6	-0.7	-17.8	-10.5	-0.5	20.2	-17.9
LL06-1E	4.55	-0.7	-2.2	3.7	-4.6	-1.8	-1.9	-15.7	-11.8	-1.7	20.2	-15.7
LL07-1E	0.47	-9.5	-6.7	-7.5	-2.2	-1.3	-2.2	-20.9	-28.7		9.0	-21.0
LL07-1E	0.77	-10.8	-6.6	-10.9	-1.0	-1.5	-3.0	-7.1	-28.4		8.0	-7.2
LL07-1E	1.43	-3.7	-1.2	4.5	-1.8	-1.0	-2.9	-5.7	-17.9		13.7	-5.7
LL07-1E	2.1	-0.4	-1.5	8.0	-3.9	-0.6	-2.0	-14.9	-11.8	-2.1	21.1	-15.0
LL07-1E	2.96	-1.6	-1.7	5.6	-3.3	-0.3	-2.3	-14.6	-12.2	-2.8	17.9	-14.6
LL07-1E	5.9	-1.1	-1.1	5.7	-3.6	-0.9	-0.4	-13.9	-10.6	-2.8	20.7	-14.0

Table B.1 Continued.

		Mineral saturation indices calculated with PHREEQC									
Location	Depth (m)	Covellite [CuS]	Dolomite [$CaMg(CO_3)_2$]	Epsomite [$MgSO_4 \cdot 7H_2O$]	Ferrihydrite [$Fe(OH)_3$]	FeS ppt.	Gibbsite [$Al(OH_3$]	Goethite [α-FeOOH]	Gypsum [$CaSO_4 \cdot 2H_2O$]	Hematite [Fe_2O_3]	Jarosite-K
LL01-1E	0.85	8.3		-3.6	-6.2	-8.5	-8.3	-1.0	-1.1	0.0	-8.5
LL01-1E	1.27	10.2		-3.7	-4.4	-7.6	-0.8	0.9	-1.1	3.7	-11.8
LL01-1E	1.6	9.3		-3.5	-5.7	-6.7	-0.9	-0.5	-0.2	1.0	-15.7
LL01-1E	1.97	12.1		-3.2	-5.5	-5.5	-0.4	-0.3	0.0	1.4	-15.1
LL01-1E	3	12.9	-4.3	-3.5	-1.9	-0.7	3.1	3.4	-0.4	8.7	-10.5
LL01-1E	3.89	7.6	-5.1	-2.9	-2.1	-1.4	1.1	3.2	0.0	8.3	-8.9
LL01-1E	4.9	8.4	-5.1	-2.5	-0.4	-0.2	1.2	4.9	0.1	11.7	-3.9
LL03-1E	0.3	9.4			-2.8	-8.1	-3.3	2.5		6.9	
LL03-1E	0.5	12.6		-2.5	-4.4	-1.3	-1.8	0.8	0.0	3.5	-9.8
LL03-1E	0.5	12.3		-2.5	-2.5	-0.3	-1.8	2.7	0.1	7.4	-3.8
LL03-1E	1	12.6	-5.2	-2.5	0.2	-1.2	1.5	5.5	0.0	12.8	-1.1
LL03-1E	1.58	12.3	-4.2	-2.5	0.6	-0.6	1.5	5.9	0.0	13.6	-1.2
LL03-1E	1.86	10.8	-2.6	-2.4	1.1	0.9	1.4	6.3	0.0	14.5	-0.4
LL03-1E	2.29	13.3	-3.1	-2.5	0.9	-1.3	1.8	6.1	-0.1	14.2	-1.3
LL03-1E	3	9.7	-2.0	-2.9	1.3	-6.2	1.6	6.5	-0.5	14.9	-2.7
LL03-1E	4.56	11.3	-1.6	-3.5	1.5	-1.2	1.0	6.7	-1.0	15.4	-3.8
LL03-1E	6	11.8	-2.4	-3.3	1.5	-0.2	2.5	6.8	-0.6	15.5	-2.2
LL06-1E	0.47	13.5	-5.8	-4.2	0.9	-1.9	2.1	6.1	-1.4	14.2	-3.0
LL06-1E	1	12.8	-1.6	-5.8	1.4	-0.4	1.4	6.6	-2.5	15.1	-7.7
LL06-1E	1.54	13.2	-1.5	-6.0	1.2	-1.4	0.9	6.4	-3.1	14.8	-8.3
LL06-1E	2	12.9	-1.2	-6.8	0.9	-1.5	1.8	6.2	-4.1	14.3	-10.4
LL06-1E	2.4	11.7	-1.4	-6.0	1.4	-1.2	2.6	6.7	-3.5	15.2	-7.7
LL06-1E	2.9	12.6	-1.3	-4.8	1.6	-2.0	1.6	6.9	-2.3	15.8	-5.6
LL06-1E	4.55	13.5	-3.7	-4.1	0.8	-2.9	2.1	6.0	-1.6	14.0	-4.4
LL07-1E	0.47	8.9		-3.8	-2.9	-9.4	-6.7	2.4	-1.0	6.8	-0.1
LL07-1E	0.77	7.6		-3.2	-5.4	-9.3	-7.9	-0.2	-1.3	1.6	-7.3
LL07-1E	1.43	8.9		-2.9	-2.2	-4.8	-0.9	3.1	-0.7	8.1	-3.4
LL07-1E	2.1	12.6	-4.5	-2.8	1.8	-1.1	2.5	7.1	-0.3	16.1	2.1
LL07-1E	2.96	11.3	-5.7	-2.4	0.6	-3.0	1.2	5.9	-0.1	13.8	0.0
LL07-1E	5.9	12.0	-5.7	-3.0	1.7	-0.9	1.7	7.0	-0.6	15.9	1.7

Table B.1 Continued.

		Mineral saturation indices calculated with PHREEQC									
Location	Depth (m)	Mackinawite [$Fe_{1+x}S$]	Maghemite [γ-Fe2O3]	Melanterite [$FeSO_4 \bullet 7H_2O$]	$Mn_3(AsO_4)_2$	Orpiment [As_2S_3]	Pyrite [FeS_2]	Realgar [As_4S_4]	Scorodite [$FeAsO_4 \bullet 2H_2O$]	Siderite [$FeCO_3$]	ZnS (amorph.)
LL01-1E	0.85	-8.8	-9.1	-1.6	-25.5	-2.8	12.6	-8.1	-5.1		-7.5
LL01-1E	1.27	-4.8	-5.4	-3.0	-17.5	-1.5	12.2	-5.3	-6.9		-2.2
LL01-1E	1.6	-4.1	-8.1	-2.7	-23.4	1.5	10.5	-2.6	-10.6		-2.4
LL01-1E	1.97	-4.1	-7.7	-2.2	-22.8	0.5	9.2	-2.4	-10.8		-2.6
LL01-1E	3	0.1	-0.4	-2.4	-11.3	0.4	12.7	-2.2	-8.2	0.8	1.1
LL01-1E	3.89	0.0	-0.8	-1.8	-12.5	1.1	13.9	-2.5	-8.0	0.5	0.9
LL01-1E	4.9	-0.1	2.6	-1.5	-5.4	-0.3	16.3	-4.4	-3.7	0.6	0.7
LL03-1E	0.3	-6.2	-2.1		-16.2	-7.2	16.9	-11.2	-2.3		-4.2
LL03-1E	0.5	-4.4	-5.5	-1.6	-17.4	0.3	11.7	-4.0	-7.2		-2.7
LL03-1E	0.5	-4.3	-1.6	-1.5	-12.4	-2.4	15.6	-7.3	-2.8		-2.7
LL03-1E	1	-1.1	3.9	-1.7	-5.5	-3.6	17.5	-7.1	-1.8	0.4	0.0
LL03-1E	1.58	-0.6	4.7	-1.8	-5.5	-5.1	17.3	-7.6	-2.3	0.7	0.8
LL03-1E	1.86	0.0	5.6	-1.9	-7.6	-8.0	18.6	-9.4	-3.4	1.5	0.9
LL03-1E	2.29	-0.9	5.1	-2.3	-8.4	-10.3	17.8	-10.6	-3.6	0.9	0.8
LL03-1E	3	-0.2	6.0	-3.0	-8.1	-10.4	18.5	-10.6	-4.0	1.2	2.1
LL03-1E	4.56	0.2	6.5	-3.9	-7.6	-11.6	19.1	-11.3	-4.5	1.0	2.8
LL03-1E	6	-0.3	6.5	-3.0	-5.9	-10.3	17.4	-10.0	-3.1	1.2	1.6
LL06-1E	0.47	-1.2	5.1	-3.3	-6.8	-8.9	17.4	-9.8	-2.4	0.0	0.8
LL06-1E	1	0.3	6.2	-5.7	-5.3	-7.6	17.9	-8.6	-3.3	1.1	2.2
LL06-1E	1.54	-0.6	5.8	-6.0	-7.1	-9.7	17.0	-9.7	-3.2	1.3	1.0
LL06-1E	2	-0.8	5.3	-7.0	-8.0	-10.2	17.4	-10.3	-3.6	1.2	0.5
LL06-1E	2.4	-0.5	6.2	-7.0	-10.2	-14.0	20.9	-13.8	-4.2	0.5	1.7
LL06-1E	2.9	-1.2	6.7	-5.6	-9.0	-16.1	19.2	-14.3	-3.5	0.7	0.9
LL06-1E	4.55	-2.2	4.9	-4.6	-10.2	-14.1	18.2	-13.3	-3.3	-0.2	0.1
LL07-1E	0.47	-8.7	-2.3	-2.6	-23.3	-17.7	19.1	-18.9	-2.7		-6.2
LL07-1E	0.77	-8.5	-7.5	-1.9	-23.6	-3.9	13.8	-9.2	-3.8		-7.2
LL07-1E	1.43	-4.0	-1.0	-1.4	-13.9	-2.4	15.9	-7.2	-2.3		-2.6
LL07-1E	2.1	-0.4	7.0	-2.0	-6.0	-11.1	20.8	-12.2	-1.9	0.8	0.5
LL07-1E	2.96	-2.2	4.7	-2.6	-6.0	-11.7	19.4	-12.8	-2.0	-0.7	0.5
LL07-1E	5.9	-0.1	6.8	-2.4	-5.3	-8.2	22.2	-11.3	-0.9	0.0	1.8

Table B.2 Saturation indices for samples from June 2017 calculated using PHREEQC.

		Mineral saturation indices calculated with PHREEQC										
Location	Depth (m)	$Al(OH)_3$ (amorph.)	$AlAsO_4$	Alunite ($KAl_3(SO_4)_2(OH)_6$)	Anglesite ($PbSO_4$)	Anhydrite ($CaSO_4$)	Ankerite [$Ca(Fe,Mg,Mn)(CO_3)_2$]	Arsenolite (As_4O_6)	$Ca_3(AsO_4)_2$	Calcite ($CaCO_3$)	Chalcopyrite ($CuFeS_2$)	Claudetite (As_2O_3)
LL01-1E	1.27	-7.7	-6.2	-5.2	-0.7	-1.5		-4.2	-27.5		9.8	-4.3
LL01-1E	1.6	-4.0	-1.9	2.4	-2.4	-0.4		-13.7	-15.8		14.8	-13.8
LL01-1E	1.97	-3.7	-1.4	3.3	-2.8	-0.3		-14.3	-14.9		13.6	-14.4
LL01-1E	3	3.0	2.4	15.3	-3.9	-0.6	-3.0	-9.4	-5.4		23.4	-9.4
LL01-1E	3.89	1.4	1.0	13.4	-3.7	-0.3	-3.0	-10.4	-9.5	-3.2	21.0	-10.5
LL01-1E	4.9	0.7	0.2	11.3	-3.6	-0.2	-2.9	-10.1	-9.5	-3.1	21.7	-10.2
LL03-1E	0.3	-8.3	-5.2	-4.9	-1.8	-0.2		-15.5	-23.7		10.9	-15.6
LL03-1E	1.58	-1.0	-1.3	6.5	-3.9	-0.2	-1.6	-9.8	-8.7	-1.5	21.0	-9.8
LL03-1E	1.86	-1.2	-2.9	4.8	-4.4	-0.3	-1.5	-12.5	-10.1	-1.4	21.6	-12.5
LL03-1E	2.29	-0.8	-2.6	4.9	-4.6	-0.5	-1.1	-13.0	-10.0	-0.9	21.1	-13.1
LL03-1E	3	-1.4	-4.0	0.8	-4.7	-0.8	-0.7	-15.0	-9.1	-0.5	21.4	-15.0
LL03-1E	4.56	-2.4	-5.9	-5.5	-6.2	-1.5	0.1	-18.0	-6.8	0.2	21.1	-18.1
LL03-1E	6	-1.6	-4.6	-5.3	-7.1	-3.0	-0.3	-15.5	-6.7	-0.2	21.6	-15.6
LL06-1E	0.47	-1.4	-2.4	0.1	-5.1	-2.1	-1.6	-19.1	-7.8	-1.6	20.6	-19.1
LL06-1E	1	-1.1	-2.9	-3.5	-7.0	-3.6	-0.6	-13.2	-6.1	-0.5	21.6	-13.2
LL06-1E	1.54	0.8	-1.7	4.2	-5.7	-2.2	-0.2	-16.5	-6.5	-0.1	23.5	-16.5
LL06-1E	2	-0.8	-3.0	-2.7	-7.5	-4.1	-0.7	-16.3	-9.2	-0.5	21.1	-16.4
LL06-1E	2.4	-0.7	-4.2	-2.0	-6.9	-4.2	-1.3	-21.5	-13.9	-1.2	20.0	-21.6
LL06-1E	2.9	-1.2	-3.0	-4.2	-6.9	-3.5	-0.7	-14.7	-7.7	-0.5	21.2	-14.8
LL06-1E	4.55	-1.9	-4.7	-4.6	-6.0	-2.1	-0.2	-14.9	-6.4	-0.1	21.5	-15.0
LL07-1E	0.47	-8.5	-7.5	-8.0	-3.0	-3.0		-27.8	-33.0		9.2	-27.9
LL07-1E	0.77	-8.9	-5.6	-8.8	-1.8	-2.8		-19.2	-28.4		7.8	-19.3
LL07-1E	1.43	-4.1	-1.6	3.1	-2.6	-1.3		-8.0	-19.3		13.6	-8.1
LL07-1E	2.1	0.5	-1.3	8.9	-3.6	-0.7	-2.0	-16.0	-10.4	-1.9	22.0	-16.0
LL07-1E	2.96	-1.2	-2.7	5.3	-3.9	-0.5	-2.3	-16.8	-12.7	-2.2	18.5	-16.9
LL07-1E	5.9				-4.6	-1.1	-0.3	-16.1	-6.5	-0.2	21.4	-16.1

Table B.2 Continued.

		Mineral saturation indices calculated with PHREEQC									
Location	Depth (m)	Covellite [CuS]	Dolomite [$CaMg(CO_3)_2$]	Epsomite [$MgSO_4 \cdot 7H_2O$]	Ferrihydrite [$Fe(OH)_3$]	FeS ppt.	Gibbsite [$Al(OH_3$]	Goethite [α-FeOOH]	Gypsum [$CaSO_4 \cdot 2H_2O$]	Hematite [Fe_2O_3]	Jarosite-K
LL01-1E	1.27	8.3		-3.7	-6.3	-8.1	-4.9	-1.1	-1.3	-0.2	-13.6
LL01-1E	1.6	10.2		-3.6	-1.2	-5.1	-1.2	4.0	-0.1	10.0	-1.8
LL01-1E	1.97	9.3		-3.4	-0.6	-5.3	-0.9	4.6	0.0	11.2	0.1
LL01-1E	3			-3.4	1.5	-0.6	5.8	6.8	-0.3	15.5	-1.5
LL01-1E	3.89	12.1	-7.0	-2.9	1.2	-0.5	4.2	6.4	0.0	14.8	0.3
LL01-1E	4.9	12.9	-6.3	-2.4	1.3	-0.8	3.5	6.6	0.0	15.2	0.8
LL03-1E	0.3	9.4		-2.4	-2.7	-8.1	-5.5	2.5	0.0	7.0	-0.7
LL03-1E	1.58	12.6	-3.2	-2.4	1.2	-1.3	1.9	6.5	0.0	14.8	0.3
LL03-1E	1.86	12.3	-3.0	-2.4	1.7	-0.3	1.6	6.9	0.0	15.7	0.8
LL03-1E	2.29	12.6	-2.0	-2.6	1.5	-1.2	2.1	6.8	-0.3	15.4	-0.9
LL03-1E	3	12.3	-1.3	-3.0	1.8	-0.6	1.5	7.0	-0.6	15.8	-2.5
LL03-1E	4.56	10.8	0.2	-3.7	3.0	0.8	0.4	8.1	-1.3	18.2	-2.2
LL03-1E	6	13.3	-0.7	-5.3	2.2	-1.3	1.3	7.4	-2.7	16.7	-6.8
LL06-1E	0.47	13.2	-4.0	-4.9	2.8	-2.2	1.4	8.1	-1.9	18.1	0.2
LL06-1E	1	12.8	-2.2	-6.6	1.8	-0.9	1.8	7.0	-3.3	15.9	-7.7
LL06-1E	1.54	15.0	-0.7	-4.7	3.4	-1.1	3.6	8.7	-2.0	19.3	-0.4
LL06-1E	2	12.9	-1.5	-6.5	2.1	-1.4	2.1	7.4	-3.9	16.7	-6.7
LL06-1E	2.4	12.2	-2.6	-6.5	1.4	-1.9	2.2	6.7	-4.0	15.3	-8.1
LL06-1E	2.9	13.0	-1.3	-5.7	2.1	-1.3	1.6	7.4	-3.2	16.8	-6.6
LL06-1E	4.55	13.1	-0.5	-4.4	2.3	-1.2	0.9	7.6	-1.9	17.1	-4.5
LL07-1E	0.47	9.3		-5.8	-2.2	-9.6	-5.7	3.1	-2.8	8.1	-1.6
LL07-1E	0.77	6.6		-5.1	-2.0	-8.4	-6.0	3.3	-2.5	8.5	-0.6
LL07-1E	1.43	9.1		-3.0	-1.9	-5.1	-1.3	3.4	-1.1	8.6	-2.8
LL07-1E	2.1	13.2	-4.0	-2.9	2.5	-0.7	3.3	7.8	-0.5	17.5	2.4
LL07-1E	2.96	12.1	-4.4	-2.5	0.3	-3.2	1.6	5.6	-0.2	13.1	-2.5
LL07-1E	5.9	11.8	-0.6	-3.2	2.5	0.0		7.8	-0.8	17.5	-1.4

Table B.2 Continued.

		Mineral saturation indices calculated with PHREEQC									
Location	Depth (m)	Mackinawite [$Fe_{1+x}S$]	Maghemite [γ-Fe2O3]	Melanterite [$FeSO_4 \bullet 7H_2O$]	$Mn_3(AsO_4)_2$	Orpiment [As_2S_3]	Pyrite [FeS_2]	Realgar [As_4S_4]	Scorodite [$FeAsO_4 \bullet 2H_2O$]	Siderite [$FeCO_3$]	ZnS (amorph.)
LL01-1E	1.27	-7.3	-9.3	-2.8	-24.1	-1.0	10.8	-5.7	-7.4		-6.0
LL01-1E	1.6	-4.3	0.9	-2.7	-15.2	-8.7	19.8	-12.5	-1.8		-3.0
LL01-1E	1.97	-4.6	2.1	-2.4	-14.1	-11.1	19.5	-13.7	-1.0		-3.0
LL01-1E	3	0.8	6.5	-2.9	-4.2	-4.7	20.0	-8.0	-1.6		2.3
LL01-1E	3.89	0.4	5.7	-1.9	-6.0	-4.8	20.5	-8.6	-1.9	-0.5	0.8
LL01-1E	4.9	0.0	6.1	-1.6	-3.7	-6.6	19.2	-9.0	-1.8	-0.1	0.8
LL03-1E	0.3	-7.3	-2.0	-1.7	-19.4	-12.1	18.2	-14.9	-2.3		-5.5
LL03-1E	1.58	-0.5	5.9	-1.9	-5.2	-7.1	18.5	-9.1	-1.8	1.1	0.5
LL03-1E	1.86	0.5	6.7	-1.9	-6.6	-8.3	19.9	-9.9	-2.7	1.3	0.3
LL03-1E	2.29	-0.4	6.4	-2.6	-6.7	-10.9	18.4	-11.0	-3.0	1.3	0.7
LL03-1E	3	0.1	6.9	-3.5	-7.3	-11.4	19.8	-11.6	-3.6	1.0	1.7
LL03-1E	4.56	1.7	9.3	-4.7	-4.1	-12.5	22.6	-12.7	-3.3	1.3	1.9
LL03-1E	6	-0.6	7.7	-6.3	-5.4	-15.7	17.6	-13.0	-3.6	0.8	1.9
LL06-1E	0.47	-1.4	9.1	-4.9	-5.2	-18.3	20.8	-16.4	-0.8	-0.1	1.6
LL06-1E	1	-0.1	7.0	-6.7	-6.2	-10.6	19.0	-10.9	-2.7	0.7	2.3
LL06-1E	1.54	-0.4	10.3	-4.4	-4.2	-18.4	18.3	-14.6	-1.7	2.0	1.7
LL06-1E	2	-0.7	7.6	-6.7	-7.9	-15.0	19.2	-13.5	-2.8	1.2	1.2
LL06-1E	2.4	-1.1	6.2	-7.5	-12.4	-17.5	21.0	-15.9	-4.7	-0.1	2.0
LL06-1E	2.9	-0.6	7.6	-6.1	-5.7	-13.7	18.8	-12.6	-2.3	1.2	1.2
LL06-1E	4.55	-0.5	8.0	-5.2	-4.1	-15.4	17.6	-12.8	-3.1	1.2	2.1
LL07-1E	0.47	-8.9	-1.0	-4.3	-28.9	-24.6	20.6	-23.2	-3.8		-6.4
LL07-1E	0.77	-7.7	-0.7	-2.8	-24.1	-16.0	19.8	-17.8	-1.3		-6.3
LL07-1E	1.43	-4.4	-0.4	-1.7	-14.9	-4.8	16.7	-9.0	-2.1		-2.7
LL07-1E	2.1	0.0	8.4	-2.3	-4.6	-13.3	20.6	-13.0	-1.9	0.8	0.8
LL07-1E	2.96	-2.5	4.0	-3.6	-6.8	-14.0	18.8	-13.8	-3.8	-1.0	0.3
LL07-1E	5.9	0.8	8.4	-4.1	-2.5	-12.4	20.9	-12.3	-2.8	1.0	2.5

Table B.3 Saturation indices for samples from September 2017 calculated using PHREEQC.

		Mineral saturation indices calculated with PHREEQC										
Location	Depth (m)	$Al(OH)_3$ (amorph.)	$AlAsO_4$	Alunite ($KAl_3(SO_4)_2(OH)_6$)	Anglesite [$PbSO_4$]	Anhydrite [$CaSO_4$]	Ankerite [$Ca(Fe,Mg,Mn)(CO_3)_2$]	Arsenolite [As_4O_6]	$Ca_3(AsO_4)_2$	Calcite [$CaCO_3$]	Chalcopyrite [$CuFeS_2$]	Claudetite [As_2O_3]
LL01-1E	1.27	-7.2	-11.3	-4.3	-0.7	-1.5		-4.1	-37.8		9.4	-4.2
LL01-1E	1.6	-4.2	-8.4	1.9	-2.4	-0.4		-3.4	-28.9		12.8	-3.4
LL01-1E	1.97	-3.7	-8.4	3.4	-2.8	-0.3		-2.7	-28.7		11.9	-2.8
LL01-1E	3	-0.4	-1.0	6.1	-4.9	-0.9	-1.9	-3.9	-8.3	-1.8	20.9	-3.9
LL01-1E	3.89	-1.7	-3.4	4.3	-4.7	-0.3	-2.4	-4.4	-12.8	-2.2	20.2	-4.5
LL01-1E	4.9	0.6	-1.2	10.2	-3.1	-0.3		-5.8	-11.0		21.7	-5.9
LL03-1E	1	-7.3	-11.1	-4.7	-3.1	-0.3		-3.3	-31.7		13.2	-3.3
LL03-1E	1.58	-1.6	-3.2	4.8	-4.2	-0.2	-1.9	-4.0	-11.6	-1.8	19.7	-4.1
LL03-1E	1.86	-1.4	-3.5	4.2	-4.9	-0.2	-1.0	-6.9	-10.8	-0.9	21.2	-6.9
LL03-1E	2.29	-1.4	-4.0	3.0	-5.1	-0.5	-1.0	-6.1	-11.7	-0.9	20.3	-6.2
LL03-1E	3	-0.8	-3.4	2.6	-5.4	-0.9	-0.8	-8.7	-9.5	-0.6	21.1	-8.8
LL03-1E	4.56	-1.8	-5.3	-3.0	-7.6	-1.6	0.0	-11.7	-8.1	0.1	20.0	-11.7
LL03-1E	6	-2.1	-5.4	-8.3	-8.6	-3.4	0.0	-12.1	-6.7	0.2	21.3	-12.1
LL06-1E	0.47	-0.8	-1.3	2.5	-5.8	-2.3	-1.8	-7.2	-8.2	-1.8	19.7	-7.3
LL06-1E	1	-1.7	-3.5	-4.7	-7.7	-3.3	-0.7	-11.3	-6.0	-0.6	20.0	-11.3
LL06-1E	1.54	-1.3	-4.3	-5.3	-8.6	-3.6	-0.1	-13.0	-7.0	0.0	20.8	-13.0
LL06-1E	2	-0.5	-3.0	-2.0	-6.7	-4.1	-0.4	-11.7	-9.3	-0.2	21.4	-11.8
LL06-1E	2.4	-0.1	-3.7	-0.5	-7.2	-4.1	-0.6	-12.8	-12.3	-0.4	19.3	-12.9
LL06-1E	2.9	-1.5	-3.4	-6.4	-7.3	-4.2	-0.6	-8.2	-9.0	-0.5	20.4	-8.3
LL06-1E	4.55	-1.9	-4.7	-4.5	-5.9	-2.1	-0.1	-10.0	-7.0	0.0	21.3	-10.0
LL07-1E	0.47	-8.2	-7.3	-7.3	-2.9	-2.5		-22.5	-31.2		10.2	-22.5
LL07-1E	0.77	-10.4	-6.6	-10.4	-1.0	-2.0		-9.8	-29.7		6.1	-9.8
LL07-1E	1.43	-3.9	-5.6	3.1	-3.7	-1.7		-3.0	-27.7		12.9	-3.0
LL07-1E	2.1	-0.2	-1.6	8.1	-4.9	-0.6	-1.8	-7.8	-11.6	-1.6	20.5	-7.8
LL07-1E	2.96	-1.2	-2.4	5.3	-4.8	-0.5	-1.9	-8.4	-12.3	-1.8	17.8	-8.4
LL07-1E	5.9				-7.5	-1.1	0.6	-20.1	-4.6	0.8	20.0	-20.1

Table B.3 Continued.

		Mineral saturation indices calculated with PHREEQC									
Location	Depth (m)	Covellite [CuS]	Dolomite [$CaMg(CO_3)_2$]	Epsomite [$MgSO_4 \cdot 7H_2O$]	Ferrihydrite [$Fe(OH)_3$]	FeS ppt.	Gibbsite [$Al(OH_3$]	Goethite [α-FeOOH]	Gypsum [$CaSO_4 \cdot 2H_2O$]	Hematite [Fe_2O_3]	Jarosite-K
LL01-1E	1.27	7.6		-3.7	-8.8	-7.8	-4.4	-3.5	-1.3	-5.2	-21.6
LL01-1E	1.6	8.4		-3.6	-7.1	-5.1	-1.3	-1.8	-0.2	-1.7	-19.3
LL01-1E	1.97	7.7		-3.4	-7.1	-5.3	-0.8	-1.8	0.0	-1.7	-19.4
LL01-1E	3	11.9	-4.4	-3.7	-0.1	-0.6	2.4	5.2	-0.7	12.2	-5.5
LL01-1E	3.89	11.2	-5.1	-2.9	-1.2	-0.6	1.1	4.1	0.0	10.1	-6.5
LL01-1E	4.9	12.3		-2.4	0.0	-0.2	3.5	5.3	-0.1	12.6	-4.1
LL03-1E	1	9.7		-2.7	-7.3	-6.2	-4.5	-2.1	-0.1	-2.3	-17.3
LL03-1E	1.58	11.3	-3.8	-2.5	-0.9	-1.2	1.3	4.3	0.0	10.5	-5.9
LL03-1E	1.86	11.8	-2.0	-2.5	0.1	-0.2	1.4	5.3	0.0	12.5	-4.0
LL03-1E	2.29	11.7	-1.9	-2.6	-0.6	-1.0	1.4	4.6	-0.3	11.2	-7.1
LL03-1E	3	12.1	-1.5	-3.0	0.2	-0.6	2.1	5.3	-0.6	12.6	-7.4
LL03-1E	4.56	9.9	-0.1	-3.8	0.9	0.7	1.0	6.1	-1.3	14.2	-7.6
LL03-1E	6	12.8	0.0	-5.7	1.2	-1.1	0.7	6.4	-3.2	14.8	-11.0
LL06-1E	0.47	12.5	-4.4	-5.0	-0.6	-2.5	2.0	4.6	-2.0	11.2	-9.5
LL06-1E	1	11.6	-2.3	-6.2	0.7	-1.1	1.2	5.9	-3.0	13.7	-10.4
LL06-1E	1.54	12.8	-0.7	-6.3	0.9	-1.6	1.5	6.2	-3.4	14.3	-11.1
LL06-1E	2	13.3	-1.0	-6.5	0.8	-1.5	2.3	6.1	-3.9	14.1	-10.5
LL06-1E	2.4	10.3	-1.1	-6.4	-0.2	-0.6	2.7	5.1	-3.9	12.2	-13.1
LL06-1E	2.9	12.2	-1.1	-6.4	0.0	-1.4	1.3	5.3	-4.0	12.5	-14.3
LL06-1E	4.55	12.6	-0.3	-4.4	1.0	-0.8	0.9	6.3	-1.9	14.4	-8.3
LL07-1E	0.47	9.7		-5.0	-3.1	-9.1	-5.3	2.2	-2.2	6.4	-4.4
LL07-1E	0.77	5.7		-4.1	-4.9	-9.1	-7.6	0.4	-1.8	2.8	-6.2
LL07-1E	1.43	8.7		-3.6	-5.6	-5.4	-1.0	-0.3	-1.5	1.2	-14.7
LL07-1E	2.1	11.8	-3.6	-2.9	-0.1	-0.8	2.7	5.2	-0.4	12.3	-4.0
LL07-1E	2.96	11.4	-3.6	-2.5	-1.7	-3.2	1.6	3.6	-0.2	9.2	-8.5
LL07-1E	5.9	10.3	1.3	-3.3	3.0	0.4		8.3	-0.9	18.5	-2.8

Table B.3 Continued.

		Mineral saturation indices calculated with PHREEQC									
Location	Depth (m)	Mackinawite [$Fe_{1+x}S$]	Maghemite [γ-Fe2O3]	Melanterite [$FeSO_4 \bullet 7H_2O$]	$Mn_3(AsO_4)_2$	Orpiment [As_2S_3]	Pyrite [FeS_2]	Realgar [As_4S_4]	Scorodite [$FeAsO_4 \bullet 2H_2O$]	Siderite [$FeCO_3$]	ZnS (amorph.)
LL01-1E	1.27	-7.0	-14.3	-2.8	-34.5	-0.9	5.5	-2.8	-15.5		-6.2
LL01-1E	1.6	-4.4	-10.8	-2.7	-28.3	1.6	8.1	-1.6	-14.0		-3.3
LL01-1E	1.97	-4.6	-10.8	-2.5	-28.3	0.5	6.6	-1.4	-14.5		-3.2
LL01-1E	3	0.3	3.1	-2.6	-4.9	0.1	16.4	-4.1	-3.3	0.8	0.8
LL01-1E	3.89	0.1	1.0	-1.9	-9.3	1.0	15.9	-3.5	-5.5	0.5	-0.5
LL01-1E	4.9	0.5	3.5	-1.6	-5.2	-1.9	16.4	-5.0	-4.4		0.7
LL03-1E	1	-5.4	-11.2	-1.8	-27.7	0.1	7.0	-2.2	-13.8		-4.3
LL03-1E	1.58	-0.5	1.6	-1.8	-8.1	-1.3	14.3	-4.1	-5.3	0.9	0.4
LL03-1E	1.86	0.5	3.5	-1.9	-7.4	-2.4	16.9	-5.4	-4.7	1.7	0.0
LL03-1E	2.29	-0.3	2.1	-2.5	-8.5	-3.3	14.7	-5.2	-5.8	1.4	-0.3
LL03-1E	3	0.1	3.7	-3.5	-7.7	-5.2	16.5	-6.9	-5.2	1.0	1.8
LL03-1E	4.56	1.6	5.3	-4.7	-5.4	-4.9	19.8	-7.6	-5.3	1.2	1.2
LL03-1E	6	-0.4	5.8	-6.9	-5.5	-11.7	16.0	-10.1	-4.8	1.0	1.5
LL06-1E	0.47	-1.7	2.1	-5.3	-7.0	-5.0	15.6	-7.2	-3.8	-0.6	0.2
LL06-1E	1	-0.3	4.7	-7.0	-7.2	-7.3	18.4	-9.0	-3.8	-0.1	1.8
LL06-1E	1.54	-0.9	5.3	-7.4	-8.0	-12.2	16.3	-10.8	-4.8	0.5	1.3
LL06-1E	2	-0.8	5.1	-6.8	-8.2	-10.6	16.5	-10.0	-4.3	1.3	0.2
LL06-1E	2.4	0.1	3.1	-7.3	-11.1	-6.9	18.4	-8.7	-6.4	0.7	1.2
LL06-1E	2.9	-0.7	3.4	-6.9	-7.3	-6.2	15.7	-7.4	-4.5	1.2	0.4
LL06-1E	4.55	-0.1	5.3	-5.1	-4.6	-9.2	15.8	-8.6	-4.5	1.4	1.2
LL07-1E	0.47	-8.3	-2.7	-3.9	-27.0	-19.3	18.4	-19.1	-4.7		-6.4
LL07-1E	0.77	-8.4	-6.3	-2.0	-25.4	-6.6	14.9	-11.0	-3.6		-8.0
LL07-1E	1.43	-4.7	-7.8	-2.4	-23.1	0.2	9.6	-3.1	-9.9		-2.7
LL07-1E	2.1	-0.1	3.2	-2.3	-6.0	-3.3	17.4	-6.4	-4.2	1.0	-0.3
LL07-1E	2.96	-2.4	0.0	-3.6	-6.4	-5.4	15.1	-7.5	-5.4	-0.6	-0.4
LL07-1E	5.9	1.3	9.4	-5.6	-1.7	-15.9	21.8	-14.3	-4.0	0.6	1.9

Table B.4 Saturation indices for samples from November 2017 calculated using PHREEQC.

		Mineral saturation indices calculated with PHREEQC										
Location	Depth (m)	$Al(OH)_3$ (amorph.)	$AlAsO_4$	Alunite ($KAl_3(SO_4)_2(OH)_6$]	Anglesite [$PbSO_4$]	Anhydrite [$CaSO_4$]	Ankerite [$Ca(Fe,Mg,Mn)(CO_3)_2$]	Arsenolite [As_4O_6]	$Ca_3(AsO_4)_2$	Calcite [$CaCO_3$]	Chalcopyrite [$CuFeS_2$]	Claudetite [As_2O_3]
LL01-1E	0.85	-8.8	-6.7	-8.3	-1.1	-2.3		-5.1	-30.0		8.4	-5.2
LL01-1E	1.27	-6.8	-13.6	-3.6	-1.1	-1.5		-4.1	-42.2		9.6	-4.2
LL01-1E	1.6	-2.1	-5.5	6.1	-3.2	-0.4		-3.4	-23.0		16.1	-3.4
LL01-1E	1.97	-4.9	-10.9	0.9	-3.5	-0.3		-2.8	-33.7		10.9	-2.9
LL01-1E	3	-0.2	-3.6	6.3	-4.9	-0.8	-1.8	-3.3	-12.9	-1.6	21.1	-3.4
LL01-1E	3.89	-1.9	-8.0	4.4	-3.5	-0.3		-4.4	-22.7		19.1	-4.4
LL01-1E	4.9	-0.7	-3.3	5.5	-3.7	-0.4		-5.5	-11.6		22.1	-5.6
LL03-1E	1	-2.4	-2.8	4.7	-3.9	-0.2	-3.0	-3.0	-13.6	-2.8	18.4	-3.1
LL03-1E	1.58	-1.5	-2.4	4.9	-4.8	-0.2	-1.7	-4.3	-10.2	-1.5	19.9	-4.3
LL03-1E	1.86	-1.6	-4.9	4.2	-4.8	-0.2	-1.4	-6.7	-14.2	-1.2	21.3	-6.8
LL03-1E	2.29	-1.3	-4.3	3.9	-4.5	-0.5	-1.3	-7.7	-13.4	-1.2	20.6	-7.8
LL03-1E	3	-1.0	-4.0	2.2	-5.5	-0.8	-0.6	-9.1	-10.4	-0.5	21.6	-9.1
LL03-1E	4.56	-2.0	-6.1	-3.7	-7.6	-1.5	0.2	-17.0	-8.7	0.3	19.8	-17.1
LL03-1E	6	-1.5	-5.1	-4.3	-7.4	-2.5	-0.1	-12.8	-7.8	0.0	21.0	-12.9
LL06-1E	1	-1.2	-3.3	-4.4	-8.2	-3.5	-0.3	-13.2	-5.3	-0.2	20.9	-13.3
LL06-1E	1.54	-1.1	-3.3	-5.7	-9.4	-4.7	-0.5	-9.4	-7.5	-0.3	21.4	-9.5
LL06-1E	2	-0.6	-3.5	-3.1	-7.4	-4.4	-0.4	-12.2	-10.0	-0.3	21.3	-12.2
LL06-1E	2.4	-0.1	-3.5	-0.4	-7.1	-3.9	-0.5	-11.1	-11.4	-0.3	20.4	-11.1
LL06-1E	2.9	-1.1	-3.3	-3.7	-6.9	-3.7	-0.7	-9.3	-9.8	-0.5	20.7	-9.3
LL06-1E	4.55	-1.4	-4.5	-3.0	-5.7	-2.1	-0.3	-11.7	-7.3	-0.1	21.9	-11.7
LL07-1E	0.47	-7.7	-6.5	-6.7	-3.0	-2.6		-8.4	-29.9		10.5	-8.5
LL07-1E	0.77	-8.8	-5.1					-18.8	-27.6		8.0	-18.9
LL07-1E	1.14	-8.1	-6.1	-5.7	-0.4	-1.9		-3.2	-28.6		9.8	-3.2
LL07-1E	1.43	-3.5	-5.4	3.5	-3.9	-1.7		-3.0	-27.0		13.6	-3.0
LL07-1E	2.1	-0.3	-1.8	8.0	-4.3	-0.6	-2.0	-9.0	-12.1	-1.8	21.1	-9.1
LL07-1E	2.96	-1.5	-3.4	4.9	-4.3	-0.4	-2.2	-6.9	-14.5	-2.1	18.2	-7.0
LL07-1E	5.9				-7.3	-1.1	0.6	-18.7	-5.1	0.7	21.9	-18.7

Table B.4 Continued.

		Mineral saturation indices calculated with PHREEQC									
Location	Depth (m)	Covellite [CuS]	Dolomite [$CaMg(CO_3)_2$]	Epsomite [$MgSO_4 \cdot 7H_2O$]	Ferrihydrite [$Fe(OH)_3$]	FeS ppt.	Gibbsite [$Al(OH_3$]	Goethite [α-FeOOH]	Gypsum [$CaSO_4 \cdot 2H_2O$]	Hematite [Fe_2O_3]	Jarosite-K
LL01-1E	0.85	7.8		-4.6	-6.6	-8.9	-6.0	-1.3	-2.1	-0.7	-14.2
LL01-1E	1.27	7.5		-3.7	-9.9	-7.5	-4.0	-4.6	-1.2	-7.3	-25.3
LL01-1E	1.6	10.3		-3.6	-5.2	-3.8	0.8	0.0	-0.2	2.0	-15.8
LL01-1E	1.97	7.4		-3.4	-8.5	-6.1	-2.0	-3.2	0.0	-4.5	-22.4
LL01-1E	3	11.9	-4.0	-3.6	-1.4	-0.4	2.6	3.9	-0.6	9.8	-9.5
LL01-1E	3.89	10.5		-2.9	-3.8	-0.9	0.9	1.5	0.0	5.0	-13.6
LL01-1E	4.9	12.5		-2.5	-0.1	0.0	2.2	5.2	-0.1	12.3	-5.1
LL03-1E	1	11.3	-6.0	-2.6	-1.9	-2.5	0.5	3.4	0.0	8.7	-6.4
LL03-1E	1.58	11.5	-3.3	-2.5	-0.5	-1.3	1.3	4.7	0.0	11.4	-4.6
LL03-1E	1.86	12.2	-2.7	-2.4	-0.9	-0.5	1.3	4.3	0.0	10.6	-6.4
LL03-1E	2.29	12.4	-2.5	-2.6	-0.8	-1.3	1.6	4.5	-0.3	10.9	-7.2
LL03-1E	3	12.8	-1.2	-2.9	-0.1	-0.8	1.8	5.0	-0.5	12.0	-7.9
LL03-1E	4.56	9.6	0.3	-3.7	1.8	0.6	0.9	7.0	-1.2	15.9	-5.3
LL03-1E	6	13.3	-0.4	-4.8	0.6	-1.9	1.3	5.9	-2.2	13.6	-10.5
LL06-1E	1	13.1	-1.5	-6.5	0.8	-1.8	1.7	6.1	-3.2	14.0	-11.2
LL06-1E	1.54	13.3	-1.3	-7.4	0.6	-1.5	1.7	5.8	-4.4	13.6	-13.2
LL06-1E	2	13.3	-1.0	-6.8	0.7	-1.6	2.2	5.9	-4.2	13.8	-11.7
LL06-1E	2.4	11.8	-0.9	-6.2	-0.4	-1.0	2.7	4.8	-3.7	11.6	-13.9
LL06-1E	2.9	12.9	-1.3	-5.9	-0.1	-1.8	1.8	5.2	-3.4	12.3	-13.2
LL06-1E	4.55	13.5	-0.6	-4.3	1.2	-1.2	1.4	6.5	-1.8	15.0	-7.5
LL07-1E	0.47	9.8		-5.1	-6.2	-8.9	-4.9	-0.9	-2.3	0.1	-14.6
LL07-1E	0.77	7.1			-2.1	-8.6	-5.9	3.2		8.3	
LL07-1E	1.14	7.4		-3.5	-6.1	-7.2	-5.2	-0.8	-1.6	0.4	-12.1
LL07-1E	1.43	9.1		-3.6	-5.4	-5.1	-0.7	-0.1	-1.5	1.7	-14.7
LL07-1E	2.1	12.6	-4.0	-2.9	0.2	-1.0	2.6	5.5	-0.4	12.8	-3.2
LL07-1E	2.96	12.0	-4.2	-2.5	-2.6	-3.3	1.4	2.7	-0.2	7.4	-10.7
LL07-1E	5.9	11.1	1.2	-3.3	3.5	1.3		8.8	-0.8	19.6	-0.9

Table B.4 Continued.

		Mineral saturation indices calculated with PHREEQC									
Location	Depth (m)	Mackinawite [$Fe_{1+x}S$]	Maghemite [γ-Fe2O3]	Melanterite [$FeSO_4 \bullet 7H_2O$]	$Mn_3(AsO_4)_2$	Orpiment [As_2S_3]	Pyrite [FeS_2]	Realgar [As_4S_4]	Scorodite [$FeAsO_4 \bullet 2H_2O$]	Siderite [$FeCO_3$]	ZnS (amorph.)
LL01-1E	0.85	-8.2	-9.8	-3.2	-26.7	-1.9	11.1	-6.7	-7.1		-7.1
LL01-1E	1.27	-6.7	-16.4	-2.8	-39.0	-0.9	3.1	-1.4	-19.3		-5.8
LL01-1E	1.6	-3.0	-7.1	-2.7	-22.5	1.4	10.3	-2.1	-11.3		-1.8
LL01-1E	1.97	-5.4	-13.5	-2.5	-32.8	0.4	4.6	-0.9	-17.1		-3.9
LL01-1E	3	0.4	0.7	-2.6	-9.7	0.2	13.4	-2.5	-7.3	1.0	1.0
LL01-1E	3.89	-0.2	-4.2	-1.9	-19.1	1.3	11.3	-1.2	-12.4		-0.2
LL01-1E	4.9	0.7	3.2	-1.7	-5.8	-2.1	15.5	-4.5	-5.3		0.9
LL03-1E	1	-1.7	-0.3	-1.7	-9.6	0.0	13.9	-3.9	-5.0	0.0	-0.6
LL03-1E	1.58	-0.5	2.4	-1.9	-6.6	-1.6	15.1	-4.7	-4.1	1.1	0.7
LL03-1E	1.86	0.2	1.6	-1.9	-10.8	-2.4	15.2	-4.7	-6.9	1.4	0.2
LL03-1E	2.29	-0.6	1.8	-2.6	-10.1	-5.2	14.5	-6.2	-6.5	1.1	0.1
LL03-1E	3	-0.1	3.1	-3.5	-8.7	-5.6	16.1	-6.9	-5.9	1.0	1.3
LL03-1E	4.56	1.4	7.0	-5.1	-6.1	-10.5	21.5	-11.3	-5.2	1.0	1.3
LL03-1E	6	-1.1	4.7	-6.4	-6.6	-12.9	15.2	-10.7	-5.7	0.4	1.8
LL06-1E	1	-1.1	5.1	-7.9	-6.8	-11.3	17.5	-11.0	-4.1	-0.4	2.4
LL06-1E	1.54	-0.7	4.6	-7.6	-7.4	-8.6	15.6	-8.6	-4.2	1.0	1.1
LL06-1E	2	-0.9	4.7	-7.2	-9.0	-11.1	16.2	-10.2	-4.8	1.2	0.7
LL06-1E	2.4	-0.2	2.5	-7.2	-10.1	-6.5	16.9	-7.9	-6.5	0.7	1.7
LL06-1E	2.9	-1.1	3.2	-6.5	-8.1	-7.8	15.3	-8.2	-5.0	1.0	0.1
LL06-1E	4.55	-0.5	5.9	-5.1	-4.9	-11.8	15.7	-10.1	-4.4	1.1	1.0
LL07-1E	0.47	-8.1	-9.0	-4.0	-25.7	-5.3	11.9	-8.7	-7.6		-6.0
LL07-1E	0.77	-7.9	-0.8		-23.5	-15.7	19.8	-17.7	-1.0		-7.0
LL07-1E	1.14	-6.4	-8.7	-2.1	-24.1	1.8	12.3	-4.5	-6.7		-5.5
LL07-1E	1.43	-4.4	-7.4	-2.5	-22.4	0.2	9.7	-3.0	-9.9		-2.3
LL07-1E	2.1	-0.3	3.7	-2.2	-6.4	-5.2	17.5	-7.5	-4.0	0.9	0.0
LL07-1E	2.96	-2.6	-1.7	-3.4	-8.6	-4.0	13.5	-6.1	-7.0	-0.8	-0.6
LL07-1E	5.9	2.2	10.5	-4.5	-1.8	-14.6	21.9	-13.3	-3.5	1.6	1.9

Table B.5 Saturation indices for samples from June 2018 calculated using PHREEQC.

		Mineral saturation indices calculated with PHREEQC										
Location	Depth (m)	$Al(OH)_3$ (amorph.)	$AlAsO_4$	Alunite $(KAl_3(SO_4)_2(OH)_6]$	Anglesite $[PbSO_4]$	Anhydrite $[CaSO_4]$	Ankerite $[Ca(Fe,Mg,Mn)(CO_3)_2]$	Arsenolite $[As_4O_6]$	$Ca_3(AsO_4)_2$	Calcite $[CaCO_3]$	Chalcopyrite $[CuFeS_2]$	Claudetite $[As_2O_3]$
LL01-1E	0.9	-7.7	-5.6	-7.4	-2.3	-3.1		-6.2	-28.7		10.2	-6.3
LL01-1E	1.3	-7.0	-4.3	-4.2	-1.5	-1.9		-5.4	-24.5		11.5	-5.4
LL01-1E	1.6	-6.0	-5.0	-2.1	-3.6	-1.3		-4.5	-24.4		12.2	-4.5
LL01-1E	2.0	-3.9	-1.7	2.7	-3.6	-0.3		-4.4	-15.3		13.3	-4.4
LL01-1E	3.0	0.0	-0.4	6.9	-4.7	-1.1	-1.9	-6.8	-7.6	-2.0	22.5	-6.9
LL01-1E	3.9	-2.2	-2.2	3.8	-3.4	-0.3	-2.8	-8.3	-11.1	-2.7	21.1	-8.4
LL01-1E	4.9	-1.2	-3.2	4.0	-4.3	-0.3	-2.2	-8.6	-10.1	-2.0	22.5	-8.6
LL03-1E	0.3	-7.9	-5.3	-5.9	-2.6	-0.3		-20.2	-24.3		11.2	-20.3
LL03-1E	0.5	-8.2	-4.6	-4.4	-2.2	-0.4		-26.1	-23.7		9.3	-26.1
LL03-1E	1.6	-1.5	-1.9	5.0	-4.5	-0.3	-2.1	-7.4	-9.8	-2.0	20.6	-7.5
LL03-1E	1.9	-1.1	-2.2	5.1	-4.7	-0.3	-1.3	-10.5	-10.1	-1.2	21.6	-10.5
LL03-1E	2.3	-1.8	-4.3	3.5	-4.7	-0.7	-2.0	-15.5	-15.7	-1.8	19.6	-15.6
LL03-1E	3.0	-1.9	-5.0	-1.0	-4.5	-1.0	-0.6	-14.6	-10.8	-0.4	21.9	-14.7
LL03-1E	4.6	-1.7	-6.4	-3.4	-6.7	-1.5	0.2	-23.9	-9.2	0.3	19.8	-23.9
LL03-1E	6.0	-1.9	-6.0	-6.5	-7.4	-2.6	0.1	-19.5	-7.1	0.3	21.7	-19.6
LL06-1E	0.5	-5.3	-4.0	-4.2	-5.3	-2.1	-3.8	-5.2	-18.1	-3.7	12.5	-5.3
LL06-1E	1.0	-1.4	-3.0	-3.4	-7.2	-3.9	-1.4	-22.3	-9.3	-1.3	18.9	-22.3
LL06-1E	1.5	-1.5	-3.4	-5.8	-9.3	-4.4	-0.6	-14.2	-7.6	-0.4	20.9	-14.3
LL06-1E	2.0	-0.6	-3.0	-3.0	-9.6	-4.5	-0.5	-14.9	-9.4	-0.3	20.7	-15.0
LL06-1E	2.4	-0.1	-4.3	-1.0	-9.7	-4.3	-0.5	-20.4	-13.5	-0.4	18.4	-20.4
LL06-1E	2.9	-1.2	-3.7	-5.3	-8.6	-4.1	-0.5	-15.9	-9.9	-0.4	20.7	-15.9
LL06-1E	4.6	-2.4	-5.7	-6.2	-7.6	-2.1	0.0	-16.4	-7.4	0.1	20.9	-16.4
LL07-1E	0.5	-9.5	-7.3	-9.1	-2.4	-2.5		-27.1	-32.1		8.4	-27.1
LL07-1E	1.4	-4.5	-2.0	1.6	-2.9	-1.7		-7.1	-20.2		13.7	-7.2
LL07-1E	2.1	-0.6	-0.9	7.8	-2.8	-0.9	-3.0	-12.5	-12.5	-2.9	20.6	-12.6
LL07-1E	3.0	-2.1	-3.3	3.5	-3.5	-0.5	-3.1	-13.8	-14.5	-2.9	17.7	-13.8
LL07-1E	5.9				-5.9	-1.1	0.5	-24.9	-5.6	0.6	21.0	-24.9

Table B.5 Continued.

		Mineral saturation indices calculated with PHREEQC									
Location	Depth (m)	Covellite [CuS]	Dolomite [$CaMg(CO_3)_2$]	Epsomite [$MgSO_4 \cdot 7H_2O$]	Ferrihydrite [$Fe(OH)_3$]	FeS ppt.	Gibbsite [$Al(OH_3$]	Goethite [α-FeOOH]	Gypsum [$CaSO_4 \cdot 2H_2O$]	Hematite [Fe_2O_3]	Jarosite-K
LL01-1E	0.9	9.2		-5.4	-6.0	-8.5	-4.9	-0.7	-2.8	0.5	-14.6
LL01-1E	1.3	9.5		-4.1	-5.0	-7.6	-4.1	0.3	-1.6	2.6	-10.6
LL01-1E	1.6	9.3		-3.8	-5.7	-6.7	-3.1	-0.5	-1.0	1.0	-13.9
LL01-1E	2.0	9.2		-3.4	-3.3	-5.5	-1.1	2.0	-0.1	5.8	-7.9
LL01-1E	3.0	13.6	-4.8	-3.7	0.9	-0.7	2.9	6.2	-0.8	14.4	-2.8
LL01-1E	3.9	12.9	-6.0	-2.8	0.0	-1.4	0.6	5.3	0.0	12.6	-1.9
LL01-1E	4.9	13.1	-4.2	-2.4	1.0	-0.2	1.6	6.3	0.0	14.6	-1.6
LL03-1E	0.3	9.5		-2.3	-1.6	-7.9	-5.1	3.7	0.0	9.2	0.5
LL03-1E	0.5	9.3		-2.1	-1.4	-9.6	-5.3	3.9	-0.1	9.7	3.4
LL03-1E	1.6	12.6	-4.4	-2.7	0.1	-1.7	1.3	5.4	-0.1	12.7	-2.7
LL03-1E	1.9	13.3	-3.0	-2.9	0.8	-1.3	1.7	6.0	-0.1	13.9	-1.8
LL03-1E	2.3	12.6	-3.8	-2.8	0.2	-2.5	1.0	5.4	-0.5	12.8	-3.1
LL03-1E	3.0	13.6	-1.1	-3.2	1.0	-1.3	1.0	6.2	-0.8	14.4	-5.2
LL03-1E	4.6	9.7	0.4	-3.8	3.1	0.4	1.1	8.3	-1.3	18.6	-1.6
LL03-1E	6.0	13.4	0.1	-5.0	2.8	-1.2	1.0	8.0	-2.4	18.0	-5.1
LL06-1E	0.5	9.7	-8.1	-4.8	-4.8	-6.7	-2.5	0.4	-1.9	2.8	-15.3
LL06-1E	1.0	11.7	-3.6	-7.0	1.9	-2.5	1.5	7.1	-3.7	16.1	-6.4
LL06-1E	1.5	12.4	-1.6	-7.1	1.9	-1.2	1.4	7.1	-4.1	16.2	-8.4
LL06-1E	2.0	12.4	-1.1	-6.9	1.6	-1.2	2.3	6.9	-4.2	15.7	-8.8
LL06-1E	2.4	9.4	-1.0	-6.5	1.4	-0.5	2.7	6.6	-4.0	15.2	-9.0
LL06-1E	2.9	12.9	-1.0	-6.3	1.5	-1.7	1.6	6.8	-3.8	15.5	-9.5
LL06-1E	4.6	12.2	-0.1	-4.3	2.3	-0.8	0.5	7.6	-1.8	17.1	-4.5
LL07-1E	0.5	8.9		-4.9	-2.3	-10.1	-6.7	3.0	-2.2	7.9	0.0
LL07-1E	1.4	9.7		-3.4	-2.7	-5.6	-1.6	2.6	-1.5	7.2	-5.5
LL07-1E	2.1	12.9	-6.0	-3.1	0.8	-1.9	2.2	6.1	-0.6	14.1	-0.3
LL07-1E	3.0	12.0	-5.9	-2.5	-1.0	-3.8	0.8	4.3	-0.2	10.5	-5.7
LL07-1E	5.9	11.6	1.0	-3.2	3.9	-0.1		9.2	-0.8	20.4	1.1

Table B.5 Continued.

		Mineral saturation indices calculated with PHREEQC									
Location	Depth (m)	Mackinawite [$Fe_{1+x}S$]	Maghemite [γ-Fe2O3]	Melanterite [$FeSO_4 \bullet 7H_2O$]	$Mn_3(AsO_4)_2$	Orpiment [As_2S_3]	Pyrite [FeS_2]	Realgar [As_4S_4]	Scorodite [$FeAsO_4 \bullet 2H_2O$]	Siderite [$FeCO_3$]	ZnS (amorph.)
LL01-1E	0.9	-7.8	-8.6	-4.0	-24.9	-3.0	12.0	-7.5	-6.5		-5.7
LL01-1E	1.3	-6.8	-6.5	-2.9	-21.1	-2.2	13.1	-7.1	-5.0		-5.5
LL01-1E	1.6	-5.9	-8.1	-3.2	-21.7	0.5	12.4	-5.0	-7.4		-4.2
LL01-1E	2.0	-4.7	-3.2	-2.5	-14.8	-1.1	14.3	-6.2	-3.7		-3.3
LL01-1E	3.0	0.0	5.3	-2.6	-4.0	-4.4	17.3	-6.9	-2.1	0.7	0.7
LL01-1E	3.9	-0.6	3.5	-1.9	-7.4	-3.3	18.7	-7.4	-2.5	0.0	-0.1
LL01-1E	4.9	0.6	5.5	-1.6	-4.3	-5.7	17.4	-7.3	-3.5	1.0	0.6
LL03-1E	0.3	-7.1	0.3	-1.7	-20.0	-16.8	20.3	-18.2	-1.6		-5.3
LL03-1E	0.5	-8.8	0.7	-3.0	-18.8	-22.7	22.4	-23.0	-0.5		-5.4
LL03-1E	1.6	-0.9	3.7	-2.1	-6.7	-4.7	16.8	-7.3	-2.9	0.5	0.4
LL03-1E	1.9	-0.5	4.9	-2.3	-7.2	-7.2	18.2	-9.0	-3.0	1.1	0.8
LL03-1E	2.3	-1.8	3.7	-2.9	-12.5	-12.7	17.9	-12.3	-5.0	0.3	-0.6
LL03-1E	3.0	-0.6	5.5	-3.9	-9.3	-12.2	17.9	-11.4	-4.9	1.0	1.3
LL03-1E	4.6	1.2	9.7	-5.4	-6.7	-17.7	24.1	-16.3	-4.3	0.7	1.5
LL03-1E	6.0	-0.5	9.0	-6.3	-6.1	-20.0	18.5	-15.6	-4.0	0.9	1.7
LL06-1E	0.5	-6.0	-6.3	-5.3	-16.0	-2.0	12.5	-6.3	-6.2	-2.6	-3.0
LL06-1E	1.0	-1.7	7.2	-8.1	-10.3	-17.9	22.7	-17.2	-2.5	-1.2	1.6
LL06-1E	1.5	-0.4	7.2	-7.1	-7.6	-12.4	18.9	-11.9	-2.7	1.1	0.9
LL06-1E	2.0	-0.5	6.7	-7.1	-8.4	-12.8	18.8	-12.1	-3.4	1.3	0.0
LL06-1E	2.4	0.2	6.1	-7.5	-12.3	-14.0	21.9	-13.9	-5.4	0.7	0.7
LL06-1E	2.9	-1.0	6.4	-6.9	-8.3	-14.4	18.4	-13.0	-3.6	1.1	0.4
LL06-1E	4.6	-0.1	8.0	-5.2	-5.1	-15.6	18.5	-13.2	-3.6	1.3	1.5
LL07-1E	0.5	-9.3	-1.2	-3.7	-28.2	-23.9	20.9	-23.2	-2.7		-7.4
LL07-1E	1.4	-4.9	-1.9	-2.3	-15.7	-3.9	15.7	-8.3	-2.8		-2.9
LL07-1E	2.1	-1.1	5.0	-2.4	-6.9	-8.6	19.6	-10.7	-2.1	-0.1	0.6
LL07-1E	3.0	-3.1	1.4	-3.5	-8.5	-10.7	17.1	-11.5	-4.8	-1.7	-0.9
LL07-1E	5.9	0.7	11.3	-5.4	-2.9	-21.2	23.9	-18.3	-2.7	0.6	2.4

Appendix C: Hydrogeology

Table C.1 Measured hydraulic head values.

		Water Level (mASL)			
Location/Well	**Matrix**	**June 13, 2017**	**Sept 17, 2017**	**Nov 7, 2017**	**June 11, 2018**
LL01-1.6	Tailings	241.80	241.80	242.43	241.76
LL01-1.97	Tailings	241.85	241.84	242.44	241.74
LL01-3.0	Soil	241.92	241.91	242.44	241.86
LL01-3.89	Soil	242.12	242.09	242.14	241.89
LL01-4.9	Soil	241.99	242.01	242.39	241.81
LL03-1.0	Tailings	241.66	241.71	242.32	N/A[a]
LL03-1.58	Tailings	241.69	241.90	242.34	241.49
LL03-1.86	Soil	241.75	241.78	242.43	241.51
LL03-2.29	Soil	242.05	242.08	242.15	241.90
LL03-3.0	Soil	242.04	242.07	242.37	241.89
LL03-4.56	Soil	242.13	241.98	241.47	242.17
LL03-6.0	Soil	242.26	241.71	240.35	242.37
LL06-1.0	Tailings	241.57	241.62	242.30	241.43
LL06-1.54	Tailings	241.59	241.63	242.34	241.45
LL06-2.0	Soil	241.61	241.65	242.07	241.46
LL06-2.4	Soil	241.83	241.83	242.10	241.74
LL06-2.9	Soil	241.92	241.91	242.11	241.85
LL06-4.55	Soil	241.92	241.82	241.69	241.89
LL07-1.14	Tailings	N/A[a]	242.18	242.56	N/A[a]
LL07-1.43	Tailings	242.37	242.37	242.66	242.27
LL07-2.1	Soil	242.39	242.38	242.67	242.30
LL07-2.96	Soil	242.53	242.47	242.82	242.44
LL07-5.9	Soil	242.36	242.42	242.57	242.29
P1		------	------	------	242.04
P2		------	------	------	242.63
P3		------	------	------	242.10
P4		------	------	------	241.98
P5		------	------	------	241.81

a – Piezometer was dry during measurement

Table C.1 Continued.

Location/Well	Matrix	Water Level (mASL)			
		July 24, 2018	Oct 25, 2018	Nov 5, 2018	July 3, 2019
LL01-1.6	Tailings	N/A[a]	242.41	242.68	241.71
LL01-1.97	Tailings	241.54	------	242.67	241.72
LL01-3.0	Soil	241.65	------	242.77	242.00
LL01-3.89	Soil	241.05	242.14	242.28	242.19
LL01-4.9	Soil	240.95	------	242.22	242.13
LL03-1.0	Tailings	N/A[a]	242.31	242.56	N/A[a]
LL03-1.58	Tailings	241.69	------	242.56	241.52
LL03-1.86	Soil	241.55	------	242.43	241.59
LL03-2.29	Soil	241.25	------	242.32	241.98
LL03-3.0	Soil	241.33	------	242.43	241.96
LL03-4.56	Soil	240.44	242.24	242.25	242.14
LL03-6.0	Soil	239.56	------	241.71	242.29
LL06-1.0	Tailings	241.72	242.41	242.07	241.58
LL06-1.54	Tailings	241.71	------	242.14	241.59
LL06-2.0	Soil	241.60	------	242.13	241.56
LL06-2.4	Soil	241.16	------	242.13	241.81
LL06-2.9	Soil	241.18	------	242.14	241.94
LL06-4.55	Soil	240.49	241.85	241.94	241.91
LL07-1.14	Tailings	N/A[a]	------	242.46	N/A[a]
LL07-1.43	Tailings	N/A[a]	242.63	242.73	242.36
LL07-2.1	Soil	241.93	------	242.75	242.40
LL07-2.96	Soil	241.83	------	242.60	242.45
LL07-5.9	Soil	241.75	242.58	242.57	242.43
P1		------	242.59	------	241.90
P2		------	242.75	------	242.52
P3		------	242.74	------	241.90
P4		------	242.66	------	241.78
P5		------	242.56	------	241.70

a – Piezometer was dry during measurement

Table C.2 Measured water levels.

		Water Level (mbgs)			
Location/Well	**Matrix**	**June 13, 2017**	**Sept 17, 2017**	**Nov 7, 2017**	**June 11, 2018**
LL01-1.6	Tailings	1.225	1.221	0.689	1.359
LL01-1.97	Tailings	1.172	1.186	0.687	1.381
LL01-3.0	Soil	1.300	1.308	0.785	1.361
LL01-3.89	Soil	0.991	1.025	0.972	1.220
LL01-4.9	Soil	1.078	1.058	0.683	1.259
LL03-1.0	Tailings	0.927	0.877	0.268	N/A[a]
LL03-1.58	Tailings	0.896	0.691	0.249	1.096
LL03-1.86	Soil	0.854	0.825	0.172	1.089
LL03-2.29	Soil	0.545	0.514	0.429	0.691
LL03-3.0	Soil	0.550	0.517	0.220	0.704
LL03-4.56	Soil	0.477	0.635	1.141	0.445
LL03-6.0	Soil	0.347	0.905	2.259	0.239
LL06-1.0	Tailings	0.579	0.533	0.122	0.721
LL06-1.54	Tailings	0.566	0.530	0.079	0.713
LL06-2.0	Soil	0.532	0.491	0.077	0.685
LL06-2.4	Soil	0.336	0.339	0.065	0.426
LL06-2.9	Soil	0.276	0.284	0.083	0.340
LL06-4.55	Soil	0.198	0.300	0.428	0.235
LL07-1.14	Tailings	N/A[a]	1.152	0.780	N/A[a]
LL07-1.43	Tailings	1.213	1.214	0.923	1.314
LL07-2.1	Soil	1.225	1.226	0.945	1.311
LL07-2.96	Soil	1.019	1.077	0.727	1.109
LL07-5.9	Soil	1.049	0.989	0.835	1.116
P1		------	------	------	0.568
P2		------	------	------	0.128
P3		------	------	------	0.833
P4		------	------	------	0.738
P5		------	------	------	1.045

a – Piezometer was dry during measurement

Table C.2 Continued.

Location/Well	Matrix	Water Level (mbgs) July 24, 2018	Oct 25, 2018	Nov 5, 2018	July 3, 2019
LL01-1.6	Tailings	N/A[a]	0.708	0.439	1.231
LL01-1.97	Tailings	1.585	------	0.453	1.246
LL01-3.0	Soil	1.572	------	0.447	1.217
LL01-3.89	Soil	2.062	0.971	0.831	0.924
LL01-4.9	Soil	2.117	------	0.846	0.943
LL03-1.0	Tailings	N/A[a]	0.277	0.032	N/A[a]
LL03-1.58	Tailings	0.899	------	0.028	1.023
LL03-1.86	Soil	1.048	------	0.166	1.014
LL03-2.29	Soil	1.344	------	0.266	0.609
LL03-3.0	Soil	1.263	------	0.159	0.626
LL03-4.56	Soil	2.172	0.373	0.362	0.466
LL03-6.0	Soil	3.051	------	0.897	0.322
LL06-1.0	Tailings	0.428	0.007	0.078	0.567
LL06-1.54	Tailings	0.451	------	0.020	0.574
LL06-2.0	Soil	0.541	------	0.010	0.587
LL06-2.4	Soil	1.009	------	0.031	0.351
LL06-2.9	Soil	1.014	------	0.051	0.256
LL06-4.55	Soil	1.634	0.275	0.176	0.207
LL07-1.14	Tailings	N/A[a]	------	0.877	N/A[a]
LL07-1.43	Tailings	N/A[a]	0.954	0.858	1.223
LL07-2.1	Soil	1.679	------	0.859	1.207
LL07-2.96	Soil	1.722	------	0.946	1.102
LL07-5.9	Soil	1.660	0.830	0.839	0.984
P1		------	0.020	------	1.070
P2		------	0.015	------	0.242
P3		------	0.193	------	1.155
P4		------	0.058	------	1.337
P5		------	0.295	------	1.172

a – Piezometer was dry during measurement

Table C.3 Hydraulic head values measured by ENDM/CH2M Hill.

	Water Level (mASL)					
Location ID	**July 12, 2013**	**August 19, 2013**	**Oct 15, 2015**	**July 14, 2016**	**Matrix**	**Location**
CH-LL-MW01	241.44	241.34	------	------	Soil	TA-01
CH-LL-MW02	241.42	241.55	------	------	Tailings	TA-01
CH-LL-MW03	242.98	243.01	------	------	Tailings	TA-01
CH-LL-MP03	242.19	242.13	------	------	Tailings	TA-01
MW15-01	------	------	241.1	241.11	Soil	TA-01
MW15-02	------	------	242.56	242.36	Bedrock	TA-01
MW15-03	------	------	242.27	241.75	Bedrock	TA-01
MW15-04	------	------	241.24	241.82	Soil	TA-01
MW15-05	------	------	242.8	242.2	Tailings	TA-01
MW16-01-1	------	------	------	241.7	Bedrock	TA-01
MW16-01-2	------	------	------	241.45	Soil	TA-01
MW16-02	------	------	------	241.61	Bedrock	TA-01
MW16-03-1	------	------	------	242.31	Bedrock	TA-01
MW16-03-2	------	------	------	242.23	Soil	TA-01
MW16-04	------	------	------	244.26	Bedrock	TA-01

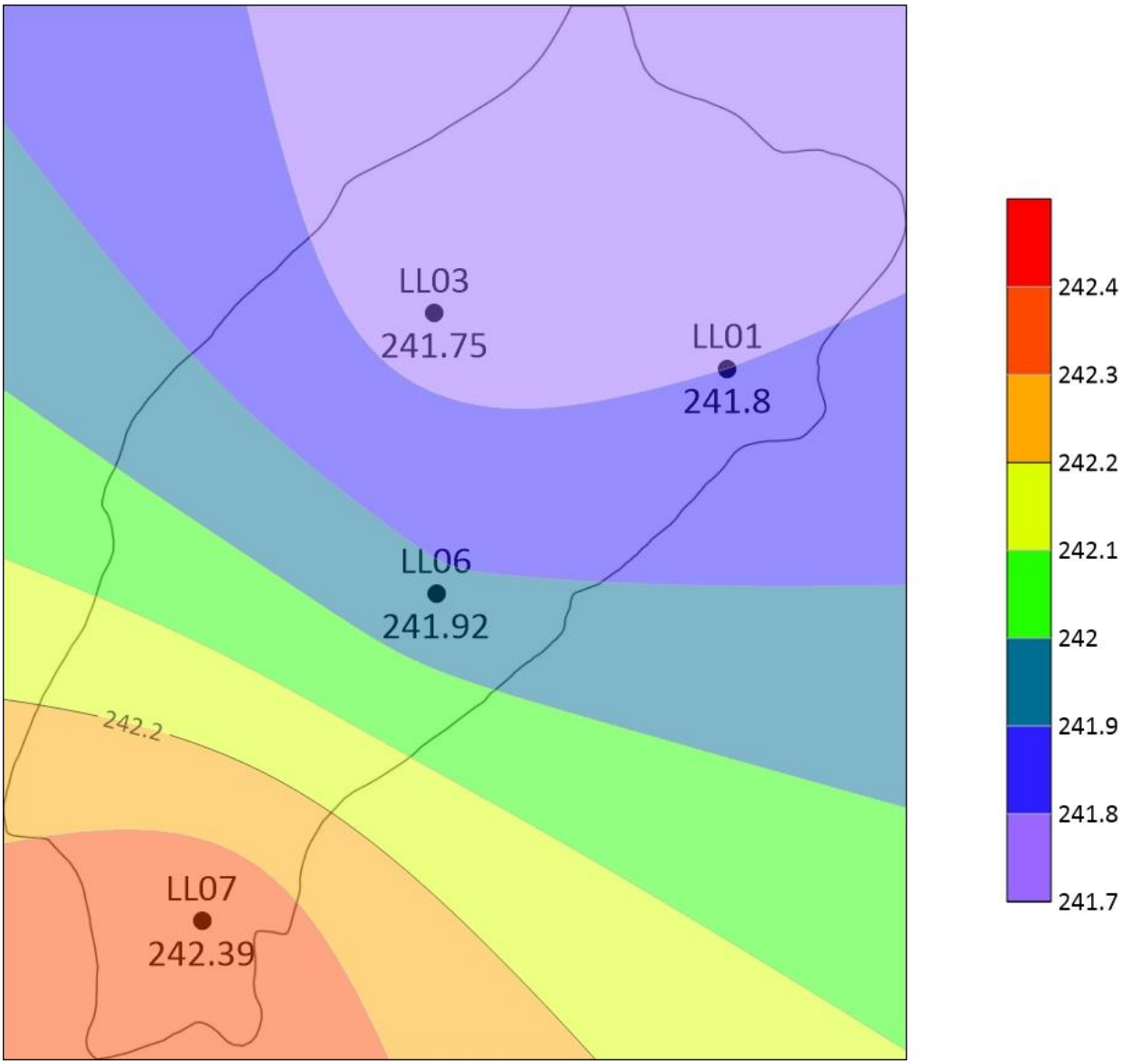

Figure C.1 Groundwater elevation contour map from June 2017.

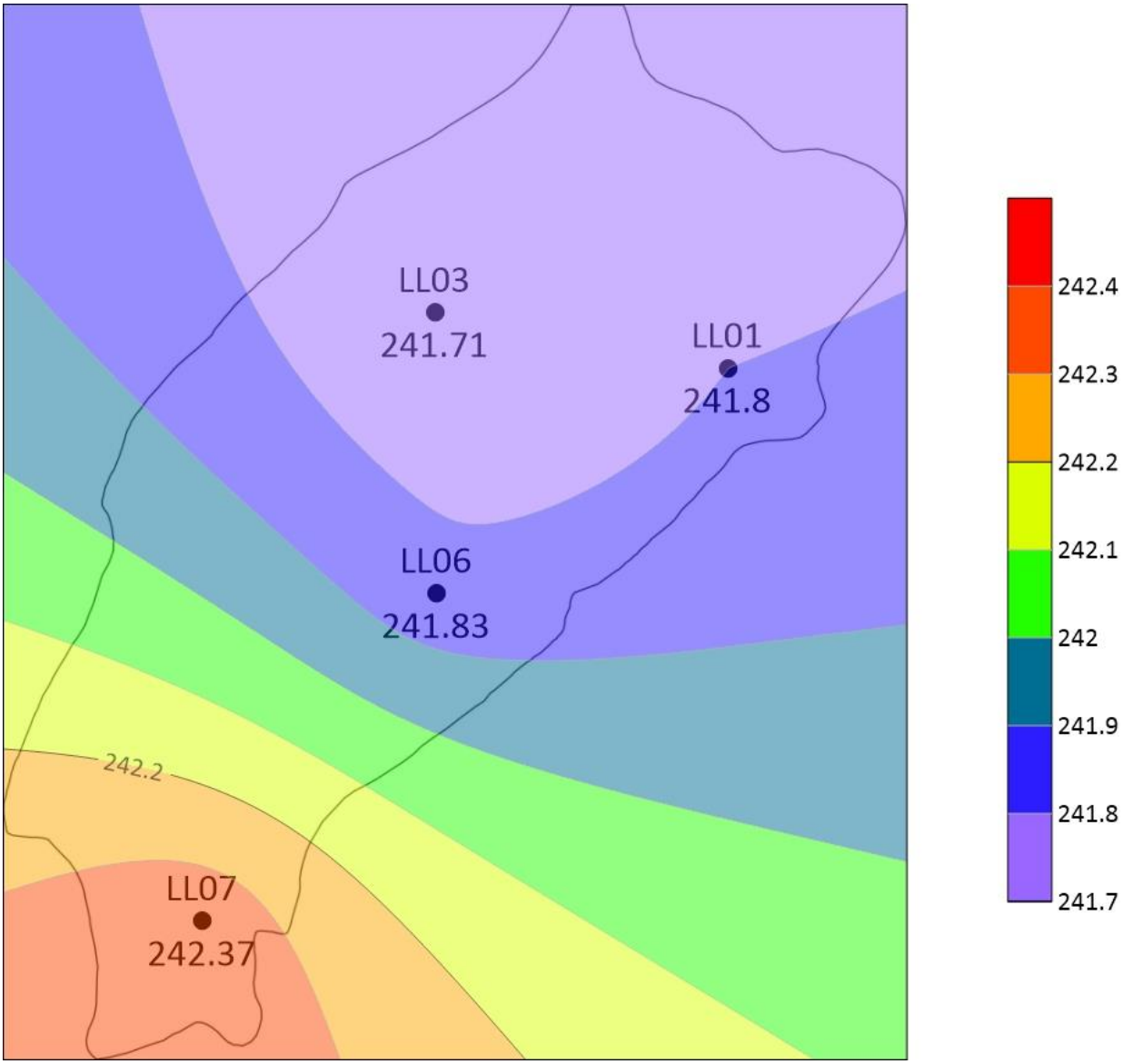

Figure C.2 Groundwater elevation contour map from September 2017.

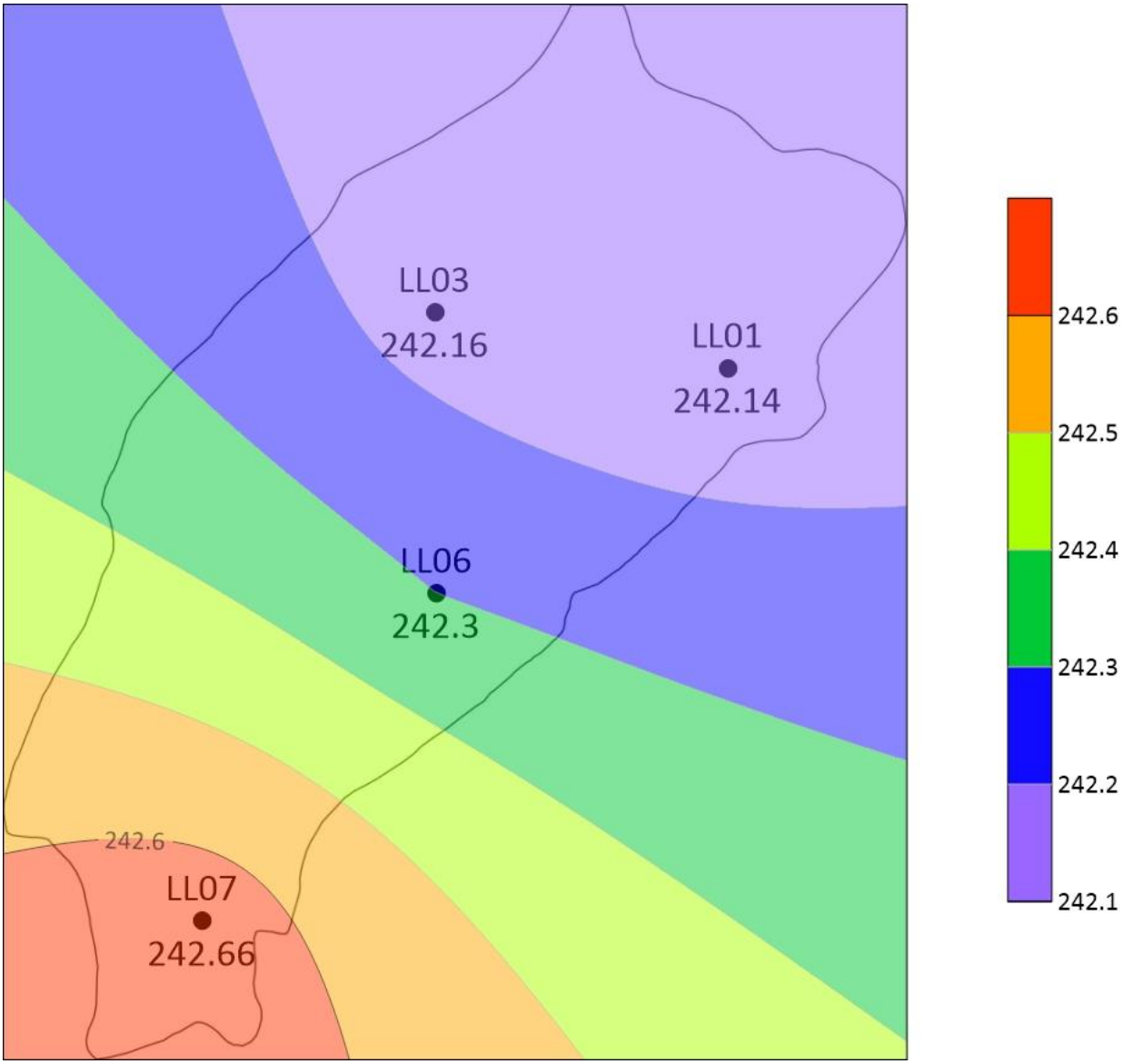

Figure C.3 Groundwater elevation contour map from November 2017.

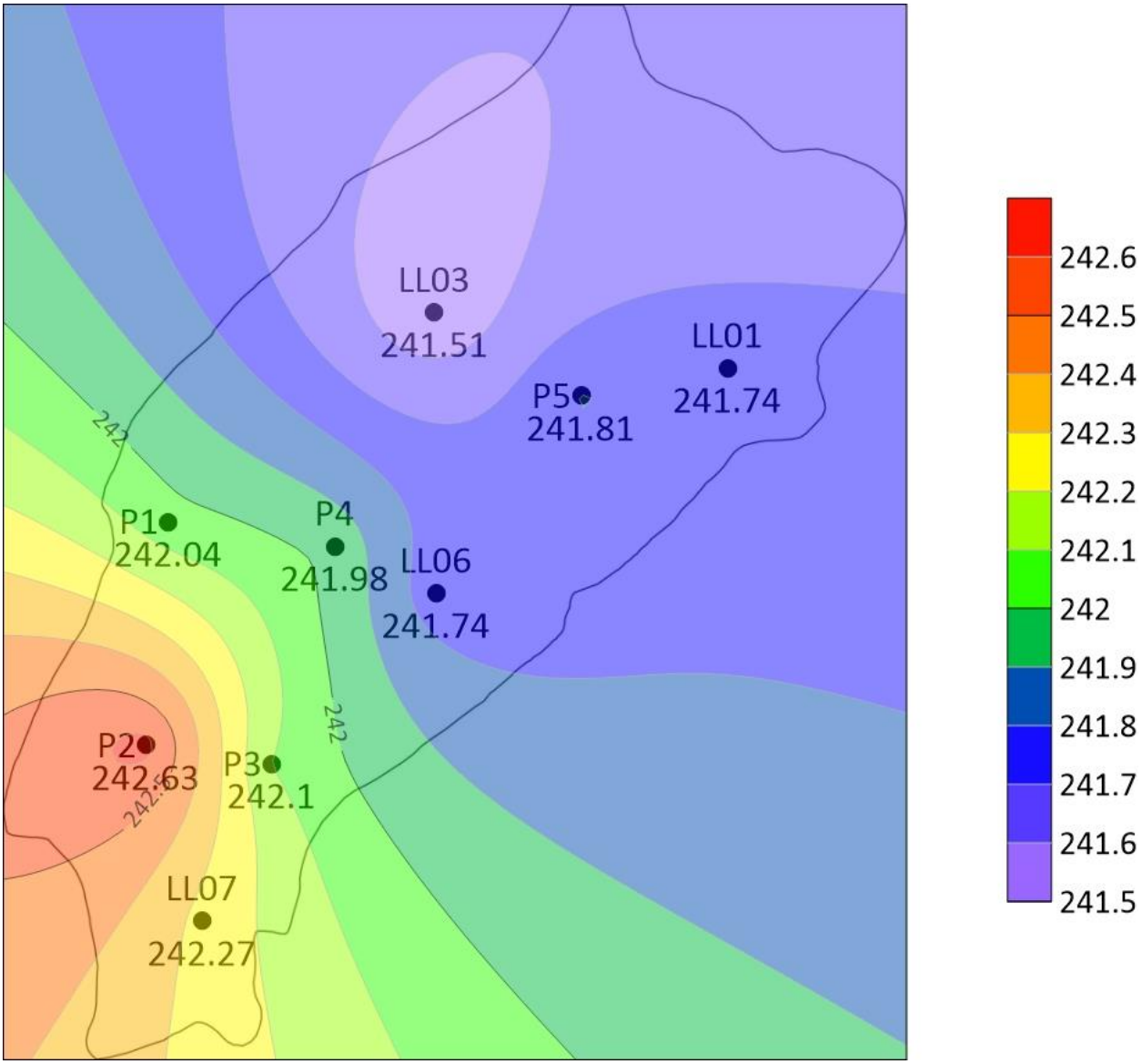

Figure C.4 Groundwater elevation contour map from June 2018.

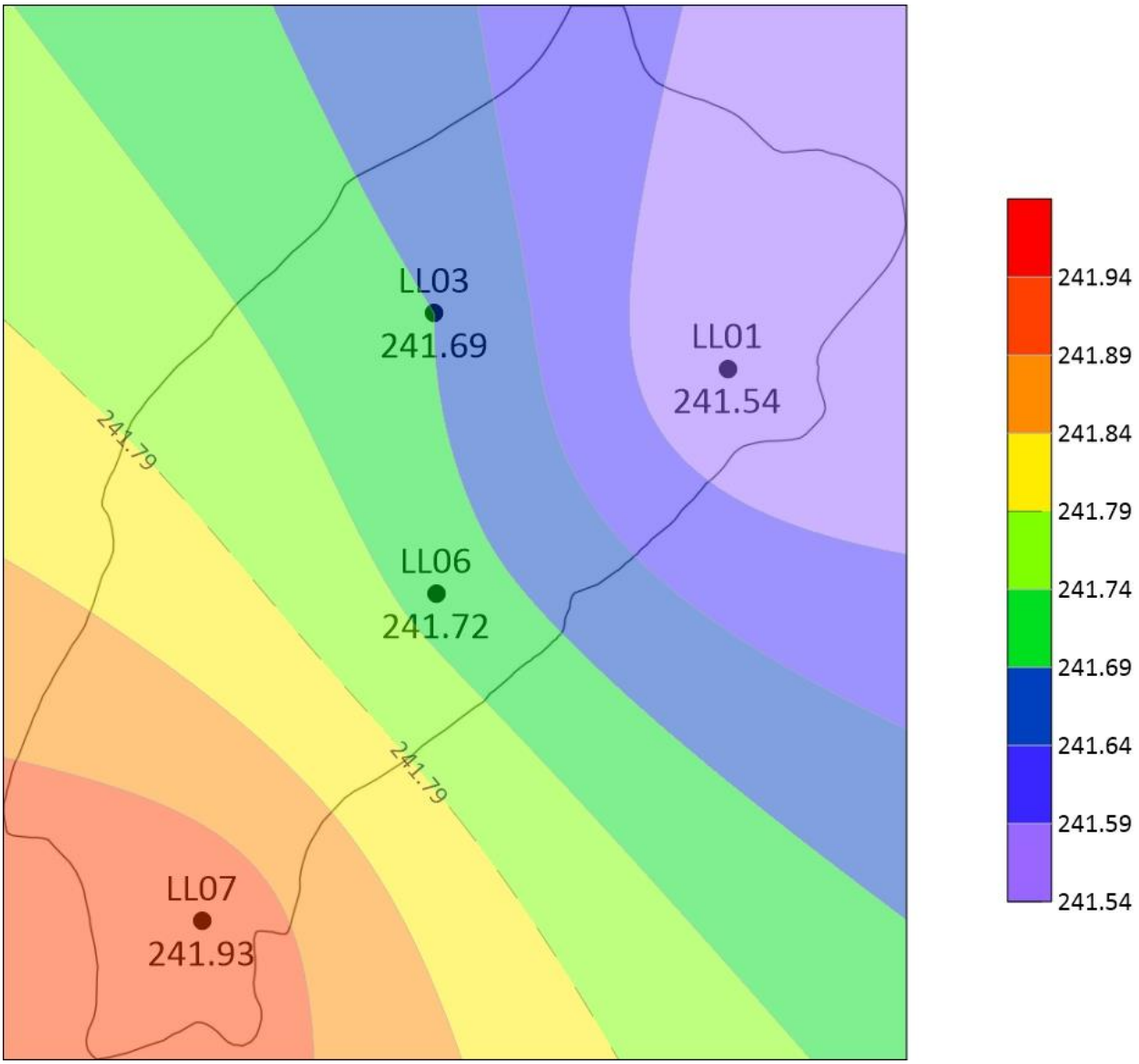

Figure C.5 Groundwater elevation contour map from July 2018.

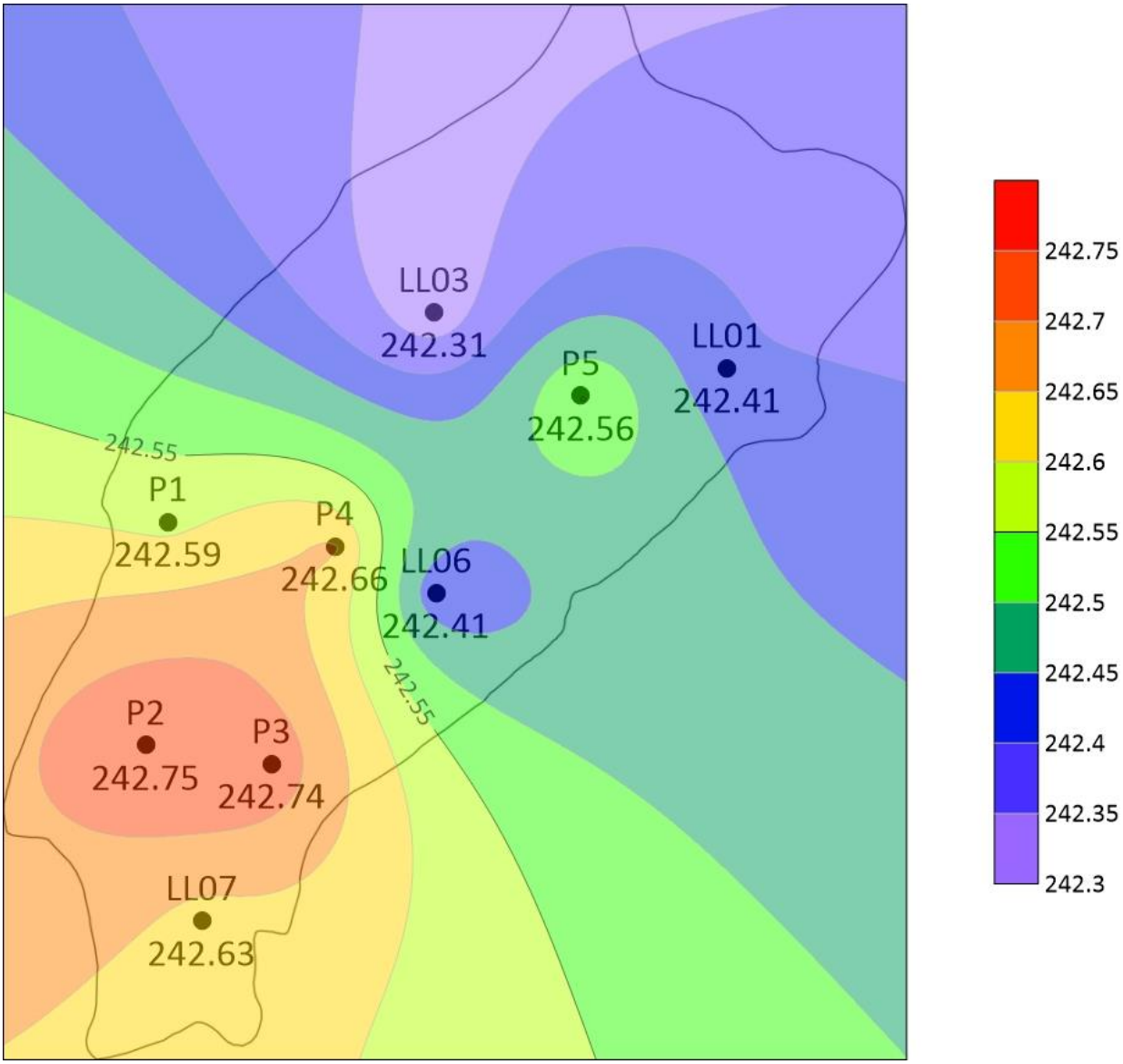

Figure C.6 Groundwater elevation contour map from October 2018.

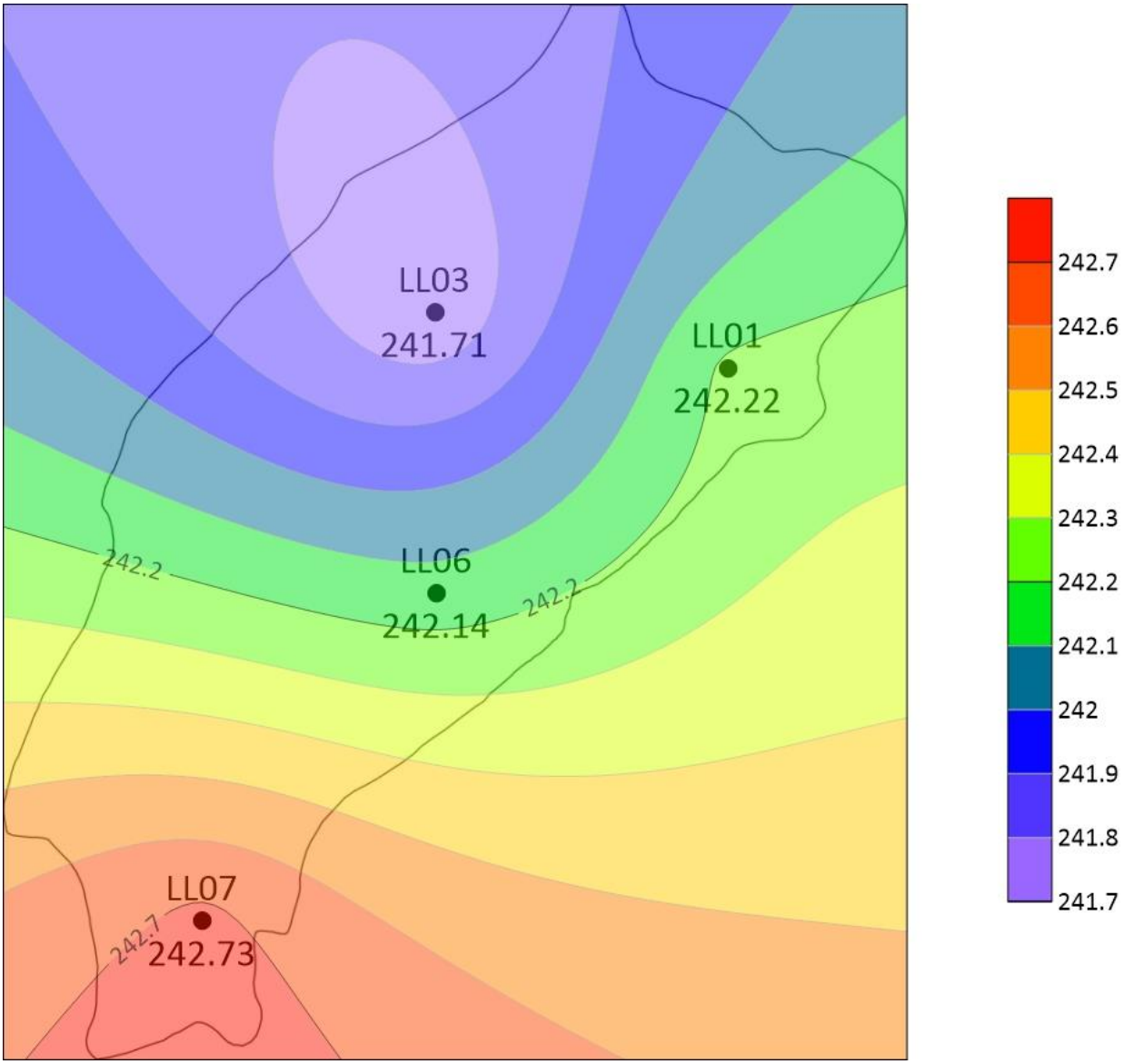

Figure C.7 Groundwater elevation contour map from November 2018.

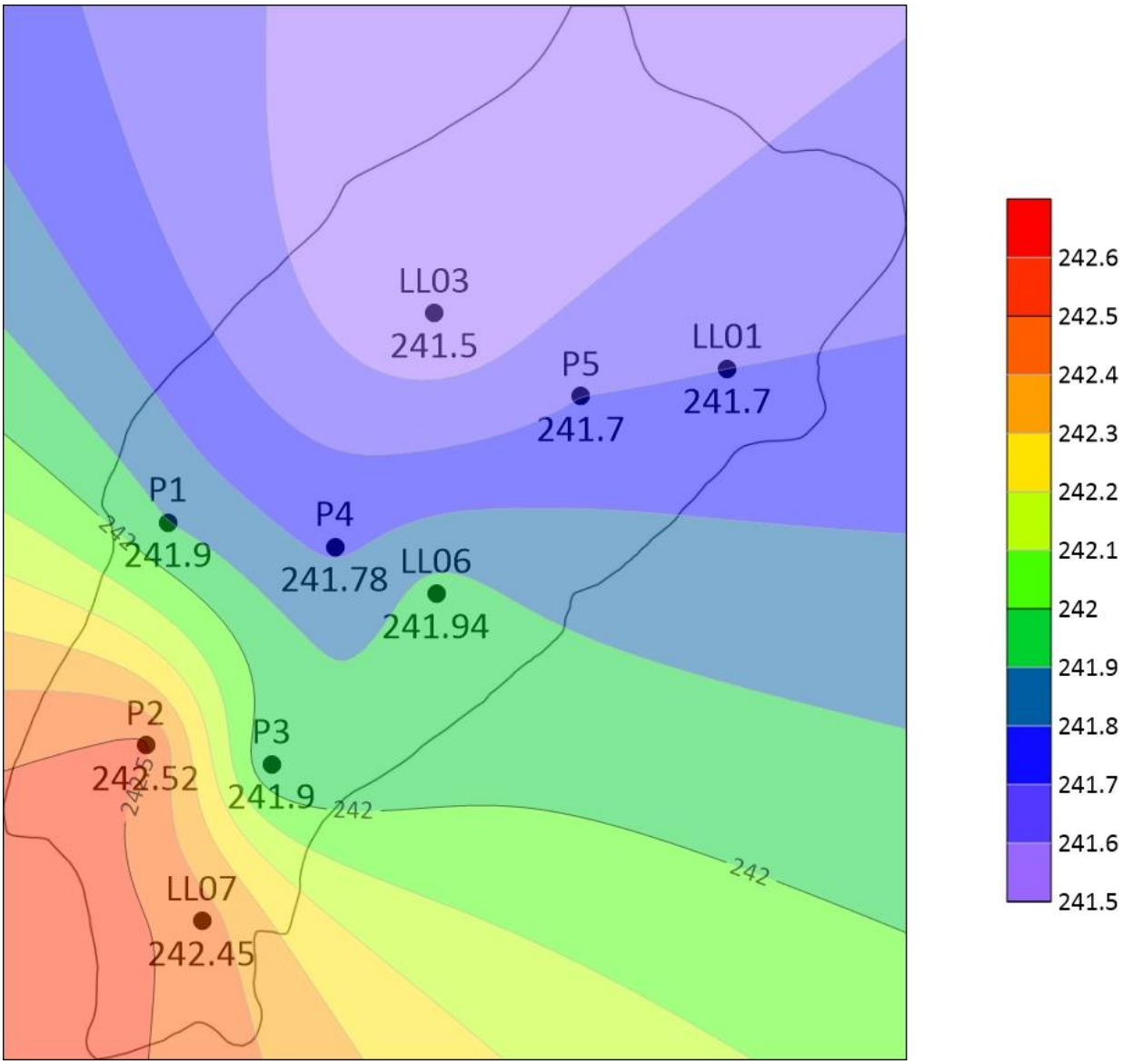

Figure C.8 Groundwater elevation contour map from July 2019.

Table C.4 Summary of D_{10}, coefficient of uniformity (CU), and calculated porosity.

Sample	Depth (m)	D_{10} (mm)	CU	Porosity
LL01	0.23	0.124	5.90	0.34
	0.57	0.063	3.15	0.40
	0.80	0.122	5.81	0.34
	1.14	0.093	3.00	0.40
	1.33	0.110	5.50	0.35
	1.88	0.103	4.29	0.37
	2.44	0.067	3.35	0.39
LL03	0.23	0.038	2.71	0.41
	0.47	0.096	3.00	0.40
	0.70	0.149	2.81	0.41
	0.94	0.064	2.46	0.42
LL06	0.25	0.151	2.85	0.40
	0.51	0.035	2.92	0.40
	0.76	0.025	4.17	0.37
	1.02	0.036	2.25	0.42
LL07	0.25	0.154	6.70	0.33
	0.50	0.168	8.40	0.31
	0.75	0.152	2.27	0.42
	1.00	0.149	2.26	0.42

Table C.5 Summary of porosity, gravimetric and volumetric moisture content, and bulk and particle density.

Location	Depth (m)	Gravimetric Moisture Content (%)	Bulk Density (g cm^{-3})	Volumetric Moisture Content (%)	Particle Denisty	Porosity (%)
LL01-1E	0.23	27.8	1.09	30.19	2.74	60.3
LL01-1E	0.51	34.8	1.07	37.38	2.94	63.5
LL01-1E	1.03	29.4	0.93	27.40	2.75	66.1
LL01-1E	1.74	29.5	1.25	36.77	2.75	54.7
LL01-1E	2.16	25.9	1.20	31.15	2.87	58.0
LL01-1E	3.21	49.3	1.01	49.61	2.74	63.3
LL03-1E	0.06	15.8	1.55	24.47	2.80	44.5
LL03-1E	0.32	19.4	1.03	19.93	2.80	63.2
LL03-1E	0.60	17.8	1.08	19.26	2.69	59.8
LL03-1E	0.91	21.2	1.11	23.60	2.75	59.5
LL03-1E	1.24	32.0	1.03	33.04	2.75	62.4
LL03-1E	1.59	59.5	0.66	39.53	2.47	73.1
LL03-1E	1.93	8.8	1.51	13.26	2.87	47.3
LL03-1E	2.47	10.6	1.27	13.53	2.87	55.7
LL03-1E	2.77	13.0	1.37	17.85	2.87	52.2
LL06-1E	0.25	35.5	1.15	40.88	2.60	55.6
LL06-1E	0.64	37.7	1.12	42.36	2.78	59.5
LL06-1E	1.21	41.8	1.16	48.68	3.98	70.8
LL07-1E	0.25	36.6	0.96	35.00	2.71	64.7
LL07-1E	0.63	30.6	1.31	40.00	3.30	60.4
LL07-1E	1.10	28.1	1.44	40.43	2.98	51.8
LL07-1E	1.49	52.1	0.91	47.55	2.71	66.3

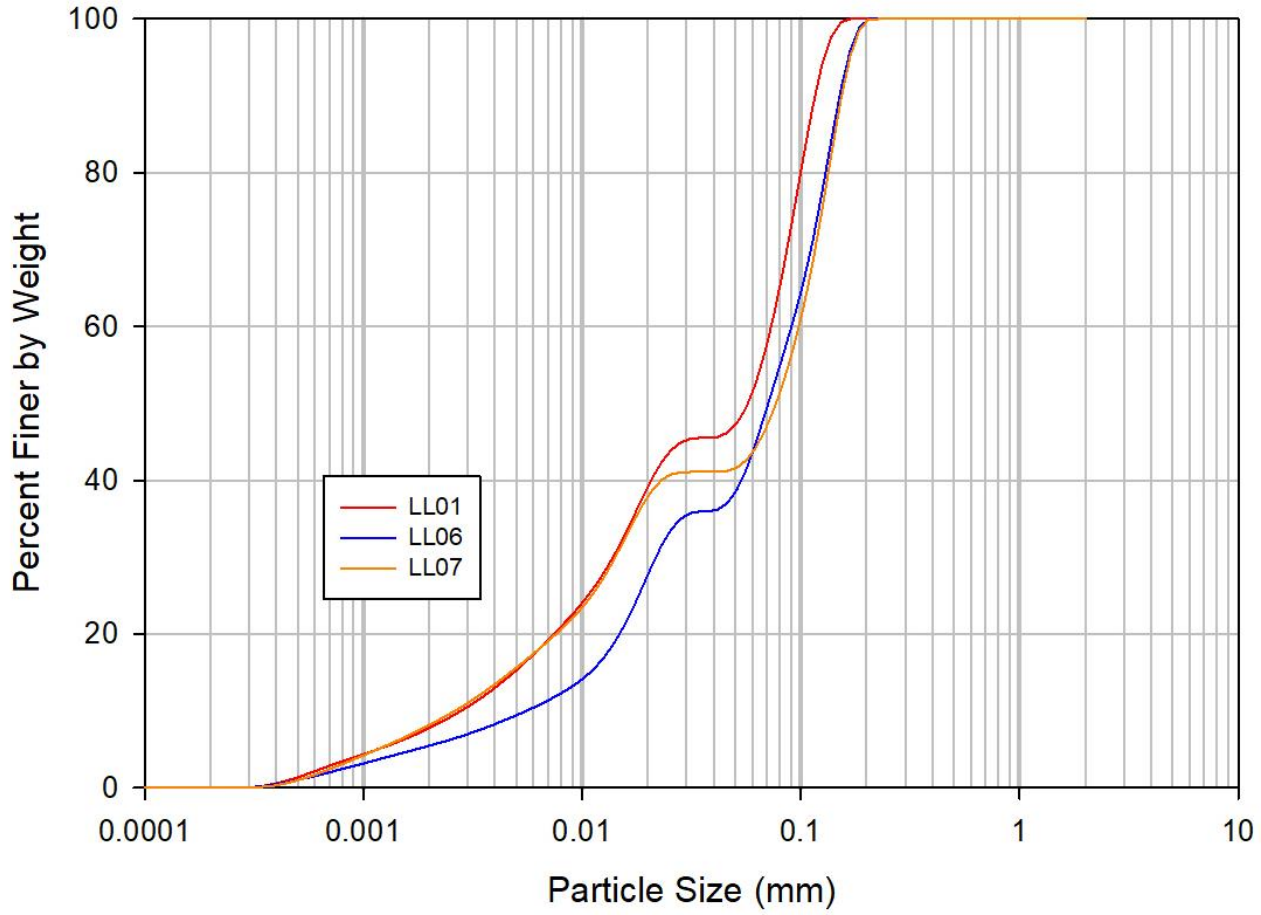

Figure C.9 Grain-size distributions of sand samples from TA-01.

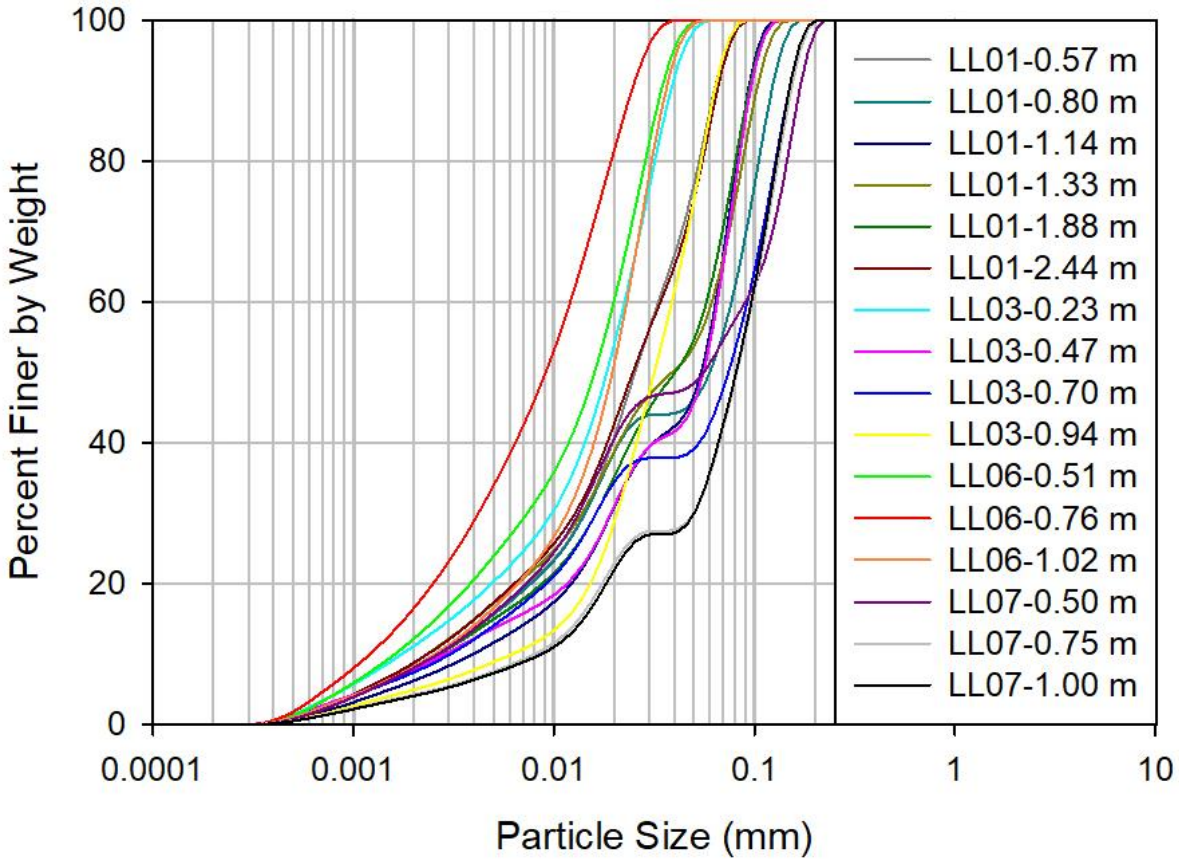

Figure C.10 Grain-size distributions of tailings samples from TA-01.

Table C.6 Comparison of hydraulic conductivity values.

Location	Depth (m)	Matrix	K (m s^{-1}) [Kozeny-Carman]	K (m s^{-1}) [Bower and Rice]
	0.23	Sand	1.25×10^{-6}	
	0.57	Tailings	1.22×10^{-6}	
	0.80	Tailings	1.42×10^{-6}	
	1.14	Tailings	2.02×10^{-6}	
	1.33	Tailings	1.25×10^{-6}	
LL01	1.60	Tailings		1.60×10^{-6}
	1.88	Tailings	1.44×10^{-6}	
	1.97	Tailings		1.97×10^{-6}
	2.44	Tailings	1.23×10^{-6}	
	3.0	Organics		2.79×10^{-6}
	3.89	Soil		2.49×10^{-9}
	0.23	Tailings	6.56×10^{-7}	
	0.47	Tailings	1.38×10^{-6}	
	0.70	Tailings	1.45×10^{-6}	
LL03	0.94	Tailings	2.43×10^{-6}	
	1.00	Tailings		6.60×10^{-6}
	1.86	Soil		1.57×10^{-7}
	6.00	Soil		1.14×10^{-9}
	0.25	Sand	2.31×10^{-6}	
	0.51	Tailings	5.88×10^{-7}	
	0.76	Tailings	3.44×10^{-7}	
LL06	1.00	Tailings		1.77×10^{-6}
	1.02	Tailings	9.48×10^{-7}	
	2.00	Soil		3.49×10^{-7}
	4.55	Soil		2.06×10^{-9}
	0.25	Tailings	1.42×10^{-6}	
	0.50	Tailings	1.48×10^{-6}	
LL07	0.75	Tailings	3.74×10^{-6}	
	1.00	Tailings	4.00×10^{-6}	
	1.43	Organics		1.61×10^{-5}
	2.1	Soil		1.61×10^{-7}

Appendix D: Solid-phase geochemistry and mineralogy data

Table D.1 Summary of carbon-sulfur data.

Location	Depth (m)	Total Carbon (wt. %)	Total Sulfur (wt. %)
LL01-1E	0.11	0.15	0.02
LL01-1E	0.23	0.23	0.05
LL01-1E	0.34	0.21	0.03
LL01-1E	0.46	0.24	0.06
LL01-1E	0.57	0.34	3.40
LL01-1E	0.69	0.21	5.09
LL01-1E	0.80	0.22	3.65
LL01-1E	0.91	0.27	3.28
LL01-1E	1.03	0.18	2.38
LL01-1E	1.14	0.21	1.78
LL01-1E	1.26	0.21	2.28
LL01-1E	1.33	0.24	5.60
LL01-1E	1.60	0.20	2.07
LL01-1E	1.88	0.18	1.82
LL01-1E	2.16	0.16	3.87
LL01-1E	2.44	0.25	3.04
LL01-1E	2.71	0.24	3.57
LL01-1E	2.85	1.87	2.89
LL01-1E	2.96	8.46	0.66
LL01-1E	3.09	2.39	0.27
LL01-1E	3.33	0.25	0.11
LL01-1E	3.58	0.16	0.20
LL01-1E	3.82	0.07	0.10
LL03-1E	0.12	0.26	1.45
LL03-1E	0.23	0.29	1.78
LL03-1E	0.35	0.35	2.30
LL03-1E	0.47	0.20	4.27
LL03-1E	0.59	0.73	3.30
LL03-1E	0.70	0.96	2.25
LL03-1E	0.82	0.67	1.66
LL03-1E	0.94	0.76	2.15
LL03-1E	1.17	0.75	3.63
LL03-1E	1.35	0.25	5.15
LL03-1E	1.56	3.68	0.50
LL03-1E	1.66	0.40	0.10
LL03-1E	1.87	0.23	0.11
LL03-1E	2.07	0.18	0.10

Table D.1 Continued.

Location	Depth (m)	Total Carbon (wt. %)	Total Sulfur (wt. %)
LL06-1E	0.13	0.22	1.30
LL06-1E	0.25	0.13	0.17
LL06-1E	0.38	0.23	2.42
LL06-1E	0.51	0.38	3.80
LL06-1E	0.64	0.35	1.55
LL06-1E	0.76	0.87	1.57
LL06-1E	0.89	0.34	5.07
LL06-1E	1.02	0.63	4.68
LL06-1E	1.27	0.36	6.03
LL06-1E	1.49	24.80	1.03
LL06-1E	1.62	20.14	0.74
LL06-1E	1.76	17.38	1.24
LL06-1E	2.03	0.52	0.10
LL06-1E	2.30	1.02	0.13
LL07-1E	0.13	0.36	0.43
LL07-1E	0.25	0.32	0.09
LL07-1E	0.38	0.43	0.08
LL07-1E	0.50	0.77	0.07
LL07-1E	0.63	0.51	8.07
LL07-1E	0.75	0.36	14.72
LL07-1E	0.88	0.30	9.93
LL07-1E	1.00	0.33	9.37
LL07-1E	1.26	0.36	7.70
LL07-1E	1.49	2.98	2.84
LL07-1E	1.61	3.05	0.42
LL07-1E	1.74	0.34	0.10
LL07-1E	1.99	0.13	0.10
LL07-1E	2.24	0.09	0.09

Table D.2 Summary of whole-rock analysis.

Location	Depth (m)	Au (ppm)	Ag (ppm)	Al (ppm)	As (ppm)	Ba (ppm)	Be (ppm)	Bi (ppm)	Ca (ppm)	Cd (ppm)
LL01-1E	0.57	1.5	0.11	1500	43700	8.1	0.01	1.2	1700	0.02
LL01-1E	0.91	2.0	0.11	1167	37700	9.1	0.01	1.1	500	0.06
LL01-1E	1.88	1.3	0.08	5333	13817	10.1	0.1	0.4	3333	0.08
LL01-1E	2.85	0.8	0.07	4400	21750	11.7	0.1	0.8	1900	0.05
LL01-1E	3.21	0.2	0.12	23667	1039	114	0.5	0.2	3467	0.11
LL01-1E	3.82	0.03	0.07	13433	1291	84	0.3	0.1	3600	0.03

Location	Depth (m)	Ce (ppm)	Co (ppm)	Cr (ppm)	Cs (ppm)	Cu (ppm)	Fe (ppm)	Ga (ppm)	Hg (ppm)	K (ppm)
LL01-1E	0.57	48.5	568	14.9	0.04	494	51167	2.1	0.08	300
LL01-1E	0.91	46.5	471	17.5	0.1	405	45267	0.9	0.08	300
LL01-1E	1.88	41.9	138	41.2	0.2	151	24100	1.6	0.05	667
LL01-1E	2.85	95.3	249	72.7	0.1	215	68100	2.1	0.10	400
LL01-1E	3.21	33.2	19.4	45.6	1.4	31.7	17600	7.2	0.06	1667
LL01-1E	3.82	34.9	18.8	45.7	0.5	24.6	22267	4.3	0.04	1400

Location	Depth (m)	Li (ppm)	Mg (ppm)	Mn (ppm)	Mo (ppm)	Na (ppm)	Ni (ppm)	P (ppm)	Pb (ppm)	S (ppm)
LL01-1E	0.57	1.0	1000	28.9	1.8	1270	360	80.0	15.7	34233
LL01-1E	0.91	0.8	700	27.0	1.8	777	310	43.3	32.2	32067
LL01-1E	1.88	3.8	2000	43.2	4.0	677	109	383	7.5	16167
LL01-1E	2.85	3.7	1733	162	1.4	903	181	550	20.9	28467
LL01-1E	3.21	21.0	3167	108	0.3	333	32.4	293	8.1	867
LL01-1E	3.82	10.9	4300	177	0.4	500	30.5	293	5.2	1333

Location	Depth (m)	Sb (ppm)	Se (ppm)	Sn (ppm)	Sr (ppm)	Ti (ppm)	U (ppm)	Zn (ppm)
LL01-1E	0.57	10.1	8.1	8.4	3.4	227	0.7	5.1
LL01-1E	0.91	4.5	6.6	3.2	2.7	163	1.1	10.1
LL01-1E	1.88	2.6	2.3	1.1	4.3	177	2.4	29.1
LL01-1E	2.85	2.8	4.8	0.8	7.2	76.7	9.7	12.5
LL01-1E	3.21	0.1	0.3	0.7	21.9	460	1.8	30.4
LL01-1E	3.82	0.3	0.4	0.5	28.1	803	1.0	25.5

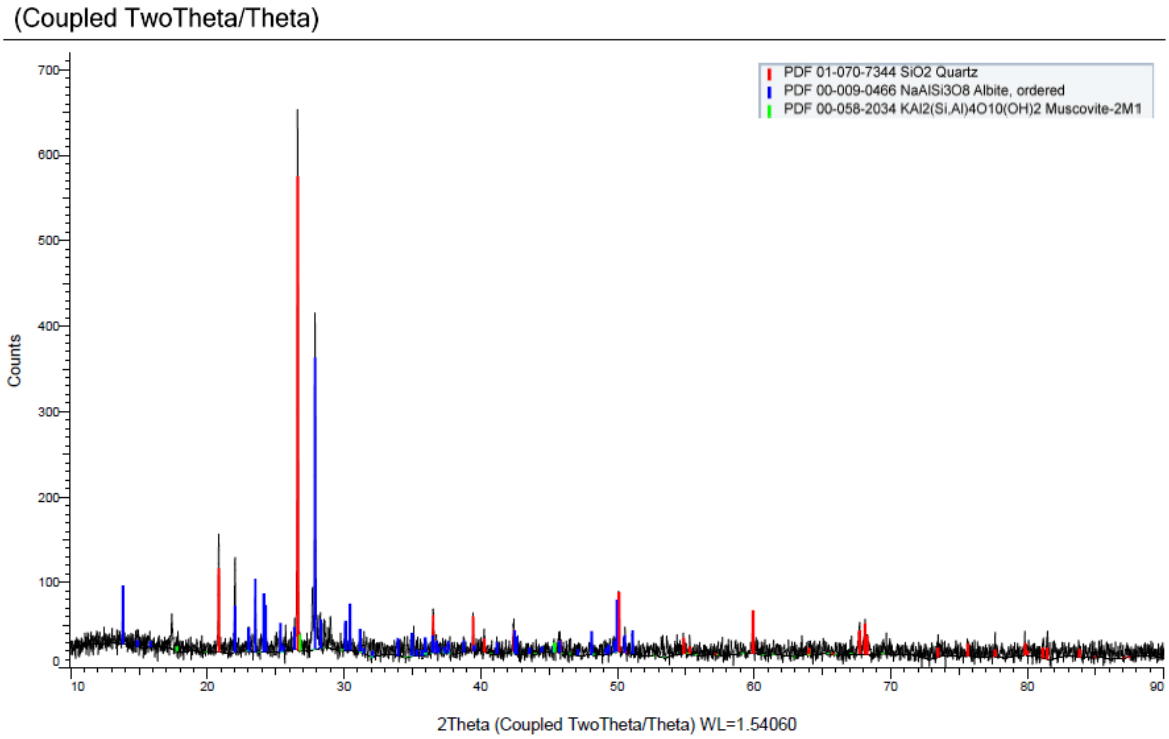

Figure D.1 XRD results of LL06-0.13 m.

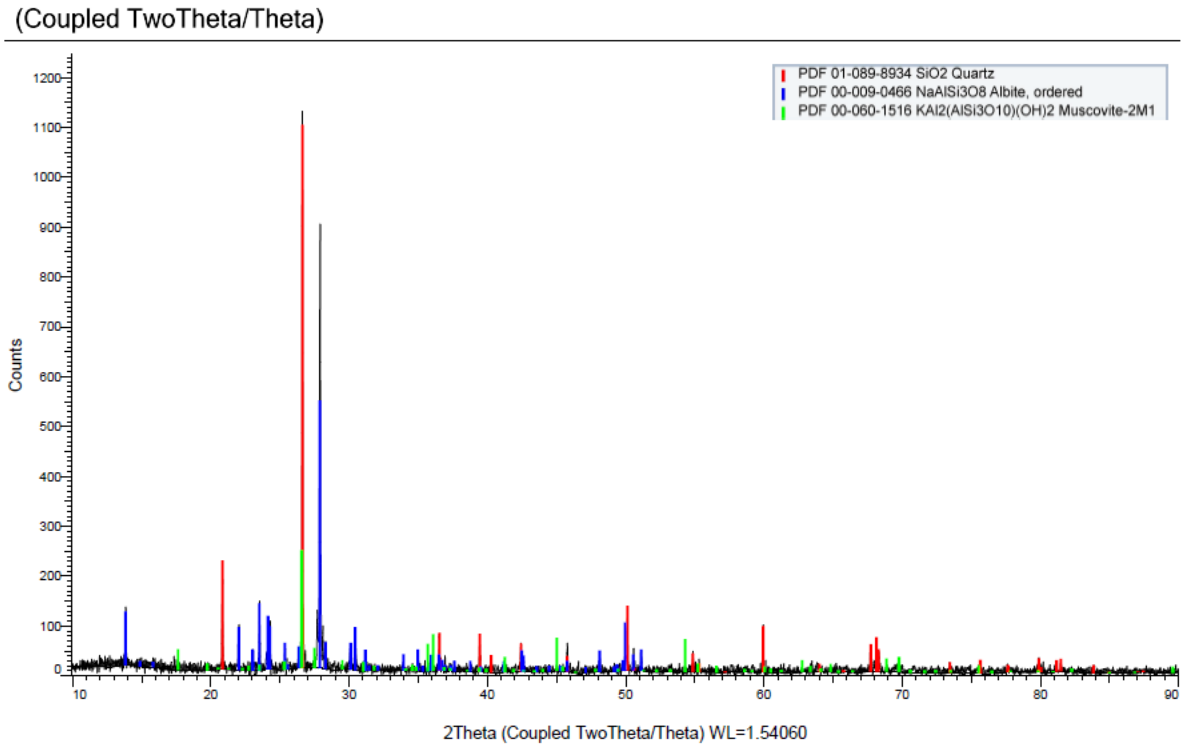

Figure D.2 XRD results of LL06-0.25 m.

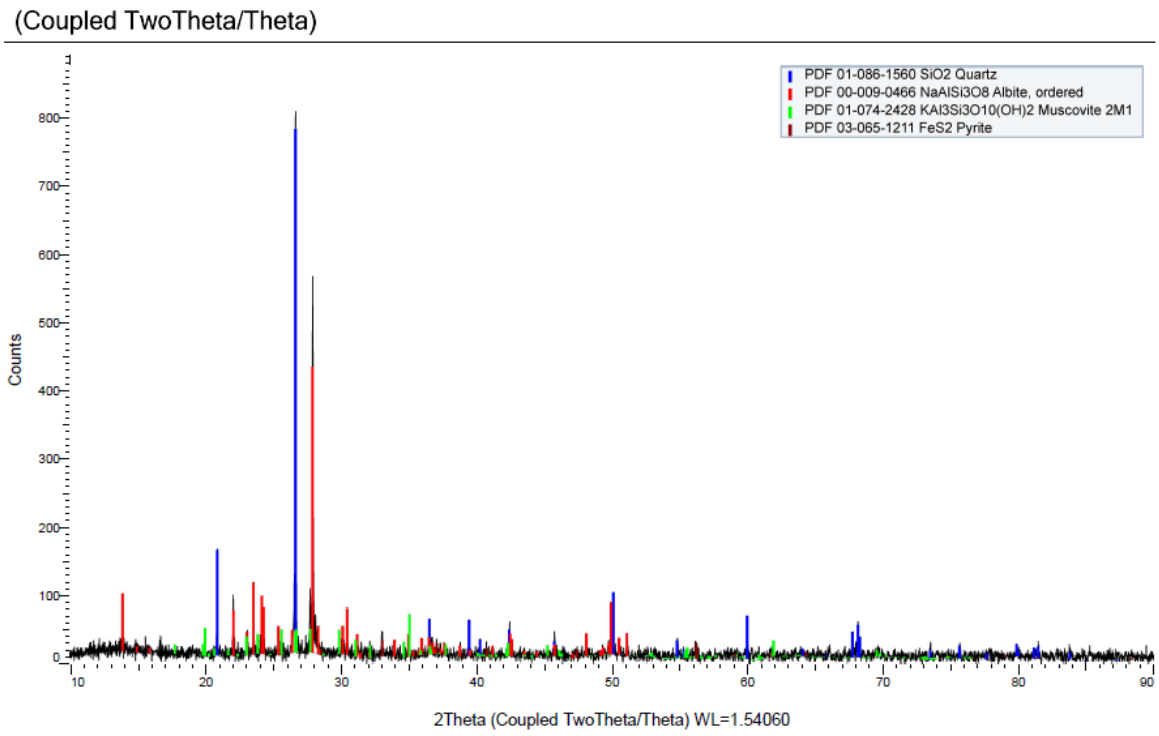

Figure D.3 XRD results of LL06-0.38 m.

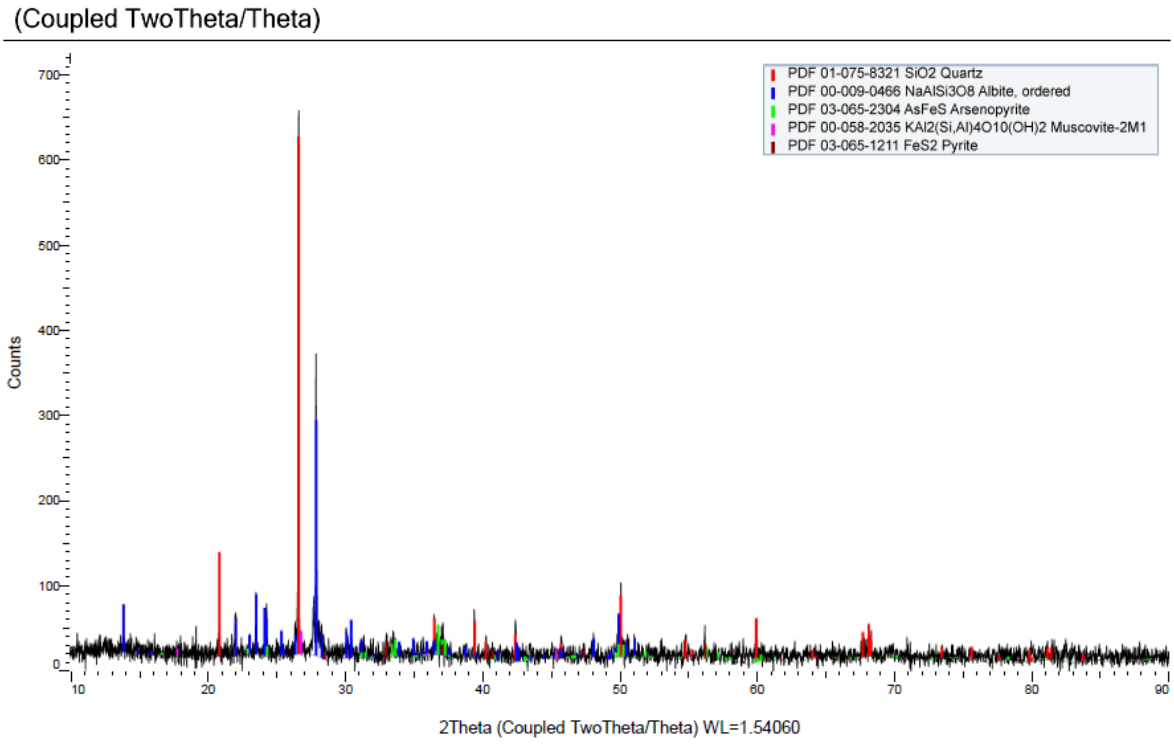

Figure D.4 XRD results of LL06-0.51 m.

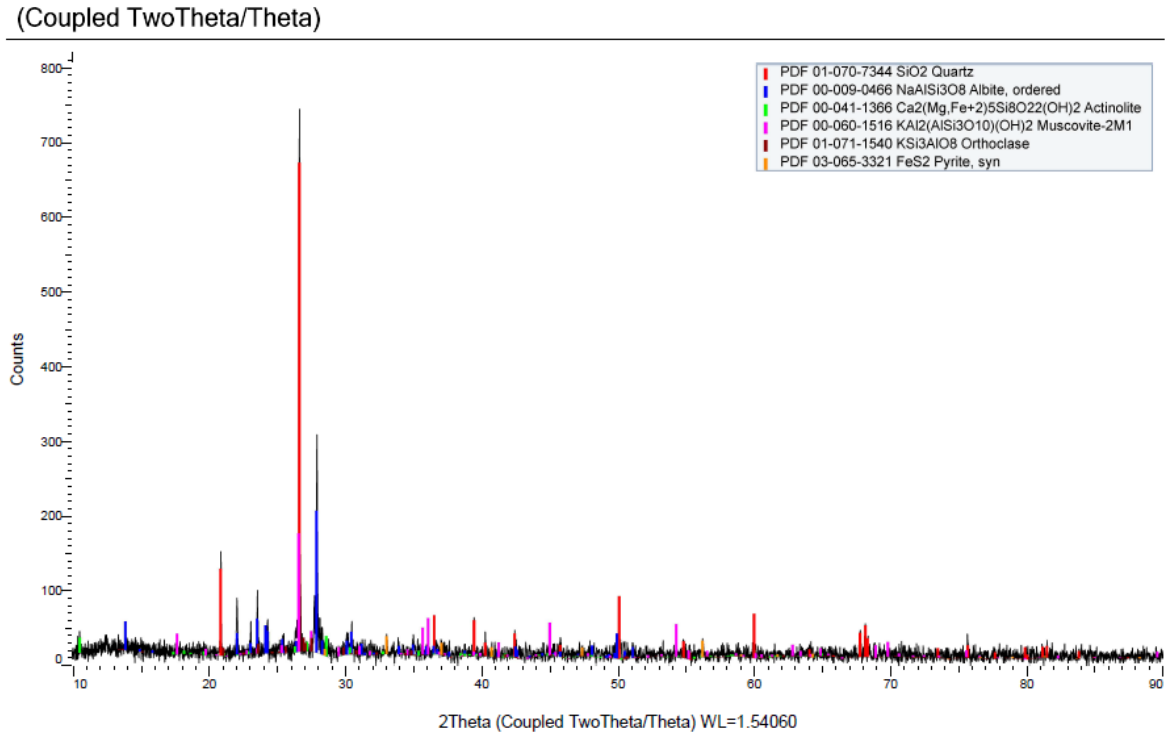

Figure D.5 XRD results of LL06-0.64 m.

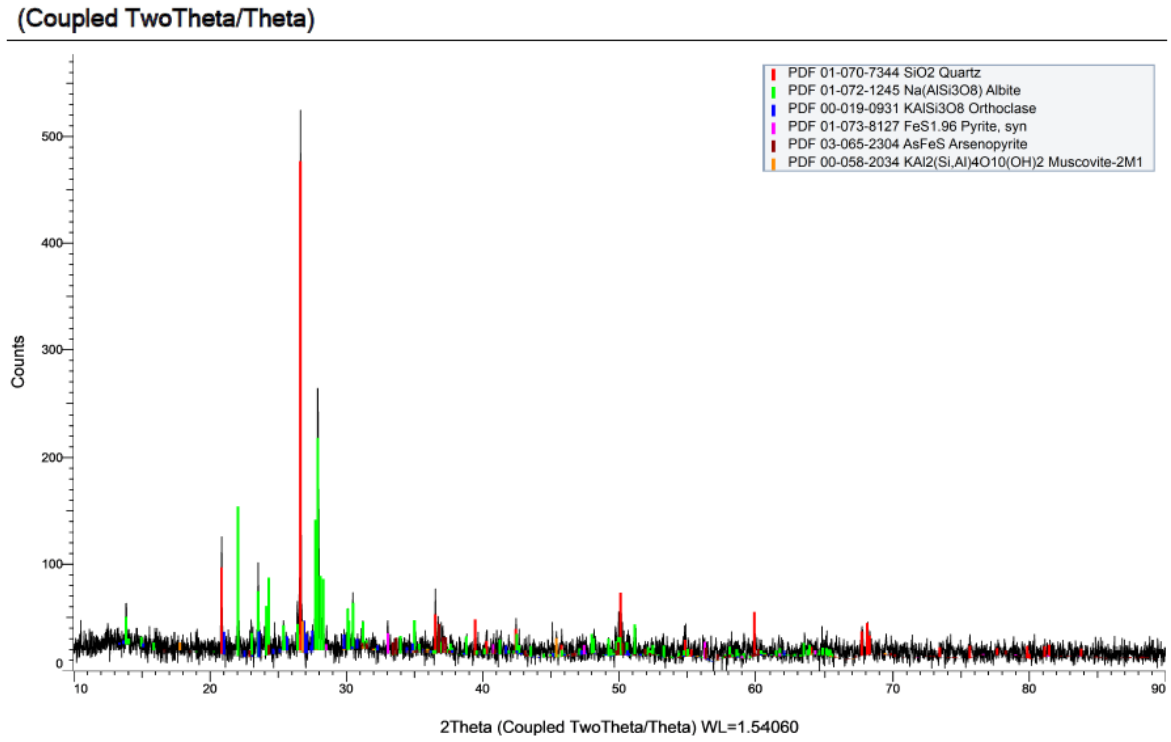

Figure D.6 XRD results of LL06-0.76 m.

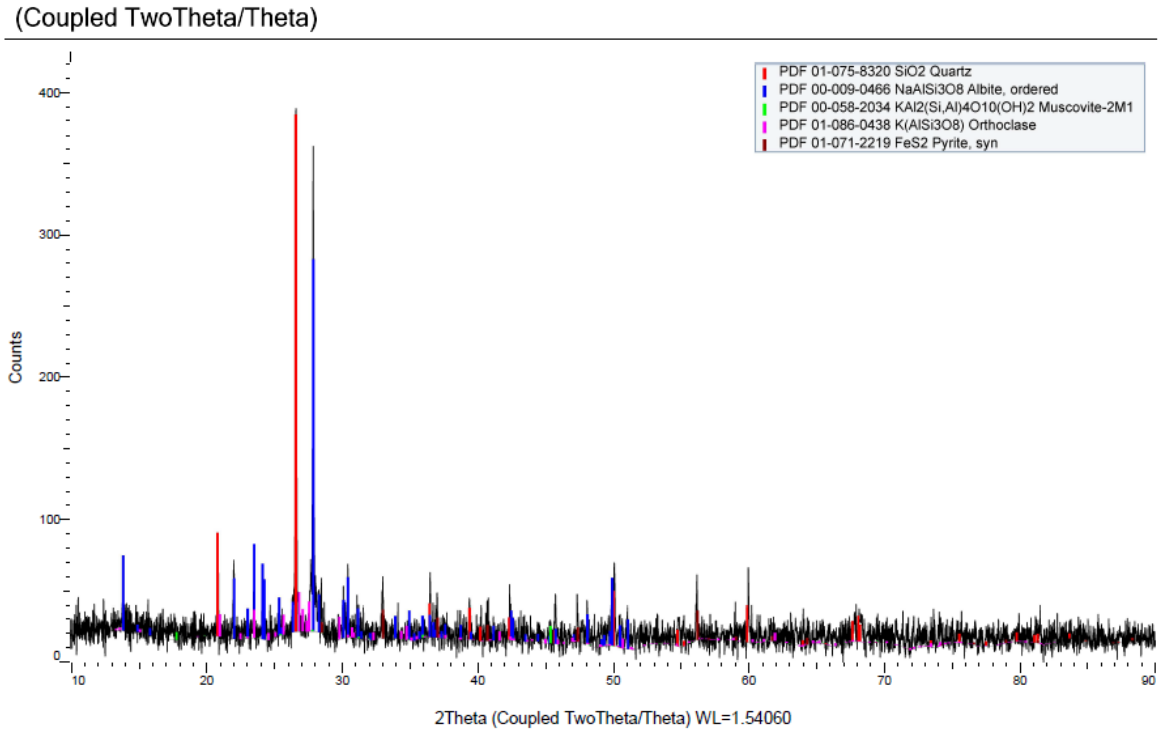

Figure D.7 XRD results of LL06-0.89 m.

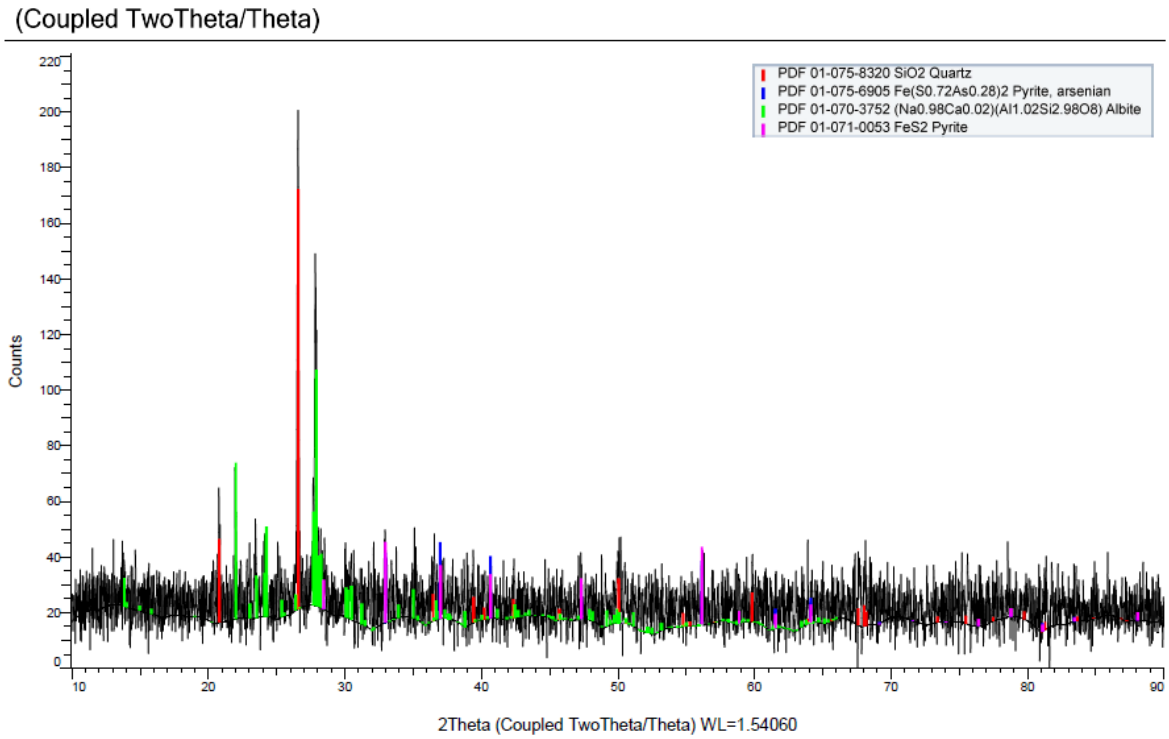

Figure D.8 XRD results of LL06-1.02 m.

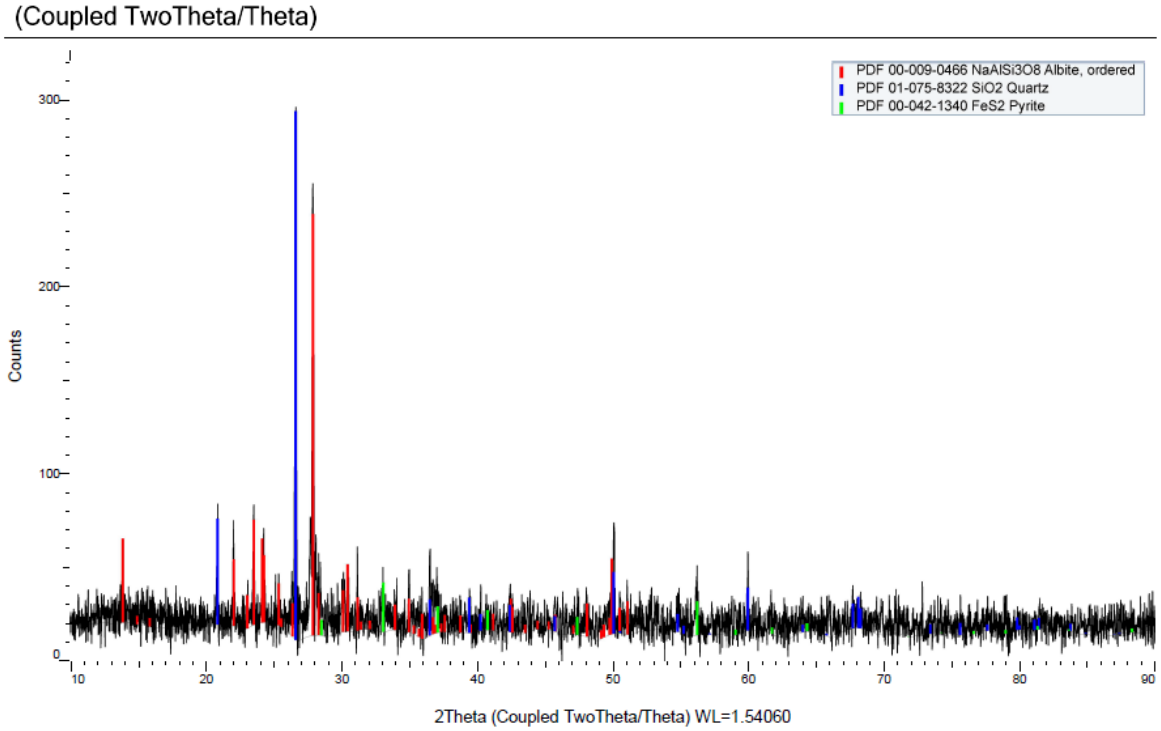

Figure D.9 XRD results of LL06-1.27 m.

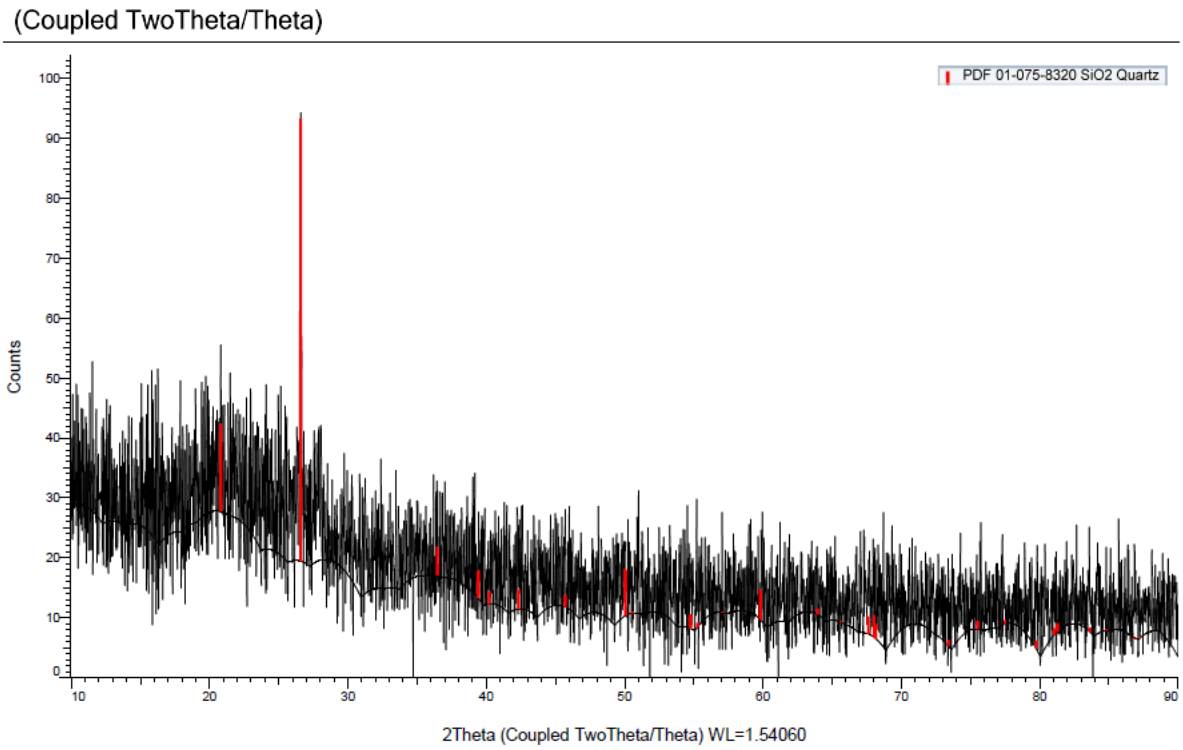

Figure D.10 XRD results of LL06-1.49 m.

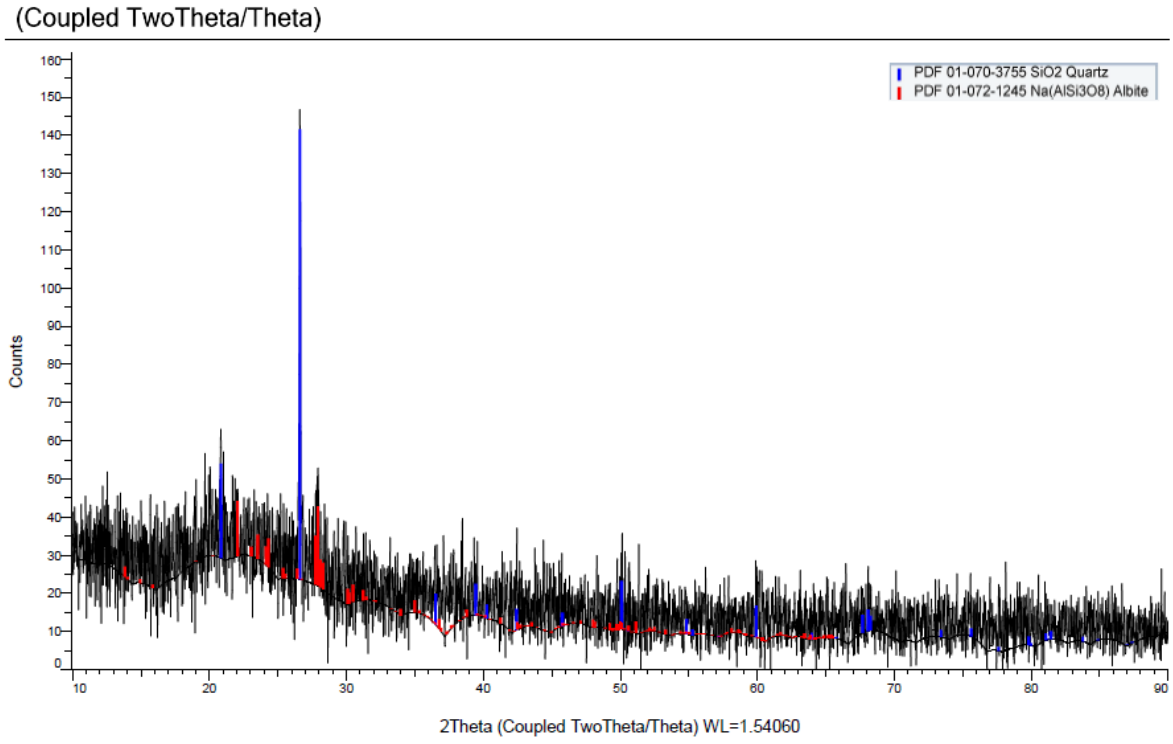

Figure D.11 XRD results of LL06-1.62 m.

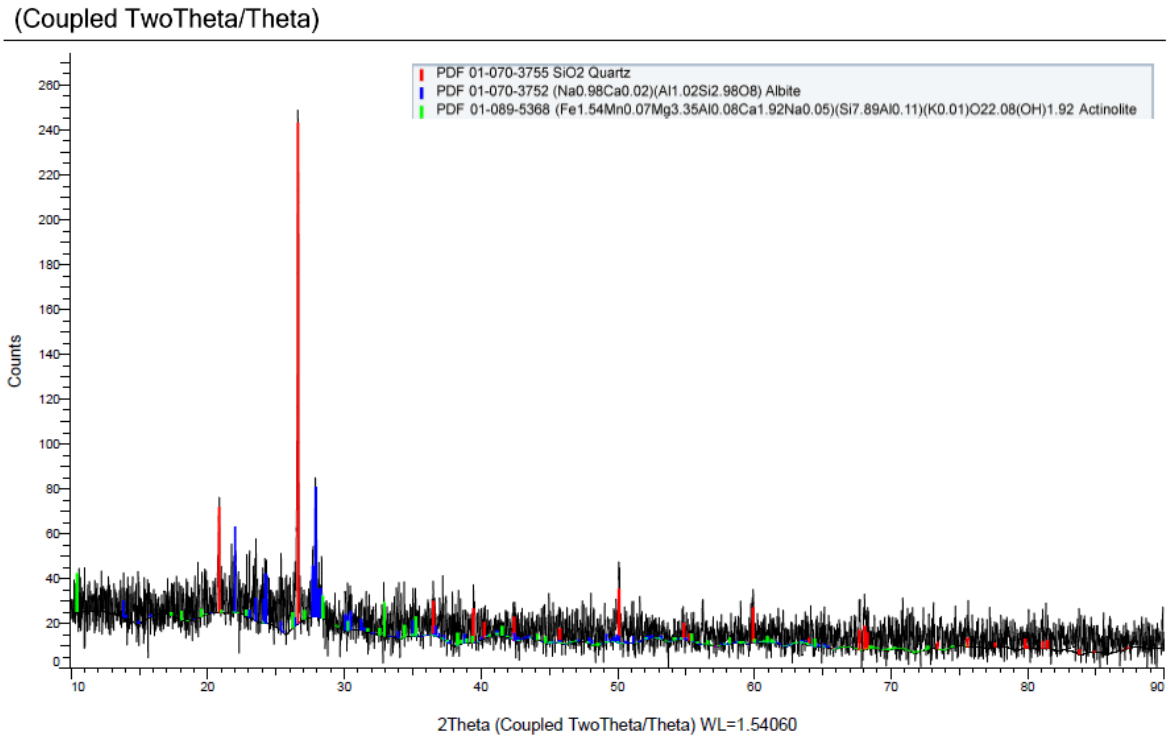

Figure D.12 XRD results of LL06-1.76 m.

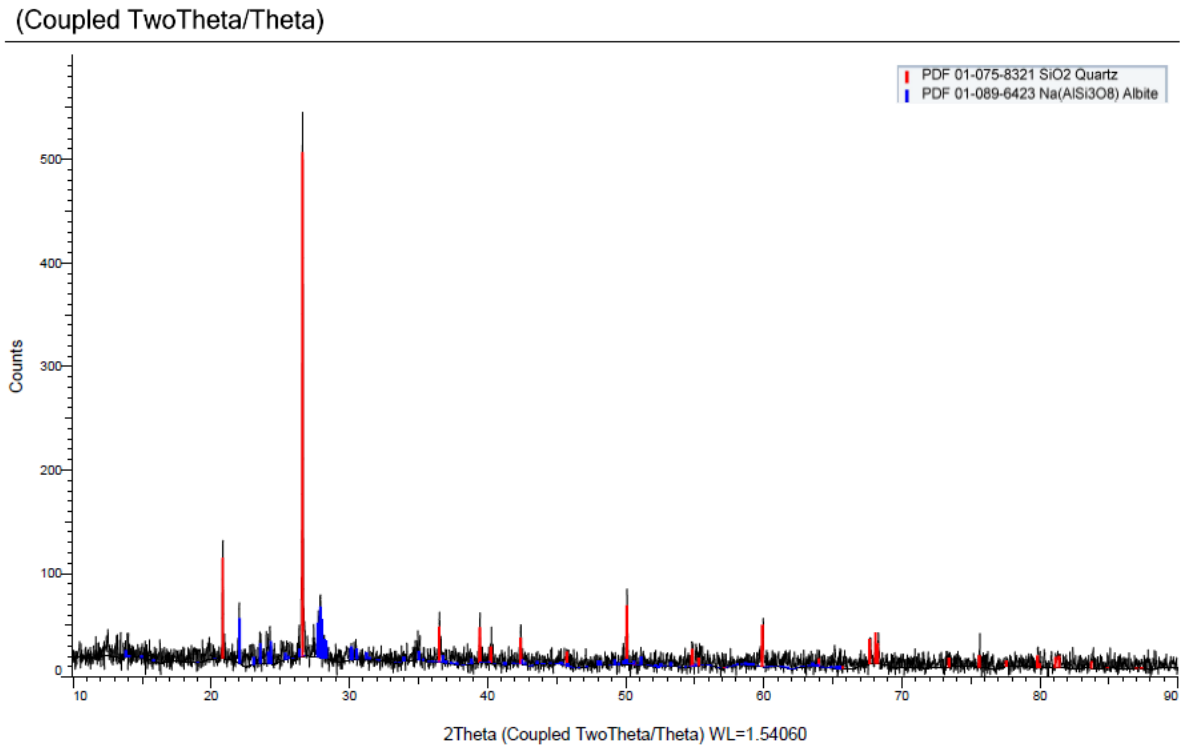

Figure D.13 XRD results of LL06-2.03 m.

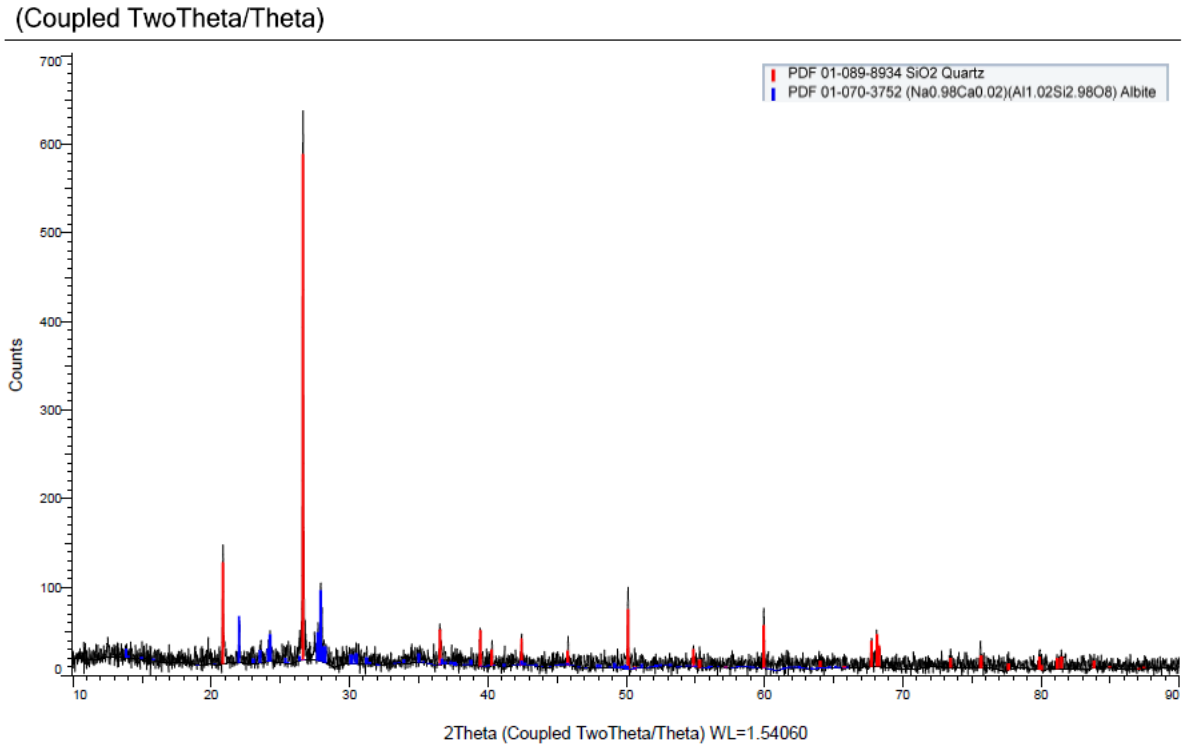

Figure D.14 XRD results of LL06-2.30 m.

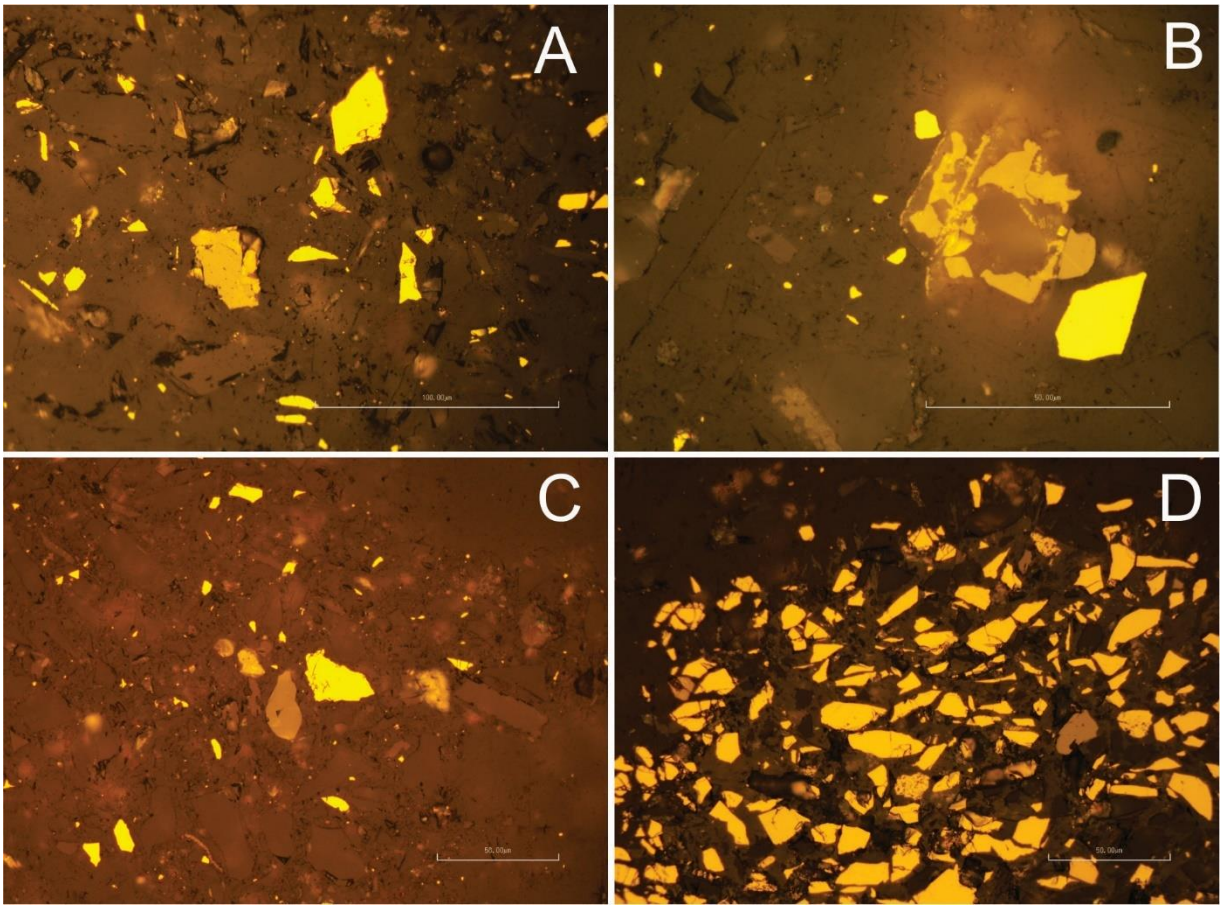

Figure D.15 Optical photomicrographs from LL06 at depths of (A) 0.44 m containing two larger sulfide grains approximately 50 um in size, (B) 0.76 m depicting an altered sulfide grain, (C) 0.76 m containing two larger sulfide grains approximately 50 um in size, (D) 1.00 m showing many unaltered sulfide grains in close proximity.

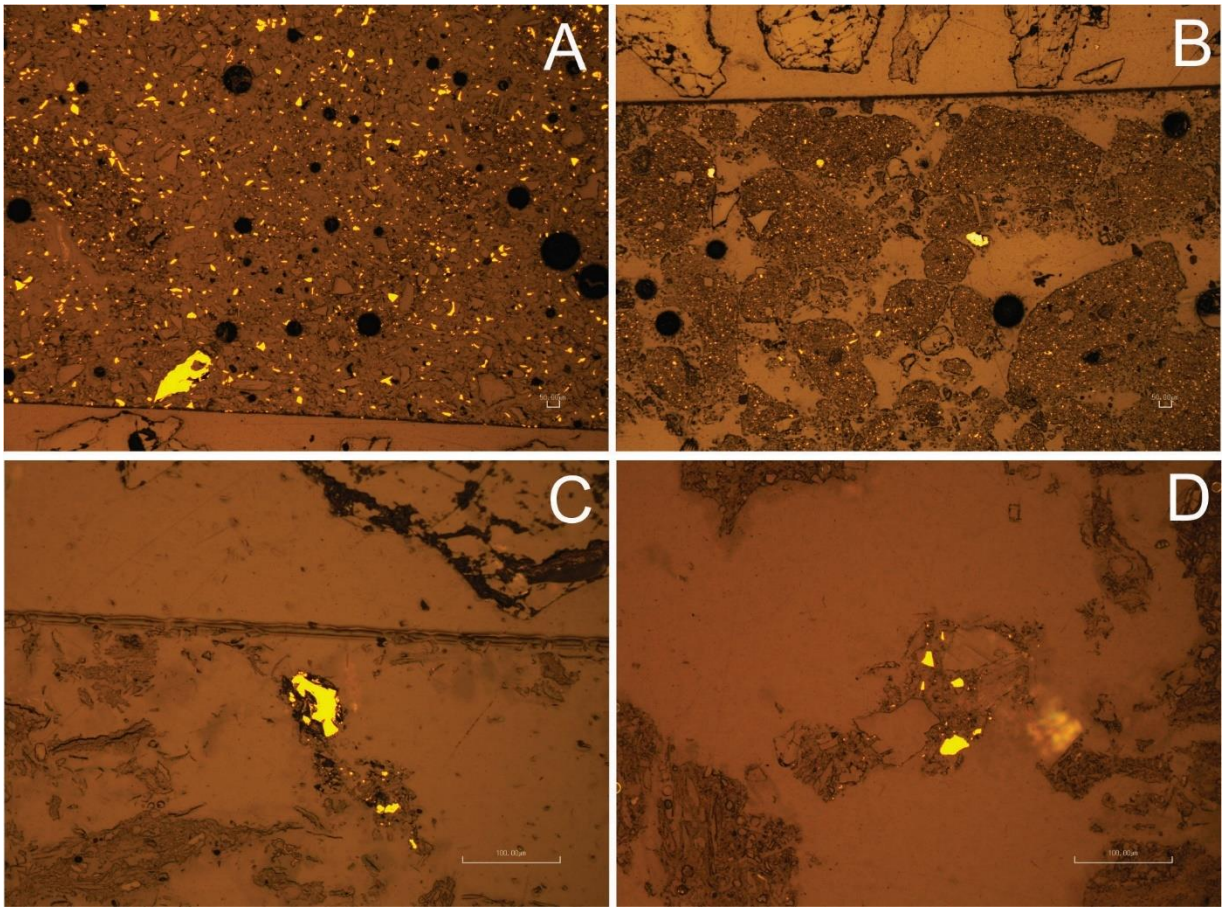

Figure D.16 Optical photomicrographs from LL06 at depths of (A) 1.21 m showing the abundance of several small sulfide grains, (B) 1.36 m showing few small sulfide grains directly beneath the tailings, (C) 1.62 m showing possibly secondary sulfide precipitation, (D) 1.89 m showing possible secondary sulfide precipitation.

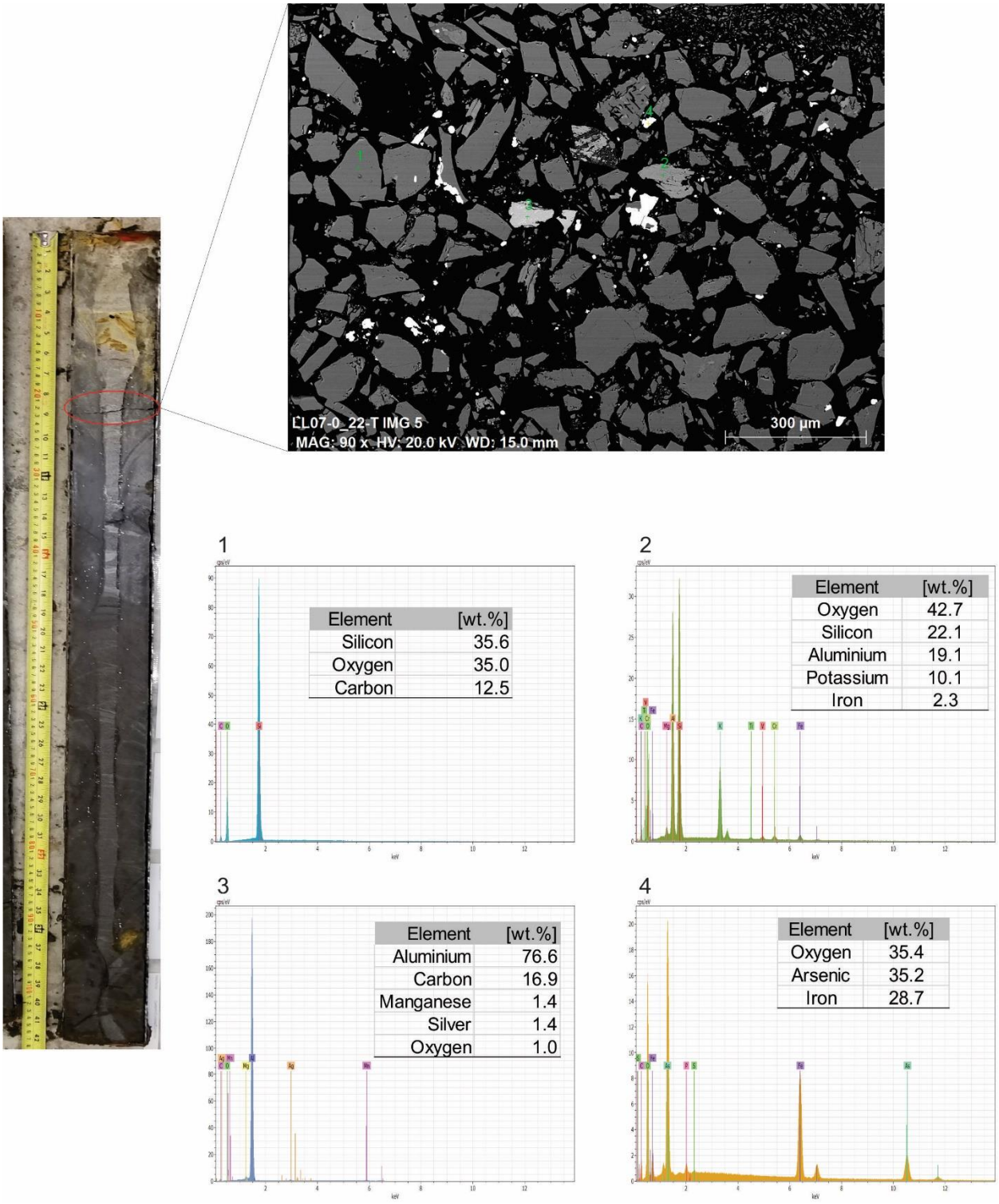

Figure D.17 Scanning electron microscope picture from location LL07-0.28 m of several aluminosilicate and pyrite grains.

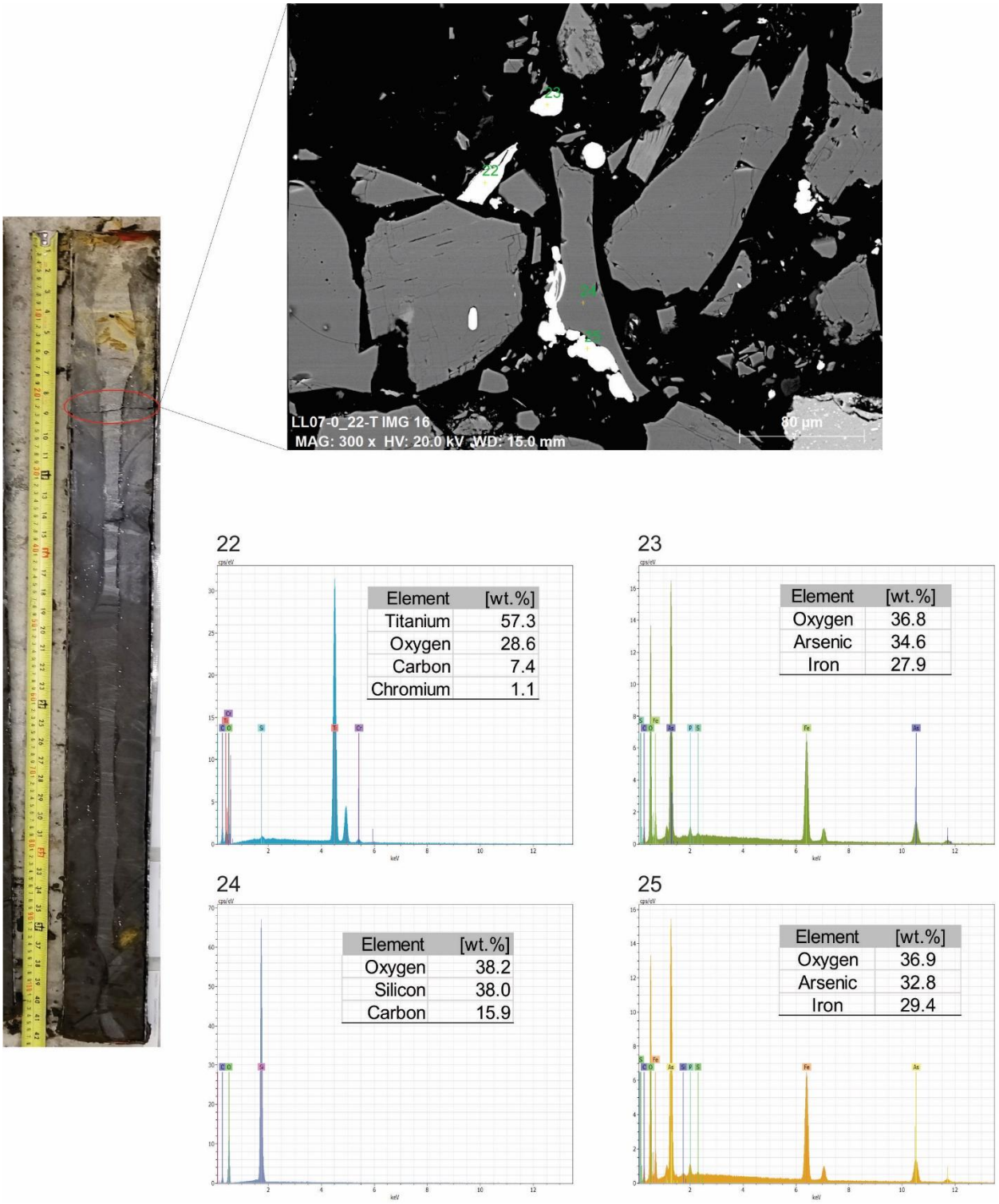

Figure D.18 Scanning electron microscope picture from location LL07-0.28 m of possible scorodite precipitation.

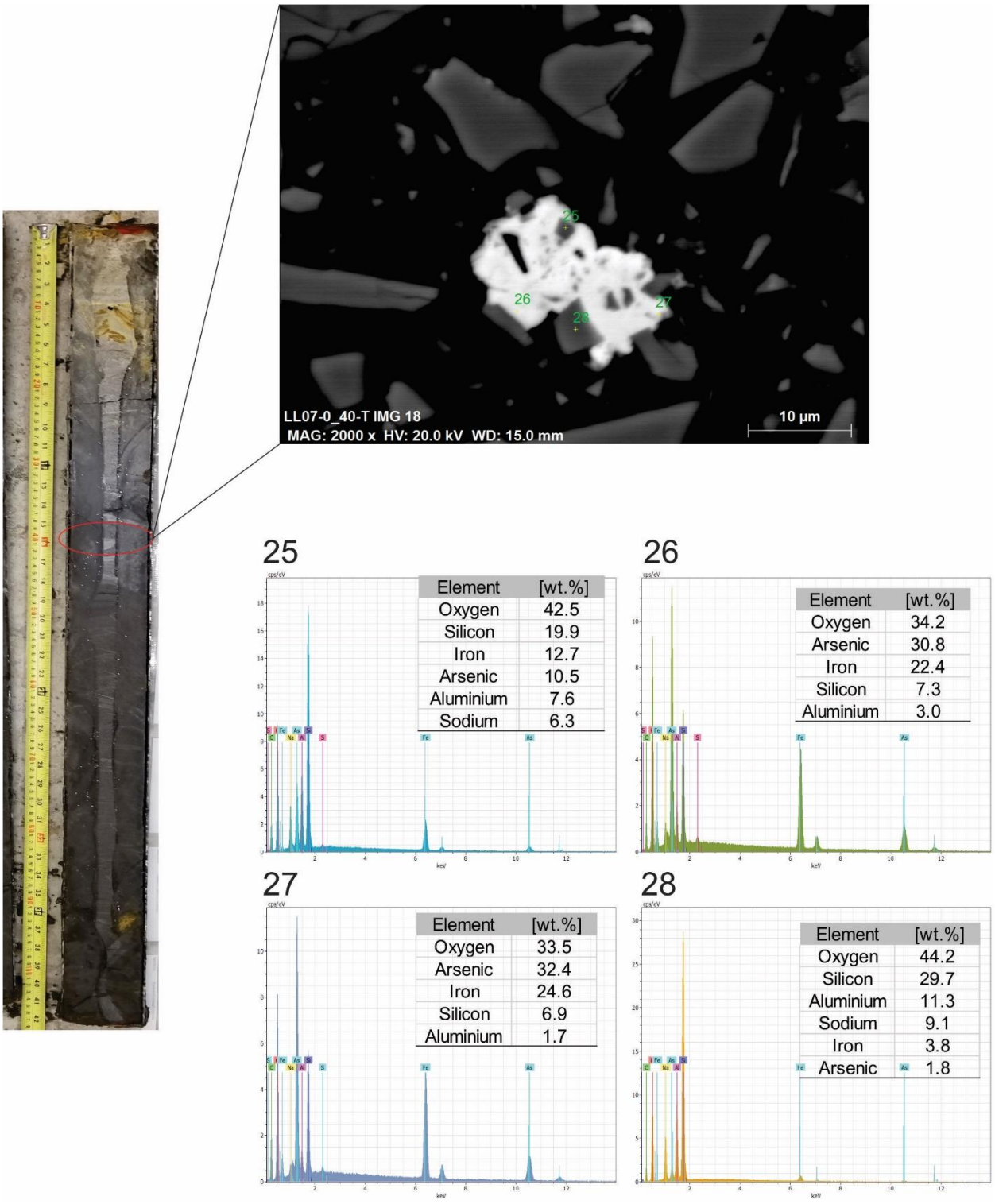

Figure D.19 Scanning electron microscope picture from location LL07-0.50 m of precipitation of an arsenic-iron phase.

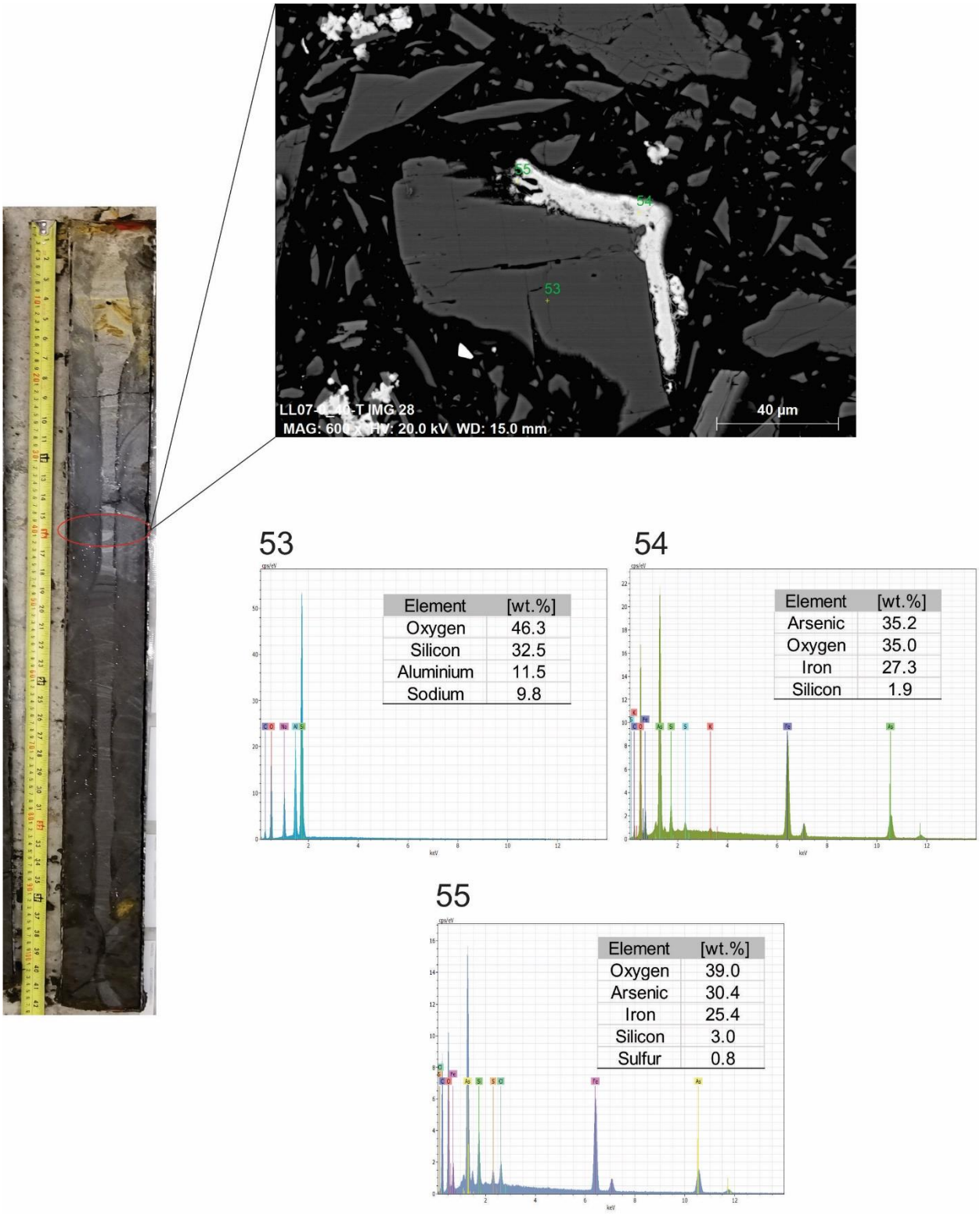

Figure D.20 Scanning electron microscope picture from location LL07-0.50 m of possible scorodite precipitation.

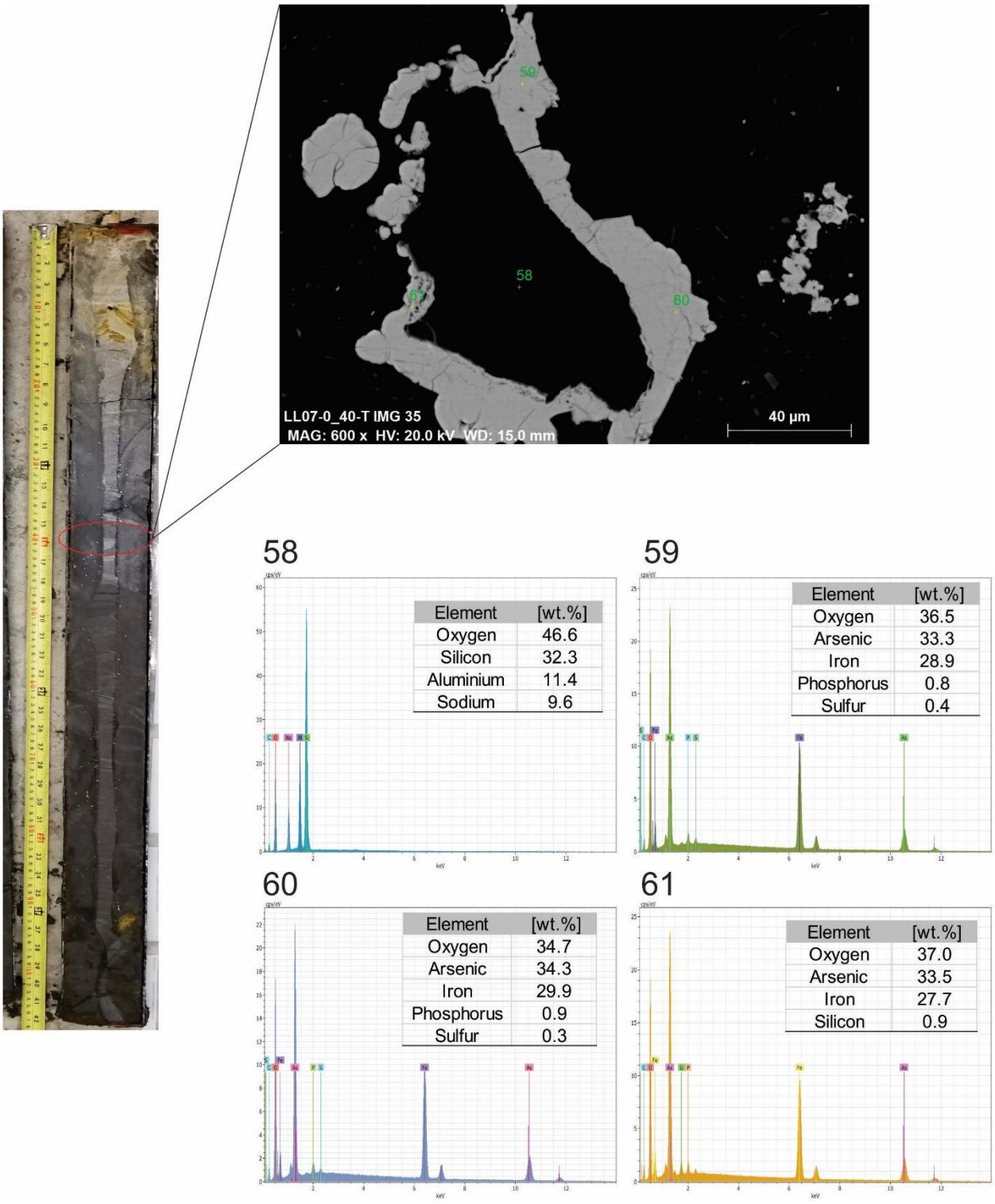

Figure D.21 Scanning electron microscope picture from location LL07-0.50 m of scorodite precipitation.

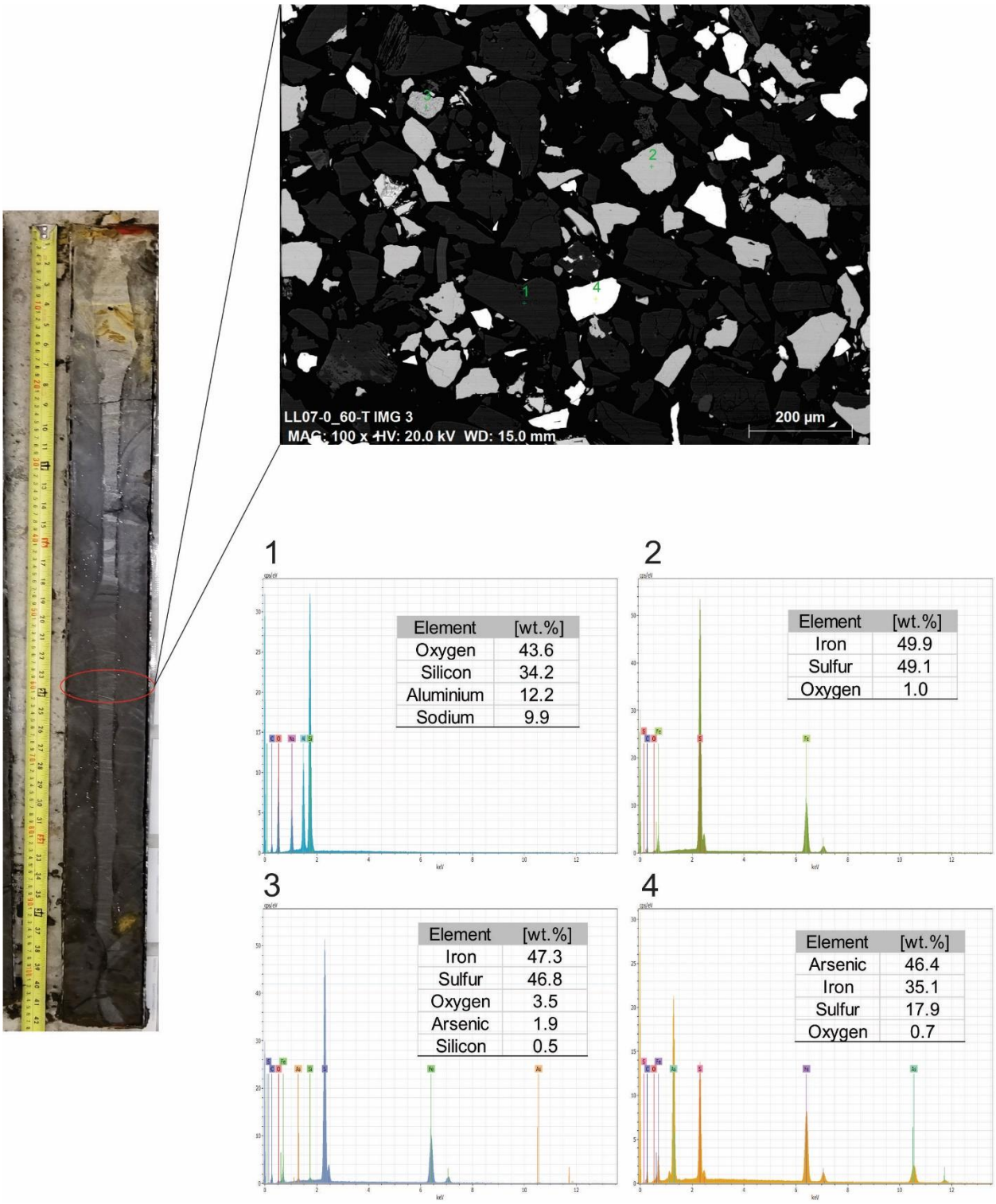

Figure D.22 Scanning electron microscope picture from location LL07-0.75 m of pyrite and arsenopyrite grains.

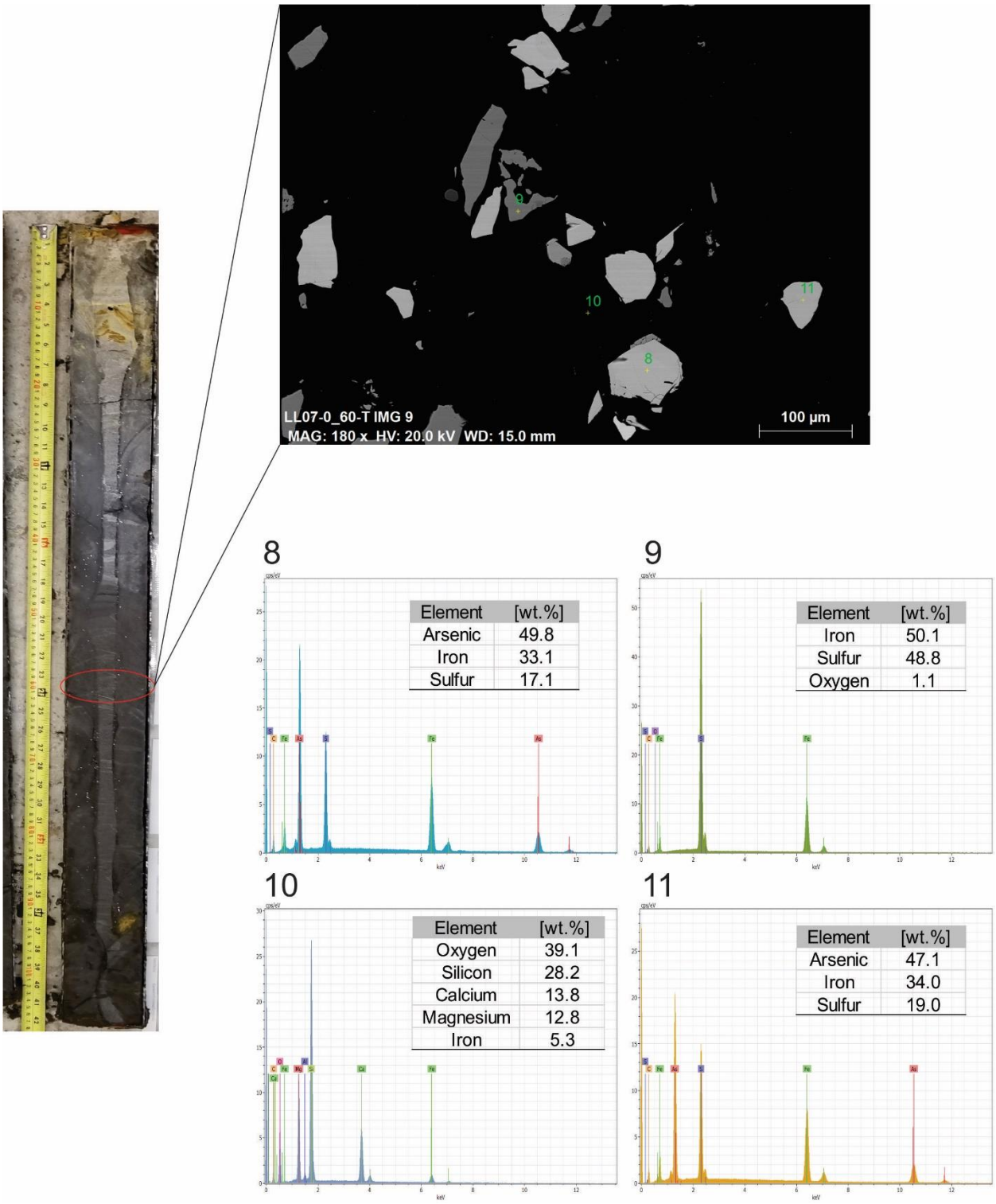

Figure D.23 Scanning electron microscope picture from location LL07-0.75 m of pyrite and arsenopyrite grains.

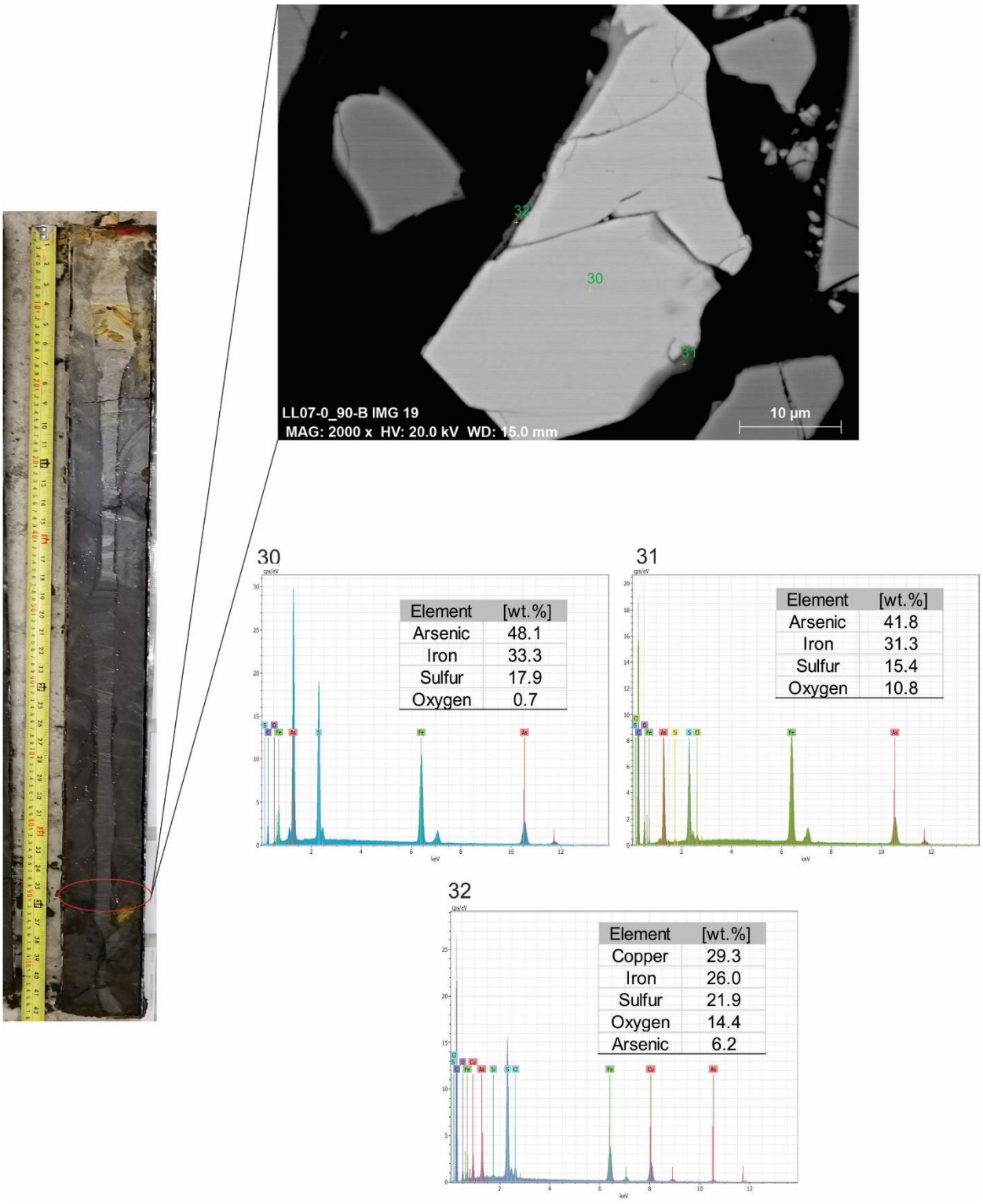

Figure D.24 Scanning electron microscope picture from location LL07-1.13 m of an arsenopyrite grain.

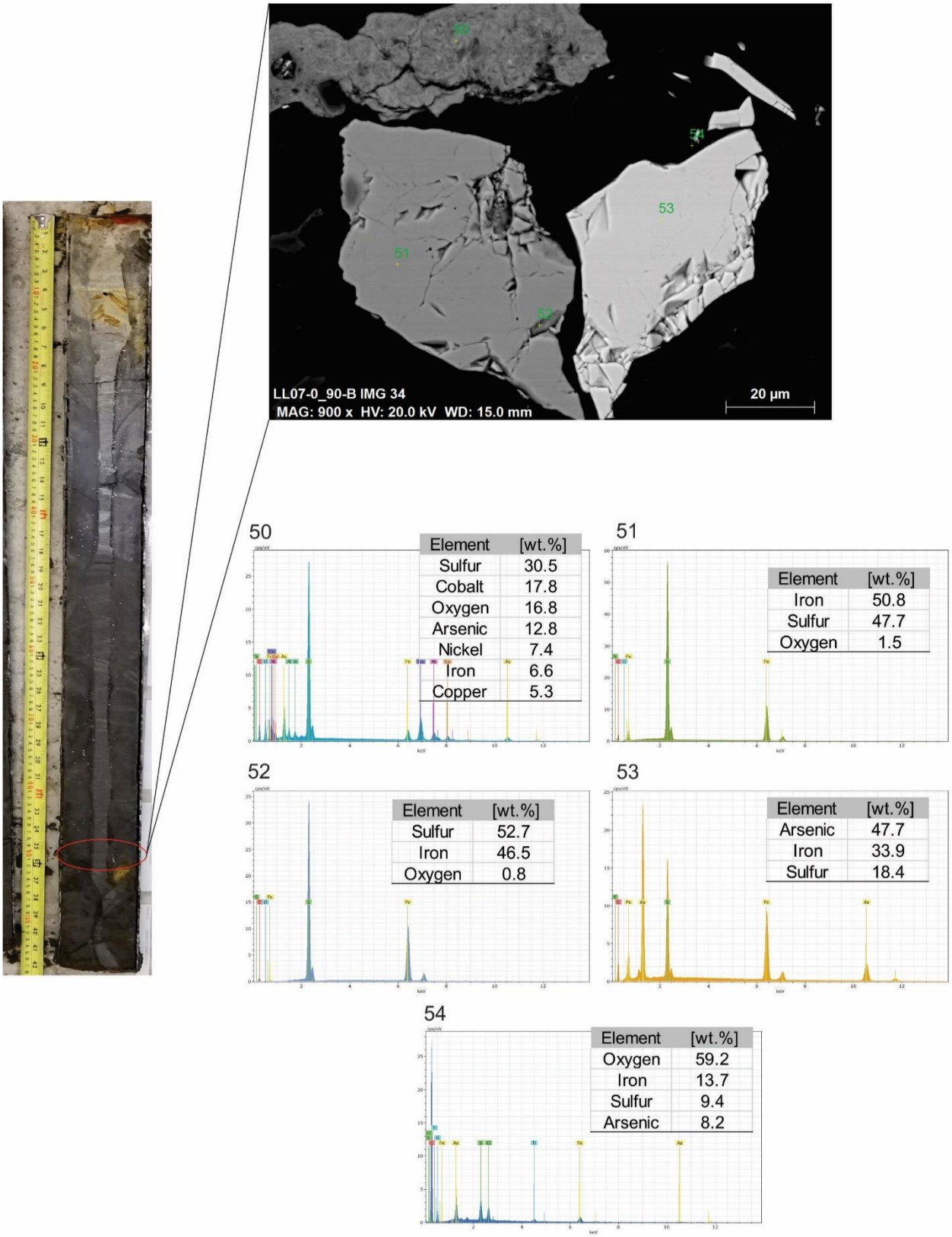

Figure D.25 Scanning electron microscope picture from location LL07-1.13 m of a pyrite and arsenopyrite grain.

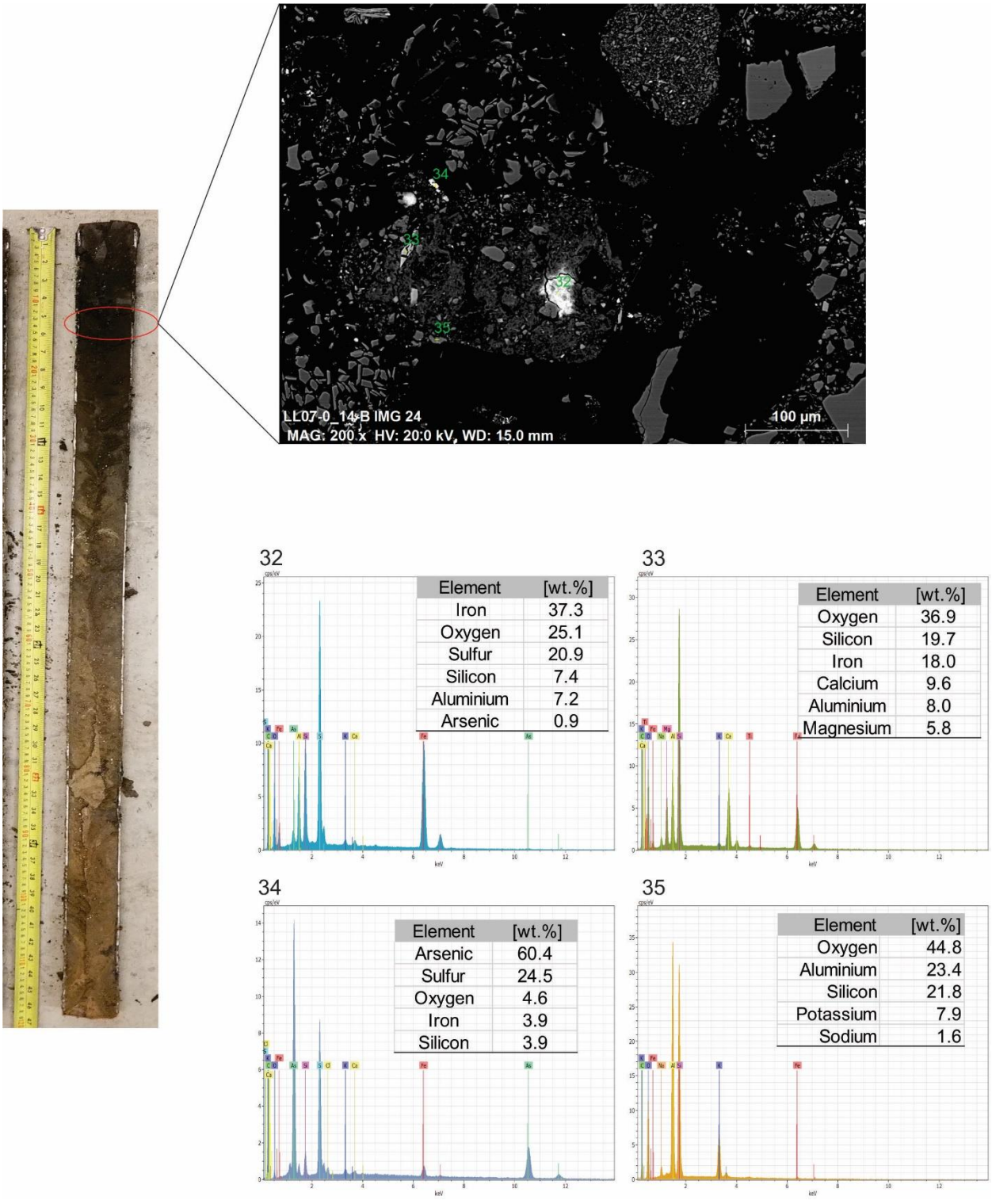

Figure D.26 Scanning electron microscope picture from location LL07-1.54 m of possible secondary sulfide precipitation.

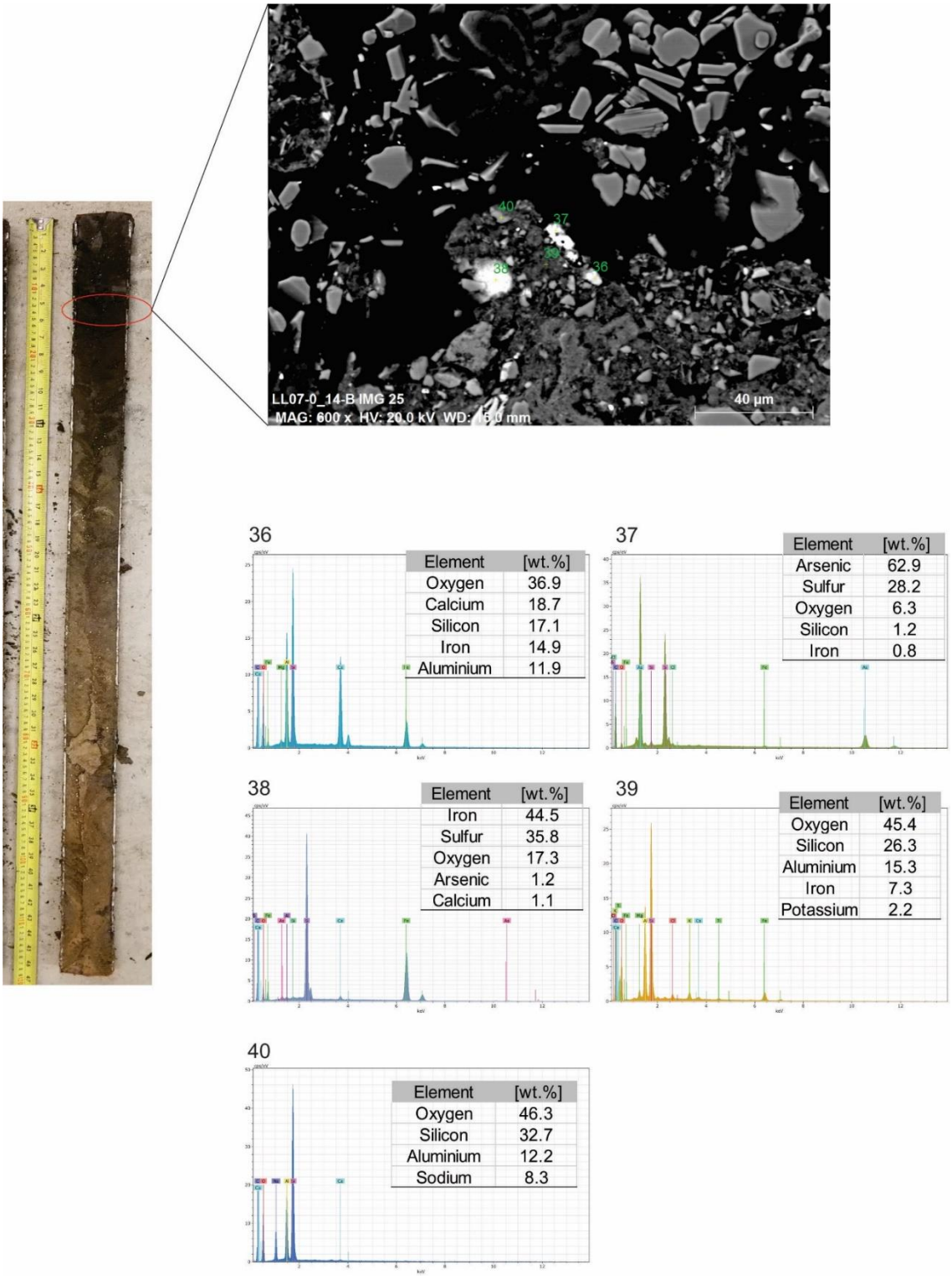

Figure D.27 Scanning electron microscope picture from location LL07-1.54 m of secondary sulfide precipitation.

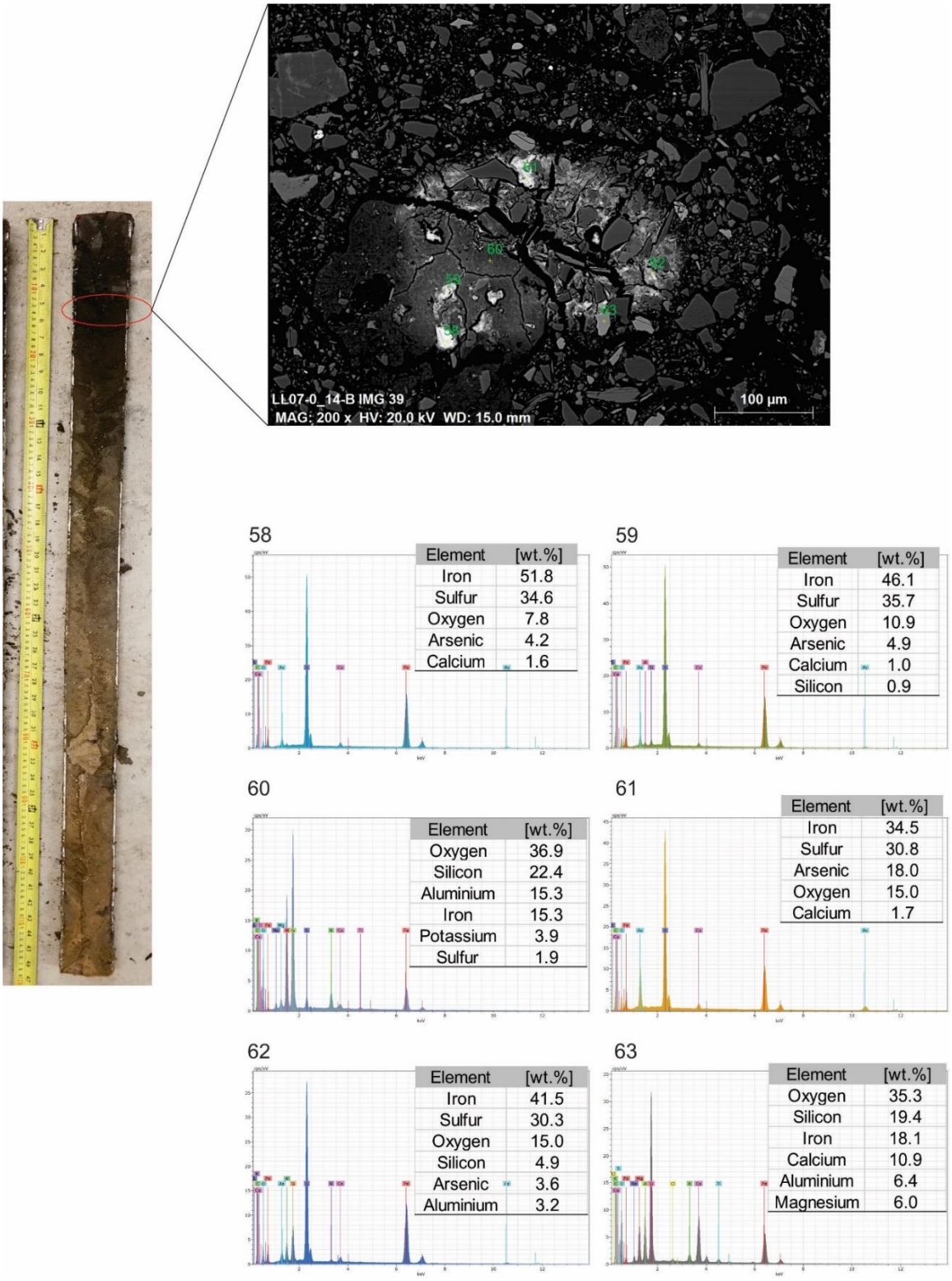

Figure D.28 Scanning electron microscope picture from location LL07-1.54 m of arsenic-iron-sulfide precipitation.

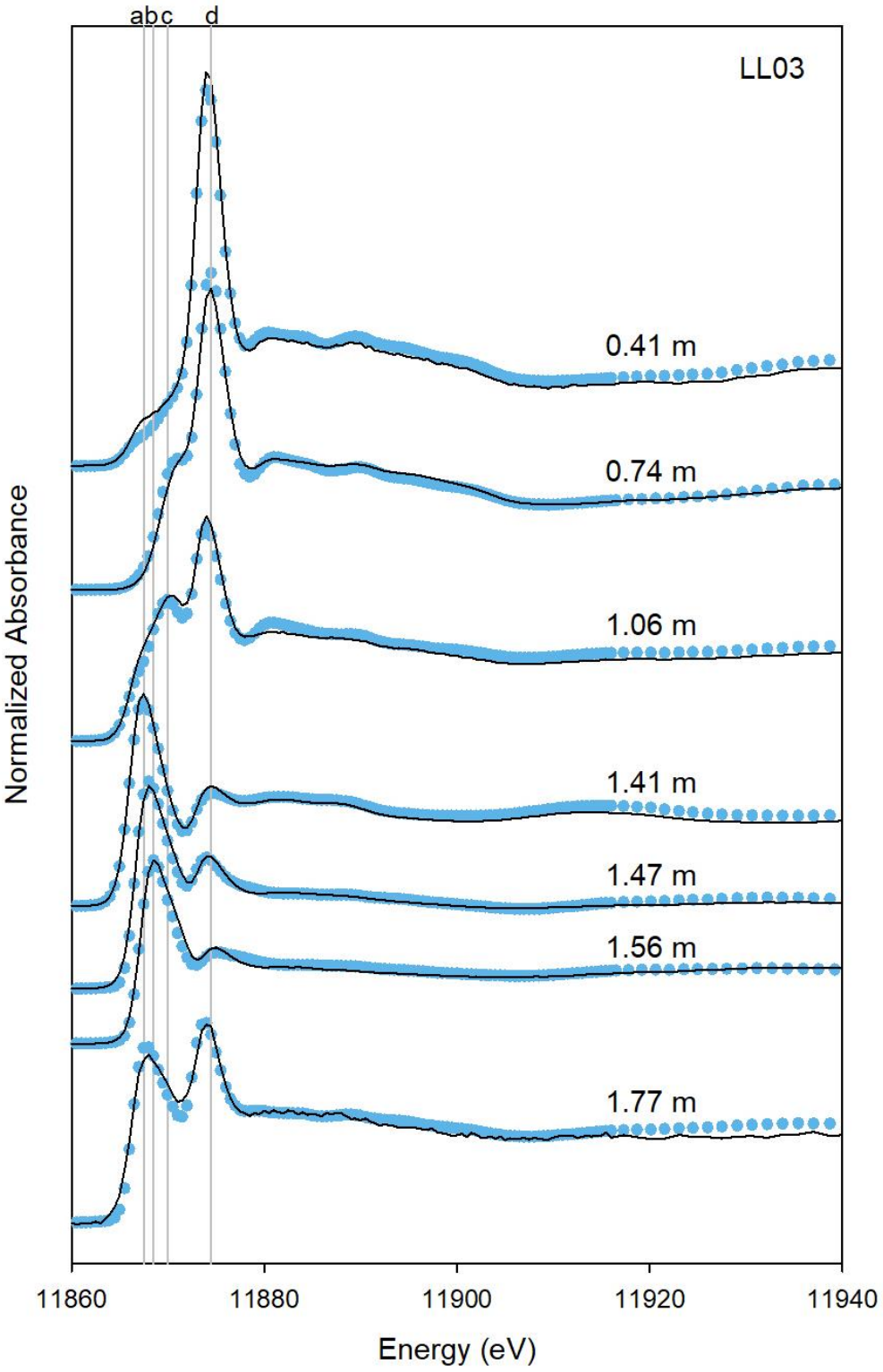

Figure D.29 Measured (line) and modeled (circles) As K-edge HERFD spectra for TA-01 tailings samples from LL03. Vertical shaded lines represent measured As K-edge white line maxima for (a) arsenopyrite, (b) orpiment, (c) arsenolite, and (d) scorodite reference standards.

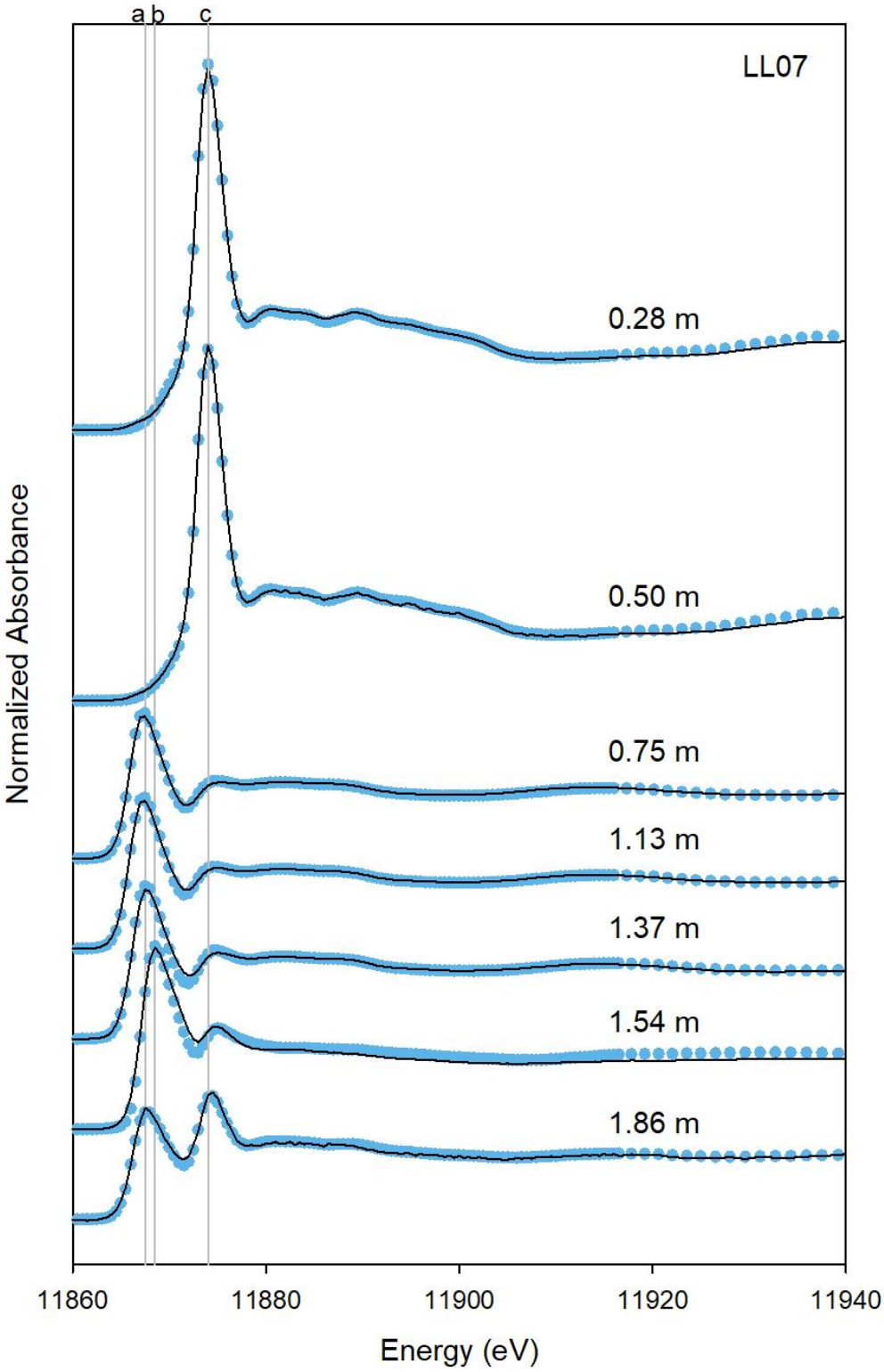

Figure D.30 Measured (line) and modeled (circles) As K-edge HERFD spectra for TA-01 tailings samples from LL07. Vertical shaded lines represent measured As K-edge white line maxima for (a) arsenopyrite, (b) orpiment, (c) scorodite reference standards.